UKRAINIAN JOURNAL OF PHYSICS

NATIONAL ACADEMY OF SCIENCES OF UKRAINE
BOGOLYUBOV INSTITUTE FOR THEORETICAL PHYSICS

8 **VOLUME 64** **2019**

SCIENTIFIC JOURNAL
12 TIMES PER YEAR
ISSUED SINCE APRIL 1956
KYIV

The present issue is dedicated to the 110-th anniversary of great scientist M.M. Bogolyubov, founder and first director of BITP

CONTENTS

УКРАЇНСЬКИЙ ФІЗИЧНИЙ ЖУРНАЛ

НАЦІОНАЛЬНА АКАДЕМІЯ НАУК УКРАЇНИ
ІНСТИТУТ ТЕОРЕТИЧНОЇ ФІЗИКИ
ім. М.М. БОГОЛЮБОВА НАН УКРАЇНИ

8 ТОМ 64 2019

НАУКОВИЙ ЖУРНАЛ
ВИХОДИТЬ 12 РАЗІВ НА РІК
ЗАСНОВАНИЙ У КВІТНІ 1956 р.
КИЇВ

ЗМІСТ

EDITORIAL FOREWORD

Issues 7 and 8 of the Ukrainian Journal of Physics (V. 64, Nos. 7 and 8, 2019) contain original papers presented at the conference on New Trends in High-Energy Physics, organized by the Bogolyubov Institute for Theoretical Physics (BITP), National Academy of Sciences of Ukraine and held in Odessa on May 12–18, 2019, https://indico.bitp.kiev.ua/event/1/. The present issues are dedicated to the 110-th anniversary of great scientist M.M. Bogolyubov, founder and first director of BITP. They collect experimental (No. 7) and theoretical/phenomenological (No. 8) papers. As guest editors, we made sure that the submitted papers, presented and discussed at the Conference, have undergone regular submission procedures and passed peer review by experts.

We thank all participants for coming to Odessa and making the Conference successful. We acknowledge the authors of the present publication for their valuable contributions, marking new trends in high-energy physics.

The Conference Program and pdf versions of all talks presented at the Conference are available at the Conference site: https://indico.bitp.kiev.ua/event/1/.

The next conference of this series is scheduled to be held in Kyiv by the end of June 2021.

László JENKOVSZKY and Rainer SCHICKER,
Guest Editors

“New Trends” in Odessa. Credit: A. Burgazli

M.M. Bogolyubov
21.08.1909–13.02.1992

https://doi.org/10.15407/ujpe64.8.665

A. AYALA,[1,2] M. HENTSCHINSKI,[3] L.A. HERNÁNDEZ,[1] M. LOEWE,[4,2,5]
R. ZAMORA [6]

[1] Instituto de Ciencias Nucleares, Universidad Nacional Autónoma de México
(Apartado Postal 70-543, CdMx 04510, Mexico)

[2] Centre for Theoretical and Mathematical Physics, and Department of Physics,
University of Cape Town
(Rondebosch 7700, South Africa)

[3] Departamento de Actuaría, Física y Matemáticas, Universidad de las Américas Puebla
(Santa Catarina Mártir, San Andrés Cholula, 72820 Puebla, Mexico)

[4] Instituto de Física, Pontificia Universidad Católica de Chile
(Casilla 306, Santiago 22, Chile)

[5] Centro Científico-Tecnológico de Valparaíso CCTVAL,
Universidad Técnica Federico Santa María
(Casilla 110-V, Valaparaíso, Chile)

[6] Instituto de Ciencias Básicas, Universidad Diego Portales
(Casilla 298-V, Santiago, Chile)

EFFECTS OF SUPERSTATISTICS ON THE LOCATION OF THE EFFECTIVE QCD CRITICAL END POINT

Effects of the partial thermalization during the chiral symmetry restoration at the finite temperature and quark chemical potential are considered for the position of the critical end point in an effective description of the QCD phase diagram. We find that these effects cause the critical end point to be displaced toward larger values of the temperature and lower values of the quark chemical potential, as compared to the case where the system can be regarded as completely thermalized. These effects may be important for relativistic heavy ion collisions, where the number of subsystems making up the whole interaction volume can be linked to the finite number of participants in the reaction.

Keywords: superstatistics, QCD phase diagram, critical end point, relativistic heavy-ion collisions.

The usual thermal description of a relativistic heavy-ion collision assumes that the produced matter reaches equilibrium, characterized by values of the temperature T and the baryon chemical potential μ, common within the whole interaction volume, after some time from the beginning of the reaction. The system evolution is subsequently described by the time evolution of the temperature down to a kinetic freeze-out, where particle spectra are established. This implicitly assumes the validity of the Gibbs–Boltzmann statistics and system's adiabatic evolution.

For expansion rates not too large compared to the interaction rate, the adiabatic evolution can perhaps be safely assumed. However, the Gibbs–Boltzmann statistics can be applied only to systems in the thermodynamical limit, namely, long after the relaxation time has elapsed and the randomization has been achieved within system's volume. In the case of a relativistic heavy-ion collision, the reaction starts off from nucleon-nucleon interactions. This means that the entire reaction volume is made, at the beginning, of a superposition of interacting pairs of nucleons. If the thermalization is achieved, it seems natural to assume that it starts off in each of the interacting nucleon pair subsystems and later spreads to the entire volume. In this scenario, the temperature and chemical potential within each subsystem may not be the same for other subsystems. Thus, a superposition of statistics, one in the usual Gibbs–Boltzmann sense for particles in each subsystem and another one, for the probability to find particular values for T and μ for different subsystem, seems appropriate. This is described by the so-called superstatistics scenario which describes a nonextensive behavior that naturally arises due to fluctuations in T or μ over the system's volume. This feature could be of particular relevance, when studying the position of the critical end point (CEP) in the QCD phase diagram, where one resorts to measuring ratios of fluctuations in conserved charges with the expectation that the volume factor cancels out in the ratio. If the thermalization is not complete, this expectation cannot hold, and a more sophisticated treatment is called for.

From the theoretical side, efforts to locate the CEP employing several techniques [1–20] were recently carried out. In all of these cases, the full thermalization over the whole reaction volume has been assumed. From the experimental side, the STAR BES-I program has recently studied heavy-ion collisions in the energy range 200 GeV $> \sqrt{s_{NN}} >$ 7.7 GeV [21]. Future experiments [22–24] will continue to thoroughly explore the QCD phase diagram, using different system sizes and varying the temperature and baryon density using different collision energies down to about $\sqrt{s_{NN}} \simeq 5$ GeV.

The superstatistics scenario has been explored in the context of relativistic heavy-ion collisions in many papers, *e.g.* Refs. [25–41] and references therein, with a particular focus on the study of imprints of the superstatistics on the particle production, using a particular version, the so-called Tsallis statistics [42]. Its use in the context of the computation of the rapidity distribution profile for the stopping in heavy ion collisions has been recently questioned in Ref. [43]. It has also been implemented to study generalized entropies and generalized Newton's law in Refs. [44–47]. The superstatistics concept has been nicely described in Refs. [48, 49]. In this work, we summarize the findings of Ref. [50] describing the implications of the superstatistics, when applied to temperature fluctuations for the location of the CEP in the QCD phase diagram.

For a system that has not yet reached a full equilibrium and contains space-time fluctuations of an intensive parameter β, such as the inverse temperature or chemical potential, one can still think of dividing the full volume into spatial subsystems, where β is approximately constant. Within each subsystem, one can apply the ordinary Gibbs–Boltzmann statistics, namely, one can use the ordinary density matrix giving rise to the Boltzmann factor $e^{-\beta\hat{H}}$, where $\hat{H}$ corresponds to the Hamiltonian for the states in each subsystem. The whole system can thus be described in terms of a space-time average over the different values that β could take for the different subsystems. In this way, one obtains a superposition of two statistics, one referring to the Boltzmann factor $e^{-\beta\hat{H}}$ and the other for β, hence, the name superstatistics.

To implement the scenario, one defines an averaged Boltzmann factor

$$B(\hat{H}) = \int_0^\infty f(\beta) e^{-\beta\hat{H}} d\beta, \tag{1}$$

where $f(\beta)$ is the probability distribution of β. The partition function then becomes

$$Z = \mathrm{Tr}[B(\hat{H})] = \int_0^\infty B(E) dE, \tag{2}$$

where the last equality holds for a suitably chosen set of eigenstates of the Hamiltonian.

When all the subsystems can be described with the same probability distribution [44], a possible choice to distribute the random variable β is the χ^2 distribution,

$$f(\beta) = \frac{1}{\Gamma(N/2)} \left(\frac{N}{2\beta_0}\right)^{N/2} \beta^{N/2-1} e^{-N\beta/2\beta_0}, \tag{3}$$

where Γ is the Gamma function, N represents the number of subsystems that make up the whole system, and

$$\beta_0 \equiv \int_0^\infty \beta f(\beta) d\beta = \langle\beta\rangle \tag{4}$$

is the average of the distribution. The χ^2 is the distribution that emerges for a random variable that is made up of the sum of the squares of random variables X_i, each of which is distributed with a Gaussian probability distribution with vanishing average and unit variance. This means that if we take

$$\beta = \sum_{i=1}^{N} X_i^2, \tag{5}$$

then β is distributed according to Eq. (3). Moreover, its variance is given by

$$\langle \beta^2 \rangle - \beta_0^2 = \frac{2}{N}\beta_0^2. \tag{6}$$

Given that β is a positive definite quantity, thinking of it as being the sum of positive definite random variables is an adequate model. Note, however, that these variables do not necessarily correspond to the inverse temperature in each of the subsystems. Nevertheless, since the use of the χ^2 distribution allows for an analytical treatment, we hereby take this as the distribution to model the possible values of β.

To add superstatistics effects to the dynamics of a given system, we first find the effective Boltzmann factor. This is achieved by taking Eq. (3) and substituting it into Eq. (1). The integration over β leads to

$$B(\hat{H}) = \left(1 + \frac{2}{N}\beta_0 \hat{H}\right)^{-\frac{N}{2}}. \tag{7}$$

Note that, in the limit as $N \to \infty$, Eq. (7) becomes the ordinary Boltzmann factor. For large, but finite N, Eq. (7) can be expanded as

$$B(\hat{H}) = \left[1 + \frac{1}{2}\left(\frac{2}{N}\right)\beta_0^2 \hat{H}^2 - \frac{1}{3}\left(\frac{2}{N}\right)^2 \beta_0^3 \hat{H}^3 + ...\right] e^{-\beta_0 \hat{H}}. \tag{8}$$

Working up to first order in $1/N$, Eq. (8) can be written as [48]

$$B(\hat{H}) = e^{-\beta \hat{H}}\left(1 + \frac{\beta^2 H^2}{N} + ...\right) = \\ = \left[1 + \frac{\beta_0^2}{N}\left(\frac{\partial}{\partial \beta_0}\right)^2 + ...\right] e^{-\beta_0 \hat{H}}. \tag{9}$$

Therefore, the partition function to the first order in $1/N$ is given by

$$Z = \left[1 + \frac{\beta_0^2}{N}\left(\frac{\partial}{\partial \beta_0}\right)^2 + ...\right] Z_0 \tag{10}$$

with

$$Z_0 = e^{-\mathtt{V}\beta_0 V^{\text{eff}}}, \tag{11}$$

where $\mathtt{V}$ and V^{eff} are the system's volume and effective potential, respectively. After a bit of a straightforward algebra, we write the expression for the partition function in terms of $T_0 = 1/\beta_0$ as

$$Z = \left[1 + \frac{\beta_0^2}{N}\left(\frac{\partial}{\partial \beta_0}\right)^2 + ...\right] Z_0 = \\ = Z_0 \left[1 + \frac{2T_0}{NZ_0}\left(\frac{\partial Z_0}{\partial T_0} + \frac{T_0}{2}\frac{\partial^2 Z_0}{\partial T_0^2}\right)\right], \tag{12}$$

and, therefore,

$$\ln[Z] = \ln[Z_0] + \ln\left[1 + \frac{2T_0}{NZ_0}\left(\frac{\partial Z_0}{\partial T_0} + \frac{T_0}{2}\frac{\partial^2 Z_0}{\partial T_0^2}\right)\right]. \tag{13}$$

To explore the QCD phase diagram from the point of view of chiral symmetry restoration, we use an effective model that accounts for the physics of spontaneous symmetry breaking at finite temperature and density: the linear sigma model. In order to account for the fermion degrees of freedom around the phase transition, we also include quarks in this model and work with the linear sigma model with quarks. The Lagrangian in the case where only the two lightest quark flavors are included is given by

$$\mathcal{L} = \frac{1}{2}(\partial_\mu \sigma)^2 + \frac{1}{2}(\partial_\mu \boldsymbol{\pi})^2 + \frac{a^2}{2}(\sigma^2 + \boldsymbol{\pi}^2) + \\ + \frac{\lambda}{4}(\sigma^2 + \boldsymbol{\pi}^2)^2 + i\bar{\psi}\gamma^\mu \partial_\mu \psi - g\bar{\psi}(\sigma + i\gamma_5 \boldsymbol{\tau}\,\boldsymbol{\pi})\psi, \tag{14}$$

where ψ is an SU(2) isospin doublet, $\boldsymbol{\pi} = (\pi_1, \pi_2, \pi_3)$ is an isospin triplet, σ is an isospin singlet, λ is the boson's self-coupling, g is the fermion-boson coupling, and $a^2 > 0$ is the squared mass parameter.

To allow for an spontaneous symmetry breaking, we let the σ field develop a vacuum expectation value v

$$\sigma \to \sigma + v, \tag{15}$$

which serves as the order parameter to identify the phase transitions. After this shift, the Lagrangian can be rewritten as

$$\mathcal{L} = \frac{1}{2}(\partial_\mu \sigma)^2 - \frac{1}{2}\left(3\lambda v^2 - a^2\right)\sigma^2 +$$

$$+\frac{1}{2}(\partial_\mu \boldsymbol{\pi})^2 - \frac{1}{2}\left(\lambda v^2 - a^2\right)\boldsymbol{\pi}^2 + \frac{a^2}{2}v^2 + \\ -\frac{\lambda}{4}v^4 + i\bar{\psi}\gamma^\mu\partial_\mu\psi - gv\bar{\psi}\psi + \mathcal{L}_I^b + \mathcal{L}_I^f, \quad (16)$$

where the sigma, three pions, and the quarks have masses given by

$$m_\sigma^2 = 3\lambda v^2 - a^2, \\ m_\pi^2 = \lambda v^2 - a^2, \\ m_f = gv, \quad (17)$$

respectively, and $\mathcal{L}_I^b$ and $\mathcal{L}_I^f$ are given by

$$\mathcal{L}_I^b = -\frac{\lambda}{4}(\sigma^2 + \boldsymbol{\pi}^2)^2 \\ \mathcal{L}_I^f = -g\bar{\psi}(\sigma + i\gamma_5 \boldsymbol{\tau}\,\boldsymbol{\pi})\psi. \quad (18)$$

Equation (18) describes the interactions among the σ, $\boldsymbol{\pi}$, and ψ fields after the symmetry breaking.

In order to analyze the chiral symmetry restoration, we compute the effective potential at finite temperature and density. In order to account for plasma screening effects, we also work up to the contribution of ring diagrams. All matter terms are computed in the high-temperature approximation. The effective potential is given by [20]

$$V^{\rm eff}(v, T_0, \mu_q) = -\frac{(a^2 + \delta a^2)}{2}v^2 + \frac{(\lambda + \delta\lambda)}{4}v^4 + \\ + \sum_{b=\sigma,\bar{\pi}}\left\{-\frac{m_b^4}{64\pi^2}\left[\ln\left(\frac{a^2}{4\pi T_0^2}\right) - \gamma_E + \frac{1}{2}\right] - \right. \\ \left. -\frac{\pi^2 T_0^4}{90} + \frac{m_b^2 T_0^2}{24} - \frac{(m_b^2 + \Pi(T_0, \mu_q))^{3/2} T_0}{12\pi}\right\} + \\ + \sum_{f=u,d}\left\{\frac{m_f^4}{16\pi^2}\left[\ln\left(\frac{a^2}{4\pi T_0^2}\right) - \gamma_E + \frac{1}{2} - \right.\right. \\ \left. -\psi^0\left(\frac{1}{2} + \frac{\mathrm{i}\mu_q}{2\pi T_0}\right) - \psi^0\left(\frac{1}{2} - \frac{\mathrm{i}\mu_q}{2\pi T_0}\right)\right] - \\ -8 m_f^2 T_0^2\left[\mathrm{Li}_2(-e^{\mu_q/T_0}) + \mathrm{Li}_2(-e^{-\mu_q/T_0})\right] + \\ \left. +32 T_0^4\left[\mathrm{Li}_4(-e^{\mu_q/T_0}) + \mathrm{Li}_4(-e^{-\mu_q/T_0})\right]\right\}, \quad (19)$$

where μ_q is the quark chemical potential, and δa^2 and $\delta\lambda$ represent the counterterms which ensure that the one-loop vacuum corrections do not shift the position of the minimum or the vacuum mass of the sigma. These counterterms are given by

$$\delta a^2 = -a^2\frac{(8g^4 - 12\lambda^2 - 3\lambda^2\ln[2])}{32\pi\lambda}, \\ \delta\lambda = \frac{(16 + 8\ln[g^2/\lambda])g^4 - (18 + 9\ln[2])\lambda^2}{64\pi^2}. \quad (20)$$

The self-energy at finite temperature and quark chemical potential, $\Pi(T_0, \mu_q)$, includes the contribution from both bosons and fermions. In the high temperature approximation, it is given by [20]

$$\Pi(T_0, \mu_q) = -N_f N_c g^2 \frac{T_0^2}{\pi^2}\left[\mathrm{Li}_2(-e^{\mu_q/T_0}) + \right. \\ \left. + \mathrm{Li}_2(-e^{-\mu_q/T_0})\right] + \frac{\lambda T_0^2}{2}. \quad (21)$$

To implement superstatistics corrections, we substitute Eq. (19) into Eq. (11). The partition function is obtained from Eq. (12) and the effective potential including superstatistics effects is obtained from the logarithm of this partition function,

$$V_{\rm sup}^{\rm eff} = -\frac{1}{\mathsf{V}\beta}\ln[Z]. \quad (22)$$

As a consequence, the effective potential of Eq. (22) has four free parameters. Three of them come from the original model, namely, λ, g and a. The remaining one corresponds to the superstatistics correction, N. In the absence of superstatistics, the effective potential in Eq. (19) allows for the second- and first-order phase transitions, depending on the values of λ, g and a, as well as of T_0 and μ_q. For given values of λ, g, and a, we now proceed to analyze the phase structure that emerges, when varying N, paying particular attention to the displacement of the CEP location in the T_0, μ_q plane.

The figure shows the effective QCD phase diagram calculated with $a = 133$ MeV, $g = 0.51$, and $\lambda = 0.36$ for different values of the number of subsystems making up the whole system, N. For the different curves, the star shows the position of the CEP. Note that this position moves to larger values of T and lower values of μ_q, with respect to the CEP position for $N = \infty$, that is, without superstatistics effects, as N decreases. Note also that, for these findings, we have not considered fluctuations in the chemical potential. Those have been included to study the CEP position in the Nambu–Jona-Lasinio model in Ref. [53].

Our findings show that fermions become more relevant for lower values of the baryon chemical potential, than they do in the case of the homogeneous system. To picture this result, as above, let (μ_c^0, T_c^0) and (μ_c, T_c) be the critical values for the baryon chemical potential and temperature at the onset of first-order phase transitions for the homogeneous and fluctuating systems, respectively. The parameter that determines, when fermions become relevant, is the combination μ_c^0/T_c^0. Since our calculation for a single-boson degrees of freedom shows that the critical temperature decreases with decreasing the number of subsystems (see Ref. [50]), this means that, for the boson-fermion fluctuating system, fermions become relevant for $\mu_c/T_c \simeq \mu_c^0/T_c^0$ and, thus, for $\mu_c < \mu_c^0$.

To apply these considerations to the context of relativistic heavy-ion collisions, we recall that temperature fluctuations are related to the system's heat capacity by

$$\frac{(1-\xi)}{C_v} = \frac{\langle (T-T_0)^2\rangle}{T_0^2}, \tag{23}$$

where the factor $(1-\xi)$ accounts for deviations [54] from the Gaussian [55] distribution for the random variable T. The right-hand side of Eq. (23) can be written in terms of fluctuations in β as

$$\frac{\langle (T-T_0)^2\rangle}{T_0^2}\frac{\langle T^2\rangle - T_0^2}{T_0^2} = \frac{\beta_0^2 - \langle \beta^2\rangle}{\langle \beta^2\rangle} = = \frac{\left(\frac{\beta_0^2}{\langle\beta^2\rangle}\right)^2\langle\beta^2\rangle - \beta_0^2}{\beta_0^2}. \tag{24}$$

Note that, according to Eq. (6),

$$\left(\frac{\beta_0^2}{\langle\beta^2\rangle}\right)^2 = \left(\frac{1}{1+2/N}\right)^2 \simeq 1 - 4/N. \tag{25}$$

Therefore, for N finite, but large,

$$\frac{\langle (T-T_0)^2\rangle}{T_0^2} \simeq \frac{\langle\beta^2\rangle - \beta_0^2}{\beta_0^2}. \tag{26}$$

Using Eqs. (6) and (26), we obtain

$$\frac{\langle (T-T_0)^2\rangle}{T_0^2} = \frac{2}{N}. \tag{27}$$

This means that the heat capacity is related to the number of subsystems by

$$\frac{(1-\xi)}{C_v} = \frac{2}{N}. \tag{28}$$

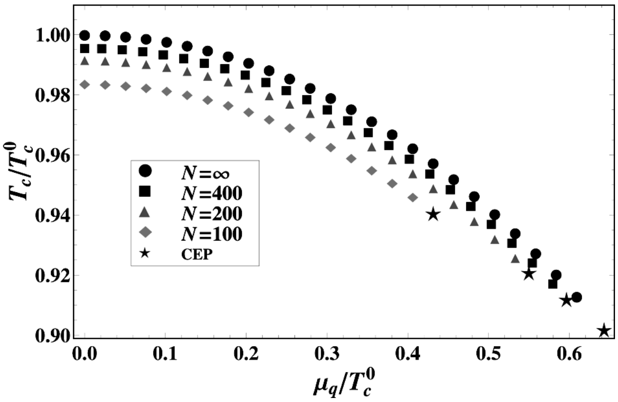

Effective QCD phase diagram calculated with $a = 133$ MeV, $g = 0.51$, and $\lambda = 0.36$ for different values of N. The star shows the position of the CEP which moves toward larger values of T and lower values of μ_q, as N decreases

To introduce the specific heat c_v for a relativistic heavy-ion collision, it is natural to divide C_v by the number of participants N_p in the reaction. Therefore, Eq. (28) can be written as

$$\frac{2}{N} = \frac{(1-\xi)}{N_p c_v}. \tag{29}$$

In Ref. [54], ξ is estimated as $\xi = N_p/A$, where A is the smallest mass number of the colliding nuclei. Equation (29) provides the link between the number of subsystems in a general superstatistics framework and a relativistic heavy-ion collision. It has been shown [56] that, at least for Gaussian fluctuations, c_v is a function of the collision energy. Therefore, in order to make a thorough exploration of the phase diagram, as the collision energy changes, we need to account for this dependence, as well as to work with values of the model parameters λ, g, and a, appropriate to the description of the QCD phase transition. Work along these lines is currently underway and will be reported elsewhere.

M.H., M.L., and R.Z. would like to thank Instituto de Ciencias Nucleares, Universidad Nacional Autónoma de México for their warm hospitality during a visit in June-July 2018. A.A. and L.A.H. would like to thank the Physics Derpartment, PUC and CIDCA for their warm hospitality during a visit in July 2018. This work was supported by UNAM-DGPA-PAPIIT grant number IG100219, by Consejo Nacional de Ciencia y Tecnología grant num-

ber 256494, by Fondecyt (Chile) grant numbers 1170107, 1150471, 11508427, Conicyt/PIA/Basal (Chile) grant number FB0821. R.Z. would like to acknowledge the support from CONICYT FONDECYT Iniciación under grant number 11160234.

1. A. Ayala, C. A. Dominguez, M. Loewe. For a recent review on the QCD sum rules technique at finite temperature. *Adv. High Energy Phys.* **2017**, 9291623 (2017).
2. P. Costa, M.C. Ruivo, C.A. de Sousa. Thermodynamics and critical behavior in the Nambu–Jona-Lasinio model of QCD. *Phys. Rev. D* **77**, 096001 (2008).
3. G.A. Contrera, D. Gomez-Dumm, N.N. Scoccola. Nonlocal SU(3) chiral quark models at finite temperature: The role of the Polyakov loop. *Phys. Lett. B* **661**, 113 (2008).
4. A. Ayala, A. Bashir, C. A. Dominguez, E. Gutierrez, M. Loewe, A. Raya. QCD phase diagram from finite energy sum rules. *Phys. Rev. D* **84**, 056004 (2011).
5. X.-Y. Xin, S.-X. Qin, Y.-X. Liu. Quark number fluctuations at finite temperature and finite chemical potential via the Dyson–Schwinger equation approach. *Phys. Rev. D* **90**, 076006 (2014).
6. C.S. Fischer, J. Luecker, C.A. Welzbacher. Phase structure of three and four flavor QCD. *Phys. Rev. D* **90**, 034022 (2014).
7. Y. Lu, Y.-L. Du, Z.-F. Cui, H.-S. Zong. Critical behaviors near the (tri-) critical end point of QCD within the NJL model. *Eur. Phys. J. C* **75**, 495 (2015).
8. A. Ayala, M. Loewe, R. Zamora. Inverse magnetic catalysis in the linear sigma model with quarks. *Phys. Rev. D* **91**, 016002 (2015).
9. A. Ayala, M. Loewe, A.J. Mizher, R. Zamora. Inverse magnetic catalysis for the chiral transition induced by thermomagnetic effects on the coupling constant. *Phys. Rev. D* **90**, 036001 (2014).
10. A. Ayala, C.A. Dominguez, L.A. Hernández, M. Loewe, R. Zamora. Magnetized effective QCD phase diagram. *Phys. Rev. D* **92**, 096011 (2015).
11. C. Shi, Y.-L. Du, S.-S. Xu, X.-J. Liu, H.-S. Zong. Continuum study of the QCD phase diagram through an OPE-modified gluon propagator. *Phys. Rev. D* **93**, 036006 (2016).
12. G.A. Contrera, A.G. Grunfeld, D. Blaschke. Supporting the search for the CEP location with nonlocal PNJL models constrained by lattice QCD. *Eur. Phys. J. A* **52**, 231 (2016).
13. A. Ayala, C.A. Dominguez, L.A. Hernández, M. Loewe, A. Raya, J.C. Rojas, C. Villavicencio. Thermomagnetic properties of the strong coupling in the local Nambu–Jona-Lasinio model. *Phys. Rev. D* **94**, 054019 (2016).
14. Z.-F. Cui, J.-L. Zhang, H.-S. Zong. Proper time regularization and the QCD chiral phase transition. *Sci. Rep.* **7**, 45937 (2017).
15. S. Datta, R.V. Gavai, S. Gupta. Quark number susceptibilities and equation of state at finite chemical potential in staggered QCD with $N_t = 8$. *Phys. Rev. D* **95**, 054512 (2017).
16. J.P. Carlomagno, M. Loewe. Comparison between the continuum threshold and the Polyakov loop as deconfinement order parameters. *Phys. Rev. D* **95**, 036003 (2017).
17. J. Knaute, R. Yaresko, B. Kämpfer. Holographic QCD phase diagram with critical point from Einstein–Maxwell-dilaton dynamics. *Phys. Lett. B* **778**, 419 (2018).
18. N.G. Antoniou, F.K. Diakonos, X.N. Maintas. C.E. Tsagkarakis. Locating the QCD critical endpoint through finite-size scaling. *Phys. Rev. D* **97**, 034015 (2018).
19. R. Rougemont, R. Critelli, J. Noronha-Hostler, J. Noronha, C. Ratti. Dynamical versus equilibrium properties of the QCD phase transition: A holographic perspective. *Phys. Rev. D* **96**, 014032 (2017).
20. A. Ayala, S. Hernández-Ortiz, L.A. Hernández. QCD phase diagram from chiral symmetry restoration: analytic approach at high and low temperature using the linear sigma model with quarks. *Rev. Mex. Fis.* **64**, 302 (2018).
21. L. Adamczyk *et al.*, [STAR Collaboration]. Energy dependence of moments of net-proton multiplicity distributions at RHIC. *Phys. Rev. Lett.* **112**, 032302 (2014); Beam energy dependence of moments of the net-charge multiplicity distributions in Au + Au collisions at RHIC. *Phys. Rev. Lett.* **113**, 092301 (2014).
22. C. Yang, [for the STAR Collaboration]. The STAR beam energy scan phase II physics and upgrades. *Nucl. Phys. A* **967**, 800 (2017).
23. P. Senger. The heavy-ion program of the future FAIR facility. *J. Phys. Conf. Ser.* **798**, 012062 (2017).
24. V. Kekelidze, A. Kovalenko, R. Lednicky, V. Matveev, I. Meshkov, A. Sorin, G. Trubnikov. Feasibility study of heavy-ion collision physics at NICA JINR. *Nucl. Phys. A* **967**, 884 (2017).
25. G. Wilk, Z. Wlodarczyk. Multiplicity fluctuations due to the temperature fluctuations in high-energy nuclear collisions. *Phys. Rev. C* **79**, 054903 (2009).
26. G. Wilk, Z. Wlodarczyk. Power laws in elementary and heavy-ion collisions. *Eur. Phys. J. A* **40**, 299 (2009).
27. G. Wilk, Z. Wlodarczyk. The imprints of superstatistics in multiparticle production processes. *Cent. Eur. J. Phys.* **10**, 568 (2012).
28. M. Rybczynski, Z. Wlodarczyk. Tsallis statistics approach to the transverse momentum distributions in p-p collisions. *Eur. Phys. J. C* **74**, 2785 (2014).
29. C.Y. Wong, G. Wilk, L.J.L. Cirto, C. Tsallis. From QCD-based hard-scattering to nonextensive statistical mechanical descriptions of transverse momentum spectra in high-energy pp and $p\bar{p}$ collisions. *Phys. Rev. D* **91**, 114027 (2015).
30. G. Wilk, Z. Wlodarczyk. Superstatistical cluster decay. *Phys. Lett. A* **379**, 2941 (2015).
31. A. Bialas. Tsallis $p_\perp$ distribution from statistical clusters. *Phys. Lett. B* **747**, 190 (2015).
32. T. Bhattacharyya, J. Cleymans, A. Khuntia, P. Pareek, R. Sahoo. Radial flow in non-extensive thermodynamics

and study of particle spectra at LHC in the limit of small $(q-1)$. *Eur. Phys. J. A* **52**, 30 (2016).
33. A. Bialas, A. Bzdak. Short-range two-particle correlations from statistical clusters. *Phys. Rev. D* **93**, 094015 (2016).
34. J. Rozynek, G. Wilk. An example of the interplay of nonextensivity and dynamics in the description of QCD matter. *Eur. Phys. J. A* **52**, 294 (2016).
35. S. Tripathy, T. Bhattacharyya, P. Garg, P. Kumar, R. Sahoo, J. Cleymans. Nuclear modification factor using Tsallis non-extensive statistics. *Eur. Phys. J. A* **52**, 289 (2016).
36. S. Grigoryan. Using the Tsallis distribution for hadron spectra in pp collisions: Pions and quarkonia at $\sqrt{s}=5$–13000 GeV. *Phys. Rev. D* **95**, 056021 (2017).
37. A. Khuntia, S. Tripathy, R. Sahoo, J. Cleymans. Multiplicity dependence of non-extensive parameters for strange and multi-strange particles in proton-proton collisions at $\sqrt{s}=7$ TeV at the LHC. *Eur. Phys. J. A* **53**, 103 (2017).
38. T. Bhattacharyya, J. Cleymans, L. Marques, S. Mogliacci, M.W. Paradza. On the precise determination of the Tsallis parameters in proton-proton collisions at LHC energies. *J. Phys. G* **45**, 055001 (2018).
39. S. Tripathy, S.K. Tiwari, M. Younus, R. Sahoo. Elliptic flow in Pb+Pb collisions at $\sqrt{s_{\mathrm{NN}}}=2.76$ TeV at the LHC using Boltzmann transport equation with non-extensive statistics. *Eur. Phys. J. A* **54**, 38 (2018).
40. M. Ishihara. Phase transition for the system of finite volume in the ϕ^4 theory in the Tsallis nonextensive statistics. *Int. J. Mod. Phys. A* **33**, 1850067 (2018).
41. G. Wilk, Z. Wlodarczyk. Some intriguing aspects of multiparticle production processes. *Int. J. Mod. Phys. A* **33**, 1830008 (2018).
42. C. Tsallis. Possible generalization of Boltzmann–Gibbs statistics. *J. Stat. Phys.* **52**, 479 (1988).
43. A. Simon, G. Wolschin. Examining nonextensive statistics in relativistic heavy-ion collisions. *Phys. Rev. C* **97**, 044913 (2018).
44. O. Obregón, A. Gil-Villegas. Generalized information entropies depending only on the probability distribution. *Phys. Rev. E* **88**, 062146 (2013).
45. A. Martínez-Merino, O. Obregón, M.P. Ryan, jr. Modified entropies, their corresponding Newtonian forces, potentials, and temperatures. *Phys. Rev. D* **95**, 124031 (2017).
46. O. Obregón. Superstatistics and gravitation. *Entropy 2010* **12**, 2067 (2010).
47. O. Obregón. Superstatistics and gravitation. *Entropy 2010* **12**, 2067 (2010).
48. C. Beck, E.G.D. Cohen. Superstatistics. *Phys. A* **322**, 267 (2003).
49. C. Beck. Superstatistics: theory and applications. *Continuum Mech. Thermodyn.* **16**, 293 (2004); C. Beck. Recent developments in superstatistics. *Braz. J. Phys.* **39**, 2A, 357 (2009).
50. Al. Ayala, M. Hentschinski, L.A. Hernandez, M. Loewe, R. Zamora. Superstatistics and the effective QCD phase diagram. *Phys. Rev. D* **98**, 114002 (2018).
51. A. Ayala, A. Sanchez, G. Piccinelli, S. Sahu. Effective potential at finite temperature in a constant magnetic field. I. Ring diagrams in a scalar theory. *Phys. Rev. D* **71**, 023004 (2005).
52. M.E. Carrington. The effective potential at finite temperature in the Standard Model. *Phys. Rev. D* **45**, 2933 (1992).
53. J. Rozynek, G. Wilk. An example of the interplay of nonextensivity and dynamics in the description of QCD matter. *Eur. Phys. J. A* **52**, 294 (2016).
54. G. Wilk, Z. Wlodarczyk. Multiplicity fluctuations due to the temperature fluctuations in high-energy nuclear collisions. *Phys. Rev. C* **79**, 054903 (2009).
55. L.D. Landau, E.M. Lifshitz. *Statistical Physics* (Elsevier, 2013), ISBN 9780080570464.
56. S. Basu, S. Chatterjee, R. Chatterjee, T.K. Nayak, B.K. Nandi. Specific heat of matter formed in relativistic nuclear collisions. *Phys. Rev. C* **94**, 044901 (2016).

Received 08.07.19

А. Аяла, М. Хентшинскі,
Л.А. Гернандез, М. Леве, Р. Замора

ВПЛИВ СУПЕРСТАТИСТИКИ
НА ПОЛОЖЕННЯ КРИТИЧНОЇ КІНЦЕВОЇ
ТОЧКИ В ЕФЕКТИВНІЙ КХД

Р е з ю м е

В рамках ефективної моделі фазової діаграми КХД розглядається вплив часткової термалізації під час відновлення кіральної симетрії при скінченних температурі і хімічному потенціалі кварків на положення критичної кінцевої точки. Ми показали, що ці ефекти спричиняють зміщення критичної точки в бік більших температур та менших значень хімічного потенціалу кварків по відношенню до повністю термалізованої системи. Ці ефекти можуть бути важливими для зіткнень релятивістських важких іонів, де число підсистем, що заповнюють весь об'єм, можна пов'язати зі скінченним числом частинок в реакції.

https://doi.org/10.15407/ujpe64.8.672

S. CATTO,[1,2] Y. GÜRCAN,[3] A. KHALFAN,[4] L. KURT,[3] B. NICOLESCU,[5] E. YU[5]

[1] CUNY Graduate School and University Center
(365, Fifth Avenue, New York, NY 10016-4309; e-mail: scatto@gc.cuny.edu)

[2] The Rockefeller University
(1230, York Avenue, New York, NY10021-6399)

[3] Department of Science, Borough of Manhattan CC
(The City University of New York, NY 10007)

[4] Physics Department, LaGuardia CC
(The City University of New York, NY 11101)

[5] Baruch College, City University of New York
(17, Lexington Ave, New York, NY 10010)

HADRONIC SUPERSYMMETRY FROM QCD

The evolution of hadronic mass formulae with special emphasis on group theoretical descriptions and supersymmetry suggested by QCD and based on quark-antidiquark symmetry is shown, with further comments on possible applications to a Skyrme-type models that may compete with the potential quark models in the future.

K e y w o r d s: supersymmetry, quark models, skyrmions.

1. Introduction

The quark model with potentials derived from QCD, including the quark-diquark model for excited hadrons gives mass formulae in a very good agreement with experiments and goes a long way in explaining the approximate symmetries and supersymmetries of the hadronic spectrum, including the symmetry breaking mechanism.

The mathematical expression of supersymmetry arises through a generalization of Lie algebras to superalgebras. When a Lie algebra is $su(n)$ it can be extended to a graded algebra (superalgebra) $su(n/m)$ with even and odd generators, the even generators being paired with commuting (bosonic) parameters and the odd generator with the Grassmann (fermionic) parameters. The algebra can then be exponentiated to the supergroup SU(n/m). This was done by Miyazawa [1] who derived the correct commutation and anticommutation relations for such a superalgebra, as well as the generalized Jacobi identity. This discovery predates the supersymmetry in dual resonance models or supersymmetry in quantum field theories invariant under the super-Poincaré group that generalizes special relativity. Miyazawa looked for a supergroup that would contain SU(6) and settled on broken SU(6/21). He showed that an SU(3) singlet-octet of this supergroup leads to a new kind of mass formulae relating fermionic and bosonic mass splittings.

2. Quark-Diquark Model

We shall first discuss the validity domain of SU(6/21) supersymmetry [2, 3, 6]. The diquark structure with spins $s = 0$ and $s = 1$ emerges in inelastic inclusive lepton-baryon collisions with high impact parameters that excite the baryon rotationally, resulting in inelastic structure functions based on point-like quarks and diquarks instead of three point-like quarks. In this case, both mesons and baryons are bilocal with large separation of constituents.

In addition, there is a symmetry between color antitriplet diquarks with $s = 0$ and $s = 1$ and color antitriplet antiquarks with $s = \frac{1}{2}$. This is only possible, if the force between quark q and antiquark $\bar{q}$, and between q and diquark D is mediated by a zero spin object that sees no difference between the spins of $\bar{q}$ and D. The object can be in color states that are either singlet or octet since q and D are both triplets. Such an object is provided by scalar flux tubes of gluons that dominate over the one gluon exchange at large distances. Various strong coupling approximations to QCD, like lattice gauge theory [4, 5], 't Hooft's $\frac{1}{N}$ approximation [7], when N, the number of colors, is very large, or the elongated bag model [8] all give a linear potential between widely separated quarks and an effective string that approximates the gluon flux tube. In such a theory, it is energetically favorable for the three quarks in a baryon to form a linear structure with a quark in the middle and two at the ends or, for a high rotational excitation, a bilocal linear structure (diquark) at one end and a quark at the other end. In order to illustrate these points, we start with the suggestion of Johnson and Thorn [8] that the string-like hadrons may be pictured as the vortices of color flux lines which terminate on the concentration of color at the end points. The color flux connecting opposite ends is the same for mesons and baryons giving an explanation for the same slope of meson and baryon trajectories [3].

To construct a solution, which yields a maximal angular momentum for a fixed mass, we consider a bag with elongated shape rotating about the center of mass with an angular frequency ω. Its ends have the maximal velocity allowed, which is the speed of light ($c = 1$). Thus, a given point inside the bag, at a distance r from the axis of rotation moves with a velocity

$$v = |\boldsymbol{\omega} \times \mathbf{r}| = \frac{2r}{L}, \tag{1}$$

where L is the length of the string. In this picture, the bag surface will be fixed by balancing the gluon field pressure against the confining vacuum pressure B, which (in analogy to electrodynamics) can be written in the form

$$\frac{1}{2}\sum_{\alpha=1}^{8}(E_\alpha^2 - B_\alpha^2) = B. \tag{2}$$

Using Gauss' law, the color electric field E through the flux tube connecting the color charges at the ends of the string is given by

$$\int \mathbf{E}_\alpha \, d\mathbf{S} = E_\alpha A = g\frac{1}{2}\lambda_\alpha, \tag{3}$$

where $A(r)$ is the cross-section of the flux tube at distance r from the center and $g\frac{1}{2}\lambda_\alpha$ is the color electric charge, which is the source of E_α. By analogy with classical electrodynamics, the color magnetic field $\mathbf{B}_\alpha(r)$ associated with the rotation of the color electric field is

$$\mathbf{B}_\alpha(r) = \mathbf{v}(r) \times \mathbf{E}_\alpha(r), \tag{4}$$

at a point moving with a velocity $\mathbf{v}(r)$. For the absolute values, this yields

$$B_\alpha = v \; E_\alpha, \tag{5}$$

because $\mathbf{v}(r)$ is perpendicular to $\mathbf{E}_\alpha(r)$. Using last three equations together with

$$\left\langle \sum_{\alpha=1}^{8} \left(\frac{1}{2}\lambda_\alpha\right)^2 \right\rangle = \frac{4}{3} \tag{6}$$

for the $SU(3)^c$ triplet in Eq. (2), we obtain that the cross-section of the bag

$$A(r) = \sqrt{\frac{2}{3B}}\; g\; \sqrt{1 - v^2}, \tag{7}$$

which shows the expected Lorentz contraction.

The total energy E of the bag

$$E = E_q + E_G + BV \tag{8}$$

is the sum of the quark energy E_q, the gluon field energy E_G, and the volume energy of the bag, BV. Because the quarks at the ends move with the a speed close to the speed of light, their energy is simply given by

$$E_q = 2p, \tag{9}$$

where p is the momentum of a quark, a diquark, or an antiquark, respectively. By analogy with electrodynamics, Eqs. (3)–(5) yield

$$E_G = \frac{1}{2}\int d^3x \sum_{\alpha=1}^{8}(E_\alpha^2 + B_\alpha^2) = \\ = \sqrt{\frac{2}{3}}\, g\sqrt{B}\, L \int_0^1 dv \frac{1+v^2}{\sqrt{1-v^2}} = \sqrt{\frac{2}{3}}\, g\sqrt{B}\, L\frac{3\pi}{4} \tag{10}$$

for the gluon energy and

$$BV = 2B\int_0^{\frac{L}{2}} A(r)\; dr = \\ = 2B\int_0^1 \sqrt{\frac{2}{3B}}\, g\sqrt{1-v^2}\,\frac{L}{2}\, dv = \\ = \sqrt{\frac{2}{3}}\, g\sqrt{B} L\frac{\pi}{4} = \frac{BA(0)L\pi}{4} \tag{11}$$

for the volume energy. It is obvious from Eq. (10) that the gluon field energy is proportional to the length L of the bag. The gluon field energy and the volume energy of the bag together correspond to a linear rising potential of the form

$$V(L) = E_G + BV = bL, \tag{12}$$

where

$$b = \sqrt{\frac{2B}{3}}\, g\pi. \tag{13}$$

The total angular momentum J of this classical bag is the sum of the angular momenta of the quarks at the two ends

$$J_q = pL \tag{14}$$

and the angular momentum J_G of the gluon field. From Eq. (4), we get

$$\mathbf{E}_\alpha \times \mathbf{B}_\alpha = \mathbf{v}E_\alpha^2, \tag{15}$$

for the momentum of the gluon field. Hence,

$$J_G = \left| \int\limits_{\text{bag}} d^3\mathbf{r} \sum_{\alpha=1}^{8} \mathbf{r} \times (\mathbf{E}_\alpha \times \mathbf{B}_\alpha) \right| = \\ = 2\int\limits_0^{\frac{L}{2}} dr A(r) r v E_\alpha^2 = \frac{16}{3L} g^2 \int\limits_0^{\frac{L}{2}} \frac{r^2 dr}{A(r)} = \sqrt{\frac{2}{3}} g\sqrt{B} L^2 \frac{\pi}{4}, \tag{16}$$

where we have used Eq. (1) and Eq. (3) in the third step. We can now express the total energy of the bag in terms of angular momenta. Putting these results back into the formulae for E_q and E_G, we arrive at

$$E_q = \frac{2J_q}{L}, \quad E_G = \frac{3J_G}{L}, \tag{17}$$

so that the bag energy now becomes

$$E = \frac{2J_q}{L} + \frac{3J_G}{L} + \sqrt{\frac{2B}{3}} Lg\frac{\pi}{L} = \\ = \frac{2J_q + 4J_G}{L} = \frac{2(J + J_G)}{L} = \\ = \frac{1}{L}\left(2J + \sqrt{\frac{2}{3}} g\sqrt{B} L^2 \frac{\pi}{2}\right). \tag{18}$$

Minimizing the total energy for a fixed angular momentum with respect to the length of the bag, $\frac{\partial E}{\partial L} = 0$ gives the relation

$$-\frac{2J}{L^2} + \sqrt{\frac{2}{3}} g\sqrt{B}\frac{\pi}{2} = 0 \tag{19}$$

so that

$$L^2 = \frac{4J}{g\pi}\sqrt{\frac{3}{2B}}. \tag{20}$$

Re-inserting this into Eq. (18), we arrive at

$$E = 2\sqrt{Jg\pi}\left(\frac{2B}{3}\right)^{\frac{1}{4}}, \tag{21}$$

or

$$J = \left(\sqrt{\frac{3}{2B}}\frac{1}{4\pi g}\right) E^2 = \\ = \left(\sqrt{\frac{3}{2B}}\frac{1}{8\pi^{\frac{3}{2}}}\frac{1}{\sqrt{\alpha_s}}\right) E^2 = \alpha'(0) M^2, \tag{22}$$

where $M = E$, and $\alpha_s = \frac{g^2}{4\pi}$ is the unrationalized color gluon coupling constant. We can now let $\alpha'(0)$ defined by the last equation, which is the slope of the Regge trajectory, be expressed as

$$\alpha'(0) = \sqrt{\frac{3}{2B}}\frac{1}{8\pi^{\frac{3}{2}}}\frac{1}{\sqrt{\alpha_s}} = \frac{1}{4b}, \tag{23}$$

where b was defined in Eq. (12).

The parameters B and α_s have been determined [9, 10] using the experimental information from the low lying hadron states: $B^{\frac{1}{4}} = 0.146$ GeV and $\alpha_s = 0.55$ GeV. If we use these values in Eq. (23), we find

$$\alpha'(0) = 0.88 \ (\text{GeV})^{-2} \tag{24}$$

in the remarkable agreement with the slope determined from experimental data, which is about $0.9\ (\text{GeV})^{-2}$.

Then the total phenomenological non-relativistic potential is the well-known superposition of the Coulomb-like and confining potentials $V(r) = \frac{a}{r} + br$, where $r = |\mathbf{r}_1 - \mathbf{r}_2|$ is the distance between q and $\bar{q}$ in a meson or between q and D in a baryon with high angular momentum. This was verified in lattice QCD to a high degree of accuracy [11] ($a = \frac{-c\alpha_c}{r}$, where

c is the color factor, and α_c is the strong coupling strength).

It is interesting to know that all this is related very closely to the dual strings. Indeed, we can show that the slope given in Eq. (23) is equivalent to the dual string model formula for the slope, if we associate the "proper tension" in the string with the proper energy per unit length of the color flux tube and the volume. By the proper energy per unit length, we mean the energy per unit length at a point in the bag evaluated in the rest system of that point. This will be

$$T_0 = \frac{1}{2}\sum_\alpha E_\alpha^2 A_0 + BA_0. \tag{25}$$

The relation $\frac{1}{2}\sum_\alpha E_\alpha^2 = B$ in the rest system gives

$$T_0 = 2BA_0, \tag{26}$$

where A_0 is the cross-sectional area of the bag. Let $A = A_0$ in Eq. (7), when $v = 0$. Then, using

$$A_0 = \sqrt{\frac{2}{3B}}\, g, \tag{27}$$

we find

$$T_0 = 2\sqrt{\frac{2}{3}}\, g\sqrt{B} = 4\sqrt{\frac{2\pi}{3}}\,\sqrt{\alpha_s}\sqrt{B} \tag{28}$$

for the proper tension. In the dual string, the slope and the proper tension are related by the formula [12]

$$T_0 = \frac{1}{2\pi\alpha'}, \tag{29}$$

so that the slope is

$$\alpha' = \frac{1}{8}\sqrt{\frac{3}{2}}\,\frac{1}{\pi^{\frac{3}{2}}}\,\frac{1}{\sqrt{\alpha_s}}\,\frac{1}{\sqrt{B}}, \tag{30}$$

which is identical to the earlier formula we produced in Eq. (23).

It would appear from Eq. (28) that the ratio of volume to field energy would be one-to-one in one space dimension in contrast to the result one-to-three, which holds for a three-dimensional bag [13]. However, the ratio one-to-one is true only in the rest system at a point in the bag, and each position along the x-axis is, of course, moving with a different velocity. Indeed, we see from Eq. (10) and Eq. (11) that the ratio of the total volume energy to the total field energy is given by one-to-three in conformity with the virial theorem [13].

In the string model of hadrons, we have $E^2 \sim J$ between the energy and the angular momentum of the rotating string. If we denote, by $\rho(r)$, the mass density of a string, and, by v and ω, its linear and angular velocities, respectively, the energy and the angular momentum of the rotating string are given by

$$E = 2\int \frac{\rho(r)}{\sqrt{1-\omega^2 r^2}}\,dr = \frac{2}{\omega}\int_0^1 \frac{\rho(v)}{\sqrt{1-v^2}}dv \tag{31}$$

and

$$J = 2\int \frac{\rho(r)}{\sqrt{1-\omega^2 r^2}}\,r^2\omega dr = \frac{2}{\omega^2}\int_0^1 \frac{\rho(v)}{\sqrt{1-v^2}}v^2 dv. \tag{32}$$

Hence, the relation

$$E^2 \propto J \tag{33}$$

holds. If the string is loaded with mass points at its ends, they no longer move with the speed of light. However, the above relation still holds approximately for the total energy and angular momentum of the loaded string.

We now look at various ways of the partitioning of the total angular momentum into two subsystems. Figures a, b, and c show the possible configurations of three quarks in a baryon. If we put the proportionality constant in Eq. (33) equal to unity, then the naive evaluation of energies yield

$$E^2 = J_1 + J_2 = E_1^2 + E_2^2 \le (E_1 + E_2)^2 = E'^2, \tag{34}$$

where E and E' denote the energies corresponding to Figures a or c. In the case of Figure b, J_1 and J_2 are the angular momenta corresponding to the energies E_1 and E_2 of the subsystems. The equality in Eq. (34) holds, only if E_1 or E_2 is zero. Therefore, for each fixed total angular momentum, its most unfair partition into two subsystems gives us the lowest energy levels, and its more or less fair partition gives rise to energy levels on daughter trajectories. Hence, on the leading baryonic trajectory, we have a quark-diquark structure (Fig. a) or a linear molecule structure (Fig. c). On the other hand, on low-lying trajectories, we have more or less symmetric ($J_1 \sim J_2$) configuration of quarks.

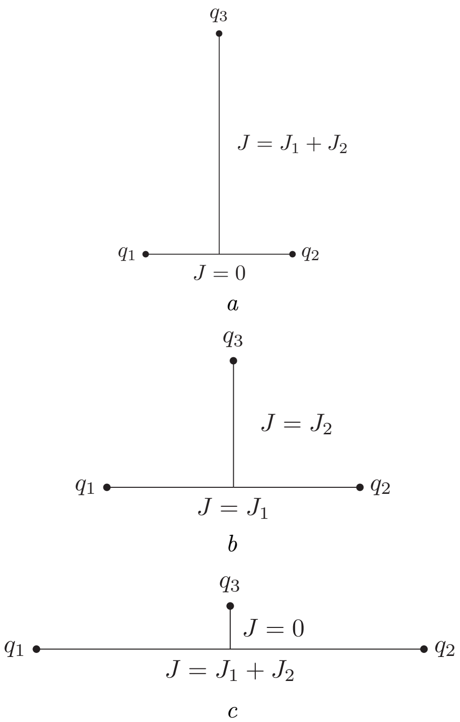

Since the high-J hadronic states on leading Regge trajectories tend to be bilocal with large separation of their constituents, they fulfill all the conditions for supersymmetry between $\bar{q}$ and D. Then the only difference between the energies of $(q\bar{q})$ mesons and (qD) baryons comes from the different masses of their constituents, namely, $m_q = m_{\bar{q}} = m$, and $m_D \sim 2m$. For high J, this is the main source of symmetry breaking, which is spin-independent. We will show how we can obtain sum rules from this breaking. The part of the mass operator that gives rise to this splitting is a diagonal element of U(6/21) that commutes with SU(6).

Let us now consider the spin-dependent breaking of SU(6/21). For low J states, the (qD) system becomes trilocal(qqq), and the flux tube degenerates to a single gluon propagator that gives spin-dependent forces in addition to the Coulomb term $\frac{a}{r}$. In this case, we have the regime studied by de Rujula, Georgi, and Glashow, where the breaking is due to the hyperfine splitting caused by the exchange of single gluons that have spin 1. These mass splittings give rise to different intercepts of the Regge trajectories given by

$$\Delta m_{12} = k\frac{\mathbf{S}_1\,\mathbf{S}_2}{m_1 m_2}, \quad k = |\psi(0)|^2, \tag{35}$$

both for baryons and mesons at high energies. But, at low energies, the baryon becomes a trilocal object (with three quarks), and the mass splitting is given by

$$\Delta m_{123} = \frac{1}{2}k\left(\frac{\mathbf{S_1}\,\mathbf{S_2}}{m_1 m_2} + \frac{\mathbf{S}_2\,\mathbf{S}_3}{m_2 m_3} + \frac{\mathbf{S}_3\,\mathbf{S}_1}{m_3 m_1}\right), \tag{36}$$

where m_1, m_2, and m_3 are the masses of the three different quark constituents.

The element of SU(6/21) that gives rise to such splittings is a diagonal element of its U(21) subgroup and gives rise to $s(s+1)$ terms that behave like an element of the (405) representation of SU(6) in the SU(6) mass formulae. The splitting of isospin multiplets is due to a symmetry breaking element in the (35) representation of SU(6). Hence, all symmetry breaking terms are in the adjoint representation of SU(6/21). If we restrict ourselves to the non-strange sector of hadrons with approximate SU(4) symmetry, the effective supersymmetry will relate the splitting in m^2 between Δ $(s = \frac{3}{2}, I = \frac{3}{2})$, and N $(s = \frac{1}{2}, I = \frac{1}{2})$ to the splitting between ω $(s = 1, I = 0)$ and π $(s = 0, I = 1)$, so that

$$m_\Delta^2 - m_N^2 = m_\omega^2 - m_\pi^2, \tag{37}$$

which is satisfied to within 5%. Our potential model gives a more accurate symmetry breaking

$$\frac{9}{8}(m_\Delta^2 - m_N^2) = m_\omega^2 - m_\pi^2 \tag{38}$$

to within 1%, where the $\frac{8}{9}$ arises from $\frac{1}{2}(\frac{4}{3}\alpha_s)^2 = \frac{8}{9}\alpha_s^2$. For a classification of supergroups including SU(m/n), we refer to the paper by Viktor Kac [14].

3. Conclusions and Future Prospects

Effective Hamiltonians and new mass relations including quark and diquark masses were worked out in our previous works that included the complete understanding of hadronic color algebras as well. In the case of heavy quarks, one can also use the non-relativistic approximation, so that the potential models for the spectrum of charmonium and the $b\bar{b}$ system can be worked out. In such an approach, gluons can be eliminated leaving quarks interacting through potentials.

It is also possible to take an opposite approach by eliminating quarks as well as gluons, leaving only an effective theory that involves mesons and baryons as collective excitations (solitons) in a way by Skyrme. A Skyrme model that can compete with the potential model is not yet realized.

It is a pleasure to acknowledge helpful conversations with Professors Vladimir Akulov, Cestmir Burdik, and Francesco Iachello.

The work is supported in part by DOE contracts Nos. DE-AC-0276-ER 03074 and 03075; NSF Grant No. DMS-8917754; and several PSC-CUNY research grants.

1. H. Miyazawa. Baryon number changing currents. *Prog. Theor. Phys.* **36**, 1266 (1966); Spinor currents and symmetries of baryons and mesons. *Phys. Rev.* **170**, 1586 (1968).
2. S. Catto, F. Gürsey. New realizations of hadronic supersymmetry. *Nuovo Cimento A* **99**, 685 (1988).
3. S. Catto, F. Gürsey. Algebraic treatment of effective supersymmetry. *Nuovo Cimento A* **86**, 201 (1985).
4. K.N. Wilson. Confinement of quarks. *Phys. Rev. D* **10**, 2445 (1974).
5. R.L. Jaffe. Multiquark hadrons. II. Methods. *Phys. Rev. D* **15**, 281 (1977).
6. S. Catto. Exceptional projective geometries and internal symmetries. ArXiv: Hep-th/0302079.
7. G. 't Hooft. A planar diagram theory for strong interactions. *Nucl. Phys. B* **72**, 461 (1974).
8. K. Johnson, C.B. Thorn. Stringlike solutions of the bag model. *Phys. Rev. D* **13**, 1934 (1976).
9. A. Chodos, R.L. Jaffe, K. Johnson, C.B. Thorn. Baryon structure in the bag theory. *Phys. Rev. D* **10**, 2599 (1974).
10. T. De Grand, R.L. Jaffe, K. Johnson, J. Kiskis. Masses and other parameters of the light hadrons. *Phys. Rev. D* **12**, 2060 (1975).
11. S.W. Otto, J.D. Stark. SU(3) heavy-quark potential with high statistics. *Phys. Rev. Lett.* **52**, 2328 (1984).
12. P. Goddard, J. Goldstone, C. Rebbi, C.B. Thorn. Quantum dynamics of a massless relativistic string. *Nucl. Phys. B* **56**, 109 (1973).
13. A. Chodos *et al.* New extended model of hadrons. *Phys. Rev. D* **9**, 3471 (1974).
14. V.G. Kac. A sketch of Lie superalgebra theory. *Comm. Math. Phys.* **53**, 31 (1977).

Received 08.07.19

С. Катто, І. Гюркан,
Ф. Хальфан, Д. Курт, Б. Ніколеску, Е. Ю

ГАДРОННА СУПЕРСИМЕТРІЯ З КХД

Р е з ю м е

Запропоновано модифікацію масових формул для гадронів, з наголосом на теоретико-груповий опис і суперсиметрію, яка відповідає КХД і базується на кварк-антикварковій симетрії, із подальшими коментарями щодо можливих застосувань до моделей типу Скірма, які в майбутньому можуть конкурувати з потенціальними кварковими моделями.

https://doi.org/10.15407/ujpe64.8.678

V.S. FADIN[1,2]

[1] G.I. Budker Institute of Nuclear Physics of SD RAS
(630090 Novosibirsk Russia; e-mail: fadin@inp.nsk.su)
[2] Novosibirsk State University
(630090 Novosibirsk, Russia; e-mail: fadin@inp.nsk.su)

REGGE CUTS AND NNLLA BFKL

In the leading and next-to-leading logarithmic approximations, QCD amplitudes with gluon quantum numbers in cross-channels and negative signature have the pole form corresponding to a reggeized gluon. The famous BFKL equation was derived using this form. In the next-to-next-to-leading approximation (NNLLA), the pole form is violated by contributions of Regge cuts. We discuss these contributions and their impact on the derivation of the BFKL equation in the NNLLA.

K e y w o r d s: gluon Reggeization, BFKL equation, Regge cuts.

1. Introduction

The equation, which is called now BFKL (Balitskii–Fadin–Kuraev–Lipatov), was first derived in non-Abelian gauge theories with spontaneously broken symmetry [1–3]. Then its applicability to QCD was shown in [4]. The derivation of the equation was based on the Reggeization of gauge bosons in non-Abelian gauge theories (gluons in QCD). The Reggeization determines the high-energy behavior of cross-sections non-decreasing, as the energy increases. In the Regge and multi-Regge kinematics in each order of perturbation theory, dominant (having the largest $\ln s$ degrees) are the amplitudes with gluon quantum numbers and negative signatures in cross-channels. They determine the s-channel discontinuites of amplitudes with the same and all other possible quantum numbers.

It is extremely important that, both in the leading logarithmic approximation (LLA) and in the next-to-leading one (NLLA), the amplitudes used in the unitarity relations are determined by the Regge pole contributions and have a simple factorized form (pole Regge form). Due to this, the Reggeization provides a simple derivation of the BFKL equation in the LLA and in the NLLA. The s-channel discontinuities are presented by Fig. 1 and symbolically can be written as $\Phi_{A'A} \otimes G \otimes \Phi_{B'B}$, where the impact factors $\Phi_{A'A}$ and $\Phi_{B'B}$ describe the transitions $A \to A'$ and $B \to B'$, G is Green's function for two interacting Reggeized gluons, $\hat{\mathcal{G}} = e^{Y\hat{\mathcal{K}}}$, $Y = \ln(s/s_0)$, $\hat{\mathcal{K}}$ is the universal (process-independent) BFKL kernel, which determines the energy dependence of scattering amplitudes and is expressed through the gluon trajectory and the Reggeon vertices. Validity of the pole Regge form is proved now in all orders of perturbation theory in the coupling constant g both in the LLA [5], and in the NLLA (see [6, 7] and references therein).

The first observation of the violation of the pole Regge form was done [8] in the high-energy limit of the results of direct two-loop calculations of the two-loop amplitudes for gg, gq, and qq scattering. Then the terms breaking the pole Regge form in two- and three-loop amplitudes of the elastic scattering were found in [9–11] using the techniques of infrared factorization.

It is worth to say that, in general, the breaking of the pole Regge form is not a surprise. It is well known that Regge poles in the complex angular momenta plane generate Regge cuts. Moreover, in amplitudes with positive signature, the Regge cuts appear already in the LLA. In particular, the BFKL Pomeron is the two-Reggeon cut in the complex angular momenta plane. But, in amplitudes with negative signature due to the signature conservation, a cut must be at least three-Reggeon one and can appear only in the NNLLA. It is natural to expect that the observed violation of the pole Regge form can be explained by their contributions.

Indeed, all known cases of breaking the pole Regge form are now explained by the three-Reggeon cuts

[12, 13]. Unfortunately, the approaches used and the explanations given in these papers are different. Their results coincide in the three-loop approach, but may diverge for more loops. It requires a further investigation.

Here, we consider the contributions of a three-Reggeon cut to the amplitudes of elastic scattering of partons (quarks and gluons) with negative signature up to four loops.

2. Three-Reggeon Cut

Since our Reggeon is the Reggeized gluon, the three-Reggeon cut first contributes to the amplitudes corresponding to the diagrams shown in Fig. 2. In contrast to the Reggeon which contribute only to amplitudes with the adjoint representation of the color group (color octet in QCD) in the t-channel, the cut can contribute to various representations. Possible representations for the quark-quark and quark-gluon scatterings are only singlet (**1**) and octet (**8**), whereas, for the gluon-gluon scattering, there are also **10**, **10***, and **27**. The account for the Bose statistics for gluons, symmetry of the representations **1** and **27**, antisymmetry **10** and **10***, and the existence of both symmetric $\mathbf{8_s}$ and antisymmetric $\mathbf{8_a}$ representations for them, gives that, in addition to the Reggeon channel, the amplitudes with negative signature are in the representations **1** for the quark-quark-scattering and in the representation **10** and **10*** for the gluon-gluon scattering. The amplitude of the process $\mathcal{A}_{AB}^{A'B'}$ depicted by the diagrams in Fig. 2 can be written as the sum over the permutations σ of products of color factors and color-independent matrix elements:

$$\mathcal{A}_{AB}^{A'B'} = \sum_{\sigma} \left(C_{AB}^{(0)\sigma}\right)^{\alpha\beta}_{\alpha'\beta'} M_{AB}^{(0)\sigma}(s,t), \qquad (1)$$

where α and β (α' and β') are the color indices of an incoming (outgoing) projectile A and a target B, respectively. We use the same letters for the quark and gluon color indices; it should be remembered, however, that there is no difference between upper and lower indices (running from 1 to N_c^2-1) for gluons, whereas, for quarks, lower and upper indices (running from 1 to N_c) refer to mutually related representations.

The color factors can be decomposed into irreducible representations $\mathcal{R}$ of the color group in the

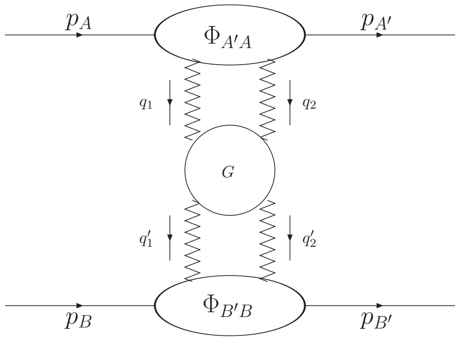

Fig. 1. Schematic representation of the s-channel discontinuities of amplitudes $A + B \to A' + B'$

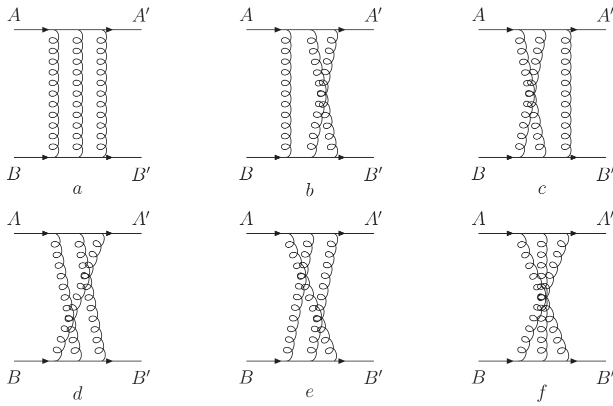

Fig. 2. Feynman diagrams of the process $A + B \to A' + B'$ with three-gluon exchanges

t-channel:

$$\left(C_{AB}^{(0)\sigma}\right)^{\alpha\beta}_{\alpha'\beta'} = \sum_{R} [\mathcal{P}_{AB}^{R}]^{\alpha\beta}_{\alpha'\beta'} \sum_{\sigma} \mathcal{G}(R)_{AB}^{(0)\sigma}, \qquad (2)$$

where

$$[\mathcal{P}_{AB}^{R}]^{\alpha\beta}_{\alpha'\beta'} = \sum_{n} [\mathcal{P}_{A}^{R,n}]^{\alpha}{}_{\alpha'} [\mathcal{P}_{B}^{R,n}]^{\beta}{}_{\beta'}, \qquad (3)$$

$\hat{\mathcal{P}}^{R,n}$ is the projection operator on the state n in the representation $\mathcal{R}$,

$$\mathcal{G}(R)_{AB}^{(0)\sigma} = \frac{1}{N_R\, T_A\, T_B} \left(\mathcal{T}_A^{c_1}\mathcal{T}_A^{c_2}\mathcal{T}_A^{c_3}\right)^{\alpha'}_{\alpha} \times$$
$$\times \left(\mathcal{T}_B^{c_1^\sigma}\mathcal{T}_B^{c_2^\sigma}\mathcal{T}_B^{c_3^\sigma}\right)^{\beta'}_{\beta} [\mathcal{P}_{AB}^{R}]^{\alpha\beta}_{\alpha'\beta'}, \qquad (4)$$

N_R is the dimension of the representation R, $\mathcal{T}^a$ are the color group generators in the corresponding representations, $[\mathcal{T}^a, \mathcal{T}^b] = if_{abc}\mathcal{T}^c$; $(\mathcal{T}^a)^{\alpha'}_{\alpha} = -if_{\alpha'\alpha}$ for

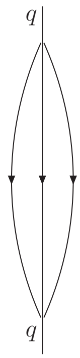

Fig. 3. Schematic representation of $A_2(q_\perp)$

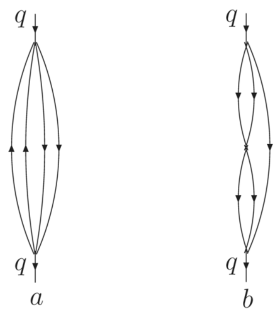

Fig. 4. Schematic representation of $A_3^a(q_\perp)$ and $A_3^b(q_\perp)$

gluons and $(\mathcal{T}^a)_\alpha^{\alpha'} = (t^a)_\alpha^{\alpha'}$ for quarks; $\mathrm{Tr}(\mathcal{T}_i^a \mathcal{T}_i^b) = T_i\delta_{ab}$, $T_q = 1/2$, $T_g = N_c$.

In [12] the Reggeon channel (R=8) was considered. It was discovered that that the terms violating the pole factorization in $\mathcal{G}(8)_{AB}^{(0)\sigma}$ do not depend on σ (let us call them $\mathcal{G}(8)_{AB}^{(0)}$), so that the momentum-dependent factors for them are summed up to the eikonal amplitude

$$\sum_\sigma M_{AB}^{(0)\sigma} = A^{eik} = g^6 \frac{s}{t}\left(\frac{-4\pi^2}{3}\right)\mathbf{q}^{\,2} A_2(q_\perp), \tag{5}$$

where $A_2(q_\perp)$ is depicted by the diagram presented in Fig. 3 and is written as

$$A_2(q_\perp) = \int \frac{d^{2+2\epsilon}l_1 d^{2+2\epsilon}l_2}{(2\pi)^{2(3+2\epsilon)}\mathbf{l}_1^2\mathbf{l}_2^2(\mathbf{q}-\mathbf{l}_1-\mathbf{l}_2)^2}. \tag{6}$$

Note that we use the "infrared" ϵ, $\epsilon = (D-4)/2$, D is the space-time dimension.

This result is very important, because the contribution of the cut must be gauge-invariant, whereas $M_{AB}^{(0)\sigma}$ taken separately are gauge-dependent.

In [14], other channels with possible cut contributions were considered. It was shown that, for them, the color coefficients $\mathcal{G}(R)_{AB}^{(0)\sigma}$ do not depend on σ,

$$\mathcal{G}(10+\bar{1}0)_{gg}^{(0)} = \frac{-3}{4}N_c,\ \ \mathcal{G}(1)_{qq}^{(0)} = \frac{(N_c^2-4)(N_c^2-1)}{16N_c^3}, \tag{7}$$

so that the momentum-dependent factors for them are also summed up to the eikonal amplitude (5).

The separation of the pole and cut contributions in the octet channel is impossible in the two-loop approximation, because of the ambiguity of the allocation of parts of the amplitudes violating the factorization. The separation becomes possible for higher loops, due to the different energy dependences of the pole and cut contributions. The energy dependence of the pole contribution is determined by the Regge factor of a Reggeized gluon $\exp(\omega(t)\ln s)$, where $\omega(t)$ is the gluon trajectory, whereas, for the three-Reggeon cut, it is

$$e^{[(\hat\omega_1+\hat\omega_2+\hat\omega_3+\hat{\mathcal{K}}_r(1,2)+\hat{\mathcal{K}}_r(1,3)+\hat{\mathcal{K}}_r(2,3))\ln s]}, \tag{8}$$

where $\hat{\mathcal{K}}_r(m,n)$ is the real part of the BFKL kernel describing the interaction between Reggeons m and n.

The calculations of the first logarithmic correction to the cut contribution in the octet channel was performed in [12, 14, 15] and, in the other channels, in [14]. In the latter case, the correction is

$$\mathcal{G}(10+\bar{1}0)_{gg}^{(0)}\ g^6\frac{s}{t}\left(\frac{-4\pi^2}{3}\right)\mathbf{q}^{\,2}g^2N_c\times$$
$$\times\ln s\left(-\frac{1}{2}A_3^a(q_\perp)-\frac{1}{2}A_3^b(q_\perp)\right), \tag{9}$$

$$\mathcal{G}(1)_{qq}^{(0)}\ g^6\frac{s}{t}\left(\frac{-4\pi^2}{3}\right)\mathbf{q}^{\,2}g^2N_c\times$$
$$\times\ln s\left(\frac{3}{2}A_3^a(q_\perp)-\frac{3}{2}A_3^b(q_\perp)\right), \tag{10}$$

and in the first case as

$$\mathcal{G}(8)_{AB}^{(0)}\ g^6\frac{s}{t}\left(\frac{-4\pi^2}{3}\right)\mathbf{q}^{\,2}g^2N_c\times$$
$$\times\ln s\left(\frac{1}{2}A_3^a(q_\perp)-A_3^b(q_\perp)\right), \tag{11}$$

where $A_3^a(q_\perp)$ and $A_3^b(q_\perp)$ are depicted by the diagrams presented in Figs. 4, a and 4, b, respectively,

$$A_3^a(q_\perp) = \int \frac{d^{2+2\epsilon}l_1\, d^{2+2\epsilon}l_2 d^{2+2\epsilon}l_3}{(2\pi)^{3(3+2\epsilon)}\mathbf{l}_1^2\mathbf{l}_2^2\mathbf{l}_3^2(\mathbf{q}-\mathbf{l}_1-\mathbf{l}_2-\mathbf{l}_3)^2}, \tag{12}$$

$$A_3^b(q_\perp) = \\ = \int \frac{d^{2+2\epsilon}l_1\, d^{2+2\epsilon}l_2 d^{2+2\epsilon}l_3 (\mathbf{q}-l_1)^2}{(2\pi)^{3(3+2\epsilon)}\mathbf{l}_1^2\mathbf{l}_2^2\mathbf{l}_3^2(\mathbf{q}-\mathbf{l}_1-\mathbf{l}_2)^2(\mathbf{q}-\mathbf{l}_1-\mathbf{l}_3)^2}. \tag{13}$$

It was shown in [12, 14, 15] that the violation of the pole Regge form, analyzed in this approximation in [9]–[11] with the help of the infrared factorization, can be explained by the pole and cut contributions. In other words, the restrictions imposed by the infrared factorization on the parton scattering amplitudes with the adjoint representation of the color group in the t-channel and negative signature can be fulfilled in the NNLLA with two and three loops, if, in addition to the Regge pole contribution, there is the Regge cut contribution. It should be noted that this result is limited to three loops and cannot be considered as a proof that, in the NNLLA, the only singularities in the J plane are the Regge pole and the three-Reggeon cut. Moreover, the explanation of the violation of the pole Regge form given in [13] differs from that described above. In this paper, in addition to the cut with the vertex of interaction with particles i having the color structure

$$(C^{(0)c})^{\alpha}_{\alpha'} = (\mathcal{T}^c)^{\alpha}_{\alpha'}\frac{1}{3!}\,\mathrm{Tr}\sum_\sigma \Big(\mathcal{T}_i^{c_1^\sigma}\mathcal{T}_i^{c_2^\sigma}\mathcal{T}_i^{c_3^\sigma}\mathcal{T}_i^{c}\Big), \tag{14}$$

the Reggeon-cut mixing is introduced. Actually, in the three-loop approximation, the mixing is not required.

Whether the mixing is necessary can be verified in the four-loop approximation.

The four-loop calculations should answer the questions whether the existence of a pole and a cut is sufficient in this approximation, with or without mixing.

In the four-loop approximation, there are three types of corrections. The first (simplest) ones come from the account for the Regge factors of each of three Reggeons. The second type of the corrections is given by the products of the trajectories and real parts of the BFKL kernels, and the third one comes from the account for Reggeon–Reggeon interactions. All types of corrections are expressed through the integrals over the transverse momentum space corresponding to the diagrams in Fig. 5:

$$I_i = \int \frac{d^{2+2\epsilon}l_1\, d^{2+2\epsilon}l_2\, d^{2+2\epsilon}l_3}{(2\pi)^{3(3+2\epsilon)}\mathbf{l}_1^2\mathbf{l}_2^2\mathbf{l}_3^2}F_i\delta^{2+2\epsilon}(\mathbf{q}-\mathbf{l}_1-\mathbf{l}_2-\mathbf{l}_3), \tag{15}$$

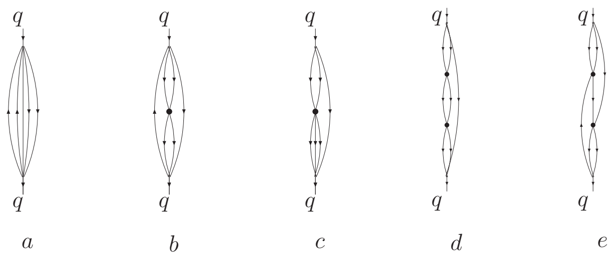

Fig. 5. Four-loop diagrams

$$F_a = f_1(\mathbf{l}_1)f_1(\mathbf{l}_2),\quad F_b = f_1(\mathbf{l}_1)f_1(\mathbf{l}_1),\quad F_c = f_2(\mathbf{l}_1+\mathbf{l}_2),$$
$$F_d = f_1(\mathbf{l}_1+\mathbf{l}_2)f_1(\mathbf{l}_1+\mathbf{l}_2),\quad F_e = f_1(\mathbf{q}-\mathbf{l}_1)f_1(\mathbf{q}-\mathbf{l}_3), \tag{16}$$

$$f_1(\mathbf{k}) = \mathbf{k}^{\,2}\int \frac{d^{2+2\epsilon}l}{(2\pi)^{(3+2\epsilon)}\mathbf{l}^{\,2}(\mathbf{l}-\mathbf{k})^2},$$
$$f_2(\mathbf{k}) = \int \frac{d^{2+2\epsilon}l f_1(\mathbf{l})}{(2\pi)^{(3+2\epsilon)}\mathbf{l}^{\,2}(\mathbf{l}-\mathbf{k})^2}. \tag{17}$$

These integrals enter the total four-loop correction with different color factors in the approaches with or without Reggeon-cut mixing. The question of whether the four-loop amplitudes of the elastic scattering in QCD are given by the Regge pole and cut contributions, with or without mixing, can be solved by comparing these corrections with the result obtained with the use of the infrared factorization.

3. Discussion

The gluon Reggeization is the basis of the BFKL approach. The BFKL equation was derived assuming the pole Regge form of amplitudes with gluon quantum numbers in cross channels and negative signature. It is proved now in all orders of perturbation theory that this form is valid both in the leading and in the next-to-leading logarithmic approximations. However, this form is violated in the NNLLA.

Currently, there are two evidences of the violation. First, it was discovered, using the results of direct calculations of parton (gg, gq and qq) scattering amplitudes in the two-loop approximation, that the non-logarithmic terms (the lowest terms of the NNLLA) do not agree with the pole Regge form of the amplitudes. Second, it was shown using the techniques of infrared factorization that there are single-logarithmic terms with three loops wihich can not be attributed to the Regge pole contribution.

It was shown that the observed violation can be explained by the three-Reggeon cuts [12, 13]. But the assertion that the QCD amplitudes with gluon quantum numbers in cross-channels and negative signature are given in the NNLLA by the contributions of the Regge pole and the three-Reggeon cut is only a hypotheses. Since there is no general proof of it, it should be checked in each order of perturbation theory. In addition, the approaches used and the explanations given in [12] and [13] are different. Their results coincide in the three-loop case but may diverge for more loops.

The calculations of the cut contributions presented here aim to prove this hypothesis in the four-loop case. Unfortunately, direct calculations in that order in the NNLLA do not exist, and there is no hope for that they will be done in the foreseeable future. But it seems possible to obtain the corresponding results using the infrared factorization. The comparison of the results should answer the questions whether the existence of a pole and a cut is sufficient with or without mixing.

Work supported in part by the Ministry of Science and Higher Education of the Russian Federation, in part by RFBR, grant 19-02-00690.

1. V.S. Fadin, E.A. Kuraev, L.N. Lipatov. On the Pomeranchuk singularity in asymptotically free theories. *Phys. Lett. B* **60**, 50 (1975).
2. E.A. Kuraev, L.N. Lipatov, V.S. Fadin. Multi-reggeon processes in the Yang–Mills theory. *Sov. Phys. JETP* **44**, 443 (1976).
3. E.A. Kuraev, L.N. Lipatov, V.S. Fadin. The Pomeranchuk singularity in non-Abelian gauge theories. *Sov. Phys. JETP* **45**, 199 (1977).
4. I.I. Balitsky, L.N. Lipatov. The Pomeranchuk singularity in quantum chromodynamics. *Sov. J. Nucl. Phys.* **28**, 822 (1978).
5. Ya.Ya. Balitskii, L.N. Lipatov, V.S. Fadin. Regge processes in non-Abelian gauge theories. In: *Materials of IV Winter School of LNPI* (1979), p. 109.
6. B.L. Ioffe, V.S. Fadin, L.N. Lipatov. *Quantum Chromodynamics: Perturbative and Nonperturbative Aspects* (Cambridge Univ. Press, 2010).
7. V.S. Fadin, M.G. Kozlov, A.V. Reznichenko. Gluon reggeization in Yang–Mills theories. *Phys. Rev. D.* **92**, 085044 (2015).
8. V. Del Duca, E.W.N. Glover. The high-energy limit of QCD at two loops. *JHEP* **0110** 035 (2001).
9. V. Del Duca, G. Falcioni, L. Magnea, L. Vernazza. High-energy QCD amplitudes at two loops and beyond. *Phys. Lett. B.* **732**, 233 (2014).
10. V. Del Duca, G. Falcioni, L. Magnea, L. Vernazza. Beyond reggeization for two- and three-loop QCD amplitudes. PoS RADCOR **2013**, 046 (2013).
11. V. Del Duca, G. Falcioni, L. Magnea, L. Vernazza. Analyzing high-energy factorization beyond next-to-leading logarithmic accuracy. *JHEP* **1502**, 029 (2015).
12. V.S. Fadin. Particularities of the NNLLA BFKL. *AIP Conf. Proc.* **1819**, 060003 (2017).
13. S. Caron-Huot, E. Gardi, L. Vernazza. Two-parton scattering in the high-energy limit. *JHEP* **1706**, 016 (2017).
14. V.S. Fadin. Violation of a simple factorized form of QCD amplitudes and Regge cuts. *PoS DIS* **2017**, 042 (2018).
15. V.S. Fadin, L.N. Lipatov. Reggeon cuts in QCD amplitudes with negative signature. *Eur. Phys. J. C* **78**, 439 (2018).

Received 08.07.19

В.С. Фадін

РЕДЖЕВСЬКІ РОЗРІЗИ
І BFKL У НАБЛИЖЕННІ NNLLA

Р е з ю м е

У головному та наступному логарифмічному наближеннях КХД амплітуди з глюонними квантовими числами в кросканалі та від'ємною сигнатурою мають полюсну форму, яка відповідає реджезованому глюону. За допомогою цієї форми виводиться знамените рівняння BFKL. В наближенні NNLLA полюсна форма порушена внесками реджевських розрізів. Ми обговорюємо ці внески та їх вплив на отримання рівняння BFKL у наближенні NNLLA.

https://doi.org/10.15407/ujpe64.8.683

I. GKIGKITZIS,[1] I. HARANAS,[2] E. CAVAN[2]

[1] NOVA, Department of Mathematics
(8333 Little River Turnpike, Annandale, VA 22003, USA; e-mail: igkigkitzis@nvcc.edu)
[2] Wilfrid Laurier University
(Waterloo, ON, Canada; e-mail: iharanas@wlu.ca, cava0920@mylaurier.ca)

BLACK HOLE TORSION EFFECT AND ITS RELATION TO INFORMATION

In order to study the effects of the torsion on the gravitation in space-time and its relation to information, we use the Schwarzschild metric, where the torsion is naturally introduced through the spin particle density. In the black hole scenario, we derive an analytic solution for the black hole gravitational radius with the spin included. Then we calculate its entropy in the cases of parallel and antiparallel spins. Moreover, four analytical solutions for the spin density as a function of the number of information are found. Using these solutions in the case of parallel spin, we obtain expressions for the Ricci scalar as a function of the information number N, and the cosmological constant λ is also revealed.

Keywords: gravitation, quantization, torsion, spin, black holes.

1. Introduction

A natural way to talk about spin effects in gravitation is through torsion. Its introduction becomes significant for the understanding of the last stage in the black hole evaporation. It could be the case of an evaporating black hole of mass M_H that disappears via an explosion burst, which can last for the time $t_p = 10^{-44}$ s, when it reaches a mass of the order of Planck's mass

$$m_p = \sqrt{\frac{\hbar c}{G}} = 10^{-15} \text{ s.} \tag{1}$$

If this happens, there might be three distinct possibilities for the fate of the evaporating black hole [3]: The black hole may evaporate completely leaving no residue, in which case it would give rise to a serious problem of quantum consistency. If the final state of evaporation leaves a naked singularity behind, then it might violate the cosmic censorship at the quantum level. If a stable remnant of the residue with approximately Planck's mass remains, the emission process might stop.

If somebody tries to quantize the gravitational field, he must know that the quantization has to be directed with the unique structure of the space-time itself. The quantization will also imply that somebody might try to discretize the space and, probably, the time. Progress in this direction will also be related to the introduction of a spin in the theory of general relativity. The general relativity (GR) is the simplest theory of gravity which agrees with all present-day data. A major recent success is the detection of the lensed emission near the event horizon in the center of M-87 supergiant elliptic galaxy in the constellation Virgo. All the data obtained are consistent with the presence of a central Kerr black hole, as predicted by the general theory of relativity [1]. Somebody might want to formulate a generalized theory of general relativity to compare GR with various theories that explain other physical interactions. As an example, we say that the electromagnetic forces, strong interactions, and weak interactions are described with the help of quantum relativistic fields interacting in a flat Minkowski space. Furthermore, the fields that represent the interactions are defined over the space-time. But, at the same time, they are distinguished from the space-time which, we must say, is not affected by them. On the other hand, the gravitational interactions can modify the space-time geometry, but they are not represented by a new field. They are just represented by their effect on the geometry of the space itself. Thus, we can say that most parts of the modern physics are successful in being described in a flat rigid space-time geometry. But a small fraction of the remaining physics, i.e., macroscopic gravitational physics, requires the use of a curved dynamical geometric background. To overcome this difficulty, somebody might try to extend the geometric principles of GR into microphysics in order to establish a direct comparison and possibly some connection between gravity and other interactions. In GR theory, the matter is represented by the energy-momentum tensor, which essentially gives description of the mass density distribution in space-time. Therefore, the idea of mass-energy in GR is enough to define the properties of classical macroscopic bodies.

Looking at the microscopic level, we know that the matter is composed of elementary particles that obey the laws of special relativity and quantum mechanics. Each particle is characterized not only by its mass, but also by a spin measured in units of $\hbar$. At the microscopic level, the mass and the spin are two independent quantities. The mass distributions in space-time are described by the energy-momentum tensor, whereas the spin distribution is described, in field theory, by the spin density tensor. Inside any microscopic body, the spins of elementary particles are, in general, randomly oriented with the total average spin equal to zero. Therefore, the spin density tensor of a macroscopic body is zero. This explains why the energy-momentum tensor is adequate to dynamically characterize a macroscopic matter. Thus, the gravitational interactions can be sufficiently described by the Riemannian geometry. Another point that should be stressed is that the spin density tensor represents the intrinsic angular momentum of particles, and not the classical orbital angular momentum due to the macroscopic rotation. A fundamental difference is that the latter can be eliminated by an appropriate coordinate transformation. On the other hand, the spin density can be eliminated at a point only. The spin density tensor is a non-vanishing quantity, if the spins inside a body are oriented at least partially along a preferred direction and, at the same time, are not affected by the rotation of the macroscopic body. At the macroscopic level, the energy-momentum tensor is not enough to characterize the dynamics of the matter sources, because the spin density tensor is also needed, unless we are considering scalar fields that correspond to spineless particles. In the case where GR must be extended to include microphysics, the matter must be considered and described, by using the mass and the spin density. On the other hand, the mass is related to a curvature in a generalized theory of GR, and the spin should be related to the spin density tensor or, probably, to a different property of the space-time. The geometric property of the space-time in relation to spin in the U4 theory is the torsion.

The torsion, thus, can be described by the antisymmetric part of Christoffel symbols of the second kind. Therefore, the torsion tensor reads [5]:

$$Q^{\mu}_{\nu\lambda} = \frac{1}{2}\left(\Gamma^{\mu}_{\nu\lambda} - \Gamma^{\mu}_{\lambda\nu}\right) = \Gamma^{\mu}_{[\nu\lambda]}. \tag{2}$$

The torsion is characterized by a third-rank tensor that is antisymmetric in the first two indices and has 24 independent components. If the torsion does not vanish, the affine connection is not coincident with the Christoffel connection. Therefore, the geometry is not any longer the Riemannian, but rather Riemann–Cartan space-time with a non-symmetric connection. To introduce the torsion simply represents a very natural way of modifying GR. The relation of the torsion and the spin allows one to modify the GR theory and Riemannian geometry resulting in a more natural and complete description of the matter at the microscopical level as well. Finally, the early Universe is the place, where GR must be applied together with quantum theory. On the other hand, GR is a classical field theory. So far, the quantization of the gravity has been a problem in our effort to develop a consistent and coherent theory in understanding the physics of the early Universe.

In the presence of a torsion, the space-time is called a Riemann–Cartan manifold and is denoted by U4. When the torsion is taken into consideration, one can define distances in the following way. Supposing that we consider a small close circuit, we can write [5] the non-closure property given by the integral:

$$\ell^{\mu} = \oint Q^{\mu}_{\nu\lambda} dx^{\nu} \wedge dx^{\mu} \neq 0, \tag{3}$$

where $dx^{\nu}dx^{\mu}$ is the area element enclosed by the loop, ι^{μ} represents the so-called closure failure, and the torsion tensor $Q^{\mu}_{\nu\lambda}$ is a true tensorial quantity. In other words, the geometric meaning of the torsion can be represented by the failure of the loop closure. It has now the dimension of length, andn the torsion tensor itself has the dimension of L^{-1} .

2. Quantum Gravity and Torsion

The inclusion of the torsion into GR might constitute a way to the quantization of gravity, by considering the effect of the spin and connecting the torsion to the defects in the topology of space-time. For that, we can define a minimal unit of length l, as well as a minimal unit of time t. In GR and quantum field theory, there are now, indeed, difficulties due to the existence of infinities and singularities. One of the reasons is the consideration of point mass particles, which results in the divergence of the energy integrals going to infinity. In the case of collapsing bodies in GR, we have singularities. All these difficulties can disappear, if, together with the introduction of a torsion, we introduce the minimal time and length or, in other words, if we consider a discretized space-time. If we want to quantize the gravity, we cannot exactly follow the same procedure of quantization used in other fields. Indeed, the gravity is not a force, but the curvature and torsion of the space-time. The inclusion of the torsion in the space-time gives rise to space-time topology defects. The problem may be avoided, if the torsion is included. In this case, the asymmetric part of the connection $\Gamma^{\mu}_{[\nu\lambda]}$ or, in other words, the torsion tensor $Q^{\mu}_{\nu\lambda}$ is a true tensorial quantity. Since the torsion is related to the intrinsic spin, we see that the intrinsic spin $\hbar$ and, hence, the spin are quantized. We can conclude that the space-time defect in topology should occur in multiples of Planck's length $l_p = \sqrt{\frac{G\hbar}{c^3}}$. In other words, we can write [5]

$$\oint Q^{\mu}_{\nu\lambda} dx^{\nu} \wedge dx^{\lambda} = n\sqrt{\frac{\hbar G}{c^3}} n^{\mu}, \tag{4}$$

where n is an integer, and n^{μ} is a unit point vector. This is a relation analogous to the Bohr–Sommerfeld relation in quantum mechanics. The torsion tensor $Q^{\mu}_{\nu\lambda}$ plays the role of a field strength, which is analogous to that of the electromagnetic field tensor $F_{\mu\nu}$. Equation (4) defines the minimal fundamental length, a minimal length that enters the picture through the unit of action $\hbar$. In other words, $\hbar$ represents the intrinsic defect that is built in the torsion structure of space-time, in quantized units of $\hbar$ related to a quantized time like-vector with the dimension of length. This vector is related to the intrinsic geometric structure, when the torsion is considered. The intrinsic spin in units of $\hbar$ characterizes all the matter, and, therefore, the torsion is now entering the geometry. Thus, the Einstein–Cartan theory of gravitation can provide the corresponding quantum gravity effects. At the same time, we can also define the time at the quantum geometric level again through the torsion according to the equation:

$$t = \frac{1}{c}\oint Q^{\mu}_{\nu\lambda} dx^{\nu} \wedge dx^{\lambda} = n\sqrt{\frac{\hbar G}{c^5}}. \tag{5}$$

So, when the torsion is included, it is important that a minimal time interval given by Eq. (5) exists and is different from zero. This is the smallest unit of time $t_p = 5.391 \times 10^{-44}$ s. In the limit as $\hbar \to 0$, we recover the classical geometry of GR and, if $c \to \infty$, the Newtonian case. Finally, the geodesic equations in the case of a nonzero spin turn to

$$\frac{d^2x^{\mu}}{dp^2} + \Gamma^{\mu}_{\nu\lambda}\frac{dx^{\mu}}{dp}\frac{dx^{\nu}}{dp} = -2Q^{\mu}_{\nu\lambda}\frac{dx^{\nu}}{dp}\frac{dx^{\lambda}}{dp}, \tag{6}$$

where p is an affine parameter. To understand the spin effects in gravitation, we can use the torsion. Consequently, let us first write a Schwarzschild metric that includes torsion effects [4]:

$$ds^2 = c^2\left(1 - \frac{2GM}{c^2r} \pm \frac{3G^2s^2}{2r^4c^6}\right)dt^2 - \\ - \left(1 - \frac{2GM}{c^2r} \pm \frac{3G^2s^2}{2r^4c^6}\right)^{-1} dr^2 - r^2\left(d\theta^2 + \sin^2\theta d\phi^2\right), \tag{7}$$

where s is the torsion. We can write $s = \sigma r^3$, where σ is the spin density [4]. So, the Schwarzschild metric is modified by the inclusion of torsion effects. The torsion gives a natural way to understand the spin effects in gravitation. Making use of an expression that relates the torsion to the spin density, we can eliminate s and include σ in Eq. (7). Our primary goal is to establish a possible relation between the spin density σ and the information number N and between the Ricci scalar, as derived from Eq. (7), and information. This is an effort to understand why information plays an important role in the space-time structure in the case wherethe torsion effects are included in gravitation.

3. Analysis

Consider the case of a Schwarzschild metric with the torsion. Substituting $s = \sigma r^3$ [4], we get the gravitational radius:

$$\left(1 - \frac{2GM}{c^2 r} \pm \frac{3G^2\sigma^2}{2c^6} r^2\right) = 0. \tag{8}$$

In the case of a spin parallel to the gravitation (plus sign), we have

$$\left(1 - \frac{2GM}{c^2 r} + \frac{3G^2\sigma^2}{2c^6} r^2\right) = 0. \tag{9}$$

From whence, we obtain

$$r_{H_{\uparrow\downarrow}} = \frac{1}{3}\big[-\big(2^{2/3}c^6\big)/\big(\big(9c^4G^5M\sigma^4 + + \sqrt{c^8G^6\sigma^6\left(2c^{10}+81G^4M^2\sigma^2\right)}\big)^{1/3}\big)\big] \pm \pm \frac{1}{3}\big[\big(2^{1/3}\big(9c^4G^5M\sigma^4 + + \sqrt{c^8G^6\sigma^6(2c^{10}+81G^4M^2\sigma^2)}^{1/3}\big)\big)/\big(G^2\sigma^2\big)\big], \tag{10}$$

where the plus sign in Eq. (10) corresponds to the plus sign of the second term in Eq. (8). The negative sign in Eq. (10) corresponds to the negative sign in the second term of Eq. (8). In other words, we deal with parallel and antiparallel spins. Let us write the entropy formula as [6]

$$S = \frac{k_\mathrm{B}}{4\ell_p^2} A_H, \tag{11}$$

where k_B is the Boltzmann constant, $l_p^2 = \frac{G\hbar}{c^3}$ is Planck's length, and A_H is horizon area [2]. This is the Bekenstein–Hawking area-entropy law. This is a macroscopic formula, and it should be viewed in the same light as the classical macroscopic thermodynamic formulae. It describes how the properties of event horizons in general relativity change as their parameters are varied. Substituting Eq. (10) in Eq. (12), we obtain

$$S = \frac{\pi k_\mathrm{B}}{\ell_p^2}(r_{H_{\uparrow\downarrow}})^2 = = \frac{\pi k_\mathrm{B}}{\ell_p^2}\left[\frac{1}{3}\left[-\left(2^{2/3}c^6\right)/\left(\left(9c^4G^5M\sigma^4 + + \sqrt{c^8G^6\sigma^6\left(2c^{10}+81G^4M^2\sigma^2\right)}\right)^{1/3}\right) \pm \pm \left(2^{1/3}\left(9c^4G^5M\sigma^4 + + \sqrt{c^8G^6\sigma^6(2c^{10}+81G^4M^2\sigma^2)}\right)^{1/3}\right)/(G^2\sigma^2)\right]\right]^2, \tag{12}$$

where the minus sign in the root stands for the parallel torsion and plus stands for the antiparallel one. We note that the information number in nats is given by [8]

$$N = \frac{S}{k_\mathrm{B}\ln 2}. \tag{13}$$

Using the positive sign, equating Eqs. (12) and (13), and solving for the spin density as a function of information in nat N, we obtain the following solutions:

$$\sigma_{1_\uparrow} = \sigma_{2_\uparrow} = \pm i\left(\frac{4c^4M}{G\ell_p^3 N^{\frac{3}{2}}}\left(\frac{\pi}{\ln 2}\right)^{3/2} + \frac{\pi c^6}{G\ell_p^2 N\ln 2}\right)^{1/2}, \tag{14}$$

$$\sigma_{3_\uparrow} = \sigma_{4_\uparrow} = \pm i\left(\frac{4c^4M}{G\ell_p^3 N^{\frac{3}{2}}}\left(\frac{\pi}{\ln 2}\right)^{3/2} - \frac{\pi c^6}{G\ell_p^2 N\ln 2}\right)^{1/2}. \tag{15}$$

Similarly, the negative sign (or antiparallel spin) gives the only real solution:

$$\sigma_{1_\downarrow} = \left[\frac{8\pi^3c^8M^2}{3G^2\ell_p^6\left(\Phi_0 + \frac{6\sqrt{\Gamma_0}}{G^5\ell_p^9}\right)^{1/3}} + \frac{2\left(\Phi_0 + \frac{6\sqrt{\Gamma_0}}{G^5\ell_p^9}\right)^{1/3}}{9N^3\ln 2^3} + + \frac{4\pi c^6}{9G^2\ell_p^2 N\ln 2} + \frac{2\pi^2c^{12}N\ln 2}{9G^4\ell_p^6(\Phi_0 + \frac{6\sqrt{\Gamma_0}}{G^5\ell_p^9})^{1/3}}\right]^{1/2}, \tag{16}$$

where the quantities Γ_0 and Φ_0 are defined as follows:

$$\Gamma_0 = -48\pi^9c^{24}\ln 2^9 M^6N^9 + + 24\pi^8c^{28}G^2\ell_p^2M^4\ln 2^{10}N^{10} + + \pi^7c^{32}\ell_p^4M^2N^{11}\ln 2^{11}, \tag{17}$$

$$\Phi_0 = \frac{36\pi^4c^{14}M^2N^5\ln 2^5}{G^4\ell_p^8} + \frac{\pi^3c^{18}N^6\ln 2^6}{G^6\ell_p^6}. \tag{18}$$

4. Calculation of the Ricci Scalar and Its Relation to Information

Next, we are going to calculate the Ricci scalar in the cases of parallel and antiparallel spins. So, we define the metric coefficients to be

$$A(r) = c^2\left[1 - \frac{2GM}{rc^2} \pm \frac{3G^2\sigma^2}{2c^6}r^2\right], \tag{19}$$

and

$$B(r) = \left[1 - \frac{2GM}{rc^2} \pm \frac{3G^2\sigma^2}{2c^6} r^2\right]^{-1}. \tag{20}$$

The correspondent Ricci scalar is given by [9]

$$R = -\frac{2}{r^2 B(r)}\left[1 - B(r) + \frac{r^2 A''(r)}{2A(r)} + \right.$$

$$\left. + \frac{A'(r)}{A(r)}\left(r - \frac{r^2 A'(r)}{4A(r)}\right) - \frac{B'(r)}{B(r)}\left(r + \frac{r^2 A'(r)}{4A(r)}\right)\right]. \tag{21}$$

In the case of the torsion parallel to the gravity, we get

$$R = -\frac{18G^2\sigma^2}{c^6} = -\frac{9}{2}\left(\frac{R_{\rm Sch}}{M}\right)^2 \left(\frac{\sigma}{c}\right)^2. \tag{22}$$

Similarly, in the case of the torsion antiparallel to the gravity, we obtain

$$R = \frac{18G^2\sigma^2}{c^6} = \frac{9}{2}\left(\frac{R_{\rm Sch}}{M}\right)^2 \left(\frac{\sigma}{c}\right)^2. \tag{23}$$

Next, we proceed in writing the Ricci scalar as a function of the information number in nats N. In this calculation, we will only deal with a parallel spin. Therefore, we use Eqs. (22) and (15) and obtain

$$R\,(\sigma_1/\sigma_2)_\uparrow =$$

$$= \frac{18G^2}{c^6}\left[\left(\frac{\pi}{\ln 2}\right)^{3/2} \frac{4c^4 M}{3G\ell_p^3 N^{3/2}} + \frac{2\pi c^6}{3G^2 \ell_p^2 N \ln 2}\right]^2, \tag{24}$$

$$R\,(\sigma_3/\sigma_4)_\uparrow =$$

$$= -\frac{18G^2}{c^6}\left[\left(\frac{\pi}{\ln 2}\right)^{3/2} \frac{4c^4 M}{3G\ell_p^3 N^{\frac{3}{2}}} - \frac{2\pi c^6}{3G^2 \ell_p^2 N \ln 2}\right]^2, \tag{25}$$

which simplifies to

$$R\,(\sigma_1/\sigma_2)_\uparrow = 12\left(\frac{\pi}{\ln 2}\right)^{3/2}\left(\frac{R_{\rm Sch}}{\ell_p^3 N^{\frac{3}{2}}}\right) + \frac{12\pi}{N\ell_p^2 \ln 2}, \tag{26}$$

$$R\,(\sigma_3/\sigma_4)_\uparrow = 12\left(\frac{\pi}{\ln 2}\right)^{3/2}\left(\frac{R_{\rm Sch}}{\ell_p^3 N^{\frac{3}{2}}}\right) + \frac{12\pi}{N\ell_p^2 \ln 2}. \tag{27}$$

With reference to [6] and [7], we note that

$$\Lambda = \frac{3\pi}{N\ell_p^2 \ln 2}. \tag{28}$$

Equation (28) gives the cosmological constant as a function of the information number N. Therefore, Eqs. (26) and (27) for the Ricci scalar become

$$R\,(\sigma_1/\sigma_2)_\uparrow = 12\left(\frac{\pi}{\ln 2}\right)^{3/2}\left(\frac{R_{\rm Sch}}{\ell_p^3 N^{3/2}}\right) + 4\Lambda, \tag{29}$$

$$R\,(\sigma_3/\sigma_4)_\uparrow = 12\left(\frac{\pi}{\ln 2}\right)^{3/2}\left(\frac{R_{\rm Sch}}{\ell_p^3 N^{3/2}}\right) + 4\Lambda. \tag{30}$$

5. Conclusion

We have examined the effect of a torsion in the Schwarzschild metric corrected for torsion effects and its relation to information. In this case, the torsion effects can be represented by the spin density. We start by calculating the entropy at the horizon of such a black hole, and then we equate the entropy to a known expression that gives the entropy in terms of the information number N. Thus, we obtain analytical expressions for the spin density as a function of the information number N. We obtain two spin density solutions. One of them is real, and another one is imaginary. Moreover, we have found that, for the spin density, both real and imaginary roots scale proportionally to the information number N according to the relation $\sigma \propto \frac{1}{N^{\frac{3}{2}}} - \frac{1}{N}$. In the case of parallel spin, we find that Ricci scalar also depends on the information number according to the relation $R \propto N^{\frac{3}{2}} + N^{-1}$ for both parallel and antiparallel spins. This comes from an extra term that is equal to the cosmological constant λ expressed as a function of the information number N adds the information dependence to the Ricci scalar via the cosmological constant λ. In this aspect, we can perceive the cosmological constant as a cosmological depository of information that affects the space-time structure or is included as an important parameter in the space-time structure and in the geometry of the Universe. Therefore, we conclude that information enters this torsion-corrected metric via the dependence of the spin density on the information number N, as well as the cosmological constant itself.

1. K. Akiyama *et al*. First M 87 event horizon telescope results. I. The shadow of the supermassive black hole. *Astrophys. J. Lett.* **875**, L1 (2019).
2. J.D. Bekenstein . Black holes and entropy. *Phys. Rev. D* **7**, 2333 (1973).
3. V. De Sabbata, D. Wang, C. Sivaram. Torsion effects in black hole evaporation. *Ann. Phys.* **47**, 508 (1990).

4. *Black Hole Physics.* Edited by V. De Sabbata, Z. Zhang (Kluwer Academic, 1992).
5. *The Early Universe*, edited by V.B. Johri (Hadronic Press, 1996).
6. I. Haranas, I. Gkigkitzis. The number of information bits related to the minimum quantum and gravitational masses in a vacuum dominated universe. *Astrophys. Space-Sci.* **346**, No. 1, 213 (2013).
7. I. Haranas, I. Gkigkitzis. Bekenstein bound of information number N and its relation to cosmological parameters in a universe with and without cosmological constant. *Modern Phys. Lett. A* **28**, No.19, Article ID1350077 (2013).
8. S. Lloyd. *Ultimate physical limits to computation. Nature* **406**, 1047 31 (2000).
9. M. Sharif, H. Kausar, R. *Dust Static Spherically Symmetric Solution in f(R) Gravity,*, arXiv:1102.4124v1 [physics.gen-ph] (2011).

Received 08.07.19

Й. Ґікіціс, Й. Харанас, Е. Praveen

ЕФЕКТ КРУЧЕННЯ ЧОРНОЇ ДІРИ
ТА ЇЇ ВІДНОШЕННЯ ДО ІНФОРМАЦІЇ

Р е з ю м е

Для вивчення впливу кручення на гравітацію в просторі-часі та його відношення до інформації ми користуємося метрикою Шварцшільда, де кручення природно вводиться через спінову щільність частинки. В сценарії чорної діри ми отримали аналітичний розв'язок для гравітаційного радіуса чорної діри з включенням спіну, звідки ми обчислили ентропію для випадків паралельних та антипаралельних спінів. Більше того, ми знайшли чотири аналітичні розв'язки для спінової щільності в залежності від числа інформації. Користуючись цими розв'язками, ми отримали вирази для коефіцієнтів Річчі як функції числа інформації N; отримано також значення для космологічної константи.

https://doi.org/10.15407/ujpe64.8.689

V.M. GORKAVENKO

Taras Shevchenko National University of Kyiv, Ukraine
(64, Volodymyrs'ka Str., Kyiv 01601, Ukraine; e-mail: gorkavol@gmail.com)

SEARCH FOR HIDDEN PARTICLES IN INTENSITY FRONTIER EXPERIMENT SHiP

*Despite the undeniable success of the Standard Model of particle physics (SM), there are some phenomena (neutrino oscillations, baryon asymmetry of the Universe, dark matter, etc.) that SM cannot explain. This phenomena indicate that the SM have to be modified. Most likely, there are new particles beyond the SM. There are many experiments to search for new physics that can be can divided into two types: energy and intensity frontiers. In experiments of the first type, one tries to directly produce and detect new heavy particles. In experiments of the second type, one tries to directly produce and detect new light particles that feebly interact with SM particles. The future intensity frontier SHiP experiment (**S**earch for **Hi**dden **P**articles) at the CERN SPS is discussed. Its advantages and technical characteristics are given.*

K e y w o r d s: physics beyond the Standard Model, hidden particles, hidden sectors, renormalizable portals, intensity frontier experiment, SHiP, SPS.

1. Introduction

The Standard Model of particle physics (SM) [1–3] was developed in the mid-1970s. It is one of the greatest successes of physics. It is experimentally tested with high precision for the processes of electroweak and strong interactions with the participation of elementary particles up to the energy scale ∼100 GeV and for individual processes up to several TeV. It predicted a number of particles, last of them (Higgs boson) has been observed in 2012. However, the SM cannot explain several phenomena in particle physics, astrophysics, and cosmology. Namely: the SM does not provide the dark matter candidate; the SM does not explain neutrino oscillations and the baryon asymmetry of the Universe; the SM cannot solve the strong CP problem in particle physics, the primordial perturbations problem and the horizon problem in cosmology, *etc.*

The presence of the problems in the SM indicates the incompleteness of the Standard Model and the existence of as yet "hidden" sectors with particles of a new physics. Although it may seem surprising, but some of the above-mentioned SM problems really can be solved with help either heavy or light new particles. Neutrino oscillations and the smallness of the active neutrino mass can be explained as with help of a new particle with sub-eV mass, as well as with help of heavy particles of the GUT scale, see, e.g., [4]. The same can be said about the problem of baryon asymmetry of the Universe and dark matter problem: physics on the very different scales can be responsible for it, see, e.g., [5].

Can the new light particles exist in the SM extensions? The answer is positive. There are many theories beyond SM that have light particles in the spectrum (e.g., GUT, SUSY, theories with extra dimensions), see, e.g., [6]. Light particles in those theories can be, e.g., (pseudo)-Goldstone bosons that were produced as a result of the spontaneous breaking of some not exact symmetry. Alternatively, a particle can be massless at the tree level, but it can obtain a light mass as a result of loops-involving corrections.

So, two answers on the question "why do we not observe particles of the new physics?" are possible. First, the new particles can be very heavy (e.g., with the mass $M_X \gtrsim 100$ TeV), so they cannot be directly produced at the present-day powerful accelerators like LHC. On other hand, the new particles can be light (with mass below or of order of the electroweak scale) and can feebly interact with particles of the SM (otherwise, we would have already seen them in the experiments). In this case, the light new particles can be produced at many high-energy experiments, but it were not still observed due to the

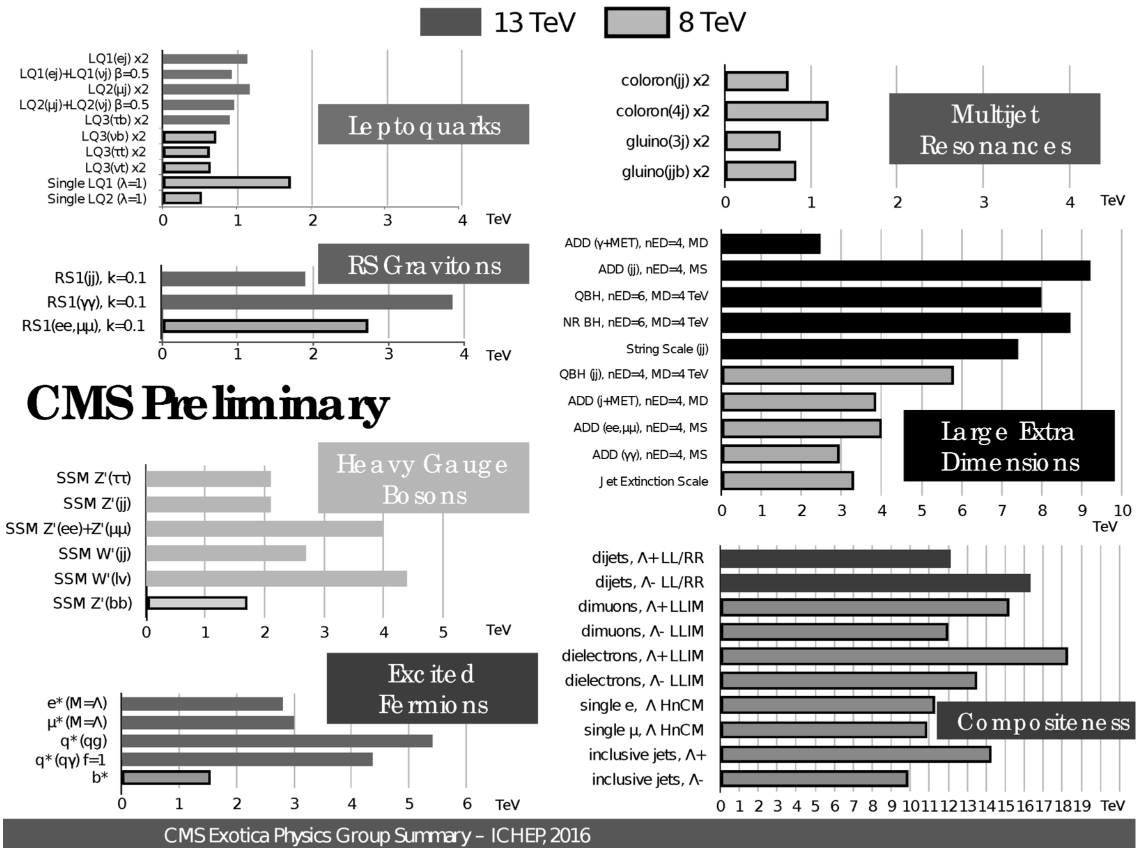

Fig. 1. Search for new particles beyond SM with mass at the TeV region at CERN CMS

extreme rarity of events with their production and to the complexity of their detection.

Based on the above, there are two types of particle search experiments.

First of them is energy frontier experiments like those at LHC or Fermilab. In these experiments, one tries to directly produce and detect new heavy particles assuming that the coupling of new particles to the SM particles is not very small. The new particles with mass of several TeV are actively searched in such experiments, see Fig. 1. Last decades, a lot of attention were paid to the energy frontier experiments.

Second of them is intensity frontier experiments. In this experiments, we try to search for the particles that feebly interact with the SM particles. So, in the intensity frontier experiments, we search for very rare events. For the successful production of hidden particles (to compensate their feeble interaction), those experiments must have the largest possible luminosity. In this sense, the beam-dump experiments are good as the intensity frontier experiments to seek the GeV-scale hidden particles, because of their luminosities is several orders of magnitude larger than those at colliders. The detection of hidden particles is possible only due to observing their decays into the SM particles. So, these experiments must be background-free. Because of the feeble interaction with the SM particles, one can expect their small decay width and long lifetime (here, we suppose that a hidden particle does not decay in non-SM channels, or the corresponding partial decay width is very small). So, the detector have to be placed as far as possible from the point of the production of hidden particles.

The intensity frontier experiments have been paid much less attention in the recent years. These experiments include PS 191 (early 1980s), CHARM (1980s), NuTeV (1990s), DONUT (late 1990s – early 2000). However, as was shown in [7, 9], the search for the new physics in the region of masses below the electroweak scale is not sufficiently investigated.

The difference between the energy and intensity frontier experiments for seeking the hidden particles can be schematically illustrated with the help of Fig. 2.

In this paper, we consider the future intensity frontier SHiP (**S**earch for **Hi**dden **P**articles) beam-dump experiment at the CERN Super Proton Synchrotron (SPS) accelerator. Its advantages and technical characteristics will be considered, and the class of theories that can be tested on SHiP will be discussed.

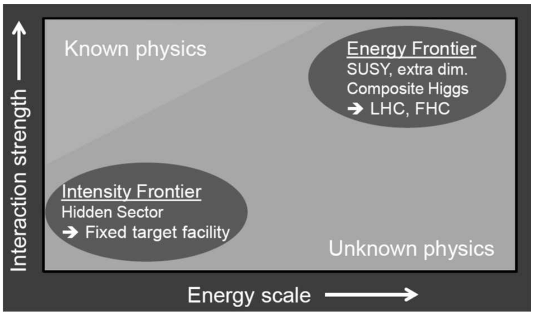

Fig. 2. Different strategies for the search for hidden particles in the energy and intensity frontier experiments

2. Interaction of New Particles with the SM Particles. Portals

If we will focused on detecting a new light particle, we have understand that this particle can originate from the large number of beyond-SM theories that predict different parameters for it (masses of new particles and their coupling to the SM particles). In particular, such relatively light particles can be mediators due to the interaction with particles of the SM and very heavy particles of "hidden sectors". Those light particles can be coupled to the Standard Model sectors either via renormalizable interactions with small dimensionless couplings ("portals") or by higher-dimensional operators suppressed by the dimensionful couplings Λ^{-n} corresponding to a new energy scale of the hidden sector [7].

Because of a limited number of possible types of particles (scalar, pseudoscalar, vector, pseudovector, fermion), there is limited number of possible effective Lagrangians of interaction of such particles with the SM particles that satisfy the Lorentz conditions and gauge invariance ones.

Renormalizable portals can be classified into the following 3 types:

Vector portal: new particles are vector Abelian fields (A'_μ) with the field strength $F'_{\mu\nu}$ that couple to the hypercharge field $F_Y^{\mu\nu}$ of the SM as

$$\mathcal{L}_{\text{Vectorportal}} = \epsilon F'_{\mu\nu} F_Y^{\mu\nu}, \tag{1}$$

where ϵ is a dimensionless coupling characterising the mixing between a new vector field with the fields of Z-bosons and photons.

Scalar portal: new particles are neutral singlet scalars, S_i, that couple to the Higgs field

$$\mathcal{L}_{\text{Scalarportal}} = (\lambda_i S_i + g_i S_i^2)(H^\dagger H), \tag{2}$$

where λ_i are dimensionless couplings, and g_i are the couplings with a dimension of mass.

Neutrino portal: new particles are neutral singlet fermions N_I

$$\mathcal{L}_{\text{Neutrinoportal}} = F_{\alpha I} \bar{L}_\alpha \tilde{H} N_I, \tag{3}$$

where index $\alpha = e, \mu, \tau$ corresponds to the lepton flavors, L_α is for the lepton doublet, $F_{\alpha I}$ is for the new matrix of the Yukawa constants, and $\tilde{H} = i\sigma_2 H^*$.

Non-renormalizable couplings of new particles to the SM operators are also possible. For example, pseudo-scalar axion-like particles A couple to SM as

$$\mathcal{L}_{\text{A}} = \sum_f \frac{C_{Af}}{2\,f_a} \bar{f}\gamma^\mu\gamma^5 f\,\partial_\mu A - \\ - \frac{\alpha}{8\pi}\frac{C_{A\gamma}}{f_a} F_{\mu\nu}\tilde{F}^{\mu\nu} A - \frac{\alpha_3}{8\pi}\frac{C_{A3}}{f_a} G^b_{\mu\nu}\tilde{G}^{b\,\mu\nu} A, \tag{4}$$

where $f = \{\text{quarks}, \text{leptons}, \text{neutrinos}\}$, $F_{\mu\nu}$ is the electromagnetic field strength tensor, $G^b_{\mu\nu}$ the field strength for a strong force, and the dual field strength tensors are defined as $\tilde{Q}^{\mu\nu} = \frac{1}{2}\epsilon^{\mu\nu\rho\sigma} Q_{\rho\sigma}$.

Another important example is a Chern–Simons-like gauge interaction [8] of a new pseudo-vector X_μ particle

$$\mathcal{L}_1 = \frac{C_Y}{\Lambda_Y^2} \cdot X_\mu (\mathfrak{D}_\nu H)^\dagger H B_{\lambda\rho} \cdot \epsilon^{\mu\nu\lambda\rho} + \text{h.c.} \tag{5}$$

$$\mathcal{L}_2 = \frac{C_{SU(2)}}{\Lambda_{SU(2)}^2} \cdot X_\mu (\mathfrak{D}_\nu H)^\dagger F_{\lambda\rho} H \cdot \epsilon^{\mu\nu\lambda\rho} + \text{h.c.}, \tag{6}$$

where the Λ_Y, $\Lambda_{SU(2)}$ are new scales of the theory, C_Y, $C_{SU(2)}$ are new dimensionless coupling constants, and $B_{\mu\nu}$, $F_{\mu\nu}$ are the field strength tensors of the

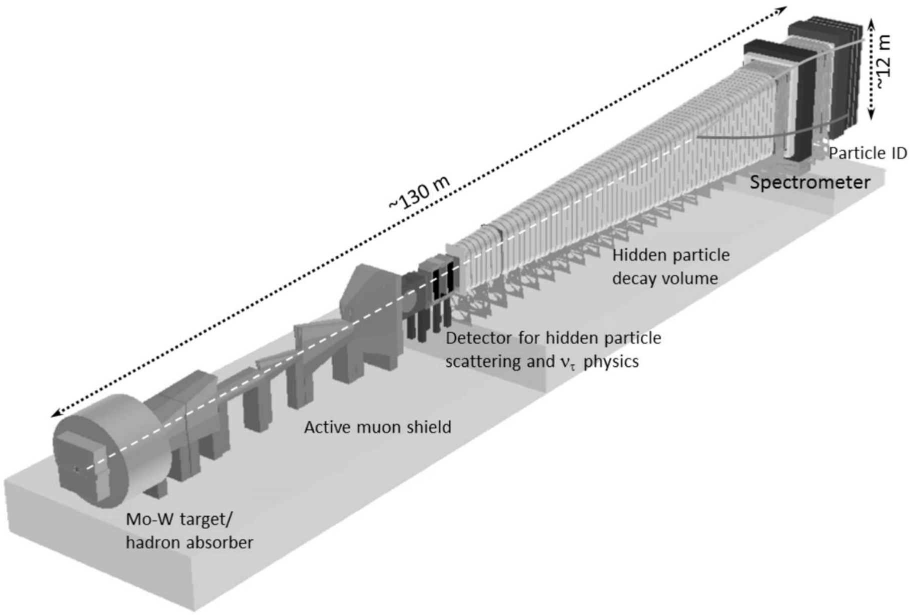

Fig. 3. General scheme of the SHiP facility

$U_Y(1)$ and $SU_W(2)$ gauge fields. After the spontaneous symmetry breaking of the Higgs field, this interaction is effectively reduced to a renormalizable interaction of the form

$$\mathcal{L}_{\rm CS} = c_z\epsilon^{\mu\nu\lambda\rho}X_\mu Z_\nu\partial_\lambda Z_\rho + c_\gamma\epsilon^{\mu\nu\lambda\rho}X_\mu Z_\nu\partial_\lambda A_\rho + + c_w\epsilon^{\mu\nu\lambda\rho}X_\mu W^-_\nu\partial_\lambda W^+_\rho. \quad (7)$$

So, from the experimental point of view, one has to test all of the above-mentioned possible new interactions in the wide range of new particle masses and couplings.

3. SHiP Experiment

The SHiP experiment was first proposed in 2013 [10]. The technical proposal was presented in 2015 [11]. The theoretical background, main channels of production and decay of new particles, and preliminary estimations of the sensitivity region for different portals for the SHiP experiment were considered in 2016 [7]. Somewhat later, the clarifying complementary works were published [12–15]. Currently, the SHiP collaboration [16] includes nearly 250 scientists from 53 institutions. The experiment will begin its work allegedly in 2026 year [17].

The main goal of the future SHiP beam-dump experiment at the CERN SPS accelerator is to search for the new physics in the region of feebly interacting long-lived light particles including Heavy Neutral Leptons (HNL), vector, scalar, axion portals to the Hidden Sector, and light supersymmetric particles. The experiment provides great opportunities for the study of neutrino physics as well.

Now, we describe the work of the SHiP experiment, see Fig. 3. A beam line from the CERN SPS accelerator will transmit 400-GeV protons at the SHiP. The proton beam will strike in a Molybdenum and Tungsten fixed target at a center-of-mass energy $E_{\rm CM} \approx 27$ GeV. Approximately 2×10^{20} proton-target collisions are expected in 5 years of the SHiP operation. The great number of the SM particles and hadrons will be produced under such collisions. Hidden particles are expected to be predominantly produced in the decays of the hadrons.

The main concept of the SHiP functioning is following. Almost all the produced SM particles should be either absorbed or deflected in a magnetic field (muons). Remaining events with SM particles can be rejected using specially developed cuts. If the hidden particles will decay into SM particles inside the decay volume, the last will be detected. This will mean the existence of hidden particles.

So, the target will be followed by a 5-m-long iron hadron absorber. It will absorb the hadrons and the electromagnetic radiation from the target, but the decays of mesons result in a large flux of muons and neutrinos. After the hadron stopper, a system of shielding magnets (which extends over a length of ∼40 m) is located to deflect muons away from the fiducial decay volume [12].

Despite the aim to search for the long-lived particles, the sensitive volume should be situated as close as possible to the proton target due to relatively large transverse momenta of the hidden particles with respect to the beam axis. The minimum distance is determined by the necessity for the system to absorb the electromagnetic radiation and hadrons produced in the proton-target collisions and to reduce the beam-induced muon flux.

The system of detectors of the SHiP consists of two parts. Just after the hadron absorber and muon shield, the detector system for recoil signatures of hidden-sector particle scattering and for neutrino physics is located. The neutrino detector has mass of nearly 10 tons. The study of neutrino physics is based on a hybrid detector similar to the detector of the OPERA Collaboration [18]. In addition, this system allows one to detect and veto charged particles produced outside the main decay volume.

The second detector system consist of the fiducial decay volume that is contained in a nearly 50-m-long rectangular vacuum tank. In order to suppress the background from neutrinos interacting in the fiducial volume, it is maintained at a pressure of $O(10^{-3})$ bar. The decay volume is surrounded by background taggers to tag the neutrino and muon inelastic scatterings in the surrounding structures, which may produce long-lived neutral Standard Model particles whose decay can mimic signal events. The vacuum tank is followed by a large spectrometer with a rectangular acceptance of 5 m in width and 10 m in height and a calorimeter. The system is constructed in such a way to detect as many final states as possible in order to be sensitive to a very wide range of models that can be tested. With the help of Table, one can see what modification of the SM is tested depending on final states of the hidden particles decay.

Modification of the SM that can be tested on SHiP depending on final states of the hidden particles decay

Decay modes	Final states	Models tested
Meson and lepton	πl, Kl, l ($l = e, \mu, \tau$)	ν portal, HNL, SUSY neutralino
Two leptons	$e^+ e^-$, $\mu^+\mu^-$	V, S and A portals, SUSY s-goldstino
Two mesons	$\pi^+ \pi^-$, $K^+ K^-$	V, S and A portals, SUSY s-goldstino
3 bodies	$l^+ l^- \nu$	HNL, neutralino

It should be noted that the SHiP experiment gives great opportunities for the study of neutrino physics. As a result of nearly 2×10^{20} proton-target collisions, $N_{\nu_\tau} = 5.7 \times 10^{15}$ ν_τ and $\nu_{\bar{\tau}}$ neutrino, $N_{\nu_e} = 5.7 \times 10^{18}$ electron neutrino, and $N_{\nu_\mu} = 3.7 \times 10^{17}$ muon neutrino will be produced. It is expected to detect nearly 10^4 τ-neutrino and at first to detect anti τ-neutrino. It is very important, because only 14 τ-neutrino candidates by the experiment DONUT in Fermilab and 10 τ-neutrino candidates by the experiment OPERA in CERN were found till now. No event with anti τ-neutrino was still observed.

4. Conclusions

There are some indisputable phenomena that point to the fact that SM has to be modified and complemented by a new particle (particles). We are sure that there is a new physics, but we do not know where to search for it. There are many theoretical possibilities to modify the SM by scalar, pseudoscalar, vector, pseudovector, or fermion particles of the new physics. These particles may be sufficiently heavy on the electroweak scale and the scale of energy of the present colliders. But these particles may be light (with masses less than that on the electroweak scale) and may feebly interact with the SM particles. The main task now is to experimentally observe particles of the new physics.

Since the possibilities for increasing the energies of the present colliders are limited by high costs, and the heavy new particles are difficult to be produced, it seems reasonable to check another variant and to find light particles of the new physics in intensity frontier experiments.

The goal of the SHiP experiment is to search for the new physics in the region of feebly interacting long-lived light particles including HNL, vector, scalar, axion particles with mass ≤10 GeV. There are theoretical predictions for the sensitivity region of the SHiP experiment for each type of new-physics particles (in the mass versus coupling constant coordinates). The experiment will provide great opportunities for the study of neutrino physics as well.

Since the idea of searching for new light feebly interacting particles is very tempting and promising, there are another projects such as REDTOP at the PS beam lines, NA64++, NA62++, LDMX, AWAKE, KLEVER at the SPS beam lines, and FASER, MATHUSLA, CODEX-b at the LHC. All these experiments are compared and summarized in [17]. It is possible that great discoveries in particle physics are right ahead.

The work was presented on the conference "New trends in high-energy physics", May 12-18, Odessa, Ukraine. I also thank Kyrylo Bondarenko for the useful discussion and helpful comments.

1. S.L. Glashow. Partial symmetries of weak interactions. *Nucl. Phys.* **22**, 579 (1961).
2. S. Weinberg. A Model of leptons. *Phys. Rev. Lett.* **19**, 1264 (1967).
3. A. Salam. Weak and electromagnetic interactions. In: *Proc. of 8th Nobel Symposium.* Edit. by N. Svartholm (Almquist and Wiksells, 1968), p. 367.
4. A. Strumia, F. Vissani. Neutrino masses and mixings and... arXiv:hep-ph/0606054 (2010).
5. D.S. Gorbunov, V.A. Rubakov. *Introduction to the Theory of the Early Universe: Hot Big Bang Theory* (World Scientific, 2011).
6. W. de Boer. Grand unified theories and supersymmetry in particle physics and cosmology. *Prog. Part. Nucl. Phys.* **33**, 201 (1994).
7. S. Alekhin. *et al.* A facility to search for hidden particles at the CERN SPS: the SHiP physics case. *Rept. Prog. Phys.* **79**, 124201 (2016).
8. I. Antoniadis, A. Boyarsky, S. Espahbodi, O. Ruchayskiy, J.D. Wells. Anomaly driven signatures of new invisible physics at the Large Hadron Collider. *Nucl. Phys. B* **824**, 296 (2010).
9. J. Alexander *et al.* Dark Sectors 2016 Workshop: Community report. arXiv:1608.08632, FERMILAB-CONF-16-421 (2016).
10. W. Bonivento *et al.* Proposal to search for Heavy Neutral Leptons at the SPS. arXiv:1310.1762 (2013).
11. M. Anelli *et al.* A facility to Search for Hidden Particles (SHiP) at the CERN SPS. arXiv:1504.04956, CERN-SPSC-2015-016, SPSC-P-350 (2015).
12. A. Akmete *et al.* The active muon shield in the SHiP experiment. *JINST* **12**, P05011 (2017).
13. C. Ahdida *et al.* Sensitivity of the SHiP experiment to Heavy Neutral Leptons. *J. High Energ. Phys.* **2019**, 77 (2019).
14. C. Ahdida *et al.* The experimental facility for the Search for Hidden Particles at the CERN SPS. *JINST* **14**, P03025 (2019).
15. I. Boiarska, K. Bondarenko, A. Boyarsky, V. Gorkavenko, M. Ovchynnikov, A. Sokolenko. Phenomenology of GeV-scale scalar portal. arXiv:1904.10447v2 (2019).
16. https://ship.web.cern.ch/ship.
17. J. Beacham *et al.* Physics Beyond Colliders at CERN: Beyond the Standard Model Working Group Report. arXiv:1901.09966, CERN-PBC-REPORT-2018-007 (2019).
18. R. Acquafredda *et al.* OPERA collaboration. The OPERA experiment in the CERN to Gran Sasso neutrino beam. *JINST* **4**, P04018 (2009).

Received 08.07.19

В.М. Горкавенко

ПОШУК ЧАСТИНОК НОВОЇ
ФІЗИКИ В ЕКСПЕРИМЕНТІ SHiP

Р е з ю м е

Незважаючи на величезні успіхи Стандартної Моделі фізики елементарних частинок (СМ), існують окремі явища (нейтринні осциляції, баріонна асиметрія Всесвіту, темна матерія тощо), які СМ пояснити не в змозі. Дані явища вказують на необхідність модифікації СМ та введення нових частинок. Експерименти з пошуку частинок нової фізики можна розділити на два типи: експерименти, в яких намагаються досягти найбільшої енергії частинок, що зіштовхуються, та експерименти, в яких намагаються досягти найбільшої кількості необхідних реакцій. В експериментах першого типу намагаються безпосередньо утворити та зареєструвати нові важкі частинки. В експериментах другого типу намагаються безпосередньо утворити та зареєструвати нові легкі частинки, що слабко взаємодіють з частинками СМ. В роботі обговорюється майбутній експеримент з високою інтенсивністю подій SHiP, що проводитиметься на прискорювачі SPS CERN, його технічні характеристики та переваги.

https://doi.org/10.15407/ujpe64.8.695

P. LEBIEDOWICZ,[1] A. SZCZUREK,[1] O. NACHTMANN [2]

[1] Institute of Nuclear Physics, Polish Academy of Sciences
(Radzikowskiego 152, PL-31342 Cracow, Poland; e-mail: Piotr.Lebiedowicz@ifj.edu.pl)

[2] Institut fur Theoretische Physik, Universitat Heidelberg
(Philosophenweg 16, D-69120 Heidelberg, Germany)

SEARCHING FOR ODDERON IN EXCLUSIVE REACTIONS

We discuss the possibility to use the $pp \to pp\phi\phi$ process in identifying the odderon exchange. So far, there is no unambiguous experimental evidence for the odderon, the charge conjugation $C = -1$ counterpart of the $C = +1$ pomeron. Last year, the results of the TOTEM collaboration suggest that the odderon exchange can be responsible for a disagreement of theoretical calculations and the TOTEM data for the elastic proton-proton scattering. Here, we present recent studies for the central exclusive production (CEP) of $\phi\phi$ pairs in proton-proton collisions. We consider the pomeron-pomeron fusion to $\phi\phi$ ($\mathbb{PP} \to \phi\phi$) through the continuum processes, due to the $\hat{t}$- and $\hat{u}$-channel reggeized ϕ-meson, photon, and odderon exchanges, as well as through the s-channel resonance process ($\mathbb{PP} \to f_2(2340) \to \phi\phi$). This f_2 state is a candidate for a tensor glueball. The amplitudes for the processes are formulated within the tensor-pomeron and vector-odderon approach. Some model parameters are determined from the comparison to the WA102 experimental data. The odderon exchange is not excluded by the WA102 data for high $\phi\phi$ invariant masses. The measurement of large $M_{\phi\phi}$ or $Y_{\rm diff}$ events at the LHC would therefore suggest the presence of the odderon exchange. The process is advantageous, as here the odderon does not couple to protons.

Keywords: exclusive reactions, meson, Regge physics, pomeron, odderon, LHC.

1. Introduction

Diffractive studies are one of the important parts of the physics program for the RHIC and LHC experiments. A particularly interesting class is the central-exclusive-production (CEP) processes, where all centrally produced particles are detected.

In recent years, there has been a renewed interest in the exclusive production of $\pi^+\pi^-$ pairs at high energies related to successful experiments by the CDF [1] and the CMS [2] collaborations. These measurements are important in the context of the resonance production, in particular, in searches for glueballs. In the CDF and CMS experiments, the large rapidity gaps around the centrally produced dimeson system were checked, but the forward- and backward-going (anti)protons were not detected. Preliminary results of similar CEP studies have been presented by the ALICE and LHCb collaborations at the LHC. Although such results will have a diffractive nature, further efforts are needed to ensure their exclusivity. Ongoing and planned experiments at the RHIC (see, e.g., [3]) and future experiments at the LHC will be able to detect all particles produced in central exclusive processes, including the forward- and backward-going protons. The feasibility studies for the $pp \to pp\pi^+\pi^-$ process with the tagging of scattered protons, as carried out for the ATLAS and ALFA detectors, are in [4]. Similar possibilities exist using the CMS and TOTEM detectors.

In [21], the tensor-pomeron and vector-odderon concepts were introduced for soft reactions. In this approach, the $C = +1$ pomeron and the reggeons $\mathbb{R}_+ = f_{2\mathbb{R}}, a_{2\mathbb{R}}$ are treated as effective rank-2 symmetric tensor exchanges, while the $C = -1$ odderon and the reggeons $\mathbb{R}_- = \omega_\mathbb{R}, \rho_\mathbb{R}$ are treated as effective vector exchanges. For these effective exchanges, a number of propagators and vertices, respecting the standard rules of quantum field theory, were derived from comparisons with experiments. This allows for an easy construction of amplitudes for specific processes. In [22], the helicity structure of a

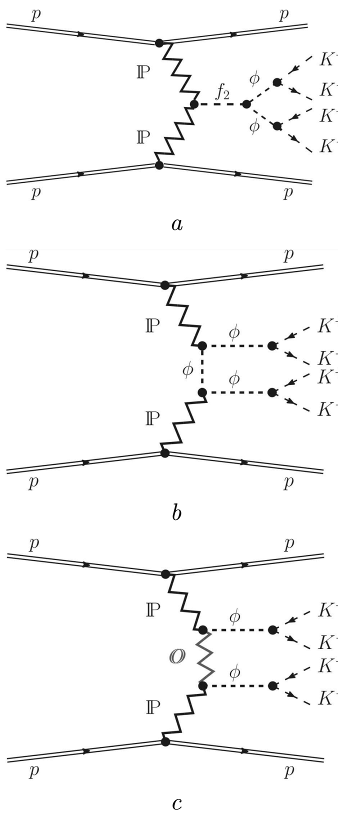

Fig. 1. Born-level diagrams for the double pomeron central exclusive $\phi\phi$ production and their decays into $K^+K^-K^+K^-$: $\phi\phi$ production via an f_2 resonance (a). Other resonances, e.g., of f_0- and η-type, can also contribute here. The continuum $\phi\phi$ production via an intermediate ϕ and odderon ($\mathbb{O}$) exchanges, respectively, (b) and (c). $\mathbb{P}$-γ-$\mathbb{P}$ and $\mathbb{O}$-$\mathbb{P}$-$\mathbb{O}$ contributions are also possible, but negligibly small

small-$|t|$ proton-proton elastic scattering was considered in three models for the pomeron: tensor, vector, and scalar ones. Only the tensor ansatz for the pomeron was found to be compatible with the high-energy experiment on the polarized pp elastic scattering [10].

Applications of the tensor-pomeron and vector-odderon ans'atze were given for the photoproduction of pion pairs in [11] and for a number of central-exclusive-production (CEP) reactions in pp collisions in [12–20]. In addition, contributions from the subleading exchanges, $\mathbb{R}_+$ and $\mathbb{R}_-$, were discussed in these works. As an example, for the $pp \to ppp\bar{p}$ reaction [17], the contributions involving an odderon are expected to be small since its coupling to a proton is very small. We have predicted asymmetries in the (pseudo)rapidity distributions of the centrally produced antiproton and proton. The asymmetry is caused by interference effects of the dominant $(\mathbb{P}, \mathbb{P})$ with the subdominant $(\mathbb{O}+\mathbb{R}_-, \mathbb{P}+\mathbb{R}_+)$ and $(\mathbb{P}+\mathbb{R}_+, \mathbb{O}+\mathbb{R}_-)$ exchanges. We find only very small effects for the odderon, roughly a factor of 10 smaller than the effects due to reggeons.

So far, there is no unambiguous experimental evidence of the odderon, the charge conjugation $C = -1$ counterpart of the $C = +1$ pomeron, introduced on theoretical grounds in [5]. A hint of the odderon was seen in ISR results [6] as a small difference between the differential cross-sections of elastic proton-proton (pp) and proton-antiproton ($p\bar{p}$) scatterings in the diffractive dip region at $\sqrt{s} = 53$ GeV. Recently, the TOTEM Collaboration has published data from high-energy elastic pp scattering experiments at the LHC. In [7], results were given for the ρ parameter, the ratio of the real part to the imaginary one of the forward scattering amplitude. The interpretation of these results is controversial at the moment.

As was discussed in [8], the exclusive diffractive J/ψ and ϕ productions from the pomeron-odderon fusion in high-energy pp and $p\bar{p}$ collisions are a direct probe for a possible odderon exchange. For a nice review of the odderon physics, see [9]. In the diffractive production of ϕ meson pairs, it is possible to have the pomeron-pomeron fusion with intermediate $\hat{t}/\hat{u}$-channel odderon exchange [20]; see the corresponding diagram in Fig. 1, *c*. Thus, the $pp \to pp\phi\phi$ reaction is a good candidate for the odderon-exchange searches, as it does not involve the coupling of the odderon to the proton.

Studies of different decay channels in the central exclusive production would be very valuable also in the context of identification of glueballs. One of the promising reactions is $pp \to pp\phi\phi$ with both $\phi \equiv \phi(1020)$ mesons decaying into the K^+K^- channel. Structures in the $\phi\phi$ invariant-mass spectrum were observed by several experiments, e.g., in the exclusive $\pi^-p \to \phi\phi n$ [23] and $K^-p \to \phi\phi\Lambda$ [24] reactions, and in the central production [25]. Three tensor states, $f_2(2010)$, $f_2(2300)$, and $f_2(2340)$, observed previously in [23], were also observed in the radiative decay $J/\psi \to \gamma\phi\phi$ [26]. The nature of these resonances is not understood at present and a tensor glueball has still not been clearly identified. According to lattice-QCD simulations, the lightest tensor glueball has a mass between 2.2 and 2.4 GeV, see, e.g. [27]. The $f_2(2300)$ and $f_2(2340)$ states are good candidates to be tensor glueballs.

For an interesting approach to the exclusive diffractive resonance production in pp collisions at high energies, see also Ref. [28, 29].

2. A Sketch of Formalism

In [20], we considered the CEP of four charged kaons via the intermediate $\phi\phi$ state. Explicit expressions for the $pp \to pp\phi\phi$ amplitudes involving the pomeron-pomeron fusion to $\phi\phi$ ($\mathbb{PP} \to \phi\phi$) through the continuum processes, due to the $\hat{t}$- and $\hat{u}$-channel reggeized ϕ-meson, photon, and odderon exchanges, as well as through the s-channel resonance reaction ($\mathbb{PP} \to \to f_2(2340) \to \phi\phi$) were given there. Here, we discuss briefly the continuum processes for the $pp \to pp\phi\phi$ reaction.

The "Born-level" amplitude for the $pp \to pp\phi\phi$ reaction is

$$\mathcal{M}^{\rm Born} = \mathcal{M}^{(f_2-\text{exchange})} + \mathcal{M}^{(\phi-\text{exchange})} + + \mathcal{M}^{(\mathbb{O}-\text{exchange})}. \tag{1}$$

For the continuum process with the odderon exchange (Fig. 1, c), the amplitude is a sum of $\hat{t}$- and $\hat{u}$-channel amplitudes. The $\hat{t}$-channel term can be written as

$$\begin{aligned}\mathcal{M}^{(\hat{t})} &= (-i)\bar{u}(p_1,\lambda_1) i\Gamma^{(\mathbb{P}pp)}_{\mu_1\nu_1}(p_1,p_a)u(p_a,\lambda_a) \times \\ &\times i\Delta^{(\mathbb{P})\,\mu_1\nu_1,\alpha_1\beta_1}(s_{13},t_1) \times \\ &\times i\Gamma^{(\mathbb{PO}\phi)}_{\rho_1\rho_3\alpha_1\beta_1}(\hat{p}_t,-p_3)\left(\epsilon^{(\phi)\,\rho_3}(\lambda_3)\right)^* \times \\ &\times i\Delta^{(\mathbb{O})\,\rho_1\rho_2}(s_{34},\hat{p}_t) \times \\ &\times i\Gamma^{(\mathbb{PO}\phi)}_{\rho_4\rho_2\alpha_2\beta_2}(p_4,\hat{p}_t)\left(\epsilon^{(\phi)\,\rho_4}(\lambda_4)\right)^* \times \\ &\times i\Delta^{(\mathbb{P})\,\alpha_2\beta_2,\mu_2\nu_2}(s_{24},t_2) \times \\ &\times \bar{u}(p_2,\lambda_2) i\Gamma^{(\mathbb{P}pp)}_{\mu_2\nu_2}(p_2,p_b)u(p_b,\lambda_b),\end{aligned} \tag{2}$$

where $p_{a,b}$, $p_{1,2}$ and $\lambda_{a,b},\lambda_{1,2} = \pm\frac{1}{2}$ denote the four-momenta and helicities of the protons and $p_{3,4}$ and $\lambda_{3,4} = 0, \pm 1$ denote the four-momenta and helicities of the ϕ mesons, respectively. $\hat{p}_t = p_a - p_1 - p_3$, $\hat{p}_u = p_4 - p_a + p_1$, $s_{ij} = (p_i + p_j)^2$, $t_1 = (p_1 - p_a)^2$, $t_2 = (p_2 - p_b)^2$. $\Gamma^{(\mathbb{P}pp)}$ and $\Delta^{(\mathbb{P})}$ denote the proton vertex function and the effective propagator, respectively, for the tensorial pomeron. The corresponding expressions are as follows [21]:

$$\begin{aligned}i\Gamma^{(\mathbb{P}pp)}_{\mu\nu}(p',p) &= -i3\beta_{\mathbb{P}NN}F_1(t) \times \\ &\times \left\{\frac{1}{2}\left[\gamma_\mu(p'+p)_\nu + \gamma_\nu(p'+p)_\mu\right] - \frac{1}{4}g_{\mu\nu}(\not{p}'+\not{p})\right\},\end{aligned} \tag{3}$$

$$\begin{aligned}i\Delta^{(\mathbb{P})}_{\mu\nu,\kappa\lambda}(s,t) &= \frac{1}{4s}\left(g_{\mu\kappa}g_{\nu\lambda} + g_{\mu\lambda}g_{\nu\kappa} - \frac{1}{2}g_{\mu\nu}g_{\kappa\lambda}\right) \times \\ &\times (-is\alpha'_{\mathbb{P}})^{\alpha_{\mathbb{P}}(t)-1},\end{aligned} \tag{4}$$

where $\beta_{\mathbb{P}NN} = 1.87\ \text{GeV}^{-1}$. The pomeron trajectory $\alpha_{\mathbb{P}}(t)$ is assumed to be of the standard linear form (see, e.g., [30]): $\alpha_{\mathbb{P}}(t) = \alpha_{\mathbb{P}}(0) + \alpha'_{\mathbb{P}}\,t$, $\alpha_{\mathbb{P}}(0) = 1.0808$, $\alpha'_{\mathbb{P}} = 0.25\ \text{GeV}^{-2}$.

Our ansatz for the effective propagator of the $C = = -1$ odderon is [21]

$$i\Delta^{(\mathbb{O})}_{\mu\nu}(s,t) = -ig_{\mu\nu}\frac{\eta_{\mathbb{O}}}{M_0^2}(-is\alpha'_{\mathbb{O}})^{\alpha_{\mathbb{O}}(t)-1}$$

with

$$M_0 = 1\ \text{GeV}, \quad \eta_{\mathbb{O}} = \pm 1. \tag{5}$$

Here, $\alpha_{\mathbb{O}}(t) = \alpha_{\mathbb{O}}(0) + \alpha'_{\mathbb{O}}\,t$ and we choose, as an example, $\alpha'_{\mathbb{O}} = 0.25\ \text{GeV}^{-2}$, $\alpha_{\mathbb{O}}(0) = 1.05$.

For the $\mathbb{PO}\phi$ vertex, we use an ansatz with two rank-four tensor functions [20]:

$$\begin{aligned}i\Gamma^{(\mathbb{PO}\phi)}_{\mu\nu\kappa\lambda}(k',k) &= iF^{(\mathbb{PO}\phi)}((k+k')^2,k'^2,k^2) \times \\ &\times \left[2\,a_{\mathbb{PO}\phi}\,\Gamma^{(0)}_{\mu\nu\kappa\lambda}(k',k) - b_{\mathbb{PO}\phi}\,\Gamma^{(2)}_{\mu\nu\kappa\lambda}(k',k)\right].\end{aligned} \tag{6}$$

We take the factorized form for the $\mathbb{PO}\phi$ form factor:

$$\begin{aligned}&F^{(\mathbb{PO}\phi)}((k+k')^2,k'^2,k^2) = \\ &= F((k+k')^2)\,F(k'^2)\,F^{(\mathbb{PO}\phi)}(k^2),\end{aligned} \tag{7}$$

where $F(k^2) = (1 - k^2/\Lambda^2)^{-1}$ and $F^{(\mathbb{PO}\phi)}(m_\phi^2) = 1$. The coupling parameters $a_{\mathbb{PO}\phi}$, $b_{\mathbb{PO}\phi}$ and the cutoff parameter Λ^2 could be adjusted to the WA102 experimental data [25].

At low $\sqrt{s_{34}} = \text{M}_{\phi\phi}$, the Regge type of interaction is not realistic and should be switched off. To achieve this, we multiplied the $\mathbb{O}$-exchange amplitude by a purely phenomenological factor: $F_{\rm thr}(s_{34}) = 1 - - \exp[(s_{\rm thr} - s_{34})/s_{\rm thr})]$ with $s_{\rm thr} = 4m_\phi^2$.

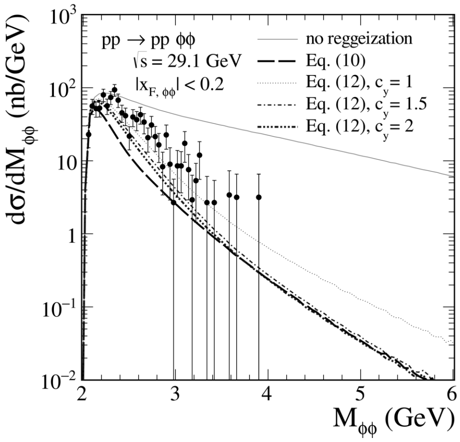

a

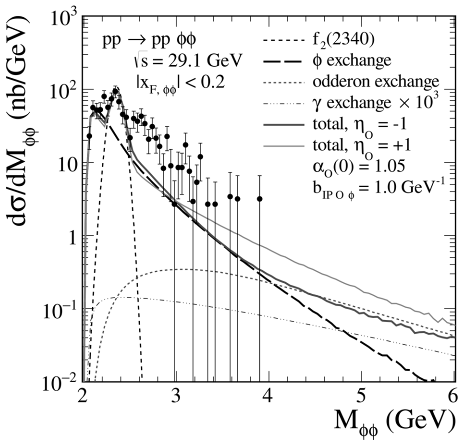

b

Fig. 2. Distributions in the $\phi\phi$ invariant mass. The calculations were done for $\sqrt{s} = 29.1$ GeV and $|x_{F,\phi\phi}| \leqslant 0.2$. The WA102 experimental data from [25] are shown. In the top panel, the green solid line corresponds to the non-reggeized ϕ-exchange contribution. The results for two prescriptions of the reggeization, (10) and (12), are shown by the black and blue lines, respectively. In the bottom panel, we show the complete results including the $f_2(2340)$-resonance contribution and the continuum processes due to the reggeized-ϕ, odderon, and photon exchanges. The black long-dashed line corresponds to the ϕ-exchange contribution and the black dashed line corresponds to the $f_2(2340)$ contribution. The red dotted line represents the odderon-exchange contribution for $a_{\mathbb{P}\mathbb{O}\phi} = 0$ and $b_{\mathbb{P}\mathbb{O}\phi} = 1.0$ GeV^{-1} in (6)

The amplitude for the process shown in Fig. 1, *b* has the same form as the amplitude with the $\mathbb{O}$ exchange, but we have to make the following replacements:

$$i\Gamma^{(\mathbb{P}\mathbb{O}\phi)}_{\mu\nu\kappa\lambda}(k', k) \to i\Gamma^{(\mathbb{P}\phi\phi)}_{\mu\nu\kappa\lambda}(k', k), \tag{8}$$

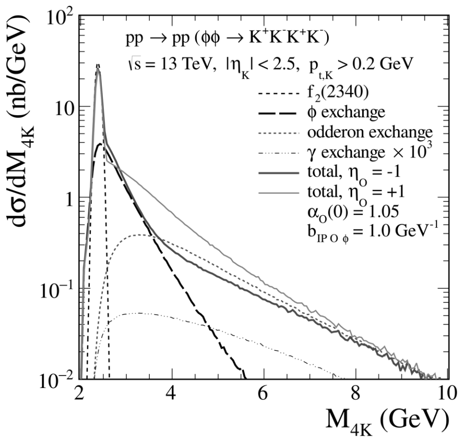

a

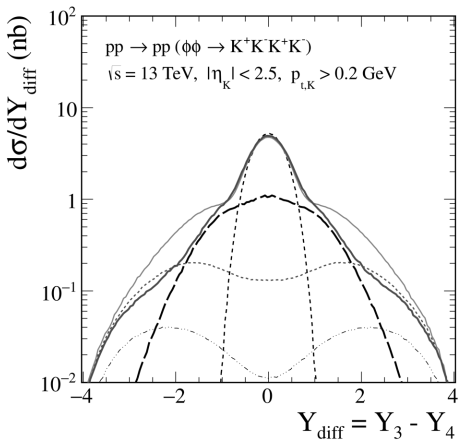

b

Fig. 3. Distributions in M_{4K} (left) and in $Y_{\rm diff}$ (right) for the $pp \to pp(\phi\phi \to K^+K^-K^+K^-)$ reaction calculated for $\sqrt{s} = 13$ TeV and $|\eta_K| < 2.5$, $p_{t,K} > 0.2$ GeV. The coherent sum of all terms is shown by the red and blue solid lines for $\eta_{\mathbb{O}} = -1$ and $\eta_{\mathbb{O}} = +1$, respectively. Here, we take $\alpha_{\mathbb{O}}(0) = 1.05$. The absorption effects are included in the calculations

$$i\Delta^{(\mathbb{O})}_{\mu\nu}(s_{34}, \hat{p}^2) \to i\Delta^{(\phi)}_{\mu\nu}(\hat{p}). \tag{9}$$

We have fixed the coupling parameters of the tensor pomeron to the ϕ meson, based on the HERA experimental data for the $\gamma p \to \phi p$ reaction; see [18].

We should take the reggeization of the intermediate ϕ meson into account. We consider two prescriptions of the reggeization (only expected to hold in the $|\hat{p}^2|/s_{34} \ll 1$ regime):

$$\Delta^{(\phi)}_{\mu\nu}(\hat{p}) \to \Delta^{(\phi)}_{\mu\nu}(\hat{p}) \left(\exp(i\phi(s_{34}))\,\frac{s_{34}}{s_{\rm thr}}\right)^{\alpha_\phi(\hat{p}^2)-1} \tag{10}$$

 ISSN 2071-0186. Ukr. J. Phys. 2019. Vol. 64, No. 8

$$\phi(s_{34}) = \frac{\pi}{2}\exp\left(\frac{s_{\rm thr} - s_{34}}{s_{\rm thr}}\right) - \frac{\pi}{2}, \tag{11}$$

where $s_{\rm thr} = 4m_\phi^2$. Alternatively, we use

$$\Delta^{(\phi)}_{\rho_1\rho_2}(\hat{p}) \to \Delta^{(\phi)}_{\rho_1\rho_2}(\hat{p})\, F(\mathrm{Y_{diff}}) +$$
$$+\, \Delta^{(\phi)}_{\rho_1\rho_2}(\hat{p})\, [1 - F(\mathrm{Y_{diff}})] \times$$
$$\times \left(\exp(i\phi(s_{34}))\, \frac{s_{34}}{s_{\rm thr}}\right)^{\alpha_\phi(\hat{p}^2)-1}, \tag{12}$$

where $F(\mathrm{Y_{diff}}) = \exp(-\mathrm{c_y}|\mathrm{Y_{diff}}|)$. Here, $\mathrm{c_y}$ is an unknown parameter which measures, how rapidly one approaches the Regge regime. This gives the proper Regge behavior for $s_{34} - 4m_\phi^2 \gg 1$ GeV^2; whereas, for smaller s_{34}, we have the mesonic behavior. We take $\alpha_\phi(\hat{p}^2) = \alpha_\phi(0) + \alpha'_\phi\,\hat{p}^2$, $\alpha_\phi(0) = 0.1$ [31], and $\alpha'_\phi = 0.9$ GeV^{-2}.

In order to give realistic predictions, we shall include the absorption effects calculated at the amplitude level and related to the pp nonperturbative interactions. The full amplitude includes the pp-rescattering corrections (absorption effects)

$$\mathcal{M}_{pp\to pp\phi\phi} = \mathcal{M}^{\rm Born} + \mathcal{M}^{\rm absorption},$$
$$\mathcal{M}^{\rm absorption}(s, \boldsymbol{p}_{1t}, \boldsymbol{p}_{2t}) =$$
$$= \frac{i}{8\pi^2 s}\int d^2\boldsymbol{k}_t\, \mathcal{M}^{\rm Born}(s, \tilde{\boldsymbol{p}}_{1t}, \tilde{\boldsymbol{p}}_{2t})\, \mathcal{M}^{(\mathbb{P})}_{\rm el}(s, -\boldsymbol{k}_t^2), \tag{13}$$

where $\tilde{\boldsymbol{p}}_{1t} = \boldsymbol{p}_{1t} - \boldsymbol{k}_t$ and $\tilde{\boldsymbol{p}}_{2t} = \boldsymbol{p}_{2t} + \boldsymbol{k}_t$. $\mathcal{M}^{(\mathbb{P})}_{\rm el}$ is the elastic pp-scattering amplitude with the momentum transfer $t = -\boldsymbol{k}_t^2$.

3. Results

It is very difficult to describe the WA102 data for the $pp \to pp\phi\phi$ reaction including resonances and the ϕ-exchange mechanism only [20]. Inclusion of the odderon exchange improves the description of the WA102 data [25]. The result of our analysis is shown in Fig. 2.

Having fixed the parameters of our quasifit to the WA102 data, we wish to show our predictions for the LHC. In Fig. 3, we show the results for the ATLAS experimental conditions ($|\eta_K| < 2.5$, $p_{t,K} > 0.2$ GeV). The distribution in the four-kaon invariant mass is shown in the top panel, and the difference in rapidities between the two ϕ mesons in the bottom panel. The small intercept of the ϕ-reggeon exchange, $\alpha_\phi(0) = 0.1$, makes the ϕ-exchange contribution steeply falling with increasing M_{4K} and $|\mathrm{Y_{diff}}|$. Therefore, an odderon with an intercept $\alpha_{\mathbb{O}}(0)$ around 1.0 should be clearly visible in the region of large four-kaon invariant masses and for large rapidity distance between the ϕ mesons.

4. Conclusions

By confronting our model results, including the odderon, the reggeized ϕ exchange, and the $f_2(2340)$ resonance exchange contributions, with the WA102 data from [25], we derived an upper limit for the $\mathbb{P}\mathbb{O}\phi$ coupling. advantage of this process for experimental studies is the following. With regard for the typical kinematic cuts for LHC experiments in the $pp \to pp\phi\phi \to ppK^+K^-K^+K^-$ reaction, we have found that the odderon exchange contribution should be distinguishable from other contributions for a large rapidity distance between the outgoing ϕ mesons and in the region of large four-kaon invariant masses. At least, it should be possible to derive an upper limit on the odderon contribution in this reaction.

Our results can be summarized in the following way:

• CEP is a particularly interesting class of processes which provides insight to the unexplored soft QCD phenomena. The fully differential studies of the exclusive $pp \to pp\phi\phi$ reaction within the tensor-pomeron and vector-odderon approaches were executed; for more details, see [20].

• Integrated cross-sections of order of a few nb are obtained, including the experimental cuts relevant for the LHC experiments. The distribution in the rapidity difference of both ϕ-mesons could shed light on the $f_2(2340) \to \phi\phi$ coupling, not known at present. Here, we used only one type of $\mathbb{P}\mathbb{P}f_2$ coupling (out of 7 possible; see [14]). We have checked that, for the distributions studied here, the choice of $\mathbb{P}\mathbb{P}f_2$ coupling is not important. This is a different situation compared to the one observed by us for the $pp \to pp(\mathbb{P}\mathbb{P} \to f_2(1270) \to \pi^+\pi^-)$ reaction [14].

• From our model, we have found that the odderon-exchange contribution should be distinguishable from other contributions for a relatively large rapidity separation between the ϕ mesons.

Hence, to study this type of mechanism, one should investigate events with rather large four-kaon invariant masses, outside of the region of resonances. These events are then “three-gap events”: proton–gap–ϕ–gap–ϕ–gap–proton. Experimentally, this should be a clear signature.

• Clearly, an experimental study of CEP of a ϕ-meson pair should be very valuable for clarifying the status of the odderon. At least, it should be possible to derive an upper limit on the odderon contribution to this reaction.

I thank the Organizers of the New Trends in High-Energy Physics conference in Odessa, Ukraine for the hospitality and good organization. P.L. was partially supported by the Polish Scientific Center of the PAS in Kiev.

1. T. Aaltonen *et al.* (CDF Collaboration). Measurement of central exclusive $\pi^+\pi^-$ production in pp collisions at $\sqrt{s} =$ $= 0.9$ and 1.96 TeV at CDF. *Phys. Rev. D* **91**, 091101 (2015).
2. CMS Collaboration. Measurement of total and differential cross sections of central exclusive $\pi^+\pi^-$ production in proton-proton collisions at 5.02 and 13 TeV. CMS-PAS-FSQ-16-006.
3. R. Sikora (STAR Collaboration). Recent results on Central Exclusive Production with the STAR detector at RHIC. arXiv:1811.03315 [hep-ex].
4. R. Staszewski, P. Lebiedowicz, M. Trzebinski, J. Chwastowski, A. Szczurek. Exclusive $\pi^+\pi^-$ production at the LHC with forward proton tagging. *Acta Phys. Polon. B* **42**, 1861 (2011).
5. L. Łukaszuk, B. Nicolescu. A possible interpretation of pp rising total cross-sections. *Lett. Nuovo Cim.* **8**, 405 (1973).
6. A. Breakstone. Measurement of $\bar{p}p$ and pp elastic scattering in the dip region at $\sqrt{s} = 53$ GeV. *Phys. Rev. Lett.* **54**, 2180 (1985).
7. TOTEM Collaboration. First determination of the ρ parameter at $\sqrt{s} = 13$ TeV – probing the existence of a colourless three-gluon bound state. arXiv:1812.04732 [hep-ex]; arXiv:1812.08610 [hep-ex].
8. A. Schäfer, L. Mankiewicz, O. Nachtmann. Double-diffractive J/ψ and φ production as a probe for the odderon. *Phys. Lett. B* **272**, 419 (1991).
9. C. Ewerz. The odderon in quantum chromodynamics. arXiv:0306137 [hep-ph].
10. L. Adamczyk *et al.* (STAR Collaboration). Single spin asymmetry AN in polarized proton–proton elastic scattering at $\sqrt{s} = 200$ GeV. *Phys. Lett. B* **719**, 62 (2013).
11. A. Bolz, C. Ewerz, M. Maniatis, O. Nachtmann, M. Sauter, A. Schoning. Photoproduction of $\pi^+\pi^-$ pairs in a model with tensor-pomeron and vector-odderon exchange. *JHEP* **1501**, 151 (2015).
12. P. Lebiedowicz, O. Nachtmann, A. Szczurek. Exclusive central diffractive production of scalar and pseudoscalar mesons; tensorial vs. vectorial pomeron. *Annals Phys.* **344**, 301 (2014).
13. P. Lebiedowicz, O. Nachtmann, A. Szczurek. ρ^0 and Drell–Soding contributions to central exclusive production of $\pi^+\pi^-$ pairs in proton-proton collisions at high energies. *Phys. Rev. D* **91**, 074023 (2015).
14. P. Lebiedowicz, O. Nachtmann, A. Szczurek. Central exclusive diffractive production of the $\pi^+\pi^-$ continuum, scalar, and tensor resonances in pp and $p\bar{p}$ scattering within the tensor Pomeron approach. *Phys. Rev. D* **93**, 054015 (2016).
15. P. Lebiedowicz, O. Nachtmann, A. Szczurek. Exclusive diffractive production of $\pi^+\pi^-\pi^+\pi^-$ via the intermediate $\sigma\sigma$ and $\rho\rho$ states in proton-proton collisions within tensor Pomeron approach. *Phys. Rev. D* **94**, 034017 (2016).
16. P. Lebiedowicz, O. Nachtmann, A. Szczurek. Central production of ρ^0 in pp collisions with single proton diffractive dissociation at the LHC. *Phys. Rev. D* **95**, 034036 (2017).
17. P. Lebiedowicz, O. Nachtmann, A. Szczurek. Central exclusive diffractive production of $p\bar{p}$ pairs in proton-proton collisions at high energies. *Phys. Rev. D* **97**, 094027 (2018).
18. P. Lebiedowicz, O. Nachtmann, A. Szczurek. Towards a complete study of central exclusive production of K^+K^- pairs in proton-proton collisions within the tensor Pomeron approach. *Phys. Phys. D* **98**, 014001 (2018).
19. P. Lebiedowicz, O. Nachtmann, A. Szczurek. Extracting the pomeron-pomeron-$f_2(1270)$ coupling in the $pp \to$ $\to pp\pi^+\pi^-$ reaction through angular distributions of the pions. arXiv:1901.07788 [hep-ph].
20. P. Lebiedowicz, O. Nachtmann, A. Szczurek. Central exclusive diffractive production of $K^+K^-K^+K^-$ via the intermediate $\phi\phi$ state in proton-proton collisions. *Phys. Rev. D* **99**, 094034 (2019).
21. C. Ewerz, M. Maniatis, O. Nachtmann. A model for soft high-energy scattering: Tensor pomeron and vector odderon. *Annals Phys.* **342**, 31 (2014).
22. C. Ewerz, P. Lebiedowicz, O. Nachtmann, A. Szczurek. Helicity in proton–proton elastic scattering and the spin structure of the pomeron. *Phys. Lett. B* **763**, 382 (2016).
23. A. Etkin *et al.* Increased statistics and observation of the g_T, $g_{T'}$, and $g_{T''}$ 2^{++} resonances in the Glueball enhanced channel $\pi^-p \to \varphi\varphi n$. *Phys. Lett. B* **201**, 568 (1988).
24. D. Aston *et al.* Strangeonium production from LASS. *Nucl. Phys. Proc. Suppl.* **21**, 5 (1991).
25. D. Barberis *et al.* (WA102 Collaboration). A Study of the centrally produced phi phi system in pp interactions at 450-GeV/c. *Phys. Lett. B* **432**, 436 (1998).
26. M. Ablikim *et al.* (BESIII Collaboration). Observation of pseudoscalar and tensor resonances in $J/\psi \to \gamma\phi\phi$. *Phys. Rev. D* **93**, 112011 (2016).
27. C.J. Morningstar, M.J. Peardon. Glueball spectrum from an anisotropic lattice study. *Phys. Rev. D* **60**, 034509 (1999).
28. R. Fiore, L. Jenkovszky, R. Schicker. Resonance production in Pomeron–Pomeron collisions at the LHC. *Eur. Phys. J. C* **76**, 38 (2016).

29. R. Fiore, L. Jenkovszky, R. Schicker. Exclusive diffractive resonance production in proton–proton collisions at high energies. *Eur. Phys. J. C* **78**, 468 (2018).
30. A. Donnachie, H.G. Dosch, P.V. Landshoff, O. Nachtmann. *Pomeron Physics and QCD* (Cambridge Univ. Press, 2002).
31. P.D.B. Collins. *Regge Theory and Particle Physics* (Univ. of Durham, 1970).

Received 08.07.19

П. Лебедович

ПОШУКИ ОДДЕРОНА
В ЕКСКЛЮЗИВНИХ РЕАКЦІЯХ

Р е з ю м е

Обговорюємо можливість користуватися процесом $pp \to \to pp\phi\phi$ для ідентифікації обміну оддероном. До цього часу немає однозначного експериментального доказу існування оддерона – партнера померона з негативним зарядовим спряженням, $C = -1$. Минулорічні результати Колаборації TOTEM вказують на те, що оддерон може спричиняти розбіжність між теоретичними розрахунками та даними TOTEM про пружне розсіяння протонів. Ми презентуємо нові результати досліджень центрального ексклюзивного народження (CEP) пар $\phi\phi$ в протонних зіткненнях. Ми разглядаємо фузію померонів у $\phi\phi$ ($\mathbb{PP} \to \phi\phi$) через континуум завдяки обміну в $\hat{t}$- і $\hat{u}$-каналах реджезованого ϕ-мезона, фотона та оддерона, а також резонансного процесу в s-каналі ($\mathbb{PP} \to f_2(2340) \to \phi\phi$). Частинка f_2 є кандидатом на тензорний глюбол. Амплітуда процесу формулюється в рамках підходу, де померон є тензором, а оддерон є вектором. Деякі з параметрів моделі визначаються з порівняння з експериментальними даними WA102. Дані WA102 не виключають обмін оддероном для великих інваріантних мас $\phi\phi$. Сигнал з великими значеннями $M_{\phi\phi}$ або $Y_{\rm diff}$ на LHC буде таким чином вказувати на присутність обміну оддероном. Цей процес привабливий ще тим, що в ньому оддерон не прив'язується до протона.

https://doi.org/10.15407/ujpe64.8.702

S.A. LUKASHEVICH, N.V. MAKSIMENKO

Francisk Skorina Gomel State University
(98, Sovetskaya Str., Gomel 246019, Belarus; e-mail: lukashevich@gsu.by)

THE CONSTRUCTION OF RELATIVISTICALLY INVARIANT EQUATIONS OF MOTION AND THE MOMENTUM ENERGY TENSOR FOR SPIN-1/2 PARTICLES WITH POLARIZABILITIES IN AN ELECTROMAGNETIC FIELD

Within the covariant Lagrangian formalism, the equations of motion for spin-1/2 particles with polarizabilities in an electromagnetic field have been obtained. We have analyzed the phenomenological tensor constant quantities as well.

Keywords: covariant Lagrangian, equations of motion, energy-momentum tensor.

1. Introduction

The interaction of an electromagnetic field with structural particles in the electrodynamics of hadrons is based on the main principles of relativistic quantum field theory. In the model conceptions, where basically the diagram technique is used, a number of features for the interaction of photons with hadrons have been determined [1, 2]. However, the diagram technique is mainly employed for the description of electromagnetic processes in the simplest quark systems. In the case of interaction for the electromagnetic field with complex quark-gluon systems in the low-energy region, the perturbative methods of QCD are nonapplicable. That is why, the low-energy theorems and sum rules were widely used lately [3–6]. In the present time, the low-energy electromagnetic characteristics which are connected with a hadron structure, such as the formfactor and polarizabilities, can be obtained from nonrelativistic theory [5]. Passing from the nonrelativistic electrodynamics to the relativistic field theory, one can use the correspondence principle. But it is necessary to investigate, step-by-step, a transition from the covariant Lagrangian formalism to the Hamiltonian one [7–9].

The determination of the interaction vertex of γ-photons with protons taking the polarizabilities into account [10] has recently been used to fit experimental data on the Compton scattering on a proton in the energy neighborhood of a birth of the $\Delta(1232)$-resonance [11].

This work is a continuation of the researches which have been presented in our previous articles [6–8]. Using the covariant Lagrangian of interaction of the electromagnetic field with a structural polarizable particle, the equations of motion and the canonical and metric energy-momentum tensors have been obtained.

2. Total Lagrangian

The total Lagrangian of the interaction of spin-1/2 particles with the electromagnetic field consists of the Lagrangian for the free electromagnetic field L_{e-m}, the spinor or Dirac field L_D, the Lagrangian of the interaction of the free electromagnetic field with the Dirac field $L_{\text{int}-D}$, and the Lagrangian which considers electric and magnetic polarizabilities of particles $L_{\alpha_0\beta_0-D}$:

$$L_{\text{total}-D} = L_{e-m} + L_D + L_{\text{int}-D} + L_{\alpha_0\beta_0-D},$$

thus,

$$L_{\text{total}-D} = -\frac{1}{4}F_{\alpha\beta}F^{\alpha\beta} + \overline{\psi}\left(\frac{1}{2}i\gamma_\alpha \overset{\leftrightarrow}{\partial^\alpha} - m\right)\psi - - e(\overline{\psi}\gamma_\alpha\psi)A^\alpha + K_{\sigma\nu}\Theta^{\sigma\nu}, \quad (1)$$

where

$$K_{\sigma\nu} = \frac{2\pi}{m}\left(\alpha_0 F_{\sigma\mu}F^\mu_\nu + \beta_0 \tilde{F}_{\sigma\mu}\tilde{F}^\mu_\nu\right),$$

$$\overset{\leftrightarrow}{\partial_\nu} = \overset{\leftarrow}{\partial_\nu} - \overset{\rightarrow}{\partial_\nu},$$

$$\Theta^{\sigma\nu} = \frac{i}{2}\left(\bar{\psi}\,\gamma^{\sigma}\,\overleftrightarrow{\partial^{\nu}}\,\psi\right),$$

ψ is the wave function of spin-1/2 particles.

In this expression $\tilde{F}_{\mu\nu} = \frac{1}{2}\varepsilon_{\mu\nu\rho\sigma}F^{\rho\sigma}$, where $F_{\mu\nu}$ and $\tilde{F}_{\mu\nu}$ are the tensors of the electromagnetic field, α_0 and β_0 are electric and magnetic polarizabilities, and $\varepsilon_{\mu\nu\rho\sigma}$–Levi-Civita antisymmetric tensor ($\varepsilon^{0123} = 1$).

The part of the Lagrangian with polarizabilities can be rewritten as

$$L^{(\alpha\beta)} = -\frac{1}{4}F_{\mu\nu}G^{\mu\nu} = K_{\sigma\nu}\Theta^{\sigma\nu}, \tag{2}$$

where $G^{\mu\nu}$ is the antisymmetric tensor $G^{\mu\nu} = -G^{\nu\mu}$ and is equal to

$$G^{\mu\nu} = -\frac{\partial L^{(\alpha\beta)}}{\partial(\partial_\mu A_\nu)} = \frac{4\pi}{m}\big((\alpha_0+\beta_0)(F^{\mu}_{\sigma}\widetilde{\Theta}^{\rho\nu} -$$
$$- F^{\nu}_{\rho}\widetilde{\Theta}^{\rho\mu}) - \beta_0\Theta^{\rho}_{\rho}F^{\mu\nu}\big), \tag{3}$$

where
$\widetilde{\Theta}^{\rho\nu} = 1/2(\Theta^{\rho\nu} + \Theta^{\nu\rho})$.

3. Equations of Motion

For the interaction of the spinor and electromagnetic fields, the following system of equations is used:

$$-\frac{\partial L}{\partial A_\mu} + \partial_\gamma\frac{\partial L}{\partial(\partial_\gamma A_\mu)} = 0, \tag{4}$$
$$-\frac{\partial L}{\partial\overline{\psi}} + \partial_\gamma\frac{\partial L}{\partial(\partial_\gamma\overline{\psi})} = 0, \tag{5}$$
$$-\frac{\partial L}{\partial\psi} + \partial_\gamma\frac{\partial L}{\partial(\partial_\gamma\psi)} = 0, \tag{6}$$

where A_μ is the vector-potential of the electromagnetic field.

From Lagrangian (1) and expressions (4–6), we get the equations of motion for a charged spin-1/2 particle with α_0-electric and β_0-magnetic polarizabilities:

$$\partial_\mu F^{\mu\nu} = e\overline{\psi}\gamma^\nu\psi - \partial_\mu G^{\mu\nu}, \tag{7}$$

$$(i\gamma^\nu\,\overrightarrow{\partial_\nu} - m)\psi = eA_\nu\gamma^\nu\psi - \frac{i}{2}(\partial^\nu K_{\sigma\nu}\gamma^\sigma)\psi -$$
$$- iK_{\sigma\nu}\gamma^\sigma\partial^\nu\psi, \tag{8}$$

$$\bar{\psi}\,(i\,\overleftarrow{\partial_\nu}\,\gamma^\nu + m) = -e\,\bar{\psi}\,A_\nu\gamma^\nu -$$
$$- \frac{i}{2}\,\bar{\psi}\,(\partial^\nu K_{\sigma\nu}\gamma^\sigma) - i(\partial^\nu\,\bar{\psi})\gamma^\sigma K_{\sigma\nu}. \tag{9}$$

In expression (7), $e\overline{\psi}\gamma^\nu\psi$ is the current associated with a charge, $-\partial_\mu G^{\mu\nu}$ is the current associated with the polarizabilities of the particle.

Following work [12], we perform a relativistic generalization of the phenomenological energy-momentum tensor of the interaction of the electromagnetic field with a polarizable particle as

$$T^{\mu\nu} = T^{\mu\nu}_0 + T^{\mu\nu}_{(\alpha\beta)\mathrm{int}}. \tag{10}$$

Lagrangian (1) takes the form

$$L_{\mathrm{total}-D} = L_0 + L_{\mathrm{int}}, \tag{11}$$

where
$$L_0 = -\frac{1}{4}F_{\alpha\beta}F^{\alpha\beta} + \overline{\psi}\left(\frac{1}{2}i\gamma_\alpha\,\overleftrightarrow{\partial^\alpha} - m\right)\psi$$

is the usual Lagrangian, and

$$L_{\mathrm{int}} = -e(\overline{\psi}\gamma_\alpha\psi)A^\alpha + K_{\sigma\nu}\Theta^{\sigma\nu}$$

is the interaction Lagrangian of the electromagnetic field and a particle with polarizabilities.

With the help of Lagrangian (11), the canonical energy-momentum tensor looks like

$$T^{\mu\nu}_{\mathrm{can}} = \frac{\partial L_0}{\partial(\partial_\mu A_\rho)}(\partial^\nu A_\rho) + \partial^\nu\bar{\psi}\frac{\partial L_0}{\partial(\partial_\mu\bar{\psi})} + \frac{\partial L_0}{\partial(\partial_\mu\psi)}\partial^\nu\psi -$$
$$- g^{\mu\nu}\left(-\frac{1}{4}F_{\alpha\beta}F^{\alpha\beta} - \frac{1}{4}F_{\alpha\beta}G^{\alpha\beta}\right).$$

As a result, we get

$$T^{\mu\nu}_{\mathrm{can}} = T^{\mu\nu}_{\mathrm{can}(0)} + \frac{g^{\mu\nu}}{4}G_{\rho\sigma}F^{\rho\sigma}, \tag{12}$$

where $\frac{g^{\mu\nu}}{4}G_{\rho\sigma}F^{\rho\sigma}$ is the energy-momentum tensor of the interaction of the electromagnetic field with regard for the polarizabilities of the particle, and

$$T^{\mu\nu}_{\mathrm{can}(0)} = -F^{\mu\rho}\partial^\nu A_\rho + \frac{g^{\mu\nu}}{4}F_{\rho\sigma}F^{\rho\sigma} + \Theta^{\mu\nu}.$$

Using the unambigious definition of a energy-momentum tensor for $T^{\mu\nu}_{\mathrm{can}}$, we construct the metric energy-momentum tensor:

$$T^{\mu\nu}_{\mathrm{metr}} = T^{\mu\nu}_{\mathrm{can}(0)} + \partial_\rho(F^{\mu\rho}A^\nu) + \frac{g^{\mu\nu}}{4}G_{\rho\sigma}F^{\rho\sigma}. \tag{13}$$

Thus, $T^{\mu\nu}_{\mathrm{metr}}$ reads

$$T^{\mu\nu}_{\mathrm{metr}} = F^{\mu\rho}F^{\nu}_{\rho} + \frac{g^{\mu\nu}}{4}F_{\rho\sigma}F^{\rho\sigma} + \Theta^{\mu\nu} -$$

$$-j^{\mu}A^{\nu}+\frac{g^{\mu\nu}}{4}G_{\rho\sigma}F^{\rho\sigma}, \tag{14}$$

where j^{μ} is the current density of the charged particle.

In the rest frame of the particle, we obtain the energy density of interaction for the particle with polarizabilities and the electromagnetic field:

$$\mathcal{E}=-\frac{2\pi}{m}\Theta^{00}(\alpha_0\mathbf{E}^2+\beta_0\mathrm{H}^2),$$

where Θ^{00} is the energy density of the spin-1/2 particle.

4. Conclusion

Taking the covariant Lagrangian of interaction of the electromagnetic field with a polarizable spin-1/2 particle as a basis in the Lagrangian covariant formalism, the equations of motion have been found. The correlations between the covariant Lagrangian and the canonical and metric energy-momentum tensors have been obtained. In the rest frame of the particle, the energy density of interaction for the particle with polarizabilities and the electromagnetic field has been determined.

1. S.J. Brodsky, J.R. Primack. The electromagnetic interaction of composite systems. *Annals of Physics* **52**, 315 (1969).
2. S. Scherer, A. Yu. Korchin, J.H. Koch. Virtual Compton scattering off the nucleon at low energies. *Phys. Rev. C* **54**, 904 (1996).
3. M.I. Levchuk, L.G. Moroz. Gyration nucleon as one of the characteristics of its electromagnetic structure. *Vesti AN BSSR Ser.: fiz.-mat. nauk* **1**, 49 (1985).
4. A.J. L'vov, V.A. Petrun'kin. Dispersion theory of proton Compton scattering in the first and second resonance regions. *Phys. Rev. C* **55**, 359 (1997).
5. M.-Th. Hutt, A.J. L'vov, A.J. Milstein, M. Schumacher. Compton scattering by nuclei. *Phys. Reports* **323**, No. 6, 458 (2000).
6. N.V. Maksimenko, L.G. Moroz. Phenomenological description polarizabilities of elementary particles in a field-theory. In: *Proc. 11 Intern. School on High Energy Physics and Relativistic Nucl. Phys. Dubna JINR* **D2-11707**, 533 (1979).
7. S.A. Belousova, N.V. Maksimenko. The description for spin polarizabilities based on the covariant Lagrangian. In *Proc. of "OFTHEP'2000". Tver, Russia*, 305 (2000), hep-ph/0009334.
8. N.V. Maksimenko, O.M. Deruzhkova, S.A. Lukashevich. The electromagnetic characteristics of hadrons in the covariant Lagrangian approach. In *Proc. of Intern. School-Seminar "Actual Problems of Particles Physics", Gomel, 2001. JINR* **2**, 145 (2002).
9. D. Babusci, J. Jiordano, A.J. L'vov, J. Matone, A.N. Nathan. Low-energy Compton scattering of polarized photons on polarized nucleons. *Phys. Rev. C* **58**, 1013 (1998).
10. A. Ilyichev, S. Lukashevich, N. Maksimenko. Static polarizability vertex and its application. arXiv: hep-ph/0611327v1.
11. Y. Zhang, K. Savvidy. Proton Compton scattering in a unified proton Δ^+ model. *Phys. Rev. C* **88**, No. 6, 064614 (2013). arXiv:1305.3847 [hep-ph] NITS-PHY-2013002.
12. C. Itzykson, J.B. Zuber. *Quantum Field Theory* (McGraw-Hill, 1980).

Received 08.07.19

С.А. Лукашевич, Н.В. Максименко

ПОБУДОВА РЕЛЯТИВІСТСЬКО-ІНВАРІАНТНИХ РІВНЯНЬ РУХУ ТА ТЕНЗОР ЕНЕРГІЇ-ІМПУЛЬСУ ДЛЯ ЧАСТИНОК ЗІ СПІНОМ 1/2 З ПОЛЯРИЗОВНІСТЮ В ЕЛЕКТРОМАГНІТНОМУ ПОЛІ

Р е з ю м е

В рамках коваріантного лагранжового формалізму отримано рівняння руху для частинок зі спіном 1/2 з поляризовністю в електромагнітному полі. Нами також проаналізовано феноменологічні тензорні константи.

https://doi.org/10.15407/ujpe64.8.705

M.V.T. MACHADO

High Energy Physics Phenomenology Group, GFPAE IF-UFRGS
Caixa Postal 15051, CEP 91501-970
(Av. Bento Goncalves 9500, Porto Alegre, RS, Brazil; e-mail: magnus@if.ufrgs.br)

INVESTIGATING THE SOFT PROCESSES WITHIN THE QCD COLOR DIPOLE PICTURE

We consider the QCD parton saturation models to describe the soft interactions at the high-energy limit. The total and elastic cross-sections, as well as the elastic slope parameter, are obtained for proton-proton and pion-proton collisions and compared to recent experimental results.

Keywords: color dipole picture, QCD parton saturation, Regge theory.

1. Introduction

Describing the soft processes with the use of the QCD degrees of freedom is a quite difficult task, since they are dominated by a long distance (non-perturbative) physics. It has been shown that the soft observables as the total and elastic cross-sections depend on the transition region between the high parton density system (saturation domain) and the perturbative QCD region [1–3]. The parton saturation phenomenon [4–6] is a well-established property of high-energy systems and gives a high-quality description of inclusive and exclusive deep inelastic scattering (DIS) data. As evidences of the successfulness of such approach, we quote the description of the light meson photoproduction cross-section [7–12] and diffractive DIS (DDIS) [13, 14]. Both are semihard processes, where an important contribution to the cross-section comes from the kinematic region in a vicinity of the saturation momentum, Q_s. This dimensional scale increases in the high-energy region. A well-known formalism, which is intuitive, and where the saturation physics can be easily implemented, is the QCD color dipole picture. It is expected [1] that the soft processes measured, for instance, at the Large Hadron Collider (LHC) in hadron-hadron collisions probe the distances about $r \sim 1/Q_s \ll R_h$, with R_h being the hadron radius. In this context, the hadron scattering at the LHC could be described by color dipoles as the correct degrees of freedom even at large transverse distances. Moreover, it has been shown that the cross-sections for soft hadron-hadron collisions within saturation approaches satisfy the Froissart–Martin bound [2,3]. In this context, the role played by the unitarized hard Pomeron contribution to the soft observables has been carefully discussed in Refs. [15, 16].

Here, we will investigate the soft observable in the small-t regime within the color dipole picture and parton saturation approaches. The paper is organized as follows. In the next section, we summarize the theoretical information to compute the cross-section for hadron-hadron collisions in two color dipole approaches. First, we consider the asymptotic cross-section following Ref. [3], where the pp cross-section is assumed to be dominated by the two-gluon production in the final state, $pp \to gg + X$. There, the main ingredients are the gluon distribution of a projectile and the partonic cross-section associates to the interaction $gN \to gg + X$. We also consider the model presented in Ref. [1], where the virtual photon wave-function is replaced by the corresponding wave-function for the hadron projectile. The hadron-proton interaction is computed using the dipole-proton amplitude constrained from DIS data. The numerical results from both models are compared to experimental measurements focusing in the LHC kinematic regime. Finally, we discuss the main theoretical uncertainties and present the main conclusions.

2. Theoretical Frameworks and Their Phenomenological Applications

Our first investigation will consider the color dipole approach applied to hadron-hadron collisions proposed in Refs. [3]. For simplicity, we address initially the case for proton-proton collisions in colliders. The formalism is able to provide us the production cross-section of (heavy or light) quark pairs or gluons at the final state. Namely, similarly to photon-hadron interactions, the total quark production cross-section is given by [17, 18]

$$\sigma(pp \to q\bar{q}X) = 2 \int_0^{-\ln\left(\frac{2m_q}{\sqrt{s}}\right)} dy\, x_1 G\left(x_1, \mu_F^2\right) \times$$
$$\times\, \sigma(GN \to q\bar{q}X), \tag{1}$$

where $y = \frac{1}{2}\ln(x_1/x_2)$ is the rapidity of the pair, $\mu_F \sim m_Q$ is the factorization scale. The quantity $x_1 G(x_1, \mu_F^2)$ is the projectile gluon density on the scale μ_F, and the partonic cross-section $\sigma(GN \to$ $\to q\bar{q}X)$ is given by [17]

$$\sigma(GN \to q\bar{q}X) = \int dz\, d^2 \left|\Psi_{G\to q\bar{q}}(z,)\right|^2 \sigma_{q\bar{q}G}(z,),$$

with $\Psi_{G\to q\bar{q}}$ being the pQCD calculated distribution amplitude, which describes the dependence of the $|q\bar{q}\rangle$ Fock component on the transverse separation and the fractional momentum. It is given by,

$$|\Psi_{G\to q\bar{q}}(z,\mathbf{R})|^2 = \frac{\alpha_s(\mu_R)}{(2\pi)^2}\Big\{m_q^2 k_0^2(m_q r) +$$
$$+ \left[z^2 + (1-z)^2\right] m_q^2 k_1^2(m_q r)\Big\}, \tag{2}$$

where $\alpha_s(\mu_R)$ is the strong coupling constant, which is probed on a renormalization scale $\mu_R \sim m_Q$. We note that the wavefunction will lead to a dominance of dipole sizes around $r \sim 1/m_q$ in the corresponding r-integration. Therefore, for the heavy quark production, the color transparency behavior from the dipole cross-section, $\sigma_{\rm dip}(r) \propto r^2$, will be the main contribution (pQCD). In the charm case, an important contribution should come from the saturation region, since the typical dipole size, $r \simeq 1$ GeV^{-1}, can reach an order of magnitude similar to the saturation radius, $R_s(x) = 1/Q_s(x) \propto (\sqrt{s})^{-\lambda/2}$ (with $\lambda \simeq$ $\simeq 0.3$). On the other hand, for light quarks, $m_q \simeq$ $\simeq 0.14$ GeV, we are deep in the parton saturation (very low-x_2 and a small scale of the probe) and non-perturbative regions. This will be the case in the following calculation.

In the partonic cross-section, $\sigma_{q\bar{q}G}$ is the cross-section for the scattering of a color neutral quark-antiquark-gluon system on the target and is directly connected with the dipole cross-section:

$$\sigma_{q\bar{q}G} = \frac{9}{8}\left[\sigma_{\rm dip}(x_2, z\mathbf{R}) + \sigma_{\rm dip}(x_2, \bar{z}\mathbf{R})\right] -$$
$$- \frac{1}{8}\sigma_{\rm dip}(x_2, \mathbf{R}). \tag{3}$$

Here, the main idea is that, at high energies, a gluon G from the projectile hadron can develop a fluctuation which contains a $Q\bar{Q}$ pair. Interaction with the color field of a target then may release these heavy quarks. Such an approach is valid for high energies, where the coherence length $l_c \approx 1/x_2$ is larger than the target radius. Therefore, it is natural to include the parton saturation effects and to use the fact the dipole cross-section is universal, i.e., it is process-independent. For the sake of completeness, the parton momentum fractions are written in terms of the quark pair rapidity and masses, $x_{1,2} = \frac{2m_Q}{\sqrt{s}}\exp(\pm y)$.

Following Ref. [3], we obtain the asymptotic hadron-hadron cross-section within the color dipole approach considering the dominant process, $pp \to$ $\to GGX$, at high energies. Now, the gluon G from the projectile hadron develops a fluctuation which contains a two-gluon (GG) pair further interacting with target's color field. Accordingly, the expression for the total cross-section for the gluon production at the final state is given by [19],

$$\sigma(pp \to GGX) = 2 \int_0^{-\ln\left(\frac{2m_G}{\sqrt{s}}\right)} dy\, x_1 G\left(x_1, \mu_F^2\right) \times$$
$$\times\, \sigma(GN \to GGX), \tag{4}$$

where the effective gluon mass, m_G, was introduced in order to regularize the calculation. Thus, in this case, one has $x_{1,2} = \frac{2m_G}{\sqrt{s}}\exp(\pm y)$.

The new partonic cross-section $\sigma(GN \to GGX)$ is given by

$$\sigma(GN \to GGX) =$$
$$= \int dz\, d^2\mathbf{R}\, |\Psi_{G\to GG}(z,\mathbf{R})|^2\, \sigma_{GGG}(z,\mathbf{R}), \tag{5}$$

with $\Psi_{G\to GG}$ being the corresponding distribution amplitude associated with the $|GG\rangle$ Fock state. It is obtained from Eq. (2) in the following way: $|\Psi_{G\to GG}|^2 = 2(N_c - 1)|\Psi_{G\to q\bar{q}}|^2$. The partonic cross-section σ_{GGG} is the cross-section for the scattering a a color neutral three-gluon system on the target and is directly related to the dipole cross-section in the following way [19]:

$$\sigma_{GGG} = \frac{1}{2}\left[\sigma_{\rm dip}(x_2, z\mathbf{R}) + \sigma_{\rm dip}(x_2, \bar{z}\mathbf{R}) + \sigma_{\rm dip}(x_2, \mathbf{R})\right]. \tag{6}$$

Now, we will present the corresponding phenomenology using Eq. (4). From Ref. [3], we identify basically two main shortcomings: a very low value for the effective gluon mass, $m_G = 154$ MeV $< \Lambda_{QCD}$ and the identification of the scale μ with the starting evolution scale in the gluon PDFs considered, $\mu^2 = Q_0^2$. Here, we will use the value $m_G = 400$ MeV. Moreover, for the gluon PDF probed on the low scale, $\mu^2 = m_G^2 = 0.16$ GeV^2 will be given for a prediction from the parton saturation physics,

$$x\,G(x, Q^2) = \frac{3\,\sigma_0 Q_s^2}{4\pi^2\alpha_s}\left[1 - \left(1 + \frac{Q^2}{Q_s^2}\right) e^{-\frac{Q^2}{Q_s^2}}\right], \tag{7}$$

where the updated values for the GBW model parameters have been used [20]. Consistently, for the dipole cross-section, we have used the GBW parametrization. It should be noted that the result is parameter-free and corresponds to the soft Pomeron contribution to the cross-section.

In Fig. 1, the result for the total cross-section in proton-proton collisions is presented. Both the low-energy and cosmic rays data are presented. Experimental measurements from colliders are properly identified [21], especially the recent LHC data. The asymptotic model is in a quite good agreement compared to accelerator data, despite no further adjustment has been done. There is some room for fitting the reggeon contribution at low energies.

We have also considered another color dipole approach addressing the soft scattering processes. In such a case, other observables can be described as the elastic cross-section and the elastic slope parameter. We follow Ref. [1] and compute the total cross-section in following way:

$$\sigma_{\rm tot}^{hp}(\sqrt{s}) = 2\int d^2b \int_0^1 dz \int d^2r\,|\Psi_h(r,z)|^2\ N(s,r,b). \tag{8}$$

It depends on the color dipole amplitude, $N(s,r,b)$, and on the hadron wavefunction, $\Psi_h(r,z)$. The expressions resembles the same equation for the DIS

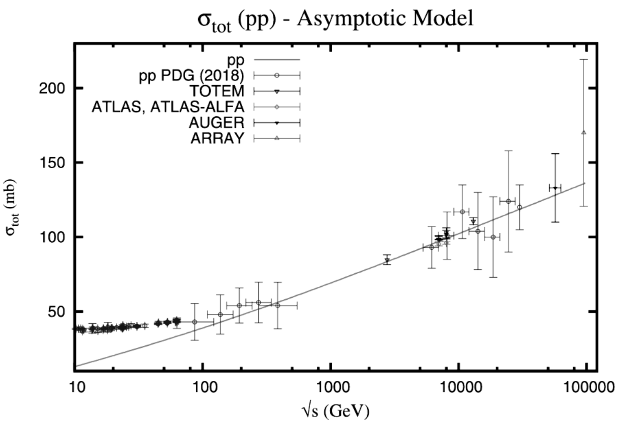

Fig. 1. (pp total cross-section as a function of the center-of-mass-energy, including low-energy and cosmic rays data. The LHC data are explicitly identified (TOTEM and ATLAS Collaborations)

description within the color dipole approach. In other words, the photon wavefunction is replaced by the hadron one. Here, in the meson-proton scattering, a meson is treated as a $q\bar{q}$ pair: the calculation implies that DIS, i.e., the interaction of a color dipole with a proton target and the saturation physics can be embedded in the dipole amplitude. A similar approach has been considered also in Refs. [22–24], where the Pomeron dynamics is written in terms of the dipole-dipole cross-section. For instance, in Ref. [22], the large dipoles are dominated by a soft Pomeron contribution, whereas small dipoles are driven by a hard Pomeron piece (two-Pomeron model with hard and soft Pomerons). On the other hand, in Ref. [23, 24] based on Mueller's cascade model, the authors discussed several contributions including the effect of Pomeron loops.

To characterize mesons and baryons, we use the phenomenological ansatz from Wirbel–Stech–Bauer (WSB) [22] which gives

$$\psi_h(z, \mathbf{r}) = \sqrt{\frac{z(1-z)}{2\pi S_h^2 N_h}}\, e^{-(z-\frac{1}{2})^2/(4\Delta z_h^2)}\, e^{-|\mathbf{r}|^2/(4S_h^2)}, \tag{9}$$

where the hadron wave function normalization to unity, $\int dz d^2r\,|\psi_h(z,\mathbf{r})|^2 = 1$, requires the following normalization constant:

$$N_h = \int_0^1 dz\ z(1-z)\ e^{-(z-\frac{1}{2})^2/(2\Delta z_h^2)}. \tag{10}$$

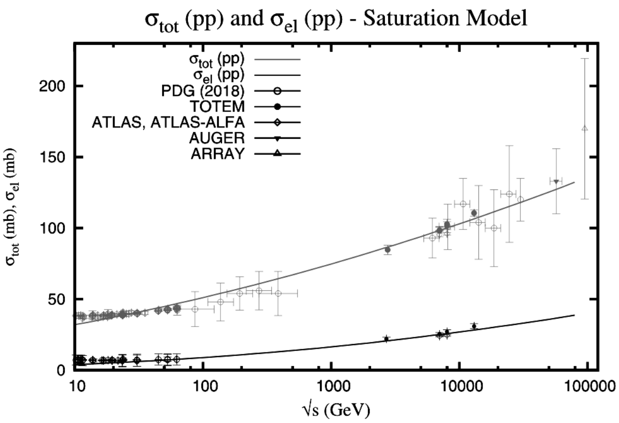

Fig. 2. The total and elastic cross-sections for *pp* collisions. The upper cross-sections are total cross-sections, while the lower ones are the elastic cross-sections. Tevatron, SPS, LHC, and cosmic rays data are presented [21]. The lines are the results from the eikonal-type (saturation) model

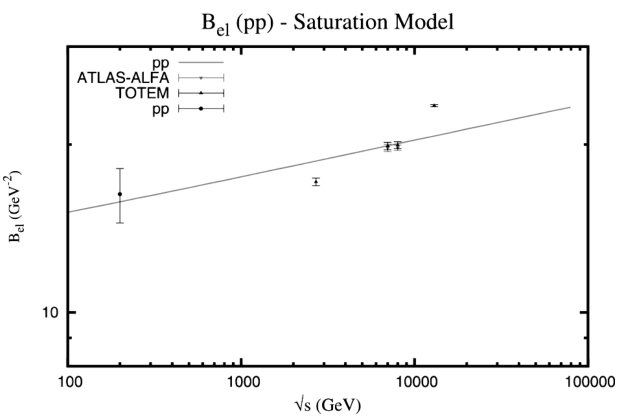

Fig. 3. Slope $B_{\rm el}(s)$ for the *pp* elastic scattering as a function of $\sqrt{s}$. The recent LHC data from TOTEM and ATLAS-ALFA are presented

Therefore, mesons and baryons are assumed to have a $q\bar{q}$ and quark–diquark valence structure. Since quark–diquark systems are equivalent to $q\bar{q}$ systems, this allows us to model not only mesons but also baryons as color-dipoles. The values of the parameters in our case are the following: $\Delta z_h = 0.3\,(2)$ and $S_h = 0.86\,(0.607)$ fm, for $p/\bar{p}\,(\pi^{\pm})$, respectively [22].

Before discussing an impact-parameter dipole amplitude extracted from DIS data, we would need to rewrite the energy dependence from the photon-hadron scattering in terms of the appropriate Bjorken scaling variable-x. In this work, the following ansatz has been considered:

$$\frac{1}{x} = \frac{sr^2}{(s_0\,R_c^2)}, \tag{11}$$

which has been successfully considered in Ref. [25]. Here, $s_0^2 \sim m_h^2$ and $R_c = 0.2$ fm. Such an ansatz is numerically equivalent to the proposal $\frac{1}{x} = \frac{s}{Q_0^2}$, with $Q_0^2 \sim (2m_q)^2 \simeq m_h^2$, done in Ref. [1]. For simplicity and faster numerical calculations, we consider the last relation, where the Q_0^2 parameter will be extracted from the total cross-section data.

We tested an eikonal-like expression for the dipole amplitude, where the impact parameter dependence is factorized from the energy dependence. The function $S(b)$ is described by the dipole profile function. Namely, the amplitude has the following form:

$$\begin{aligned} &N(x,r,b) = 1 - \exp\left(-\frac{1}{2}\hat{\sigma}(x,r)S(b)\right), \\ &\hat{\sigma}(x,r) = \sigma_0\frac{(rQ_s(x))^2}{4}, \quad S(b) = \frac{2\beta b}{\pi R^2}K_1(\beta b), \end{aligned} \tag{12}$$

where we have considered the parameters for $\hat{\sigma}$ from the GBW saturation model [20] and the value $R^2 = 4.5$ GeV^{-2}. Here, the parameter β was defined as $\beta = \frac{\sqrt{8}}{R}$. In Fig. 2, we present the results associated with the application of the model for the b-dependent color dipole amplitude to the *pp* scattering at the accelerator energy regime. Accordingly, we can say that the model adequately describes the proton-proton cross-section data, and we extend it to higher energies to make predictions for cosmic-ray energies. Moreover, in Fig. 3, we present the slope parameter, $B_{\rm el}(s)$ as a function of the center-of-mass energy. We present the comparison against the recent LHC data, and it was found that the description of data is quite reasonable.

In summary, we have applied the color dipole picture to the soft hadron-hadron scattering, by including the parton saturation phenomenon as the transition region between the soft and hard domains. We have shown that the inclusive process is mainly driven for dipole sizes near the saturation radius in the high-energy regime. The main advantage is that the corresponding phenomenology is almost free of parameters, as they are completely constrained from DIS data in *ep* interactions. The models rely on the dipole cross-section or b-dependent dipole amplitude and indicate that the impact parameter profile is crucial for a good data description. The advent of the

LHC opened a new window for the studies of the diffraction and the elastic and inelastic scatterings, as they are not strongly contaminated by non-diffractive events. This is translated in the Regge-theory language saying that the scattering amplitude is completely determined by a Pomeron exchange. The current measurements on these soft observables at the LHC in proton-proton collisions are in a very good shape, covering the energies of 0.9, 2.76, 7, 8, and 13 TeV [21]. In the context of the saturation physics, the soft Pomeron may be understood as an unitarized perturbation Pomeron [26]. It can be shown that the trajectory of a soft Pomeron could emerge as a result of the interplay between perturbative physics of a hard Pormeron and the confining properties of the QCD vacuum. Specifically, the local unitarization in the impact parameter plane can lead to a reasonable description of the intercept and the slope of a soft Pomeron [26]. Our work corroborates those statements, once the soft observable in the small-t regime is correctly described within the color dipole picture and the parton saturation approach.

The author thanks the conference organizers and other presenters for making this valuable opportunity available to all of us. Thank you for your gracious hospitality and professionalism. This work was partially financed by the Brazilian funding agencies CNPq and CAPES.

1. J. Bartels, E. Gotsman, E. Levin, M. Lublinsky, U. Maor. The Dipole picture and saturation in soft processes. *Phys. Lett. B* **556**, 114 (2003).
2. F. Carvalho, F. O. Duraes, V. P. Goncalves, F.S. Navarra. Gluon saturation and the Froissart bound: A Simple approach. *Mod. Phys. Lett. A* **23**, 2847 (2008).
3. C.A. Argueelles, F. Halzen, L. Wille, M. Kroll, M.H. Reno. High-energy behavior of photon, neutrino, and proton cross sections. *Phys. Rev. D* **92**, 074040 (2015).
4. F. Gelis, E. Iancu, J. Jalilian-Marian, R. Venugopalan. *Ann. Rev. Nucl. Part. Sci.* **60**, 463 (2010).
5. H. Weigert. Evolution at small x_bj: The color glass condensate. *Prog. Part. Nucl. Phys.* **55**, 461 (2005).
6. J. Jalilian-Marian, Y.V. Kovchegov. Saturation physics and deuteron–gold collisions at RHIC *Prog. Part. Nucl. Phys.* **56**, 104 (2006).
7. A.C. Caldwell, M.S. Soares. Vector meson production in the Golec-Biernat Wuesthoff model. *Nucl. Phys. A* **696**, 125 (2001);
8. H. Kowalski, D. Teaney. An impact parameter dipole saturation model. *Phys. Rev. D* **68**, 114005 (2003).
9. J.R. Forshaw, R. Sandapen, G. Shaw. Color dipoles and ρ, φ electroproduction. *Phys. Rev. D* **69**, 094013 (2004).
10. C. Marquet, R. Peschanski, G. Soyez. Exclusive vector meson production at HERA from QCD with saturation. *Phys. Rev. D* **76**, 034011 (2007).
11. H. Kowalski, L. Motyka, G. Watt. Exclusive diffractive processes at HERA within the dipole picture. *Phys. Rev. D* **74**, 074016 (2006).
12. N. Armesto, A.H. Rezaeain. *Phys. Rev. D* **90**, 054003 (2014).
13. J.R. Forshaw, R. Sandapen, G. Shaw. Further success of the colour dipole model. *JHEP* **0611**, 025 (2006).
14. K. Golec-Biernat, M.Wüsthoff. Saturation in diffractive deep inelastic scattering. *Phys. Rev. D* **60**, 114023 (1999).
15. J.-R. Cudell, O. V. Selyugin. Unitarisation and black-disk limit at the LHC in the presence of a hard pomeron. *Phys. Lett. B* **662**, 417 (2008).
16. J.-R. Cudell, E. Predazzi, O.V. Selyugin. New analytic unitarisation schemes. *Phys. Rev. D* **79**, 034033 (2009).
17. N.N. Nikolaev, G. Piller, B.G. Zakharov. Inclusive heavy-flavor production from nuclei. *Z. Phys. A* **354**, 99 (1996).
18. B.Z. Kopeliovich, A.V. Tarasov. Gluon shadowing in heavy flavor production off nuclei. *Nucl. Phys. A* **710**, 180 (2002).
19. N.N. Nikolaev, W. Schafer, B.G. Zakharov. Nonlinear $k \perp$ factorization for gluon-gluon dijets produced off nuclear targets *Phys. Rev. D* **72**, 114018 (2005).
20. K. Golec-Biernat, S. Sapeta. Saturation model of DIS: An update. *JHEP* **1803**, 102 (2018).
21. M. Tanabashi *et al.*, (Particle Data Group). Review of Particle Physics. *Phys. Rev. D* **98**, 030001 (2018).
22. A.I. Shoshi, F.D. Steffen, H.J. Pirner. S-matrix unitarity, impact parameter profiles, gluon saturation and high-energy scattering. *Nucl. Phys. A* **709**, 131 (2002).
23. C. Flensburg, G. Gustafson, L. Lonnblad. Elastic and quasi-elastic pp and y^*p scattering in the dipole model. *Eur. Phys. J. C* **60**, 233 (2009)
24. G. Gustafson, L. Lonnblad, A. Ster, T. Csorgo. Total, inelastic and (quasi-)elastic cross sections of high energy pA and γ^* A reactions with the dipole formalism. *JHEP* **1510**, 022 (2015).
25. A. Donnachie, H.G. Dosch. Comprehensive approach to structure functions. *Phys. Rev. D* **65**, 014019 (2002).
26. L. Motyka. Soft pomeron trajectory from a saturation model. *Acta Phys. Polon. B* **34**, 3069 (2003).

Received 08.07.19

М.В.Т. Машадо

ДОСЛІДЖЕННЯ М'ЯКИХ
ПРОЦЕСІВ В РАМКАХ КОЛЬОРОВОГО
ДИПОЛЬНОГО ПІДХОДУ КХД

Р е з ю м е

В роботі ми розглядаємо КХД-партонну модель насичення для опису м'яких процесів при високих енергіях. Отримано повний та пружний перерізи, а також параметр нахилу для розсіяння протонів на протонах та піонів на протонах. Ці результати порівнюються з експерименальними даними.

https://doi.org/10.15407/ujpe64.8.710

P. MINAIEV, V. SKALOZUB
Oles Honchar Dnipro National University
(72, Gagarin Ave., Dnipro 49010, Ukraine; e-mail: minaevp9595@gmail.com)

THE ELECTROWEAK PHASE TRANSITION IN A SPONTANEOUSLY MAGNETIZED PLASMA

We investigate the electroweak phase transition (EWPT) in the Minimal (One Higgs doublet) Standard Model (SM) with account for the spontaneous generation of magnetic and chromomagnetic fields. As it is known, in the SM for the mass of a Higgs boson greater than 75 GeV, this phase transition is of the second order. But, according to Sakharov's conditions for the formation of the baryon asymmetry in the early Universe, it has to be strongly of the first order. In the Two Higgs doublets SM, there is a parametric space, where the first-order phase transition is realized for the realistic Higgs boson mass $m_{\rm H} = 125$ *GeV. On the other hand, in the hot Universe, the spontaneous magnetization of a plasma had happened. The spontaneously generated (chromo) magnetic fields are temperature-dependent. They influence the EWPT. The color chromomagnetic fields* B_3 *and* B_8 *are created spontaneously in the gluon sector of QCD at a temperature* $T > T_d$ *higher the deconfinement temperature* T_d*. The usual magnetic field* H *has also to be spontaneously generated. For* T *close to the* T_{EWPT}*, these magnetic fields could change the kind of the phase transition.*

Keywords: electroweak phase transition, standard model, deconfinement.

1. Introduction

In the Early Universe, there are many phase transitions. The most important is EWPT, when particles acquired masses. Other important problem is baryogenesis.

As is well known, in the Minimal Standard Model (MSM) of elementary particles, EWPT is of the first order for the mass of a Higgs boson less than 75 GeV. For greater masses, it is of the second order. Experiments give $m_{\rm H} = 125$ GeV. Sakharov [1] proposed the conditions for generation of the asymmetry between baryons and antibaryons. Today, they are formulated as three baryogenesis conditions. According to them, the phase transition should be strongly of the first order. So, Sakharov's conditions are violated.

Another important property of non-Abelian gauge fields at high temperatures is a spontaneous vacuum magnetization. It is closely related to the asymptotic freedom, which happens due to a large magnetic moment of charged color gluons (gyromagnetic ratio $\gamma = 2$).

In fact, the asymptotic freedom at high temperatures is always accompanied by the background stable, temperature-dependent, and long-range chromomagnetic fields [2].

The magnetization phenomenon was investigated in the SU(3) gluodynamics in detail [3], and the supersymmetric theories [4, 5] were developed by analytic methods and in the SU(2) gluodynamics [6, 7] by Monte-Carlo simulations on a lattice. In all these cases, the spontaneous creation of magnetic fields was bdetected. Within the application to the early Universe, the spontaneous vacuum magnetization in the electroweak sector of the standard model was described in [8].

At the LHC experiments, a new matter, namely, phase–quark–gluon plasma (QGP), has to be produced in heavy ion collisions. The deconfinement phase transition (DPT) temperature is expected to be of the order of $T_d \sim$180–200 MeV. In theory, the investigation of the DPT and QGP properties were carried out by different method – analytic perturbative and nonperturbative.

In papers [9, 10], we have shown that, due to the vacuum polarization of quark fields by the color magnetic fields B_3 and B_8 existing in the QGP after DPT, the usual magnetic field H can be generated for temperatures $T_d < T < T_{\rm EWPT}$. The field H is temperature-dependent and occupies a large plasma volume as the fields B_3 and B_8 [3].

In the present paper, we will investigate the influence of the magnetic and chromomagnetic fields spontaneously created after DPT on EWPT. The magnetic fields could realize Sakharov's conditions in MSM and change the behavior of phase transitions as in the superconductivity. The proper time representation is used. The effective potential of the external fields $V(\phi, B_3, B_8, H, T)$ with one-loop plus daisy diagrams accounting for the gluons and all quark flavors at finite temperatures is calculated. This field configuration is stable due to the daisy diagram contributions, which cancel the imaginary terms presenting in the one-loop effective potential of charged gluons $V^{(1)}(B_3, B_8, T)$. To estimate the field strengths, the asymptotic high temperature expansion derived by Mellin's transformation technique is applied [2, 11].

2. Effective Potential of MSM with Magnetic Fields at Finite Temperatures

The spontaneous vacuum magnetization has been derived from the investigation of the effective potential (EP) of covariantly constant(soursless) chromomagnetic fields $H^a = H\delta^{a3}$, which is a solution to the classical Yang–Mills field equation, where $H = \text{const}$, and a is an isotopic index,

$$V(H,T) = \frac{H^2}{2} + V^{(1)}(H,T). \tag{1}$$

It includes the tree-level and one-loop parts. The minimum of the EP at a high temperature T corresponds to the nonzero magnetic field.

The Lagrangian of the boson sector of the Salam–Weinberg model is

$$L = -\frac{1}{4}F^a_{\mu\nu}F^{\mu\nu}_a - \frac{1}{4}G_{\mu\nu}G^{\mu\nu} + (D_\mu\Phi)^+(D^\mu\Phi) + \\ + \frac{m^2}{2}(\Phi^2+\Phi) - \frac{\lambda}{4}(\Phi^2+\Phi)^2, \tag{2}$$

where the following standard notations are introduced:

$$F^a_{\mu\nu} = \partial_\mu A^a_\nu - \partial_\nu A^a_\mu + g\varepsilon^{abc}A^b_\mu A^c_\nu, \\ G^a_{\mu\nu} = \partial_\mu B_\nu - \partial_\nu B_\mu, \tag{3} \\ D_\mu = \partial_\mu + \frac{1}{2}igA^a_\mu\tau^a + \frac{1}{2}ig'B_\mu.$$

The vacuum expectation value of the field Φ is

$$\langle\Phi\rangle = \frac{1}{\sqrt{2}}\binom{0}{\phi_c}. \tag{4}$$

The fields of Z-, $W^\pm$-bosons, and photons are

$$W^\pm_\mu = \frac{1}{\sqrt{2}}(A^1_\mu \pm iA^2_\mu), \\ Z_\mu = \frac{1}{\sqrt{g^2+g'^2}}(gA^3_\mu - g'B_\mu), \tag{5} \\ A_\mu = \frac{1}{\sqrt{g^2+g'^2}}(g'A^3_\mu + g'B_\mu).$$

For the investigation of EWPT, according to [9,13], the EP is

$$V(H,T,\phi_c) = \frac{H_8^2}{2} + \frac{H_3^2}{2} + \frac{H^2}{2} + \\ + V^{(0)}(\phi_c) + V^{(1)}(H,T,\phi_c) + V^{(\mathrm{Ring})}(H,T,\phi_c). \tag{6}$$

To compute the EP $V^{(1)}$ in the background magnetic fields, let us introduce the proper time, and s-representation for the Green functions:

$$G^{ab} = -i\int \exp(-is(G^{-1})^{ab})ds. \tag{7}$$

To incorporate the temperature into this formalism, the connection between the Matsubara Green function and the Green function at the zero temperature is needed:

$$G^{ab}_k(x,x';T) = \\ = \sum_{-\infty}^{+\infty}(-1)^{(n+[x])\sigma_k}G^{ab}_k(x-[x]\beta u, x'-n\beta u), \tag{8}$$

where G^{ab}_k is the corresponding function at $T = 0$, $\beta = 1/T$, $u = (0,0,0,1)$, $[x]$ denotes an integer part of $x_4/\beta, \sigma_k = 1$ in the case of physical fermions, and $\sigma_k = 0$ for bosons and ghost fields.

The one-loop contribution to EP is given by the expression

$$V^{(1)} = -\frac{1}{2}\mathrm{Tr}\ \ln G^{ab}, \tag{9}$$

where G^{ab} stands for the propagators of all the quantum fields $W^\pm, Z, ...$ in the background magnetic field H.

The term with $n = 0$ in Eqs. (8) and (9) gives the zero-temperature expression for the Green function and EP, respectively.

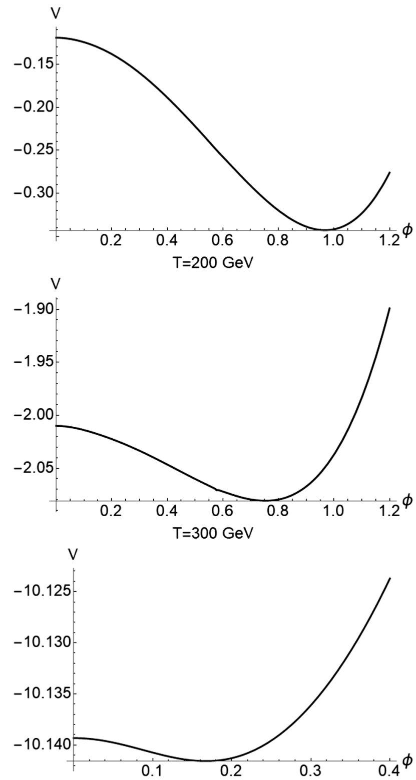

Fig. 1. Effective potential view at different temperatures; the symmetry is broken

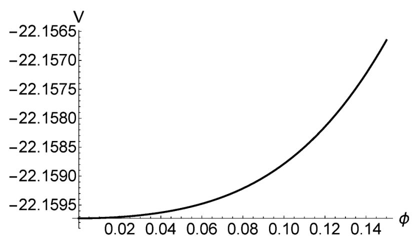

Fig. 2. Effective potential view at a temperature of 365 GeV; the symmetry is restored

Strengths of generated fields

T, GeV	ϕ	V	$H, 10^{21}$ G	$H_3, 10^{23}$ G	$H_8, 10^{23}$ G
100	0.96	−0.35	0.436	0.131	1.092
200	0.75	−2.1	1.97	0.601	3.17
260	0.4	−4.9	3.28	0.928	4.91
300	0.26	−10.14	4.70	1.20	6.66
350	0.11	−18.77	6.66	2.13	9.28
363	0.01	−21.68	6.69	2.18	9.51

In the quark sector of EP, we have the mixing of external magnetic and chromomagnetic fields, according to [9]. The next linear combinations are appear

$$\begin{cases} \mathcal{H}_f^1 = q_f H + g\left(\dfrac{H_3}{2} + \dfrac{H_8}{2\sqrt{3}}\right); \\ \mathcal{H}_f^2 = q_f H + g\left(\dfrac{H_8}{2\sqrt{3}} - \dfrac{H_3}{2}\right); \\ \mathcal{H}_f^3 = q_f H - g\dfrac{H_8}{\sqrt{3}}. \end{cases} \tag{10}$$

They are included in the quark part of EP

$$V_{\text{quark}} = \frac{1}{8\pi^2} \sum_f \sum_{a=1}^{3} \sum_{l=-\infty}^{\infty} (-1)^l \times$$
$$\times \int_0^\infty \frac{ds}{s^3}\, e^{-m_f^2 s - \frac{\beta^2 l^2}{4s}} \left(s\mathcal{H}_f^a \coth\left(s\mathcal{H}_f^a\right) - 1\right). \tag{11}$$

In our calculations, H, H_3, and H_8 are parameters. To investigate EWPT, we need to calculate EP as a function of ϕ_c at some constant temperature and for different temperatures, to look after the behavior of the symmetry, and to find the values of parameters, which minimize EP.

3. Numerical Results

For numerical calculations, we use the following dimensionless parameters:

$$V^0 = \frac{V^{(0)} e^2}{M_W^4}; \quad V^T = \frac{V^{(T)} e^2}{M_W^4}; \quad \phi = \frac{\phi_c}{\delta(0)};$$
$$\mu_f = \frac{m_f}{M_W}; \quad h_{f,a} = \frac{e\mathcal{H}_f^a}{M_W^2}; \quad \beta_p = M_W \beta. \tag{12}$$

After the calculation, we should find the minimum value depending on ϕ, H_3, H_8, and H for a fixed temperature.

The strength of generated fields at the energy minimum is shown in Table. The most important point is the next one – we have nonzero chromomagnetic and magnetic fields and a negative value of EP. The magnetic field is two orders less than the chromomagnetic one.

In Figs. 1 and 2, the behavior of the symmetry is shown. We have minimum of EP with a nonzero scalar field. The symmetry is restored at high temperatures. The critical temperature is obtained near $T_{\text{EWPT}} = 365$ GeV.

4. Conclusions

In our calculations, we applied the consistent approximation for the effective potential accounting for the one-loop plus daisy diagrams. It includes the terms of the order $\sim g^2$ and $\sim g^3$ and makes the potential real due to the cancellation of the imaginary terms. That is sufficient at high temperatures because of small couplings.

The most interesting observation of the above investigation is twofold. First, as the temperature grows, the magnetic field strengths are increased. Second, simultaneously, the value of the effective potential at the minimum is negative.

Really, as we have noted already, the asymptotic freedom at high temperatures has always to be accompanied by the temperature-dependent background magnetic fields [2].

As it follows from the obtained results, the strong chromo(magnetic) fields of the order $H_{3.8} \sim 10^{18}$–10^{19} G and $H \sim 10^{16}$–10^{17} G must be present in QGP [9]. This influences all the processes happening and may serve as the distinguishable signals of DPT. Due to the magnetization, in particular, all the initial states of charged particles have to be discrete ones. These fields are present at higher temperatures, as the deconfinement appears. At temperatures close to $T_{\rm EWPH}$, the strengths are 5 order higher than for the deconfinement temperature.

We have demonstrated that EWPT in MSM has the critical temperature near 360 GeV, and the nonzero magnetic and chromomagnetic fields should be spontaneously generated as well. In Fig. 1, we see that there is no reheating phase. This illustrates that the phase transition is of the second type, and Sakharov's conditions are not satisfied. So, even with magnetic and chromomagnetic fields, the phase transition is of the second order.

As was shown in [12], the Sakharov conditions can be satisfied in the parametric space of the Two Higgs doublet Standard Model without background magnetic fields.

This work is partially supported by the ICTP through AF-06.

1. A.D. Sakharov. Violation of CP Invariance, C asymmetry, and baryon asymmetry of the universe. *JETP Lett.* **5**, 32 (1967).
2. V. Skalozub. Effective coupling constants in gauge theories at high temperature. *Int. J. Mod. Phys. A* **11** 5643 (1996).
3. V. Skalozub, A. Strelchenko. On the generation of Abelian magnetic fields in SU(3) gluodynamics at high temperature. *Eur. Phys. J. C* **33**, 105 (2004).
4. M.D. Pollock. Magnetic fields and vacuum polarization at the Planck era. *Int. J. Mod. Phys. D* **12**, 1289 (2003).
5. V.I. Demchik, V.V. Skalozub. The spontaneous generation of magnetic fields at high temperature in a supersymmetric theory. *Eur. Phys. J. C* **27**, 601 (2003).
6. V. Demchik, V. Skalozub. The spontaneous creation of a chromomagnetic field and A_0-condensate at high temperature on a lattice. *J. Phys. A* **41**, 164051 (2008).
7. S. Antropov, M. Bordag, V. Demchik, V. Skalozub. Long range chromomagnetic fields at high temperature. *Intern. J. Mod. Phys. A* **26**, 4831 (2011).
8. V. Demchik, V. Skalozub. Spontaneous magnetization of a vacuum in the hot Universe and intergalactic magnetic fields. *Phys. Part. Nucl.* **46**, 1 (2015).
9. V. Skalozub, P. Minaiev. Magnetized quark-gluon plasma at the LHC. *Phys. Part. Nucl. Lett.* **15**, 568 (2018).
10. V. Skalozub, P. Minaiev. On magnetization of quark-gluon plasma at the LHC experiment energies. *Visnyk Dnipropetr. Univ. Fiz. Radioel.* **24**, (2016).
11. H.E. Haber, H.A. Weldon. On the relativistic Bose–Einstein integrals. *J. Math. Phys.* **23**, 1852 (1982).
12. V. Skalozub, A. Kozhushko. The parametric space of the two-Higgs-doublet model and Sakharov's baryogenesis conditions. *Ukr. J. Phys.* **56**, 431 (2011).
13. V. Skalozub, V. Demchik. Electroweak phase transition in strong magnetic fields in the standard model of elementary particles. arXiv:hep-th/9912071v1 (1999).

Received 08.07.19

П. Мінаєв, В. Скалозуб

ЕЛЕКТРОСЛАБКИЙ ФАЗОВИЙ
ПЕРЕХІД В СПОНТАННО НАМАГНІЧЕНІЙ ПЛАЗМІ

Р е з ю м е

Досліджується електрослабкий фазовий перехід в мінімальній (один дуплет хіггсівських бозонів) Стандартній Моделі (СМ) з урахуванням спонтанного народження магнітних та хромомагнітних полів при високій температурі. Як відомо, в СМ для маси бозона Хіггса, більшій за 75 ГеВ, цей фазовий перехід є переходом другого роду. Але відповідно до критеріїв Сахарова для формування баріонної асиметрії на ранніх етапах еволюції Всесвіту, він повинен бути жорстким переходом першого роду. В параметричному просторі дводуплетної СМ без магнітних полів можливий перехід першого роду. В ранньому Всесвіті існували спонтанно народжені температурозалежні магнітні та хромомагнітні поля. Хромомагнітні поля B_3 і B_8 народжувались в глюонному секторі КХД за температури $T > T_d$, більшої за температуру деконфайменту T_d. Звичайне магнітне поле народжувалось за рахунок кваркових петель. Як результат, для температур T, близьких до критичної температури $T_{\rm EWPT}$, ці поля можуть змінити характер фазового переходу.

https://doi.org/10.15407/ujpe64.8.714

T.V. OBIKHOD, I.A. PETRENKO
Institute for Nuclear Research, Nat. Acad. of Sci. of Ukraine
(47, Prosp. Nauky, Kyiv 03680, Ukraine; e-mail: obikhod@kinr.kiev.ua)

MASS RECONSTRUCTION OF MSSM HIGGS BOSON

The problems of the Standard Model, as well as questions related to Higgs boson properties led to the need to model the ttH associated production and the Higgs boson decay to a top quark pair within the MSSM model. With the help of computer programs MadGraph, Pythia, and Delphes and using the latest kinematic cuts taken from experimental data obtained at the LHC, we have predicted the masses of MSSM Higgs bosons, A and H.

Keywords: MSSM Higgs boson, top quark, b-tagging, computer modeling, the mass of a Higgs boson.

1. Introduction

The study of the properties of a Higgs boson discovered in 2012 is one of the main objectives of the LHC [1]. The importance of the experiments is related to the refinement of the channels of formation and decay of the Higgs boson, which shows that there are deviations of more than 2σ from the Standard Model (SM). Such data, together with the theoretical predictions of new physics, such as supersymmetry and the theory of extra dimensions, lead to the need to model the properties of the Higgs boson beyond the SM (BSM) such as production cross sections, angular distributions, and masses of supersymmetric Higgs bosons.

The existence of SM problems related to the impossibility of combining gravity with the other three types of interactions, the problem of radiative corrections to the Higgs boson mass, neutrino oscillations, and dark matter and dark energy problems lead to the introduction of new theories, one of which is supersymmetry. There are many supersymmetric theories. We will further use Minimal Supersymmetric Standard Model (MSSM) for the prediction of new supersymmetric particles – superpartners of the Higgs boson. The advantage of such a search lies not only in the possibility of going beyond the framework of the SM, but also in the small mass of the Higgs superparticles provided by the new theories. Such searches could be implemented both at the existing LHC collider, and at future accelerators of the type ILC or FCC. To establish a deviation from the SM behavior, the next goal is to identify the nature of the electro-weak symmetry breaking (EWSB), which is connected with properties of the top quark and Higgs boson interactions. Predictions for the coupling of the Higgs boson to top quarks directly influence the measurements of the production and decay rates and angular correlations. Therefore, this information can be used to study whether the data are compatible with the SM predictions for the Higgs boson. Since the QCD and electroweak gauge interactions of top quarks have been well established, the top Yukawa coupling might differ from the SM value. Therefore, the measurement of the ttH production rate and the tt decay of an A boson can provide a direct information about the top-Higgs Yukawa coupling, probably the most crucial coupling to fermions. The anomalous interaction of the Higgs boson with the top quark, has been experimentally studied through the measurement of the Higgs boson production in association with a top quark, [2]. According to the combined analysis of the experimental data at the LHC, the constrain on the top quark Yukawa coupling, y_t, within $[-0.9, -0.5]$ and $[1.0, 2.1] \times y_t^{\mathrm{SM}}$ were obtained. Recent ATLAS Higgs results using Run-2 data at a center-of-mass energy of 13 TeV with up to an integrated luminosity of 80 fb^{-1} to probe BSM coupling for the $tH + ttH$ processes [3] showed that the Higgs boson will continue to provide an important probe for new physics and beyond.

To implement the searches for the MSSM Higgs bosons and to facilitate their findings, we chose a specific search channels and the methods by which the corresponding superparticles were identified. Using the latest experimental data for the ttH production of a Higgs boson [4], b-tagging algorithm, MadGraph, Pythia, and Delphes programs, and latest kinematic cuts we predicted the masses of superparticles, A and H.

2. B-Tagging Identification and Reconstruction of MSSM Higgs Boson Masses

The top-quark Yukawa coupling y_t is parametrized as

$$L_{Htt} = -\frac{m_t}{v} H\bar{t}(a_t + ib_t\gamma_5)\, t,$$

where m_t is the top-quark mass, $v = 174$ GeV is the vacuum expectation value, and the coefficient a (b) denotes the CP-even (CP-odd) coupling, respectively.

Examples of Feynman diagrams for the considered tt and ttH processes are presented in Fig. 1.

It is necessary to reconstruct as many final particles as possible for the disentanglement of decay products of the exotic particles from the SM background. The B-tagging identification connected with b-quark signatures has following features and benefits for the experimental determination of primary particles:

- hadrons containing b-quarks have sufficient lifetime;
- presence of a secondary vertex (SV);
- tracks with large impact parameter (IP);
- the bottom quark is much more massive, with mass about 5 GeV, and thus its decay products have higher transverse momentum;
- b-jets have higher multiplicities and invariant masses;
- the B-decay produces often leptons.

We carried out a comprehensive computer modeling of the MSSM Higgs boson mass using MadGraph, Pythia, and Delphes programs. With the help of the program MadGraph, we carried out a calculation of the production cross-sections of the processes under consideration. The simulation of further developments, i.e. all information on decomposition products and their kinematic data, was produced using the Pythia program. In our calculations with the Pythia program, we used the latest experimental constraints on the low $\tan\beta$ region covered by the ttH, $H \to tt$ processes [5]. The calculation of the response of a detector to the resulting array of events was carried out using the Delphes program. We made a selection of events on the basis of additional kinematic restrictions associated with the peculiarities of the reactions under consideration and the b-tagging method.

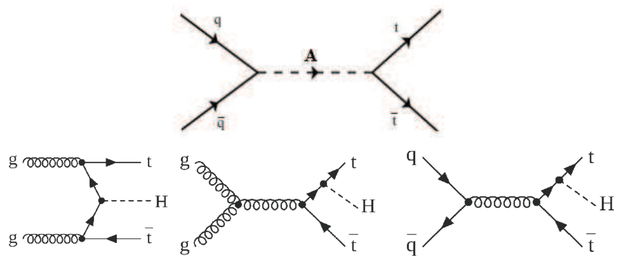

Fig. 1. Examples of Feynman diagrams for the $pp \to A$ (up) and $pp \to ttH$ (down) production process from [4]

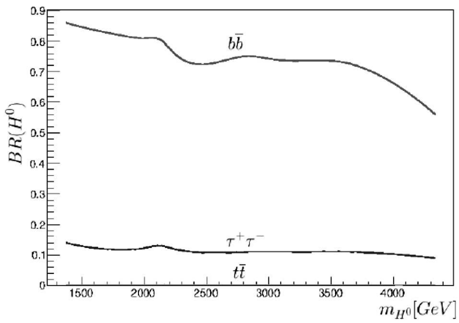

Fig. 2. Branching ratios of H to bb (red), $\tau^+\tau^-$ (blue), and tt (green)

Let us consider these processes separately and in more details.

2.1. $pp \to A \to tt$ process

The importance of the formation of a top quark pair is associated both with the possibility of a good identification of top quarks using the b-tagging algorithm and with the search for new physics due to the Yukawa constants of the top-quark and Higgs boson interaction [6]. The SM makes predictions for the coupling of the Higgs boson to a top quark. Therefore, the measurement of the decay rates of the observed state yields the information which can be used to probe whether data are compatible with the SM predictions for the Higgs boson. Loop-induced vertices allow probing for BSM contributions of new particles in the loops. In addition, it must be said that the the measuring of the properties of top pair quarks also sheds light on the stability of the electroweak vacuum [7]. The importance of this section is connected with the improvement of the searches for $H \to tt$ by studying the fully leptonic and semileptonic final states [8]. The results of our calculations presented in [9] are shown in Fig. 2.

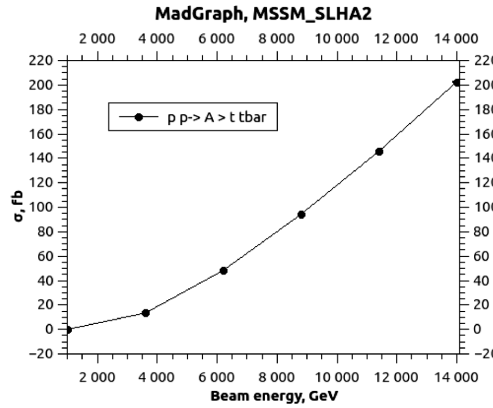

Fig. 3. Production cross section of the $pp \to A \to t\bar{t}$ process

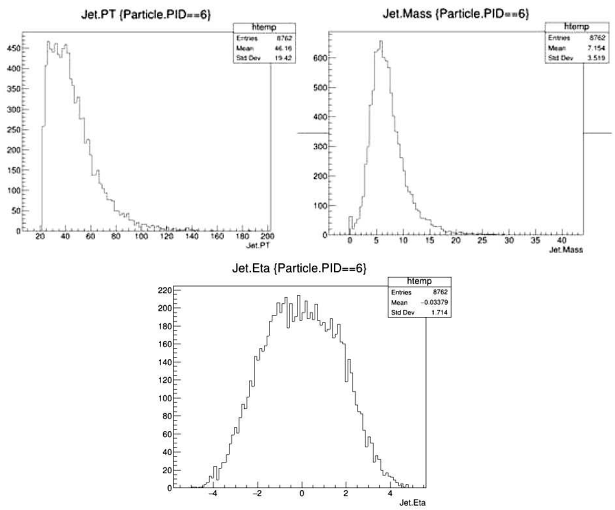

Fig. 4. Modeling of kinematic properties of jets from the reaction $pp \to A \to tt$: jet p_T distribution (left) and jet mass (right) (*a*); jet η distribution (*b*)

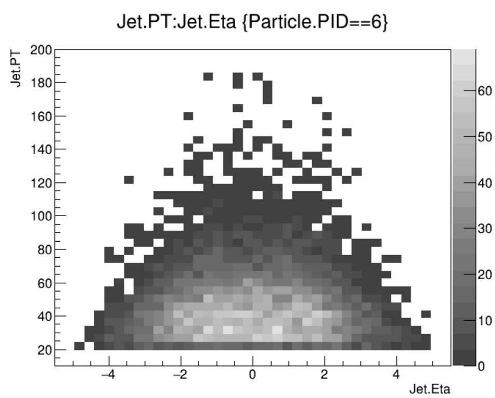

Fig. 5. Distribution for jets over the momenta and angles for the reaction $pp \to A \to tt$

The most probable decay channels for a CP-even boson, H, are the following:

- bb;
- $\tau^+\tau^-$;
- $t\bar{t}$.

We are dealing with massive MSSM particles which prefer to decay into the most massive decay products, for example, into a top-anti-top quark pair. So, we will consider the decay of the CP-odd Higgs boson into a top-anti-top quark pair, $A \to t\bar{t}$. With the help of the program MadGraph, we calculated the production cross-section of the $pp \to A \to t\bar{t}$ process presented in Fig. 3.

The increase of the production cross-section with the energy at the LHC and its large value for the formation of an A boson, about 0.2 pb at the energy of 14 TeV, lead to the conclusion about the importance of the consideration of this channel of formation and decay of the MSSM Higgs boson. Kinematic properties of decay products of A boson at the energy 14 TeV were modeled and presented in Fig. 4.

From Fig. 4, we see that jet p_T is maximal in the region of 30–50 GeV/c and then sharply decreases in the region of 120–140 GeV/c. The average jet mass is about 5–7 GeV/c, which is in accordance with the mass of the b-quark, into which the top quark decays with a probability of 99.8%. The angular distribution of the decay products shown in Fig. 4, b indicates the predominant direction of the decay products in the direction of angles from 35° to 90° to the axis of the proton-proton collision. In Fig. 5, we present the distribution for jets over the momenta and angles.

Using the distribution of Fig. 5, we can pick out the most high-energetic jets and present their separation in Fig. 6.

Using the data of Fig. 6, we can predict the mass of the A boson, which is about 360 GeV/c, since the momentum is equal to the mass at high energies.

2.2. ttH production process

We considered a combined analysis of proton-proton collision data at center-of-mass energies of $\sqrt{s} = 7$, 8, and 13 TeV, corresponding to integrated luminosities up to 5.1, 19.7, and 35.9 fb^{-1}, respectively. In this experiment, the observation of the ttH production with a significance of 5.2 standard deviations above the background-only hypothesis, at a Higgs boson mass of 125.09 GeV was reported in [4]. Then we consid-

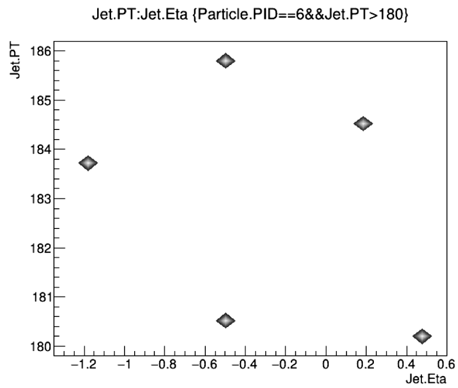

Fig. 6. The most energetic jets in the p_T range 180–186 GeV/c and the jet $\eta > |1.2|$ for the reaction $pp \to A \to tt$

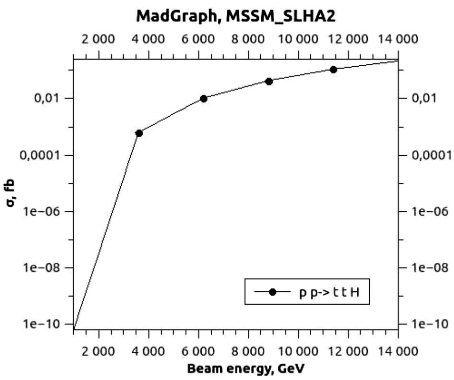

Fig. 7. Production cross-section of the $pp \to Htt$ process as a function of the energy range at the LHC

ered the decay process of the Higgs boson, $H \to bb$, as the most probable [9].

Using the program MadGraph, we calculated the production cross-sections $pp \to Htt$ of a Higgs boson via the proton-proton interaction. Our calculations for the range of 2–14 TeV at the LHC are presented in Fig. 7.

With the program Pythia, we simulated a further development of events. The detector response to the received array of events was modeled by the program Delphes. Thus, our simulation was maximally close to the experimental conditions.

The results of calculations of the jet mass range and the eta distribution of jets are presented in Fig. 8. The events were selected with the following cuts: the number of jets, $N_{\rm charged} >$ or $\sim$4, transverse momentum, $p_T > 80$ GeV, $B_{\rm tag} = 1$, mass of one b-jet, $M > 4$ GeV. From the jet distribution in Fig. 4, we

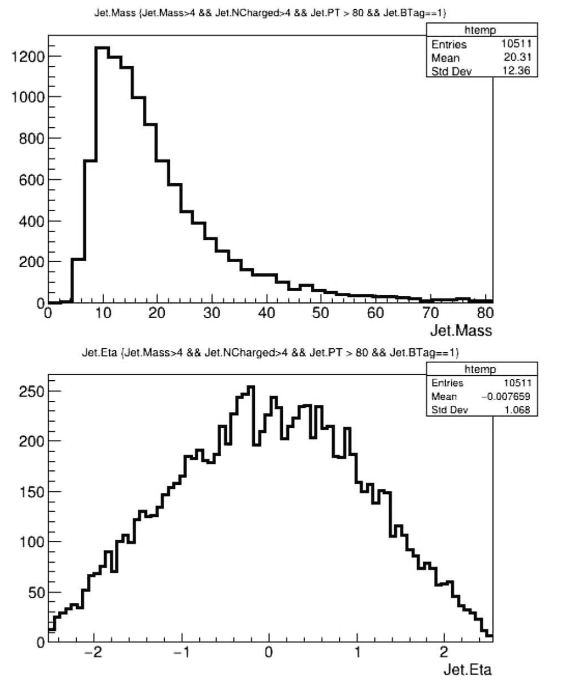

Fig. 8. Modeling of the jet mass range (a) and the angular distribution of jets (b)

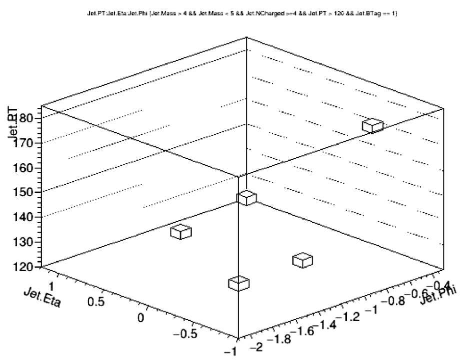

Fig. 9. Modeled angular and p_T jet distributions

conclude that the mass of jets of about 16–20 GeV for the minimal number of jets equal to 4 corresponds to the b-jet distribution and to the corresponding angular distribution of jet flux signals about the selected distribution of the jet flow in the direction perpendicular to the proton collision axis with $\theta \sim 40°$–$90°$.

As a result of the detector response calculations for the process $pp \to Htt \to Hbbbb$ with $N = 5000$ initial events and corresponding cross section of about 0.517 fb at 14 TeV at the LHC, we get the angular and p_T jet distributions presented in Fig. 9.

We have used together the following kinematic constraints: rapidity $-0.5 < y < 0.5$, mass of jets of about $4 < M < 5$ GeV, number of charge jets, $N_{\text{charged}} > 4$, transverse momentum, $p_T > 120$ GeV, parameter of the MSSM model, $M_H \sim 500$ GeV. Thus, we selected the toughest and most massive jets that can be formed from the decay process of the CP-even Higgs boson of the MSSM model. As we can see from Fig. 9, the approximate mass of one jet is about 150–170 GeV/c. We used the fact that each of the protons has an energy of 7 TeV, giving a total collision energy of 14 TeV. At this energy, the protons move at about 0.999999990 of the speed of light. Knowing the most probable Higgs boson decay channel, $H \rightarrow bb$, we conclude that the mass of the CP-even Higgs boson is about 300–340 GeV/c.

3. Conclusions

We have considered the most important channels of the MSSM Higgs boson production and decay. Since these channels are associated with the formation and decay of top quarks, whose properties shed light on the instability of the electroweak vacuum, the study of such reactions seems the most relevant to us. In addition, the MSSM Higgs bosons are the lightest supersymmetric particles predicted by supersymmetry. Therefore, finding their masses at the LHC collider is possible in the near future, which would remove a lot of theoretical questions related to the symmetries and unification of interactions. Using the programs MadGraph, Pythia, and Delphes to simulate the processes and to model the response of a detector, as well as strict kinematic cuts on the angles and momenta of particles taken from the experimental data, we have calculated the masses of the A boson equal to 360 GeV/c and H boson equal approximately to 320 GeV/c.

Our thanks to the organizers of the conference "New Trends in High-Energy Physics," Odessa, Ukraine May 12–18, 2019 and, in particular, to Laszlo L. Jenkovszky for organizing an important scientific event on topical issues of high-energy physics.

1. Y. Liu, S. Moretti. Probing anomalous top-Higgs couplings at the HL-LHC via $H \rightarrow WW^*$ decay channels. *Chin. Phys. C* **43** (1), 013102 (2019).
2. R. Goncalo. Recent highlights in top quark and Higgs boson physics from the LHC. *J. Phys.: Conf. Series* **1137**, 012012 (2019).
3. W. Leight. Studies of the SM Higgs Boson and Searches for BSM Higgs Bosons with the ATLAS Detector. *Acta Phys. Polon. B Proc. Sup.* **9** (3), 561 (2016).
4. CMS Collaboration. Observation of ttH production. *Phys. Rev. Lett.* **120**, 231801 (2018).
5. C. Gao, M. Luty, M. Mulhearn, N. Neill, Z. Wang. Searching for additional Higgs bosons via Higgs cascades. *Phys. Rev. D* **97** (7), 075040 (2018).
6. LHC Higgs Cross Section Working Group. Handbook of LHC Higgs Cross Sections: 3. Higgs Properties. arXiv:1307.1347 [hep-ph].
7. S. Alekhin, A. Djouadi, S. Moch. The top quark and Higgs boson masses and the stability of the electroweak vacuum. *Phys. Lett. B* **716**, 214 (2012).
8. M. Guchait, A. Vijay. Probing heavy charged Higgs boson at the LHC. *Phys. Rev. D* **98** (11), 115028 (2018).
9. T.V. Obikhod. Experimental searches for the extended Higgs sector at the LHC. *Prob. Atom. Sci. Technol. Series: Nucl. Phys. Invest.* **67**, 3 (2016).

Received 08.07.19

Т.В. Обіход, Е.О. Петренко

РЕКОНСТРУКЦІЯ МАСИ MSSM БОЗОНА ХІГГСА

Р е з ю м е

Проблеми Стандартної Моделі, а також питання, пов'язані з властивостями бозона Хіггса, призвели до необхідності моделювання ttH асоційованого утворення і розпаду бозона Хіггса на топ кваркову пару в рамках MSSM моделі. За допомогою комп'ютерних програм MadGraph5, Pythia8 і Delphes3 та використання останніх кінематичних обмежень, взятих з експериментальних даних, отриманих на LHC, ми передбачили маси MSSM бозонів Хіггса, A і H.

https://doi.org/10.15407/ujpe64.8.719

G.X.A. PETRONILO, S.C. ULHOA, A.E. SANTANA

Centro Internacional de Física, Universidade de Brasília
(70910-900, Brasília, DF, Brazil; e-mail: gustavopetronilo@gmail.com)

SYMPLECTIC FIELD THEORY OF THE GALILEAN COVARIANT SCALAR AND SPINOR REPRESENTATIONS

We explore the concept of the extended Galilei group, a representation for the symplectic quantum mechanics in the manifold $\mathcal{G}$, written in the light-cone of a five-dimensional de Sitter space-time in the phase space. The Hilbert space is constructed endowed with a symplectic structure. We study the unitary operators describing rotations and translations, whose generators satisfy the Lie algebra of $\mathcal{G}$. This representation gives rise to the Schrödinger (Klein–Gordon-like) equation for the wave function in the phase space such that the dependent variables have the position and linear momentum contents. The wave functions are associated to the Wigner function through the Moyal product such that the wave functions represent a quasiamplitude of probability. We construct the Pauli–Schrödinger (Dirac-like) equation in the phase space in its explicitly covariant form. Finally, we show the equivalence between the five-dimensional formalism of the phase space with the usual formalism, proposing a solution that recovers the non-covariant form of the Pauli–Schrödinger equation in the phase space.

Keywords: Galilean covariance, star-product, phase space, symplectic structure.

1. Introduction

In 1988, Takahashi *et. al.* [1] began a study of the Galilean covariance, where it was possible to develop an explicitly covariant non-relativistic field theory. With this formalism, the Schrödinger equation takes a similar form as the Klein–Gordon equation in the light-cone of a (4,1) de Sitter space [2, 3]. With the advent of the Galilean covariance, it was possible to derive the non-relativistic version of the Dirac theory, which is known in its usual form as the Pauli–Schrödinger equation. The goal in the present work is to derive a Wigner representation for such covariant theory.

The Wigner quasiprobability distribution (also called the Wigner function or the Wigner–Ville distribution in honor of Eugene Wigner and Jean–André Ville) was introduced by Eugene Wigner in 1932 [4] in order to study quantum corrections to classical statistical mechanics. The aim was to relate the wave function that appears in the Schrödinger equation to a probability distribution in the phase space. It is a generating function for all the spatial autocorrelation functions of a given quantum mechanical function $\psi(x)$. Thus, it maps the quantum density matrix onto the real phase space functions and operators introduced by Hermann Weyl in 1927 [5] in a context related to the theory of representations in mathematics (Weyl quantization in physics). Indeed, this is the Wigner–Weyl transformation of the density matrix; i.e., the realization of that operator in the phase space. It was later re-derived by Jean Ville in 1948 [6] as a quadratic representation (in sign) of the local time frequency energy of a signal, effectively a spectrogram. In 1949, José Enrique Moyal [7], who independently derived the Wigner function, as the functional generator of the quantum momentum, as a basis for an elegant codification of all expected values and, therefore, of quantum mechanics in the phase-space formulation (phase-space representation). This representation has been applied to a number of areas such as statistical mechanics, quantum chemistry, quantum optics, classical optics, signal analysis, electrical engineering, seismology, time-frequency analysis for music signals, spectrograms in biology and speech processing, and motor design. In order to derive a phase-space representation for the Galilean-covariant spin 1/2 particles, we use a symplectic representation for the Galilei group, which is associated with the Wigner approach [8–11].

This article is organized as follows. In Section 2, the construction of the Galilean covariance is presented. The Schrödinger (Klein–Gordon-like) equation and the Pauli–Schrödinger (Dirac-like) equation are derived showing the equivalence between our formalism and the usual non-relativistic formalism. In Section 4, a symplectic structure is constructed in the Galilean manifold. Using the commutation relations, the Schrödinger equation in five dimensions in the phase space is constructed. With a proposed solution, the Schrödinger equation in the phase space is restored to its non-covariant form in $(3+1)$ dimensions. The explicitly covariant Pauli–Schrödinger equation is derived in Section 5. We study a Galilean spin $1/2$ particle in a external potential, and the solutions are proposed and discussed. In Section 6, the final concluding remarks are presented.

2. Galilean Covariance

The Galilei transformations are given by

$$\mathbf{x}' = R\mathbf{x} + \mathbf{v}t + \mathbf{a}, \tag{1}$$

$$t' = t + b, \tag{2}$$

where R stands for the three-dimensional Euclidian rotations, v is the relative velocity defining the Galilean boosts, $\mathbf{a}$ and $\mathbf{b}$ stand for spatial and time translations, respectively. Consider a free particle with mass m; the mass shell relation is given by $\widehat{P}^2 - 2mE = 0$. Then we can define a 5-vector, $p^\mu = (p_x, p_y, p_z, m, E) = (p^i, m, E)$, with $i = 1, 2, 3$.

Thus, we can define a scalar product of the type

$$p_\mu p_\nu g^{\mu\nu} = p_i p_i - p_5 p_4 - p_4 p_5 = \widehat{P}^2 - 2mE = k, \tag{3}$$

where $g^{\mu\nu}$ is the metric of the space-time to be constructed, e $p_\nu g^{\mu\nu} = p^\mu$.

Let us define a set of canonical coordinates q^μ associated with p^μ, by writing a five-vector in M, $q^\mu = (\mathbf{q}, q^4, q^5)$, $\mathbf{q}$ is the canonical coordinate associated with $\widehat{P}$; q^4 is the canonical coordinate associated with E, and thus can be considered as the time coordinate; q^5 is the canonical coordinate associated with m explicitly given in terms of $\mathbf{q}$ and q^4, $q^\mu q_\mu = q^\mu q^\nu \eta_{\mu\nu} = \mathbf{q}^2 - q^4 q^5 = s^2 = 0$. From this $q^5 = \frac{\mathbf{q}^2}{2t}$, or infinitesimally, we obtain $\delta q^5 = \ \mathbf{v}\,\delta\frac{\mathbf{q}}{2}$. Therefore, the fifth component is basically defined by the velocity.

That can be seen as a special case of scalar product in G denoted as

$$(x|y) = g^{\mu\nu} x_\mu y_\nu = \sum_{i=1}^{3} x_i y_i - x_4 y_5 - x_5 y_4, \tag{4}$$

where $x^4 = y^4 = t$, $x^5 = \frac{x^2}{2t}$ e $y^5 = \frac{y^2}{2t}$. Hence, the following metric can be introduced:

$$(g_{\mu\nu}) = \begin{pmatrix} 1 & 0 & 0 & 0 & 0 \\ 0 & 1 & 0 & 0 & 0 \\ 0 & 0 & 1 & 0 & 0 \\ 0 & 0 & 0 & 0 & -1 \\ 0 & 0 & 0 & -1 & 0 \end{pmatrix}. \tag{5}$$

This is the metric of a Galilean manifold $\mathcal{G}$. In the sequence, this structure is explored in order to study unitary representations.

3. Hilbert Space and Sympletic Structure

Consider an analytical manifold $\mathcal{G}$, where each point is specified by the coordinates q_μ, with $\mu = 1, 2, 3, 4, 5$ and the metric specified by (5). The coordinates of every point in the cotangent-bundle $T^*\mathcal{G}$ will be denoted by (q_μ, p_μ). The space $T^*\mathcal{G}$ is equipped with a symplectic structure via the 2-form

$$\omega = dq^\mu \wedge dp_\mu \tag{6}$$

called the symplectic form (sum over repeated indices is assumed). We consider the following bidifferential operator on $C^\infty(T^*\mathcal{G})$ functions,

$$\Lambda = \frac{\overleftarrow{\partial}}{\partial q^\mu}\frac{\overrightarrow{\partial}}{\partial p_\mu} - \frac{\overleftarrow{\partial}}{\partial p^\mu}\frac{\overrightarrow{\partial}}{\partial q_\mu}, \tag{7}$$

such that, for C^∞ functions, $f(q,p)$ and $g(q,p)$, we have

$$\omega(f\Lambda, g\Lambda) = f\Lambda g = \{f, g\} \tag{8}$$

where

$$\{f, g\} = \frac{\partial f}{\partial q^\mu}\frac{\partial g}{\partial p_\mu} - \frac{\partial f}{\partial p^\mu}\frac{\partial g}{\partial q_\mu}. \tag{9}$$

It is the Poisson bracket, and $f\Lambda$ and $g\Lambda$ are two vector fields given by $h\Lambda = X_h = -\{h, \}$.

The space $T^*\mathcal{G}$ endowed with this symplectic structure is called the phase space and will be denoted by Γ. In order to associate the Hilbert space with the phase space Γ, we will consider the set of square-integrable complex functions, $\phi(q,p)$ in Γ such that

$$\int dpdq\ \phi^\dagger(q,p)\phi(q,p) < \infty \tag{10}$$

is a real bilinear form. In this case, $\phi(q,p) = \langle q,p|\phi\rangle$ is written with the aid of

$$\int dpdq|q,p\rangle\langle q,p| = 1, \tag{11}$$

where $\langle\phi|$ is the dual vector of $|\phi\rangle$. This symplectic Hilbert space is denoted by $H(\Gamma)$.

4. Symplectic Quantum Mechanics and the Galilei Group

In this section, we will study the Galilei group considering $H(\Gamma)$ as the space of representation. To do so, consider the unit transformations $U{:}\mathcal{H}(\Gamma) \to \mathcal{H}(\Gamma)$ such that $\langle\psi_1|\psi_2\rangle$ is invariant. Using the Λ operator, we define a mapping $e^{i\frac{\Lambda}{2}} = \star{:}\Gamma\times\Gamma\to\Gamma$ called a Moyal (or star) product and defined by

$$f\star g = f(q,p)\exp\left[\frac{i}{2}\left(\frac{\overleftarrow{\partial}}{\partial q^\mu}\frac{\overrightarrow{\partial}}{\partial p_\mu} - \frac{\overleftarrow{\partial}}{\partial p^\mu}\frac{\overrightarrow{\partial}}{\partial q_\mu}\right)\right]g(q,p),$$

it should be noted that we used $\hbar = 1$. The generators of U can be introduced by the following (Moyal–Weyl) star-operators:

$$\widehat{F} = f(q,p)\star = f\left(q^\mu + \frac{i}{2}\frac{\partial}{\partial p_\mu}, p^\mu - \frac{i}{2}\frac{\partial}{\partial q_\mu}\right).$$

To construct a representation of the Galilei algebra in $\mathcal{H}$, we define the operators

$$\widehat{P}^\mu \;=\; p^\mu\star = p^\mu - \frac{i}{2}\frac{\partial}{\partial q_\mu}, \tag{12a}$$

$$\widehat{Q}^\mu \;=\; q\star = q^\mu + \frac{i}{2}\frac{\partial}{\partial p_\mu}. \tag{12b}$$

and

$$\widehat{M}_{\nu\sigma} \;=\; M_{\nu\sigma}\star = \widehat{Q}_\nu\widehat{P}_\sigma - \widehat{Q}_\sigma\widehat{P}_\nu, \tag{12c}$$

where $\widehat{M}_{\nu\sigma}$ and $\widehat{P}_\mu$ are the generators of homogeneous and inhomogeneous transformations, respectively. From this set of unitary operators, we obtain, after some simple calculations, the following set of commutations relations:

$$\left[\widehat{P}_\mu, \widehat{M}_{\rho\sigma}\right] = -i(g_{\mu\rho}\widehat{P}^\sigma - g_{\mu\sigma}\widehat{P}^\rho),$$

$$\left[\widehat{P}_\mu, \widehat{P}_\sigma\right] = 0,$$

and

$$\left[\widehat{M}_{\mu\nu}, \widehat{M}_{\rho\sigma}\right] = -i(g_{\nu\rho}\widehat{M}_{\mu\sigma} - g_{\mu\rho}\widehat{M}_{\nu\sigma} + g_{\mu\sigma}\widehat{M}_{\nu\rho} - g_{\mu\sigma}\widehat{M}_{\nu\rho}).$$

Consider a vector $q^\mu \in G$ that obeys the set of linear transformations of the type

$$\bar{q}^\mu = G^\mu{}_\nu q^\nu + a^\mu. \tag{13}$$

A particular case of interest in these transformations is given by

$$\bar{q}^i = R^i_j q^j + v^i q^4 + a^i \tag{14}$$

$$\bar{q}^4 = q^4 + a^4 \tag{15}$$

$$\bar{q}^5 = q^5 - (R^i_j q^j)v_i + \frac{1}{2}\mathbf{v}^2 q^4. \tag{16}$$

In the matrix form, the homogeneous transformations are written as

$$G^\mu{}_\nu = \begin{pmatrix} R^1{}_1 & R^1{}_2 & R^1{}_3 & v^i & 0 \\ R^2{}_1 & R^2{}_2 & R^2{}_3 & v^2 & 0 \\ R^3{}_1 & R^3{}_2 & R^3{}_3 & v^3 & 0 \\ 0 & 0 & 0 & 1 & 0 \\ v_i R^i{}_j & v_i R^i{}_2 & v_i R^i{}_3 & \frac{\mathbf{v}^2}{2} & 1 \end{pmatrix}. \tag{17}$$

We can write the generators as

$$\begin{aligned} &\widehat{J}_i = \frac{1}{2}\epsilon_{ijk}\widehat{M}_{jk}, \quad \widehat{C}_i = \widehat{M}_{4i}, \\ &\widehat{K}_i = \widehat{M}_{5i}, \quad \widehat{D} = \widehat{M}_{54}. \end{aligned} \tag{18}$$

Hence, the non-vanishing commutation relations can be rewritten as

$$\begin{aligned} &\left[\widehat{J}_i, \widehat{J}_j\right] = i\epsilon_{ijk}\widehat{J}_k, && \left[\widehat{J}_i, \widehat{K}_j\right] = i\epsilon_{ijk}\widehat{K}_k, \\ &\left[\widehat{J}_i, \widehat{C}_j\right] = i\epsilon_{ijk}\widehat{C}_k, && \left[\widehat{K}_i, \widehat{C}_j\right] = i\delta_{ij}\widehat{D} + i\epsilon_{ijk}J_k, \\ &\left[\widehat{D}, \widehat{K}_i\right] = i\widehat{K}_i, && \left[\widehat{C}_i, \widehat{D}\right] = i\widehat{C}_i, \\ &\left[\widehat{P}_4, \widehat{D}\right] = i\widehat{P}_4, && \left[\widehat{J}_i, \widehat{P}_j\right] = i\epsilon_{ijk}\widehat{P}_k, \\ &\left[\widehat{P}_i, \widehat{K}_j\right] = i\delta_{ij}\widehat{P}_5, && \left[\widehat{P}_i, \widehat{C}_j\right] = i\delta_{ij}\widehat{P}_4, \\ &\left[\widehat{P}_4, \widehat{K}_i\right] = i\widehat{P}_i, && \left[\widehat{P}_5, \widehat{C}_i\right] = i\widehat{P}_i. \\ &\left[\widehat{D}, \widehat{P}_5\right] = i\widehat{P}_5, && \end{aligned} \tag{19}$$

These relations have the Lie algebra of the Galilei group as a subalgebra in the case of $\mathcal{R}^3\times\mathcal{R}$, considering J_i the generators of rotations K_i of the pure Galilei transformations, P_μ the spatial and temporal translations. In fact, we can observe that Eqs. (14) and (15) are the Galilei transformations given by

Eq. (1) and (2) with $x^4 = t$. Equation (16) is the compatibility condition which represents the embedding

$$\mathcal{I} : \mathbf{A} \to A = \left(\mathbf{A}, A_4, \frac{\mathbf{A}^2}{2A_4}\right); \quad \mathbf{A} \in \mathcal{E}_3, A \in \mathcal{G}.$$

The commutation of K_i and P_i is naturally nonzero in this context, so P_5 will be related to the mass, which is the extension parameter of the Galilei group or an invariant of the extended Galilei–Lie algebra. So, the invariants of this algebra in the light cone of the de Sitter space-time are

$$I_1 = \widehat{P}_\mu \widehat{P}^\mu \tag{20}$$

$$I_2 = \widehat{P}_5 = -mI \tag{21}$$

$$I_3 = \widehat{W}_{5\mu} \widehat{W}_5^\mu, \tag{22}$$

where I is the identity operator, m is the mass, $W_{\mu\nu} = \frac{1}{2}\epsilon_{\mu\alpha\beta\rho\nu} P^\alpha M^{\beta\rho}$ is the 5-dimensional Pauli–Lubanski tensor, and $\epsilon_{\mu\nu\alpha\beta\rho}$ is the totally antisymmetric tensor in five dimensions. In the scalar represantation, we can defined $I_3 = 0$. Using the Casimir invariants I_1 and I_2 and applying them to Ψ, we have

$$\widehat{P}_\mu \widehat{P}^\mu \Psi = k^2 \Psi,$$
$$\widehat{P}_5 \Psi = -m\Psi.$$

We obtain

$$\left(p^2 - i\mathrm{p}\,\nabla - \frac{1}{4}\nabla^2 - k^2\right)\Psi =$$
$$= 2\left(p_4 - \frac{i}{2}\partial_t\right)\left(p_5 - \frac{i}{2}\partial_5\right)\Psi,$$

and a solution of this equation is

$$\Psi = e^{-i2p_5 q^5} \rho(q^5) e^{-2ip_4 t} \chi(t) \Phi(\mathbf{q}, \mathbf{p}). \tag{23}$$

Thus,

$$\left(p^2\Phi - i\mathrm{p}\,\nabla\Phi - \frac{1}{4}\nabla^2\Phi - k^2\right)\frac{1}{\Phi} =$$
$$= \frac{1}{2}\left(i\partial_t\chi\right)\left(i\partial_5\rho\right)\frac{1}{\chi\rho},$$

which yields

$$i\partial_t\chi = \alpha\chi, \quad \text{and} \quad i\partial_5\rho = \beta\rho.$$

Thus, our solution for χ and ρ is

$$\chi = e^{-i\alpha t}, \quad \rho = e^{-i\beta q^5}. \tag{24}$$

Using the fact that

$$\widehat{P}_4 \Psi = \left(p_4 - \frac{i}{2}\partial_t\right) e^{-i(2p_4+\alpha)t} = -E\, e^{-i(2p_4+\alpha)t}$$

and

$$\widehat{P}_5 \Psi = \left(p_5 - \frac{i}{2}\partial_5\right) e^{-i(2p_5+\beta)q^5} = -m\, e^{-i(2p_5+\beta)q^5},$$

we can conclude that

$$\alpha = 2E, \quad \beta = 2m. \tag{25}$$

So, we have

$$\frac{1}{2m}\left(p^2 - i\boldsymbol{p}\,\nabla - \frac{1}{4}\nabla^2\right)\Phi = \left(E + \frac{k^2}{2m}\right)\Phi,$$

which is the usual form of the Schrödinger equation in the phase space for a free particle with mass m and with an additional kinetic energy of $\frac{k^2}{2m}$, that we can always set as the zero of energy.

This equation and its complex conjugate can also be obtained by using the Lagrangian density in the phase space (we use $d^\mu = d/dq_\mu$)

$$\mathcal{L} = \partial^\mu\Psi(q,p)\partial\Psi^*(q,p) + \frac{i}{2}p^\mu[\Psi(q,p)\partial^\mu\Psi^*(q,p) -$$
$$- \Psi^*(q,p)\partial^\mu\Psi(q,p)] + \left[\frac{p^\mu p_\mu}{4} - k^2\right]\Psi.$$

The association of this representation with the Wigner formalism is given by

$$f_w(q,p) = \Psi(q,p) \star \Psi^\dagger(q,p),$$

where $f_w(q,p)$ is the Wigner function. To prove this, we recall that Eq. (23) can be written as

$$\widehat{P}_\mu \widehat{P}^\mu \Psi = p^2 \star \Psi(q,p).$$

Multiplying the right-hand side of the above equation by $\Psi^\dagger$, we obtain

$$(p^2 \star \Psi) \star \Psi^\dagger = k^2 \Psi \star \Psi^\dagger. \tag{26}$$

But $\Psi^\dagger \star p^2 = k^2 \Psi^\dagger$. Thus,

$$\Psi \star (\Psi^\dagger \star p^2) = k^2 \Psi \star \Psi^\dagger. \tag{27}$$

Subtracting (27) from (26), we have

$$p^2 \star f_w(q,p) - p^2 \star f_w(q,p) = 0, \tag{28}$$

which is the Moyal brackets $\{p^2, f_w\}_M$. In view of Eq. (12a), Eq. (28) becomes

$$p_\mu \partial_{q_\mu} f_w(q,p) = 0, \tag{29}$$

where the Wigner function in the Galilean manifold is a solution of this equation.

5. Spin 1/2 Symplectic Representaion

In order to study the representations of spin-1/2 particles, we introduce $\gamma^\mu \widehat{P}_\mu$, where $\widehat{P}_\mu = p_\mu - \frac{i}{2}\partial_\mu$ in such a way that, acting on the 5-spinor in the phase space $\Psi(q,p)$, we have

$$\gamma^\mu \left(p_\mu - \frac{i}{2}\partial_\mu\right) \Psi(p,q) = k\Psi(p,q), \tag{30}$$

which is the Galilean-covariant Pauli–Schrödinger equation. Consequently, the mass shell condition is obtained by the usual steps:

$$(\gamma^\mu \widehat{P}_\mu)(\gamma^\nu \widehat{P}_\nu)\Psi(q,p) = k^2\Psi(q,p). \tag{31}$$

Therefore,

$$\gamma^\mu\gamma^\nu(\widehat{P}_\mu \widehat{P}_\nu) = k^2 = \widehat{P}^\mu \widehat{P}_\nu. \tag{32}$$

Since $\widehat{P}_\mu \widehat{P}_\nu = \widehat{P}_\nu \widehat{P}_\mu$, we have

$$\frac{1}{2}(\gamma^\mu\gamma^\nu + \gamma^\nu\gamma^\mu)\widehat{P}_\mu \widehat{P}_\nu = \widehat{P}^\mu \widehat{P}_\nu, \tag{33}$$

so

$$\{\gamma^\mu, \gamma^\nu\} = 2g^{\mu\nu}. \tag{34}$$

Equation (30) can be derived from the Lagrangian density for spin-1/2 particles in the phase space, which is given by

$$\mathcal{L} = -\frac{i}{4}\Big((\partial_\mu \bar{\Psi})\gamma^\mu \Psi - \bar{\Psi}(\gamma^\mu \partial_\mu \Psi)\Big) - (k - \gamma^\mu p_\mu)\Psi\bar{\Psi},$$

where $\bar{\Psi} = \zeta\Psi^\dagger$, with$\zeta = -\frac{i}{\sqrt{2}}\{\gamma^4 + \gamma^5\} = \begin{pmatrix} 0 & -i \\ i & 0 \end{pmatrix}$. In the Galilean-covariant Pauli–Schrödinger equation case, the association to the Wigner function is given by $f_w = \Psi \star \bar{\Psi}$, with each component satisfying Eq. (29).

Let us now examine the gauge symmetries in the phase space demanding the invariance of the Lagrangian under a local gauge transformation given by $e^{\Lambda(q,p)}\Psi$. This leads to the minimum coupling,

$$\widehat{P}_\mu \Psi \to (\widehat{P}_\mu - eA_\mu)\Psi = \left(p_\mu - \frac{i}{2}\partial_\mu - eA_\mu\right)\Psi.$$

This describes an electron in an external field with the Pauli–Schrödinger equation given by

$$\left[\gamma^\mu \left(p_\mu - \frac{i}{2}\partial_\mu - eA_\mu\right) - k\right]\Psi = 0. \tag{35}$$

In order to illustrate such result, let us consider a electron in an external field given by $A_\mu(\mathbf{A}, A_4, A_5)$, with $A_4 = -\phi$ and $A_5 = 0$. Considering the representation of the γ^μ matrices

$$\gamma^i = \begin{pmatrix} \sigma^i & 0 \\ 0 & -\sigma^i \end{pmatrix},\ \gamma^4 = \begin{pmatrix} 0 & 0 \\ \sqrt{2} & 0 \end{pmatrix},\ \gamma^5 = \begin{pmatrix} 0 & -\sqrt{2} \\ 0 & 0 \end{pmatrix}.$$

where σ^i are the Pauli matrices, and $\sqrt{2}$ is the identity 2×2 matrix multiplied by $\sqrt{2}$. We can rewrite the object Ψ, as $\Psi = \begin{pmatrix} \varphi \\ \chi \end{pmatrix}$, where φ and χ are 2-spinors dependent on $x^\mu; \mu = 1, ..., 5$. Thus, in the representation where $k = 0$, the Eq. (35) becomes

$$\begin{aligned} &\sigma \left(\mathbf{p} - \frac{i}{2}\partial_q - e\mathbf{A}\right)\varphi - \sqrt{2}\left(p_5 - \frac{i}{2}\partial_5\right)\chi = 0, \\ &\sqrt{2}\left(p_4 - \frac{i}{2}\partial_t - e\phi\right)\varphi - \boldsymbol{\sigma}\left(\mathbf{p} - \frac{i}{2}\partial_q - e\mathbf{A}\right)\chi = 0. \end{aligned} \tag{36}$$

Solving the coupled equations, we get an equation for φ and χ. Replacing the eigenvalues of $\widehat{P}_4$ and $\widehat{P}_5$, we have

$$\left[\frac{1}{2m}\left(\boldsymbol{\sigma}\left(\mathbf{p} - \frac{i}{2}\partial_q - e\mathbf{A}\right)\right)^2 + e\phi\right]\varphi = E\varphi,$$

$$\left[\frac{1}{2m}\left(\boldsymbol{\sigma}\left(\mathbf{p} - \frac{i}{2}\partial_q - e\mathbf{A}\right)\right)^2 + e\phi\right]\chi = E\chi.$$

These are the non-covariant form of the Pauli–Schrödinger equation in the phase space independent of the time with

$$f_w = \Psi \star \bar{\Psi} = i\varphi \star \chi^\dagger - i\chi \star \varphi^\dagger.$$

This leads to

$$E_n = \frac{eB}{m}\left(n + \frac{1}{2} - \frac{s}{2}\right) - \frac{k^2}{2m},$$

where $s = \pm 1$. It should be noted that the above expression represents the Landau levels which show the spin-splitting feature.

The above Figures 1 and 2 show the Wigner functions for the ground and first excited states, respec-

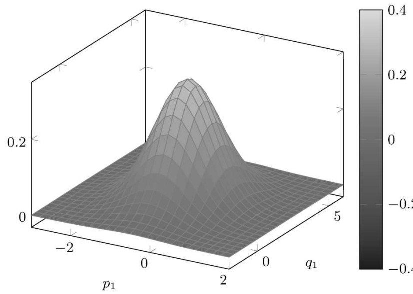

Fig. 1. Wigner Function (cut in q_1,p_1),Ground State

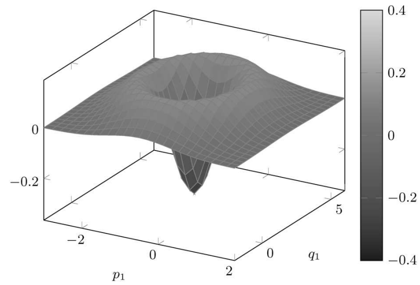

Fig. 2. Wigner Function (cut in q_1,p_1), First Excited State

tively, in the cut (q_1, p_1). These are the same solutions known in the literature using the usual Wigner method.

6. Concluding Remarks

We study the spin-1/2 particle equation, the Pauli–Schrödinger equation, in the context of the Galilean covariance, considering a symplectic Hilbert space. We begin with a presentation on the Galilean manifold which is used to review the construction of the Galilean covariance and the representations of quantum mechanics in this formalism, namely, the spin-1/2 and scalar representations and the Schrödinger (Klein–Gordon-like) and Pauli–Schrödinger (Dirac-like) equations, respectively.

The quantum mechanics formalism in the phase space is derived in this context of the Galilean covariance giving rise to the representations of spin-0 and spin-1/2 equations. For the spin-1/2 equation (the Dirac-like equation), we study the electron in an external field. Solving it, we were able to recover the non-covariant Pauli–Schrödinger equation in phase space and to analyze, in this context, the Landau levels.

This work was supported by CAPES and CNPq of Brazil.

1. Y. Takahashi. Towards the many-body theory with the Galilei invariance as a guide: Part I. *Fortschr. Phys.* **36**, 63 (1988).
2. M. Omote, S. Kamefuchi, Y. Takahashi, Y. Ohnuki. Galilean covariance and the Schrödinger equation. *Fortschr. Phys.* **37**, 933 (1989).
3. A.E. Santana, F.C. Khanna, Y. Takahashi. Galilei covariance and (4,1) de Sitter space. *Prog. Theor. Phys.* **99**, 327 (1998).
4. E. Wigner. Über das überschreiten von potentialschwellen bei chemischen reaktionen. *Z. Phys. Chem.* **19**, 203 (1932).
5. H. Weyl. Quantenmechanik und gruppentheorie. *Z. Phys.* **46**, 1 (1927).
6. J. Ville. Theorie et application de la notion de signal analytique. *Cables et Transmissions* **2**, 61 (1948).
7. J.E. Moyal. Quantum mechanics as a statistical theory. *Math. Proc. Cambr. Phil. Soc.* **45**, 99 (1949).
8. M.D. Oliveira, M.C.B. Fernandes, F.C. Khanna, A.E. Santana, J.D.M. Vianna. Symplectic quantum mechanics. *Ann. Phys.* **312**, 492 (2004).
9. R.G.G. Amorim, F.C. Khanna, A.P.C. Malbouisson, J.M.C. Malbouisson, A.E. Santana. Quantum field theory in phase space. *Int. J. Mod. Phys. A* 1950037 (2019).
10. R.A.S. Paiva, R.G.G. Amorim. Quantum physics in phase space: An analysis of simple pendulum. *Adv. Theor. Comp. Phys.* **1**, 1 (2018).
11. H. Dessano, R.A.S. Paiva, R.G.G. Amorim, S.C. Ulhoa, A.E. Santana. Wigner function and non-classicality for oscillator systems. *Brazilian J. Phys.* 1 (2019).

Received 08.07.19

Г. Петроніло, С. Уйоа, А. Сантана

СИМПЛЕКТИЧНА ТЕОРІЯ ПОЛЯ
ГАЛІЛЕЄВО-КОВАРІАНТНИХ СКАЛЯРНОГО
І СПІНОРНОГО ПРЕДСТАВЛЕНЬ

Р е з ю м е

Ми досліджуємо концепцію розширеної групи Галілея, деякого представлення для симплектичної квантової механіки на многовиді $\mathcal{G}$, заданого на світловому конусі п'ятивимірного простору-часу де Сіттера у фазовому просторі. Побудувано Гільбертів простір, наділений симплектичною структурою. Ми вивчаємо унітарні оператори, що описують повороти і трансляції, генератори яких утворюють алгебру Лі в $\mathcal{G}$. Це представлення породжує рівняння Шредінгера (типу Кляйна–Гордона) для хвильової функції у фазовому просторі, так що змінні мають зміст положення і лінійного імпульсу. Хвильові функції пов'язані з функцією Вігнера через добуток Мойала, так що хвильові функції репрезентують квазіамплітуду ймовірності. Ми будуємо рівняння Паулі–Шредінгера (типу рівняння Дірака) у фазовому просторі в явно коваріантній формі. На завершення ми показуємо еквівалентність між п'ятивимірним формалізмом фазового простору і звичайним формалізмом, пропонуючи розв'язок, що відновлює нековаріантну форму рівняння Паулі–Шредінгера у фазовому просторі.

https://doi.org/10.15407/ujpe64.8.725

J. PROCHÁZKA, V. KUNDRÁT, M.V. LOKAJÍČEK

The Czech Academy of Sciences, Institute of Physics
(18221 Prague 8, Czech Republic; e-mail: jiri.prochazka@fzu.cz, kundrat@fzu.cz, lokaj@fzu.cz)

MODELS OF ELASTIC pp SCATTERING AT HIGH ENERGIES – POSSIBILITIES, LIMITATIONS, ASSUMPTIONS, AND OPEN QUESTIONS

The simplest collision process, the elastic scattering of protons, has been measured at various energies and in a broad interval of scattering angles. Its theoretical description is, however, much more delicate, than it may seem at first glance. The widely used eikonal model allowed one to analyze the pp elastic scattering data at an ISR energy of 52.8 GeV and the TOTEM data at a much higher LHC energy of 8 TeV. The results represent the most detailed elaborated impact parameter analysis of pp data which has ever been performed. They have helped to identify several deeper open questions and problems concerning all widely used theoretical frameworks used for the description of the elastic pp scattering. The problems should be further studied and solved to derive some important proton characteristics which may be obtained with the help of the elastic scattering.

Keywords: proton-proton collisions, elastic scattering of hadrons, eikonal model, Coulomb-hadronic interference, central or peripheral scattering, impact parameter, WY approach.

1. Introduction

The elastic differential cross-section $\mathrm{d}\sigma/\mathrm{d}t$ represents a basic experimental characteristic established in the elastic collisions of hadrons. If the influence of spins is not considered then the t (four momentum transfer squared) dependence exhibits a very similar structure in all cases of elastic scattering of charged hadrons at contemporary high energies: there is a peak at very low values of $|t|$, followed by a (nearly) exponential region, and then there is a dip-bump or shoulder structure at even higher values of $|t|$ practically for all colliding hadrons [1].

The measured differential elastic cross-section of two charged hadrons (protons) is standardly described with the help of the complete elastic scattering amplitude $F^{\mathrm{C+N}}(s,t)$ as

$$\frac{\mathrm{d}\sigma}{\mathrm{d}t} = \frac{\pi}{sp^2}\left|F(s,t)\right|^2. \quad (1)$$

Here, s is the square of the total collision energy, and p is the value of the momentum of one incident proton in the center-of-mass system. The Coulomb amplitude $F^{\mathrm{C}}(s,t)$ is widely assumed to be well-known from QED (except from electromagnetic form factors). However, the t-dependence of the elastic hadronic amplitude $F^{\mathrm{N}}(s,t)$ is yet not fully known. The elastic scattering of two protons is kinematically the simplest collision process, but its description is not satisfactory in many aspects.

The description of the Coulomb-hadronic interference proposed by West and Yennie (WY) [2] in 1968 was widely used for the analysis of experimental data in the era of the ISR. However, several problems and limitations in the given model were identified later. This approach is discussed in sect. 2. The description is not usable for a reliable data analysis. It has, however, negatively influenced many recent models of elastic hadronic scattering. To overcome these problems, another approach based on the eikonal model framework has been developed. The results of analysis of experimental data using the eikonal model (under different assumptions) are summarized in sect. 3. The list of deeper open questions and problems identified in *all* contemporary descriptions of the elastic scattering is presented in sect. 4. Concluding remarks may be found in sect. 5. This paper very briefly summarizes the results obtained and discussed in more details in [3, 4].

2. Approach of West and Yennie

In 1968, West and Yennie [2] derived for the complete amplitude the following simplified formula:

$$F^{\mathrm{C+N}}_{\mathrm{WY}}(s,t) = \pm\frac{\alpha s}{t} G_1(t) G_2(t)\, \mathrm{e}^{\mathrm{i}\alpha\phi(s,t)} + \\ + \frac{\sigma^{\mathrm{tot,N}}(s)}{4\pi} p\sqrt{s}(\rho(s)+\mathrm{i})\, \mathrm{e}^{B(s)t/2}, \qquad (2)$$

where (see also Locher 1967 [5])

$$\alpha\phi(s,t) = \mp\alpha\left[\ln\left(\frac{-B(s)t}{2}\right)+\gamma\right]. \qquad (3)$$

Here, $\alpha = 1/137.036$ is the fine structure constant, $\gamma = 0.577215...$ is the Euler constant, $G_1(t)$ and $G_2(t)$ are the electric dipole form factors (being put into formula (2) by hand at the very end of the whole derivation for point-like particles). The quantity $\sigma^{\mathrm{tot,N}}$ is the total cross-section given by the optical theorem:

$$\sigma^{\mathrm{tot,N}}(s) = \frac{4\pi}{p\sqrt{s}}\,\mathrm{Im}\, F^{\mathrm{N}}(s,t=0). \qquad (4)$$

The simplified formula (2) was used widely mainly in the era of the ISR for the determination (often very misleadingly called a measurement) of three free parameters: $\sigma^{\mathrm{tot,N}}$, quantity $\rho(t=0)$, and diffractive slope $B(t=0)$. However, in the derivation of Eq. (2), two very strong assumptions concerning the t-dependence of the elastic hadronic amplitude were assumed to be valid at *all* kinematically allowed values of t:

1. t-independence of the phase of $F^{\mathrm{N}}(s,t)$, i.e., the quantity

$$\rho(s,t) = \frac{\mathrm{Re}\, F^{\mathrm{N}}(s,t)}{\mathrm{Im}\, F^{\mathrm{N}}(s,t)} \qquad (5)$$

was assumed to be t-independent;

2. purely exponential t-dependence of $\left|F^{\mathrm{N}}(s,t)\right|$, i.e., the diffractive slope defined as

$$B(s,t) = \frac{\mathrm{d}}{\mathrm{d}t}\left[\ln\frac{\mathrm{d}\sigma^{\mathrm{N}}}{\mathrm{d}t}(s,t)\right] = \frac{2}{|F^{\mathrm{N}}(s,t)|}\frac{\mathrm{d}}{\mathrm{d}t}\left|F^{\mathrm{N}}(s,t)\right| \qquad (6)$$

was assumed to be t-independent.

It has been shown in [6] that the first assumption must be valid otherwise the relative phase $\phi(s,t)$ becomes a complex function, which would lead to a contradiction (the relative phase has been defined as a real function [2]). The second assumption is in contradiction to the observed dip-bump structure in measured $\mathrm{d}\sigma/\mathrm{d}t$ data. Several other limitations and problems in the derivation of the simplified formula (2) or its application in the forward region were identified later, see [3, 7] for corresponding details and further references. The approach of WY is inapplicable for the reliable analysis of experimental data. Many recent models of elastic hadronic amplitude have been negatively influenced by the simplified formula (2). The models have been typically constrained by the values of $\sigma^{\mathrm{tot,N}}$, quantity $\rho(t=0)$, and $B(t=0)$ determined on the basis of the simplified formula, even though they have corresponded to the strongly t-dependent quantities $B(t)$ and $\rho(t)$. The measured differential cross-section data have been, therefore, described inconsistently.

3. Eikonal Model Approach

3.1. Theoretical background

In order to avoid (some of) the discrepancies and limitations related to the simplified WY formula, another approach to the description of the Coulomb-hadronic interference based on the eikonal model was proposed in 1994 by Kundrát and Lokajíček [8]. This widely used theoretical framework allowed one to derive a more general formula for the complete elastic scattering amplitude valid for *any* t-dependence of the phase and modulus of $F^{\mathrm{N}}(s,t)$ at a given (high) collision energy $\sqrt{s}$ and *any* value of t:

$$F^{\mathrm{C+N}}(s,t) = \pm\frac{\alpha s}{t} G^2_{\mathrm{eff}}(t) + F^{\mathrm{N}}(s,t)[1\mp \mathrm{i}\alpha\bar{G}(s,t)], \qquad (7)$$

where

$$\bar{G}(s,t) = \int\limits_{t_{\min}}^{0} \mathrm{d}t' \left\{\ln\left(\frac{t'}{t}\right)\frac{\mathrm{d}}{\mathrm{d}t'}\left[G^2_{\mathrm{eff}}(t')\right] - \\ - \frac{1}{2\pi}\left[\frac{F^{\mathrm{N}}(s,t')}{F^{\mathrm{N}}(s,t)} - 1\right] I(t,t')\right\}, \qquad (8)$$

and

$$I(t,t') = \int\limits_{0}^{2\pi} \mathrm{d}\Phi''\,\frac{G^2_{\mathrm{eff}}(t'')}{t''}; \qquad (9)$$

here, $t'' = t + t' + 2\sqrt{tt'}\cos\Phi''$. The upper (lower) sign corresponds to the scattering of particles with the same (opposite) charges. G^2_{eff} is the effective form factor squared reflecting the electromagnetic structure of colliding protons and was introduced in [9] as

$$G^2_{\mathrm{eff}}(t) = \frac{1}{1+\tau}\left[G^2_{\mathrm{E}}(t) + \tau\, G^2_{\mathrm{M}}(t)\right], \quad \tau = -\frac{t}{4m^2}, \quad (10)$$

where G_{E} and G_{M} stand for the electric and magnetic form factors, and m is the proton mass. The interference formula given by Eq. (7) allows one to study the t-dependence of the elastic hadronic amplitude and corresponding b-dependent properties consistently in the whole measured t range.

The b-dependent characteristics of *pp* collisions are standardly analyzed with the help of the Fourier–Bessel transform. It should be, however, consistent with a *finite* allowed region of the variable t and *finite* collision energies [10] (which is often not respected at all)

$$h_{\mathrm{el}}(s,b) = h_1(s,b) + h_2(s,b) = \\ = \frac{1}{4p\sqrt{s}}\int\limits_{-\infty}^{t_{\min}} F^{\mathrm{N}}(s,t) J_0(b\sqrt{-t})\mathrm{d}t + \\ + \frac{1}{4p\sqrt{s}}\int\limits_{t_{\min}}^{0} F^{\mathrm{N}}(s,t) J_0(b\sqrt{-t})\mathrm{d}t. \quad (11)$$

In this case, the unitarity equation in the b-space is

$$\mathrm{Im}\, h_1(s,b) = |h_1(s,b)|^2 + g_1(s,b) + K(s,b). \quad (12)$$

Here, $g_1(s,b)$ is a real inelastic overlap function which has been introduced in a similar way as the complex elastic amplitude in Eq. (11). The complex function $h_1(s,b)$ and real functions $g_1(s,b)$ oscillate at finite energies. The oscillations can be removed, if a real function $c(s,b) = -\,\mathrm{Im}\, h_2(s,b)$ fulfilling some mathematical conditions is added to both sides of the unitarity equation (12) [3]. It is then possible to define, at finite energies, the total, elastic, and inelastic profile functions $D^{\mathrm{X}}(s,b)$ (X=tot, el, inel)

$$D^{\mathrm{el}}(s,b) \equiv 4\,|h_1(s,b)|^2, \quad (13)$$

$$D^{\mathrm{tot}}(s,b) \equiv 4\,(\mathrm{Im}\, h_1(s,b) + c(s,b)), \quad (14)$$

$$D^{\mathrm{inel}}(s,b) \equiv 4\,(g_1(s,b) + K(s,b) + c(s,b)) \quad (15)$$

and rewrite the unitarity condition in the b-space as

$$D^{\mathrm{tot}}(s,b) = D^{\mathrm{el}}(s,b) + D^{\mathrm{inel}}(s,b). \quad (16)$$

These profile functions (sometimes called overlap functions) represent main b-dependent characteristics. They are used to define the root-mean-squared impact parameter $\sqrt{\langle b^2\rangle^{\mathrm{X}}}$ corresponding to the total, elastic, or inelastic hadron collisions.

Nearly all contemporary models of elastic hadron scattering a priori strongly constrain the elastic hadronic amplitude $F^{\mathrm{N}}(s,t)$ from the very beginning without sufficient reasoning, by requiring

1. dominance of the imaginary part of $F^{\mathrm{N}}(s,t)$ in a quite broad interval of t in the forward region close to $t = 0$;

2. vanishing of the imaginary part of $F^{\mathrm{N}}(s,t)$ at (or around) the dip $t = t_{\mathrm{dip}}$ (wrongly reasoned as a consequence of the minimum of $\mathrm{d}\sigma/\mathrm{d}t$ at t_{dip});

3.values of $\sigma^{\mathrm{tot,N}}]$, $B(t = 0)$ and $\rho(t = 0)$ (often misleadingly denoted as "measurement") obtained from the simplified WY formula;

4. change of a sign of the real part of $F^{\mathrm{N}}(s,t)$ at "low" values of $|t|$ (motivated by Martin's theorem [11] derived under certain (asymptotic) conditions).

The corresponding t-dependence of $F^{\mathrm{N}}(s,t)$ (its phase) is strongly constrained by these requirements. It may be shown that mainly the first requirement leads to the *central* behavior of elastic collisions corresponding to $\sqrt{\langle b^2\rangle^{\mathrm{el}}} < \sqrt{\langle b^2\rangle^{\mathrm{inel}}}$. The structure of protons which would correspond to this behavior has never been sufficiently explained.

One may, therefore, ask if it is possible to obtain a description of data which would lead to the *peripheral* behavior of elastic collisions $\sqrt{\langle b^2\rangle^{\mathrm{el}}} > \sqrt{\langle b^2\rangle^{\mathrm{inel}}}$ (without imposing the unreasoned constrains above). It was shown in 1981 [12] that the peripheral solution of the scattering problem may be obtained, if the hadronic phase has specific t-dependence.

3.2. Analysis of Measured Data

One may try to determine $F^{\mathrm{N}}(s,t)$ on the basis of experimental data under a given set of assumptions (constraints) and to study their impact on values of determined hadronic quantities. The eikonal interference formula given by Eqs. (7) to (9) may be used to subtract the Coulomb effect from the measured elastic pp $\mathrm{d}\sigma/\mathrm{d}t$ data at a given energy. The analysis of experimental elastic data in the full measured region of t values with the help of Eqs. (7) to (9) (with either effective electric or effective electromagnetic proton form factors determined from the ep scattering)

Comparison of several hadronic quantities characterizing the pp elastic scattering at energies of 52.8 GeV and 8 TeV

Particle types	pp	pp	pp	pp
$\sqrt{s}$ [GeV]	52.8	52.8	8000	8000
Fit	1	2	1	2
Case	central	peripheral	central	peripheral
$\rho(t=0)$	0.0763 ± 0.0017	0.0827 ± 0.0016	0.122 ± 0.018	0.149 ± 0.016
$B(t=0)$ [GeV^{-2}]	13.515 ± 0.035	13.444 ± 0.036	21.021 ± 0.085	20.829 ± 0.055
$\sigma^{\mathrm{tot,N}}$ [mb]	42.694 ± 0.033	42.861 ± 0.034	103.44 ± 0.35	104.12 ± 0.31
$\sigma^{\mathrm{el,N}}$ [mb]	7.469	7.539	27.6	28.0
σ^{inel} [mb]	35.22	35.32	75.9	76.1
$\sigma^{\mathrm{el,N}}/\sigma^{\mathrm{tot,N}}$	0.1750	0.1759	0.267	0.269
$\mathrm{d}\sigma^{\mathrm{N}}/\mathrm{d}t(t=0)$ [mb.GeV^{-2}]	93.67	94.51	555	566
$\sqrt{\langle b^2\rangle^{\mathrm{tot}}}$ [fm]	1.026	1.023	1.28	1.27
$\sqrt{\langle b^2\rangle^{\mathrm{el}}}$ [fm]	0.6778	1.959	0.896	1.86
$\sqrt{\langle b^2\rangle^{\mathrm{inel}}}$ [fm]	1.085	0.671	1.39	0.970
$D^{\mathrm{tot}}(b=0)$	1.29	1.30	2.01	2.04
$D^{\mathrm{el}}(b=0)$	0.530	0.0342	0.980	0.205
$D^{\mathrm{inel}}(b=0)$	0.762	1.27	1.03	1.84

requires a convenient parametrization of the complex elastic hadronic amplitude, i.e., of its modulus and phase:

$$F^{\mathrm{N}}(s,t) = \mathrm{i}\left|F^{\mathrm{N}}(s,t)\right| \mathrm{e}^{-\mathrm{i}\zeta^{\mathrm{N}}(s,t)}. \tag{17}$$

The modulus can be parametrized as

$$\left|F^{\mathrm{N}}(s,t)\right| = (a_1 + a_2 t)\,\mathrm{e}^{b_1 t + b_2 t^2 + b_3 t^3} + \\ + (c_1 + c_2 t)\,\mathrm{e}^{d_1 t + d_2 t^2 + d_3 t^3}, \tag{18}$$

and the phase can be parametrized as

$$\zeta^{\mathrm{N}}(s,t) = \zeta_0 + \zeta_1 \left|\frac{t}{t_0}\right|^{\kappa} \mathrm{e}^{\nu t}, \quad t_0 = 1\ \ \mathrm{GeV}^2. \tag{19}$$

This parametrization of the phase allows very different t-dependences according to the values of free parameters. It allows a rather fast increase of $\zeta^{\mathrm{N}}(s,t)$ with $|t|$, which is inevitable for increasing the value of $\sqrt{\langle b^2\rangle^{\mathrm{el}}}$ (for details, see, e.g., [3, 7, 8, 12, 13]). All parameters specifying the modulus and phase of the elastic hadronic amplitude $F^{\mathrm{N}}(s,t)$ may be energy-dependent. The parameter κ needs to be chosen as a positive integer to keep the analyticity of $F^{\mathrm{N}}(s,t)$.

Many fits of measured differential cross-section at 52.8 GeV [14] and 8 TeV data [15] under different additional constraints have been recently performed in [3] (see also [7]). Table shows two fits at each energy. Fit 1 corresponds to the widely imposed requirements on $F^{\mathrm{N}}(s,t)$ in many models of elastic scattering discussed in sect. 3.1. This leads to the *central* behavior of elastic collisions. Fit 2 corresponds to the *peripheral* picture of elastic collisions, and it has been obtained without imposing the strong and unreasoned constraints. The b-dependent profile functions given by Eqs. (13) to (15) corresponding to Fit 1 (central) and Fit 2 (peripheral) at an energy of 52.8 GeV are plotted in Figure.

The impact of a choice of the form factor (effective electric or effective electromagnetic one) has been found to be negligible or very small. The t-dependence of the hadronic phase $\zeta^{\mathrm{N}}(s,t)$ has, however, a fundamental impact on the character of collisions in the b-space. In a central case, relation $\sqrt{\langle b^2\rangle^{\mathrm{el}}} < \sqrt{\langle b^2\rangle^{\mathrm{tot}}}$ holds. But, in the peripheral alternative, the relation is reversed. It may be also interesting to note that Martin's theorem [11] is fulfilled in the central, as well as peripheral, alternative (at both energies).

4. Open Questions and Problems

We have reviewed many (all widely discussed) historical and contemporary models concerning the de-

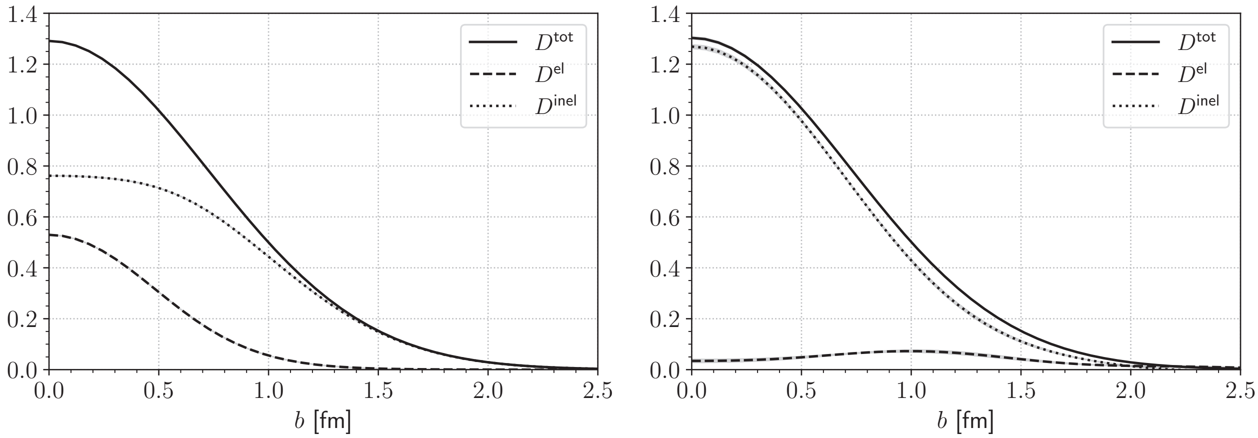

(a) central case – Fit 1 (b) peripheral case – Fit 2

Proton-proton profile functions $D(b)$ at an energy of 52.8 GeV. Full line corresponds to the total profile function, dashed line to the elastic one, and dotted line to the inelastic one

scription of elastic collisions and performed various fits of data under different conditions in order to better understand the processes with strongly interacting particles. On the basis of these studies, we have identified some deeper problems and open questions in *all* models and theoretical frameworks used in the description of the elastic scattering:

1. Coulomb interaction and experimental conditions;

a) (non-)divergence at $t = 0$

b) multiple collisions

c) electromagnetic form factors

2. Different mechanisms of Coulomb and strong forces;

3. Different types of short-ranged (contact) interactions;

4. Properties of the S matrix and the structure of a Hilbert space;

5. Optical theorem;

6. Determination of the b-dependent probability functions of hadron collisions;

7. Distribution of elastic scattering angles for a given value of the impact parameter;

8. Increase in the integrated total, elastic, and inelastic cross-sections and the dimensions of colliding particles in dependence on the collision energy;

9. extrapolations outside measured regions.

The identified open problems 1–7 were published in [4]. One may find there also the historical context concerning the dependence of proton collisions on the impact parameter, which is not widely known. Problems related specifically to the derivation of the optical theorem in particle physics are discussed in [16]. Open questions 8 and 9 are discussed in [3].

5. Conclusion

The simplified WY formula given by Eq. (2) and (3) was used widely in the era of the ISR for the analysis of experimental data. Determined values of $\sigma^{\text{tot,N}}$], $B(t = 0)$, and $\rho(t = 0)$ (at a given collision energy) on the basis of this model have often been denoted misleadingly as “measurement”. Many problems and limitations in the derivation of the formula, as well as in its application to data, have been identified, see sect. 2. The WY approach should be, therefore, abandoned in the era of the LHC, as it may lead to wrong physical conclusions. It should not be used for constraining the hadronic models based on assumptions inconsistent with the assumptions used in the derivation of a simplified WY model. One should look for the other description of the elastic scattering of (charged) hadrons.

The eikonal model approach is more general and relevant for the analysis of elastic scattering data at the present time, than the (over)simplified WY model. The former allows one to study the t-dependence of the elastic hadronic amplitude and corresponding hadronic quantities. It is more fundamental than the other contemporary models of elastic scattering as it may be used for the description of the Coulomb-hadronic interference *and* to consider the dependence of collisions on the impact parameter (in order not to mix collisions corresponding to different values of the impact parameter). We have analyzed elastic scattering data at 52.8 GeV and 8 TeV with the help of the eikonal model under different assumptions consistently in the whole measured t-range to see the impact on values of different physical quantities, see sect. 3.

This analysis of elastic scattering data with the use of the eikonal model approach has been prepared for the analysis of TOTEM data at the LHC. The first measurement of elastic differential pp data at the LHC energy of 8 TeV in the Coulomb-hadronic region published by TOTEM [15] contains the first analysis of the 8 TeV data using the eikonal model approach.

The results of our analysis (see sect. 3 and [3, 7] for more details and further references) represent the most elaborated impact parameter analysis of elastic pp collision data which has ever been performed. On the basis of our results, it may be concluded that the transparency of protons during elastic collisions (derived in widely used models of elastic pp scattering) has been based on unreasoned and unnecessary assumptions; the corresponding structure of protons has never been sufficiently explained in the literature. It is possible to say that there is no argument against the more realistic interpretation of elastic processes being peripheral and the protons regarded as rather compact (non-transparent) objects during elastic collisions.

We have reviewed basically all publicly available descriptions (models) of elastic hadron scattering over many years. Several deeper problems and open questions in *all* contemporary theoretical approaches (this includes WY model, eikonal model, Regge-based approaches, QCD-inspired approaches, ...) have been identified, see sect. 4. The proper analysis of hadron collisions in dependence on the impact parameter may provide an important insight concerning the shapes and dimensions (and other properties) of colliding particles, which can be hardly obtained in a different way. However, one should carefully study the assumptions involved in any collision model and test the consequences. It is also necessary to solve all the known fundamental problems and open questions in *any* contemporary description of the elastic pp scattering before making the far-reaching conclusions concerning the structure and properties of collided particles.

Further comments and new ideas how to move forward may be found in [4, 17]. The more fundamental analysis of the whole contemporary state of fundamental physical researches has been recently summarized in [18]. It has been argued that, to make progress in physics, one needs to return to *causal ontology* and *falsification approach* (i.e., the logic and systematic analysis of involved assumptions). In our opinion, our results may be important for new trends not only in high-energy physics, but in physics in general.

We would like to thank to the organizers, especially to L. Jenkovszky, of the “New Trends in High-Energy Physics” conference which took place in Odessa (Ukraine) in May 12–18 (2019) for the opportunity to present and discuss the achieved results.

1. M.K. Carter, P.D.B. Collins, M.R. Whalley. Compilation of nucleon-nucleon and nucleon-antinucleon elastic scattering data. Preprint RAL-86-002 (1986).
2. G.B. West, D.R. Yennie. Coulomb interference in high-energy scattering. *Phys. Rev.* **172**, 1413 (1968).
3. J. Procházka, V. Kundrát. Eikonal model analysis of elastic proton-proton collisions at 52.8 GeV and 8 TeV. *arXiv:1606.09479* (2019).
4. J. Procházka, M. V. Lokajíček, V. Kundrát. Dependence of elastic hadron collisions on impact parameter. *Eur. Phys. J. Plus* **131**, 147 (2016).
5. M.P. Locher. Relativistic treatment of structure in the Coulomb interference problem. *Nucl. Phys. B* **2**, 525 (1967).
6. V. Kundrát, M. Lokajíček, I. Vrkoč. Limited validity of West and Yennie interference formula for elastic scattering of hadrons. *Phys. Lett. B* **656**, 182 (2007).
7. J. Procházka. *Elastic Proton-Proton Collisions at High Energies*, PhD thesis (Charles University, 2018).
8. V. Kundrát, M. Lokajíček. High-energy scattering amplitude of unpolarized and charged hadrons. *Z. Phys. C* **63**, 619 (1994).
9. M.M. Block. Are we really measuring the phase of the nuclear scattering amplitude? *Phys. Rev. D* **54**, 4337 (1996).
10. M.M. Islam. *Lectures in theoretical Physics*. Edited by A.O. Barut and W.E. Brittin (Gordon and Breach, 1968), Vol. 10, B, 97.
11. A. Martin. A theorem on the real part of the high-energy scattering amplitude near the forward direction. *Phys. Lett. B* **404**, 137 (1997).
12. V. Kundrát, M. Lokajíček, jr., M. Lokajíček. Can quantum-mechanical description of physical reality be considered complete? *Czech. J. Phys. B* **31**, 1334 (1981).

13. V. Kundrát, M. Lokajíček, D. Krupa. Impact parameter structure derived from elastic collisions. *Phys. Lett. B* **544**, 132 (2002).
14. J. Bystricky *et al.* Nucleon-Nucleon and Kaon-Nucleon Scattering. In *Landolt–Bornstein, Numerical Data and Functional Relationships in Science and Technology, New Series.* Edited by H. Schopper (Springer, 1980), Vol. 9.
15. TOTEM Collaboration. Measurement of elastic pp scattering at $\sqrt{s} = 8$ TeV in the Coulomb-nuclear interference region – determination of the ρ-parameter and the total cross-section. *Eur. Phys. J. C* **76**, 661 (2016).
16. J. Procházka, V. Kundrát, M.V. Lokajíček. Elastic scattering of hadrons without optical theorem. arXiv:1502.00468 (2015).
17. M. V. Lokajíček, V. Kundrát, J. Procházka. Schrödinger equation and (future) quantum physics. In *Advances in Quantum Mechanics*, Edited by Paul Bracken (Intech, 2013).
18. M. V. Lokajíček, J. Procházka. The Contemporary State of Fundamental Physical Research and the Future Path to Scientific Knowledge. arXiv:1610.08331 (2019).

Received 08.07.19

Ї. Прохазка, В. Кундрат, М.В. Локаїчек

МОДЕЛІ ПРУЖНОГО pp-РОЗСІЯННЯ – МОЖЛИВОСТІ, ОБМЕЖЕННЯ ТА ПИТАННЯ

Р е з ю м е

Найпростіший процес зіткнень, а саме пружне розсіяння протонів вимірювалось при різних енергіях та широкому інтервалі кутів розсіяння. Відповідний теоретичний опис, однак, набагато делікатніший, ніж може здаватися. Широко відома ейкональна модель дозволила провести аналіз пружних pp-даних при енергіях прискорювачів ISR, 52,8 ГеВ та LHC 8 ТеВ. Наші результати представляють найдетальніший та ретельно опрацьований прицільний аналіз pp-даних. Вони допомогли прояснити ряд питань та проблем опису пружного розсіяння протонів. Цю програму потрібно продовжити.

https://doi.org/10.15407/ujpe64.8.732

D.A. PTASHYNSKIY, T.M. ZELENTSOVA, N.O. CHUDAK, K.K. MERKOTAN, O.S. POTIIENKO, V.V. VOITENKO, O.D. BEREZOVSKIY, V.V. OPYATYUK, O.V. ZHAROVA, T.V. YUSHKEVICH, I.V. SHARPH, V.D. RUSOV

Odessa National Polytechnic University
(1, Shevchenko Ave., Odessa, 65044, Ukraine; e-mail: sharph@ukr.net)

MULTIPARTICLE FIELDS ON THE SUBSET OF SIMULTANEITY

We propose a model describing the scattering of hadrons as bound states of their constituent quarks. We build the dynamic equations for the multiparticle fields on the subset of simultaneity, using the Lagrange method, similarly to the case of "usual" single-particle fields. We then consider the gauge fields restoring the local internal symmetry on the subset of simultaneity. Since the multiparticle fields, which describe mesons as bound states of a quark and an antiquark, are two-index tensors relative to the local gauge group, it is possible to consider a model with two different gauge fields, each one associated with its own index. Such fields would be transformed by the same laws during a local gauge transformation and satisfy the same dynamic equations, but with different boundary conditions. The dynamic equations for the multiparticle gauge fields describe such phenomena as the confinement and the asymptotic freedom of colored objects under certain boundary conditions and the spontaneous symmetry breaking under another ones. With these dynamic equations, we are able to describe the quark confinement in hadrons within a single model and their interaction during the hadron scattering through the exchange of the bound states of gluons – the glueballs.

Keywords: multiparticle fields, problem of simultaneity in relativistic quantum theory, confinement of quarks and gluons, Higgs mechanism, energy-momentum conservation law in hadron processes.

1. Introduction

Probably for the first time, the idea of multiparticle fields was proposed by H. Yukawa [1–3]. H. Yukawa called these fields "nonlocal" fields. We use another term "multiparticle fields" to show the differences between our model from the model proposed by H. Yukawa. The most essential difference between the proposed model from not only the Yukawa model, but also from models on the light cone [4, 5], quasipotential models [6–8], and models with multitime probability amplitudes [9–11] is that, in our opinion, the internal variables of such fields in different inertial reference systems cannot be related to each other, whereas these variables are connected by Lorentz transformations in the said models. We have already partially explained our viewpoint in the previous article [12]. The use of multitime probability amplitudes in [9–11, 13–15], other works of this direction, and the above-mentioned works contradicts the principles of quantum theory, because it does not consider, in our opinion, the measuring instrument influence on the state of a microsystem. In more details, we explain it in work [16], where we proposed an alternative approach to ensuring the simultaneity of quantum-mechanical measurements in different reference systems, and introduce a subset of simultaneity of the Cartesian product of several Minkowski spaces. On the other hand, the existing field theories are considered in such a way that all interaction effects are reduced only to changes in the occupation numbers of the single-particle states of free particles. This leads to the fact that, in such models, when the dynamics of processes is described, the sum of energy-momenta of these one-particle states is conserved. At the same time, the energy-momentum of hadrons, but not of constituent particles, must be conserved for the processes with hadrons. The model of multiparticle fields on the subset of simultaneity proposed in this article allows us to construct a dynamic description, which is free of the mentioned problems.

2. Scalar Product on a Subset of Simultaneity

Let us consider a meson as a two-particle system consisting of the constituent quark and antiquark. The time and coordinates of the Minkowski space of the first particle will be denoted $\left(x^0_{(1)}, x^1_{(1)}, x^2_{(1)}, x^3_{(1)}\right)$, for the second particle $\left(x^0_{(2)}, x^1_{(2)}, x^2_{(2)}, x^3_{(2)}\right)$. Here, as usual, the index 0 denotes the time coordinate of the event, and 1,2,3 are the spatial coordinates. The lower indices in parentheses identify the first and second particles. The parentheses are used to distinguish these indices from the covariant coordinates of the event. The upper indices are used to denote contravariant coordinates. The Cartesian product of Minkowski spaces for two particles is an eight-dimensional linear space. Its elements can be considered as columns

$$z^a = \begin{pmatrix} x^0_{(1)} \\ x^1_{(1)} \\ x^2_{(1)} \\ x^3_{(1)} \\ x^0_{(2)} \\ x^1_{(2)} \\ x^2_{(2)} \\ x^3_{(2)} \end{pmatrix}. \tag{1}$$

We introduce a scalar product in this eight-dimensional space by the following expression:

$$\langle z|z\rangle = \frac{1}{2}\left(g^{\mathrm{Minc}}_{ab} x^a_{(1)} x^b_{(1)} + g^{\mathrm{Minc}}_{ab} x^a_{(2)} x^b_{(2)}\right). \tag{2}$$

Here, g^{Minc}_{ab} is the Minkowski tensor. The indices a and b are repeated and summed up, and each of these indices takes the value of 0,1,2,3. Then it is convenient to use the Jacobi coordinates

$$X^a = \frac{1}{2}\left(x^a_{(1)} + x^a_{(2)}\right), \quad y^a = x^a_{(2)} - x^a_{(1)}. \tag{3}$$

In view of (3), the expression for a scalar product (2) takes the form

$$\langle z|z\rangle = g^{\mathrm{Minc}}_{ab}\left(X^a X^b + \frac{1}{4} y^a y^b\right). \tag{4}$$

A condition for the subset of simultaneity in coordinates (3) reads

$$y^0 = 0. \tag{5}$$

The coordinates of a point on a subset of simultaneity are denoted by a seven-component column

$$q^a = \begin{pmatrix} X^0 \\ X^1 \\ X^2 \\ X^3 \\ y^1 \\ y^2 \\ y^3 \end{pmatrix}. \tag{6}$$

We define the scalar product on a subset of simultaneity so that it coincides with product (4) with regard for condition (5):

$$\langle q|q\rangle = g_{ab} q^a q^b, \tag{7}$$

where the metric tensor is

$$g^{ab} = \begin{pmatrix} 1 & 0 & 0 & 0 & 0 & 0 & 0 \\ 0 & -1 & 0 & 0 & 0 & 0 & 0 \\ 0 & 0 & -1 & 0 & 0 & 0 & 0 \\ 0 & 0 & 0 & -1 & 0 & 0 & 0 \\ 0 & 0 & 0 & 0 & -4 & 0 & 0 \\ 0 & 0 & 0 & 0 & 0 & -4 & 0 \\ 0 & 0 & 0 & 0 & 0 & 0 & -4 \end{pmatrix}. \tag{8}$$

The multiparticle field will be described by a set of field functions $\Psi_a(q) = \Psi_a(X, \mathbf{y})$. Here, X is a set of coordinates X^0, X^1, X^2, X^3, and $\mathbf{y}$ is a set of internal variables y^1, y^2, y^3. The index a enumerates different components of the field, and its range space is determined by the representation of a transformation group, which describes the transition from field functions relative to one reference system to field functions relative to another reference system. The group of matrices acts on a subset of simultaneity as follows:

$$\hat{G} = \begin{pmatrix} \Lambda^0_0 & \Lambda^0_1 & \Lambda^0_2 & \Lambda^0_3 & 0 & 0 & 0 \\ \Lambda^1_0 & \Lambda^1_1 & \Lambda^1_2 & \Lambda^1_3 & 0 & 0 & 0 \\ \Lambda^2_0 & \Lambda^2_1 & \Lambda^2_2 & \Lambda^2_3 & 0 & 0 & 0 \\ \Lambda^3_0 & \Lambda^3_1 & \Lambda^3_2 & \Lambda^3_3 & 0 & 0 & 0 \\ 0 & 0 & 0 & 0 & R^1_1 & R^1_2 & R^1_3 \\ 0 & 0 & 0 & 0 & R^2_1 & R^2_2 & R^2_3 \\ 0 & 0 & 0 & 0 & R^3_1 & R^3_2 & R^3_3 \end{pmatrix}. \tag{9}$$

The indices of the G^a_b matrix take the values from 0 to 6. $\Lambda^a_b, a, b = 0, 1, 2, 3$ are the elements of the Lorentz transformation matrix, and $R^a_b, a, b = 1, 2, 3$ are the elements of the rotation matrix.

The scalar product (7) with the metric tensor (8) is invariant relative to the group transformations (9).

Hence, our further aim will be to construct a quantum field theory not on the Minkowski space with the Lorentz group, but on the above subset of simultaneity with group (9). In work [16], we show that if the Minkowski space is replaced by a subset of simultaneity and the Lorentz group is group (9), then such a theory can be constructed in the same way as a "usual" one-particle field theory. At the same time, such a model conforms to the principle of relativity.

3. Lagrangian of a Two-Particle Meson Field

We use the notation $\psi_{c_1c_2,f_1,f_2}(q)$ for a two-particle meson field, which describes, after the quantization, the processes of creation and annihilation of bound states of a quark and an antiquark. Here, q is a set of seven variables (6). Indices with subindices 1 and 2 correspond to an antiquark and a quark, respectively, c_1 is the color of an antiquark, and c_2 is the color of a quark, f_1 is the flavor of an antiquark, and f_2 is a flavor of a quark. Accordingly, the field $\psi_{c_1c_2,f_1,f_2}(q)$ takes the value, for which the mixed tensor representations of the $SU_c(3)$ and $SU_f(3)$ groups are realized:

$$\begin{aligned}&{\psi'}_{c_1c_2,f_1,f_2}(q) = \\ &= u^{(c)\dagger}_{c_1c_3}\, u^{(c)}_{c_2c_4}\, u^{(f)\dagger}_{f_1f_3}\, u^{(f)}_{f_2f_4}\, \psi_{c_3c_4,f_3,f_4}(q).\end{aligned} \tag{10}$$

Here, $u^{(c)}_{c_2c_4}$ are the elements of an arbitrary matrix of the $SU_c(3)$ group and $u^{(f)}_{f_2f_4}$ are elements of an independent matrix of the $SU_f(3)$ group. A sign † is used to denote the elements of the adjoint matrix. Duplicate indices usually mean the summation. The dynamic equations for the field $\psi_{c_1c_2,f_1,f_2}(q)$ must be symmetric relative to transformations (10).

Moreover, the dynamic equations must be symmetric relative to group (9). The simplest Lagrangian that generates such equations can be written in the form

$$\begin{aligned}&L^{(0)} = g^{ab}\frac{\partial\psi^*_{c_1c_2,f_1,f_2}(q)}{\partial q^a}\,\frac{\partial\psi_{c_1c_2,f_1,f_2}(q)}{\partial q^b} - \\ &- M^2_\mu\psi^*_{c_1c_2,f_1,f_2}(q)\,\psi_{c_1c_2,f_1,f_2}(q).\end{aligned} \tag{11}$$

Here, g^{ab} are the tensor components (8), and the term M_μ will be considered as the "bare" meson mass. The "real" meson mass was considered in [16].

Since the field $\psi_{c_1c_2,f_1,f_2}(q)$ must describe the dynamics of the bound states of a quark and an antiquark, Lagrangian (11) is obviously incomplete, because it does not involve the interaction between a quark and an antiquark, which ensures the existence of a bound state. As usual, such an interaction can be introduced, if we demand the symmetry of the Lagrangian relative to the local transformations of the internal symmetry in the form (10). Since the existence of a meson as a bound state of the quark and the antiquark is due to the strong interaction, we choose the symmetry relative to the local $SU_c(3)$-transformations. This symmetry can also be achieved in the usual way, if we will replace the "ordinary" derivatives in Lagrangian (11) by the covariant derivatives and will introduce the corresponding compensating fields $A^{(1)}_{a,g_1}(q)$ and $A^{(2)}_{a,g_1}(q)$.

Further, instead of these fields, it would be convenient to consider their linear combinations, similarly to Jacobi variables,

$$\begin{aligned}&A^{(+)}_{a,g_1}(q) = \frac{1}{2}\left(A^{(1)}_{a,g_1}(q) + A^{(2)}_{a,g_1}(q)\right),\\ &A^{(-)}_{a,g_1}(q) = A^{(2)}_{a,g_1}(q) - A^{(1)}_{a,g_1}(q).\end{aligned} \tag{12}$$

A local $SU_c(3)$ group representation is given for the domain of values of the field functions $\psi_{c_1c_2,f_1,f_2}(q)$. So, this domain may be decomposed into a direct sum of subspaces which are invariant relative to transformations of this representation. Since the hadron is colorless, we will be interested in a field that has a nonzero projection only on a subspace, on which a scalar irreducible representation is realized. This means that the field $\psi_{c_1c_2,f_1,f_2}(q)$ can be given as

$$\psi_{c_1c_2,f_1,f_2}(q) = \delta_{c_1c_2}\psi_{f_1,f_2}(q), \tag{13}$$

where $\psi_{f_1,f_2}(q)$ are the new field functions for the dynamical equations, which should describe, after the quantization, the processes of creation and annihilation of mesons. These dynamic equations can be obtained from the Lagrangian with covariant derivatives that is formed, if we substitute (13) with regard for notation (12). After these transformations, this Lagrangian takes the form

$$\begin{aligned}&L_\mu = 3g^{ab}\left(\partial\psi^*_{f_1,f_2}(q)/\partial q^a\right)\left(\partial\psi_{f_1,f_2}(q)/\partial q^b\right) + \\ &+ V(q)\psi^*_{f_1,f_2}(q)\psi_{f_1,f_2}(q) - \\ &- 3M^2_\mu\psi^*_{f_1,f_2}(q)\psi_{f_1,f_2}(q),\end{aligned} \tag{14}$$

where

$$V(q) = 2g^2 g^{ab} A^{(-)}_{a,g_1}(q)\, A^{(-)}_{b,g_1}(q). \quad (15)$$

4. Dynamic Equation for the Field $V(q)$

In order to obtain the dynamic equations for a two-gluon field, we consider the simplest tensor that can be formed from single-gluon fields

$$A_{ab,g_1g_2}(q) = g^2 \left(A^{(-)}_{a,g_1}(q)\, A^{(-)}_{b,g_2}(q)\right), \quad a,b = 4,5,6. \quad (16)$$

Extending the linear space of the tensors $A_{ab,g_1g_2}(q)$ relative to group (9) into the direct sum of invariant subspaces, we pick a term corresponding to the projection on a scalar subspace

$$A_{ab,g_1g_2}(q) = -A_{g_1g_2}(q)\, g_{ab} + \dots . \quad (17)$$

Convolving both sides of equality (17) with the metric tensor g^{ab}, we obtain

$$A_{g_1g_2}(q) = \frac{4}{7} g^2 \sum_{b=4}^{6} \left(A^{(-)}_{b,g_1}(q)\, A^{(-)}_{b,g_2}(q)\right). \quad (18)$$

Then we apply a similar procedure for internal indices. Considering the coupling equations obtained in [16] and definition (15), we get

$$\begin{aligned} &A_{g_1g_2}(q) = A(q)\, \delta_{g_1g_2} + ..., \\ &A(q) = \frac{1}{14} g^2 \sum_{b=4}^{6} \left(A^{(-)}_{b,g_1}(q)\, A^{(-)}_{b,g_1}(q)\right) = \frac{1}{14} V(q). \end{aligned} \quad (19)$$

The kinetic part of the Lagrangian for the $A_{g_1g_2}(q)$ field can be given as

$$\begin{aligned} L^{(0)}_G &= \frac{1}{2} g^{ab} \frac{\partial A_{g_1g_2}(q)}{\partial q^a} \frac{\partial A_{g_1g_2}(q)}{\partial q^b} - \\ &- \frac{1}{2} M_G^2 A_{g_1g_2}(q)\, A_{g_1g_2}(q). \end{aligned} \quad (20)$$

Replacing ordinary derivatives by covariant ones and performing some calculations described in [16], we obtain the Lagrangian

$$\begin{aligned} L_V &= \frac{1}{2} g^{ab} \frac{\partial V(q)}{\partial q^a} \frac{\partial V(q)}{\partial q^b} + \\ &+ \frac{3}{2} (V(q))^3 - \frac{1}{2} M_G^2 (V(q))^2. \end{aligned} \quad (21)$$

Having a Lagrangian for the field $V(q)$, we can obtain a dynamic equation for this field such as the Euler–Lagrange equation:

$$-g^{ca} \frac{\partial^2 V(q)}{\partial q^c \partial q^a} - M_G^2 V(q) + \frac{9}{2} (V(q))^2 = 0. \quad (22)$$

We introduce the function $V(q) = V(X, \mathbf{y})$ (with regard for (6)) in the form

$$\begin{aligned} &V(X,\mathbf{y}) = V_0(\mathbf{y}) + V_1(X,\mathbf{y}), \\ &V_1(X,\mathbf{y}) \equiv V(X,\mathbf{y}) - V_0(\mathbf{y}). \end{aligned} \quad (23)$$

Then the function $V_0(\mathbf{y})$, will enter the complete Lagrangian as the potential energy of interaction of nonrelativistic constituent quarks. At the same time, it will satisfy the equation

$$4\Delta_{\mathbf{y}} V_0(\mathbf{y}) - M_G^2 V_0(\mathbf{y}) - \frac{9}{2} (V_0(\mathbf{y}))^2 = 0. \quad (24)$$

Analyzing the properties of the solutions of Eq. (24), we can obtain information about the interaction potential for quarks. Before analyzing these properties, we will make this equation to be dimensionless.

Let us introduce the dimensionless internal coordinates $\mathbf{r}$, dimensionless glueball mass m_G, and dimensionless potential energy $u(\mathbf{r})$:

$$\begin{aligned} &\mathbf{y} = l\mathbf{r}, M_G = l^{-1} m_G, \\ &V_0(\mathbf{y}) = V_0(l\mathbf{r}) = l^{-2} u(\mathbf{r}). \end{aligned} \quad (25)$$

Then, instead of Eq. (24), we obtain

$$4\Delta_{\mathbf{r}} u(\mathbf{r}) - m_G^2 u(\mathbf{r}) - \frac{9}{2} (u(\mathbf{r}))^2 = 0. \quad (26)$$

Here, $\Delta_{\mathbf{r}} \equiv \sum_{b=1}^{3} \frac{\partial^2}{\partial (r^b)^2}$ is the Laplace operator in dimensionless variables $\mathbf{r}$.

We now consider the properties of a spherically symmetric solution of Eq. (26). In order to transform the variables $\mathbf{r}\left(r^1, r^2, r^3\right)$, we pass to spherical coordinates and make the standard replacement

$$u(r) = \frac{\chi(r)}{r}. \quad (27)$$

Finally,we obtain

$$\frac{d^2\chi(r)}{dr^2} = \frac{9}{8} \frac{\chi(r)\left(\chi(r) + \left(m_G^2/9\right) r\right)}{r}. \quad (28)$$

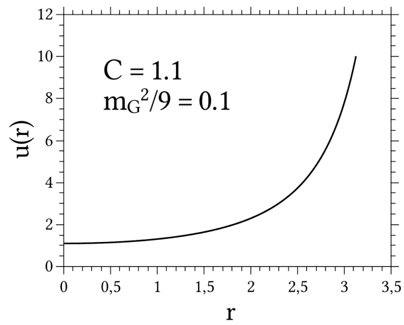

Fig. 1. Results of the numerical calculation of the dimensionless inter-quark potential $u(r)$ as a function of the dimensionless distance r for $C = 1.1$, $m_G^2/9 = 0.1$

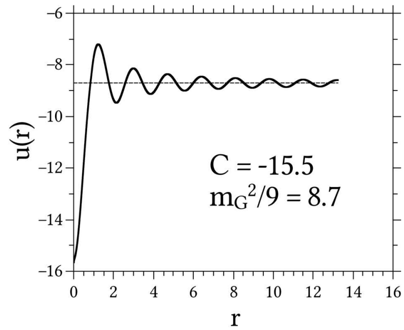

Fig. 2. Results of numerical calculations of the dimensionless inter-quark potential $u(r)$ as a function of the dimensionless distance r for $C = -15.5$, $m_G^2/9 = 8.7$

In order to analyze the properties of solutions of Eq. (28), we use an analogy with classical mechanics. We will consider the independent variable r as an analog of the time. We will call the quantity χ a "coordinate". Let its first derivative $d\chi/dr$ be a "velocity," and let the second derivative $d^2\chi/dr^2$ be an "acceleration". The dependence of "acceleration" on "coordinate", which is determined by the right part of Eq. (28), leads to the fact that, on the coordinate plane (r, χ), there are three domains [16]. Inside each of them, the "acceleration" has a constant sign. So, if the graph $\chi(r)$ gets into one of these three selected domains, then the following path of this graph is determined by the corresponding sign of the "acceleration".

Let us establish the boundary conditions for the function $\chi(r)$. We can see from Eq. (27) that if we want to obtain the finite potential energy $u(r)$ for all finite values r, we should fulfill the condition

$$\chi(r)|_{r=0} = 0. \tag{29}$$

At that, the "initial velocity" should not be equal to zero, and we can set it to a certain real number:

$$\left.\frac{d\chi(r)}{dr}\right|_{r=0} = C, \quad C \in \mathbb{R}. \tag{30}$$

We now consider the properties of a solution of Eq. (28) depending on the selection of the value C.

Let the solution satisfy the boundary conditions (29) and (30) with $C > 0$.

In Fig. 1, we see that, as r increases, the inter-quark potential $u(r)$ tends to infinity. Consequently, the considered model describes the quark confinement.

If $C < 0$, the potential $u(r)$ tends to some negative constant value. Thus, the eigenvalue of the squared internal Hamiltonian will definitely be negative. Since this eigenvalue is a coefficient at the squared field describing the bound state of two gauge bosons, this corresponds to the mechanism of spontaneous symmetry breaking. In this case, the result of numerical calculations of the $u(r)$ dependence on r is presented in Fig. 2.

5. Conclusions

In the proposed model, the strong interaction between the quarks in hadrons can be caused by the exchange of the bound states of gluons – the glueballs. The field $V(X, \mathbf{y})$, according to glueballs, can be represented as a sum of two terms,$V_0(\mathbf{y})$ and $V_1(X, \mathbf{y})$. The field $V_0(\mathbf{y})$ is not quantized and describes the strong interaction of quarks and gluons inside mesons and glueballs. This field satisfies the dynamic equation which describes the confiment of quarks and gluons under certain boundary conditions and spontaneous symmetry breaking – under another ones. When the bare mass of a glueball has a zero value, all solutions of this equation, irrespective of the boundary conditions, will lead to the confiment. The field $V_1(X, \mathbf{y})$ can be quantized. Though we did not consider the quantization procedure for multiparticle fields in this work, it is not different from the procedure described in work [17]. The operators obtained after the quantization will describe the processes of creation and annihilation of glueballs, as shown in [17]. Accordingly, the considered meson field quantization leads to the operators of creation and annihilation of the mesons. The meson interaction due to the interaction of constituent quarks can be described as the exchange by scalar glueballs. This approach differs from the one-particle field approach, because, in our model, the energy-momentum conservation law holds true precisely for hadrons, and not for the constituent particles.

1. H. Yukawa. On the radius of the elementary particle. *Phys. Rev.* **76**, 300 (1949).
2. H. Yukawa. Quantum theory of non-local fields. Part I. Free fields. *Phys. Rev.* **77**, 219 (1950).
3. H. Yukawa. Quantum theory of non-local fields. Part II. Irreducible fields and their interaction. *Phys. Rev.* **80**, 1047 (1950).
4. P. Dirac. Forms of relativistic dynamics. *Rev. Mod. Phys.* **21**, 392 (1949).
5. T. Heinzl. Light cone quantization: Foundations and applications. *Lect. Notes Phys.* **572**, 55 (2001).
6. A. Logunov, A. Tavkhelidze. Quasi-optical approach in quantum field theory. *Il Nuovo Cim. Ser. 10* **29**, 380 (1963).
7. A. Logunov, A. Tavkhelidze, I. Todorov, O. Khrustalev. Quasi-potential character of the scattering amplitude. *Il Nuovo Cim. Ser. 10* **30**, 134 (1963).
8. R. Faustov. Relativistic wavefunction and form factors of the bound system. *Ann. Phys.* **78**, 176 (1973).
9. S. Tomonaga. On a relativistically invariant formulation of the quantum theory of wave fields. *Prog. Theor. Phys.* **1**, 27 (1946).
10. P. Dirac, W. Fock, B. Podolsky. On quantum electrodynamics. *Phys. Zs. Sowjet.* **2**, 468 (1932).
11. S. Petrat, R. Tumulka. Multi-time wave functions for quantum field theory. *Ann. Phys.* **345**, 17 (2014).
12. N.O. Chudak, K.K. Merkotan, D.A. Ptashynskiy *et al.* Internal states of hadrons in relativistic reference systems. *Ukr. Fiz. Zh.* **61**, 1039 (2016).
13. E. Marx. Generalized relativistic Fock space. *Int. J. Theor. Phys.* **6**, 359 (1972).
14. H. Sazdjian. Relativistic wave equations for the dynamics of two interacting particles. *Phys. Rev. D* **33**, 3401 (1986).
15. S. Petrat, R. Tumulka. Multi-time equations, classical and quantum. *Proc. Royal Soc. of London A: Math., Phys. Eng. Sci.* **470**, 1364 (2014).
16. D.A. Ptashynskiy, T.M. Zelentsova, N.O. Chudak *et al.* Multiparticle fields on the subset of simultaneity. *arXiv:1905.07233* [physics.gen-ph].
17. N. Chudak, M. Deliyergiyev, K. Merkotan *et al.* Multiparticle quantum fields. *Phys. J.* **2**, 181 (2016).

Received 08.07.19

Д.А. Пташинський, Т.М. Зеленцова, Н.О. Чудак, К.К. Меркотан, О.С. Потієнко, В.В. Войтенко, О.Д. Березовський, В.В. Опятюк, О.В. Жарова, Т.В. Юшкевич, І.В. Шарф, В.Д. Русов

БАГАТОЧАСТИНКОВІ ПОЛЯ
НА ПІДМНОЖИНІ ОДНОЧАСНОСТІ

Р е з ю м е

В роботі пропонується модель для опису процесів розсіяння гадронів як зв'язаних станів конституентних кварків. На підмножині одночасності розглядається побудова динамічних рівнянь для багаточастинкових полів за допомогою методу Лагранжа, аналогічно тому, як це робиться для "звичайних" одночастинкових полів. Розглянуто калібрувальні поля, які відновлюють локальну внутрішню симетрію на підмножині одночасності. Для багаточастинкових полів, що описують мезони як зв'язані стани кварка і антикварка і є двоіндексними тензорами відносно локальної калібрувальної групи, запропоновано модель з двома різними калібрувальними полями, кожне з яких пов'язане зі своїм індексом. Такі поля перетворюються за однаковим законом при локальному калібрувальному перетворенні і задовольняють однаковим динамічним рівнянням, але на них накладаються різні крайові умови. При певних крайових умовах ці рівняння описують такі фізичні явища, як конфайнмент і асимптотичну свободу кольорових об'єктів, а при інших крайових умовах – механізм спонтанного порушення симетрії. Ці динамічні рівняння дозволяють в межах однієї й тієї ж моделі описати як утримання кварків всередині гадронів, так і їх взаємодію в процесах розсіяння гадронів, шляхом обміну зв'язаними станами глюонів – глюболами.

https://doi.org/10.15407/ujpe64.8.738

M. RYBCZYŃSKI,[1] G. WILK,[2] Z. WŁODARCZYK[1]
[1] Institute of Physics, Jan Kochanowski University
(25-406 Kielce, Poland; e-mail: maciej.rybczynski@ujk.edu.pl, zbigniew.wlodarczyk@ujk.edu.pl)
[2] National Centre for Nuclear Research
(02-093 Warsaw, Poland; e-mail: grzegorz.wilk@ncbj.gov.pl)

A LOOK AT MULTIPLICITY DISTRIBUTIONS VIA MODIFIED COMBINANTS

The experimentally measured multiplicity distributions exhibit, after a closer inspection, the peculiarly enhanced void probability and the oscillatory behavior of modified combinants. We show that both these features can be used as additional sources of information, not yet fully explored, on the mechanism of multiparticle production. We provide their theoretical understanding within the class of compound distributions.

Keywords: multiplicity distributions, combinants, void probabilities, compound distributions.

1. Introduction

The experimentally measured (non-single diffractive (NSD) charged) multiplicity distributions, $P(N)$ (which are one of the most thoroughly investigated and discussed sources of information on the mechanism of the production process [1]), exhibit, after a closer inspection, the peculiarly enhanced void probability, $P(0) > P(1)$ [2, 3], and the oscillatory behavior of the so-called modified combinants, C_j, introduced by us in [4, 5] (and thoroughly discussed in [6, 7]; they are closely connected with the combinants $C^\star_j$ introduced in [8] and discussed occasionally for some time [9–14]). Both features were only rarely used as a source of information. We demonstrate that the modified combinants can be extracted experimentally from the measured $P(N)$ by means of a recurrence relation involving all $P(N < j)$, and that new information is hidden in their specific distinct oscillatory behavior, which, in most cases, is not observed in the C_j obtained from the $P(N)$ commonly used to fit experimental results [4–7]. We discuss the possible sources of such behavior and the connection of C_j with the enhancement of void probabilities, and their impact on our understanding of the multiparticle production mechanism, with emphasis on understanding both phenomena within the class of compound distributions.

2. Recurence Relation and Modified Combinants

The dynamics of the multiparticle production process is hidden in the way, in which the consecutive measured multiplicities N are connected. There are two ways of characterizing the multiplicity distributions: by means of generating functions, $G(z) = \sum_{N=0}^{\infty} P(N) z^N$, or by some form of a recurrence relation between $P(N)$. In the first case, one uses the Poisson distribution as a reference and characterizes deviations from it by means of combinants $C^\star_N$ defined as [8]

$$C^\star_j = \frac{1}{j!}\frac{d^j \ln G(z)}{dz^j}\bigg|_{z=0}, \tag{1}$$

or by the expansion

$$\ln G(z) = \ln P(0) + \sum_{j=1}^{\infty} C^\star_j z^j. \tag{2}$$

For the Poisson distribution, $C^*_1 = \langle N\rangle$ and $C^*_{j>1} = 0$. The combinants were used in the analysis of experimental data in [9–14]. In [10, 13], it was demonstrated that they are particularly useful in identifying the nature of the emitting source. It turns out that, in the case of S sources emitting particles without any restrictions concerning their number, the multiplicity $P^S(N)$ is a completely symmetric function of degree N of the probabilities of emission, p_i, the generating function of which reduces for $p_i \to 0$ to the generating function of the Poisson Distribution (PD). For all probabilities remaining the same, $p_i = p$, it reduces to the generating function of the Negative Binomial Distribution (NBD). In this case, the combinants are given by a power series

$$C^\star_j = \frac{1}{j}\sum_{i=1}^{S} p_i^j \tag{3}$$

and are always positive. However, when each of the sources can emit only a given number of particles (let us assume, for definiteness, that at most only one particle), then $P^S(N)$ is an elementary symmetric function of degree N in the arguments, and the corresponding combinants are given by

$$C^\star_j = (-1)^{j+1}\frac{1}{j}\sum_{i=1}^{S}\left(\frac{p_i}{1-p_i}\right)^j, \tag{4}$$

and alternate in sign for different j's. For all probabilities remaining the same, $p_i = p$, a generating function in this scenario reduces to the generating function of the Binomial Distribution (BD) and the combinants oscillate rapidly with period equal to 2.

Note that, in both cases, we were working with probabilities p_i, which were not extracted from experiment, but their values were taken such that the measured multiplicity distributions are reproduced. They are then usually represented by one of the known theoretical formulae for multiplicity distributions, $P(N)$, which can be defined either by the generating functions mentioned above or by some recurrence relations connecting different $P(N)$. In the simplest (and most popular) case, one assumes that the multiplicity N is directly influenced only by its neighboring multiplicities, $(N \pm 1)$, i.e., we have

$$(N+1)P(N+1) = g(N)P(N), \quad g(N) = \alpha+\beta N. \tag{5}$$

This recurrence relation yields BD (when $\alpha = Kp/(1-p)$ and $\beta = -\alpha/K$), PD (when $\alpha = \lambda$ and $\beta = 0$), and NBD (when $\alpha = kp$ and $\beta = \alpha/k$, where p denotes the particle emission probability). Usually, the first choice of $P(N)$ in fitting the data is a single NBD [15] or two- [16, 17], three- [18], or multicomponent NBDs [19] (or some other forms of $P(N)$ [1,15,20]). However, such a procedure only improves the agreement at large N, whereas the ratio R = data/fit still deviates dramatically from unity at small N for all fits [4, 5]. This means that the measured $P(N)$ contains information which is not yet captured by the rather restrictive recurrence relation (5). Therefore, in [4], we proposed to use a more general form of the recurrence relation (used, e.g., in counting statistics when dealing with multiplication effects in point processes [21]):

$$(N+1)P(N+1) = \langle N\rangle \sum_{j=0}^{N} C_j P(N-j). \tag{6}$$

This relation connects multiplicities N by means of some coefficients C_j, which contain the memory of particle $N+1$ about all the $N-j$ previously produced particles. The most important feature of this recurrence relation is that C_j can be directly calculated from the experimentally measured $P(N)$ by reversing Eq. (6) [4–7]:

$$\langle N\rangle C_j = (j+1)\left[\frac{P(j+1)}{P(0)}\right] - \langle N\rangle \sum_{i=0}^{j-1} C_i \left[\frac{P(j-i)}{P(0)}\right]. \tag{7}$$

The modified combinants C_j defined by the recurrence relation (7) are closely related to the combinants $C^\star_j$ defined by Eq. (1), namely,

$$C_j = \frac{j+1}{\langle N\rangle} C^\star_{j+1}. \tag{8}$$

Using Leibnitz's formula for the j^{th} derivative of the quotient of two functions $x = G'(z)/G(z)$,

$$x^{(j)} = \frac{1}{G}\left(G'^{(j)} - j!\sum_{k=1}^{j}\frac{G'^{(j+1-k)}}{(j+1-k)!}\frac{x^{(k-1)}}{(k-1)!}\right), \tag{9}$$

where $G'(z)/G(z) = [\ln G(z)]'$ and $G(z)^{(N)}/N!|_{z=0} = P(N)$, we immediately obtain the recurrence relation (7).

The modified combinants, C_j, share with the combinants $C^\star_j$ the apparent ability of identifying the nature of the emitting source mentioned above (with, respectively, Eq. (3) corresponding to the NBD case with no oscillations, and Eq. (4) corresponding to the rapidly oscillating case of BD). This also means that C_j can be calculated from the generating function $G(z)$ of $P(N)$,

$$\langle N\rangle C_j = \frac{1}{j!}\left.\frac{d^{j+1}\ln G(z)}{dz^{j+1}}\right|_{z=0}. \tag{10}$$

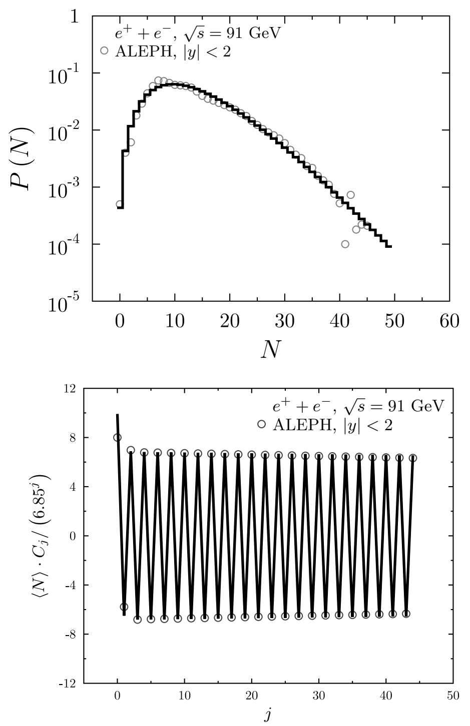

Fig. 1. Upper panel: Data on $P(N)$ measured in e^+e^- collisions by the ALEPH experiment at 91 GeV [23] are fitted by the distribution obtained from the generating function given by the product $G(z) = G_{\rm BD}(z) G_{\rm NBD}(z)$ with the parameters: $k' = 1$ and $p' = 0.8725$ for BD and $k = 4.2$ and $p = 0.75$ for NBD. Lower panel: the modified combinants C_j deduced from these data on $P(N)$. They can be fitted by C_j obtained from the same generating function with the same parameters, as used for fitting $P(N)$

Thus, whereas the recurrence relation, Eq. (7), allows us to obtain the C_j from the experimental data on $P(N)$, Eq. (10) allows for their calculation from the distribution defined by the generating function $G(z)$.

Note that C_j provide a similar measure of fluctuations as the set of cumulant factorial moments, K_q, which are very sensitive to the details of the multiplicity distribution and are frequently used in phenomenological analyses of data (cf., [1, 22]),

$$K_q = F_q - \sum_{i=1}^{q-1} \binom{q-1}{i-1} K_{q-i} F_i, \tag{11}$$

where $F_q = \langle N(N-1)(N-2)\dots(N-q+1)\rangle$ are the factorial moments, and K_q can be expressed as an infinite series in C_j,

$$K_q = \sum_{j=q}^{\infty} \frac{(j-1)!}{(j-q)!} \langle N \rangle C_{j-1}. \tag{12}$$

However, while the cumulants are best suited to study densely populated regions of the phase space, combinants are better suited for the study of sparsely populated regions, because, according to Eq. (7), the calculation of C_j requires only a finite number of probabilities $P(N < j)$ (which may be advantageous in applications).

The modified combinants share with the cumulants the property of additivity. For a random variable composed of independent random variables, with its generating function given by the product of their generating functions, $G(x) = \prod_j G_j(x)$, the corresponding modified combinants are given by the sum of the independent components. To illustrate this property, let us consider the e^+e^- data and use the generating function $G(z)$ formally treated as a generating function of the multiplicity distribution $P(N)$, in which N consists of both the particles from BD ($N_{\rm BD}$) and from NBD ($N_{\rm NBD}$):

$$N = N_{\rm BD} + N_{\rm NBD}. \tag{13}$$

In this case, the multiplicity distribution can be written as

$$P(N) = \sum_{i=0}^{\min\{N,k'\}} P_{\rm BD}(i) P_{\rm NBD}(N-i), \tag{14}$$

and the respective modified combinants as

$$\langle N \rangle C_j = \langle N_{\rm BD} \rangle C_j^{(\rm BD)} + \langle N_{\rm NBD} \rangle C_j^{(\rm NBD)}. \tag{15}$$

Figure 1 shows the results of attempts to fit both the experimentally measured [23] multiplicity distributions and the corresponding modified combinants C_j calculated from these data (cf. [24] for details). The fits shown in Fig. 1 correspond to the parameters: $k' = 1$ and $p' = 0.8725$ for BD and $k = 4.2$ and $p = 0.75$ for NBD.

Concerning the void probabilities at all energies of interest, one observes that $P(0) > P(1)$, a feature which cannot be reproduced by any composition of NBD used to fit the data [7]. To visualize the importance of this result, we note firstly that $P(0)$ is strongly connected with the modified combinants C_j, in fact:

$$P(0) = \exp\left(-\sum_{j=0}^{\infty} \frac{\langle N\rangle}{j+1} C_j\right). \tag{16}$$

From Eq. (7), one can deduce that the $P(0) > P(1)$ property is possible only when $\langle N\rangle C_0 < 1$. For most multiplicity distributions, $P(2) > P(1)$, which results in an additional condition, $C_1 > C_0(2-\langle N\rangle C_0)$; taken togethe,r this means that $C_1 > C_0$. However, because of the normalization condition $\sum_{j=0}^{\infty} C_j = 1$, such an initial increase of C_j cannot continue for all ranks j, and we should observe some kind of nonmonotonic behavior of C_j with rank j in this case. This means that all multiplicity distributions, for which the modified combinants C_j decrease monotonically with rank j, do not exhibit the enhanced void probability.

3. Compound Distributions

To continue, we use the idea of *compound distributions* (CD), which are applicable, when (as in our case) the production process consists of a number M of some objects (clusters/fireballs/etc.) produced according to a distribution $f(M)$ (defined by a generating function $F(z)$), which subsequently decay independently into a number of secondaries, $n_{i=1,\dots,M}$, following some other (always the same for all M) distribution, $g(n)$ (defined by a generating function $G(z)$). The resultant multiplicity distribution,

$$h\left(N = \sum_{i=0}^{M} n_i\right) = f(M) \otimes g(n), \tag{17}$$

is a compound distribution of f and g with the generating function

$$H(z) = F[G(z)]. \tag{18}$$

Equation (18) means that, in the case where $f(M)$ is a Poisson distribution with the generating function

$$F(z) = \exp[\lambda(z-1)], \tag{19}$$

the combinants for any other distribution $g(n)$ with a generating function $G(z)$, which are obtained from the compound distribution $h(N) = P_{\mathrm{PD}} \otimes g(n)$ and calculated with the use of Eq. (10), do not oscillate and are equal to

$$C_j = \frac{\lambda(j+1)}{\langle N\rangle} g(j+1). \tag{20}$$

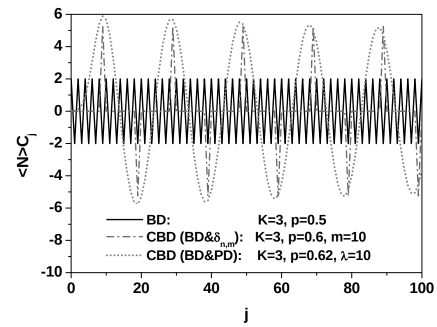

Fig. 2. C_j for BD, BD compounded with $\delta_{n,m}$ with $m = 10$ and compounded with the Poisson distribution with $\lambda = 10$

This fact explains why C_j from NBDs do not oscillate. This is because NBD is a compound distribution of the Poisson and logarithmic distributions. This means that $g(n) = -p^n/[n\ln(1-p)]$, and $h(N)$ is NBD with $k = -\lambda/\ln(1-p)$. In this case, C_j coincide with those derived before and given by Eq. (3). Actually, this reasoning applies to all more complicated compound distributions, with any distribution itself being a compound Poisson distribution. This property limits the set of distributions $P(N)$ leading to oscillating C_j, to BD, and to all compound distributions based on it. In this case, the period of oscillations is determined by the number of particles emitted from the source. For the compound distributions based on BD with $P(n) = \delta_{n,m}$, we have

$$C_j = (-1)^{j/m+1} \frac{K}{\langle N\rangle} \left(\frac{p}{1-p}\right)^{j/m+1}, \tag{21}$$

(for $j = mk$ and $C_j = 0$ for $j \neq mk$, where $k = 1, 2, 3, \dots$). For broader distributions $P(n)$, we get a smoother C_j dependence on rank j. For example, for $P(n)$ given by the Poisson distribution (with expected value λ), we obtain a Compound Binomial Distribution (CBD) with the generating function

$$H(z) = \{p\exp[\lambda(z-1)] + 1 - p\}^K, \tag{22}$$

and the modified combinants are given by

$$C_j = \frac{(-1)^{j+1} K e^{\lambda} \lambda^{j+1} \frac{1-p}{p}}{\langle N\rangle \left(e^{\lambda}\frac{1-p}{p} + 1\right)^{j+1}} A_j\left(e^{\lambda}\frac{p-1}{p}\right), \tag{23}$$

where $A_j(x)$ are the Eulerian polynomials. As an illustration, we show in Fig. 2 that, by compounding

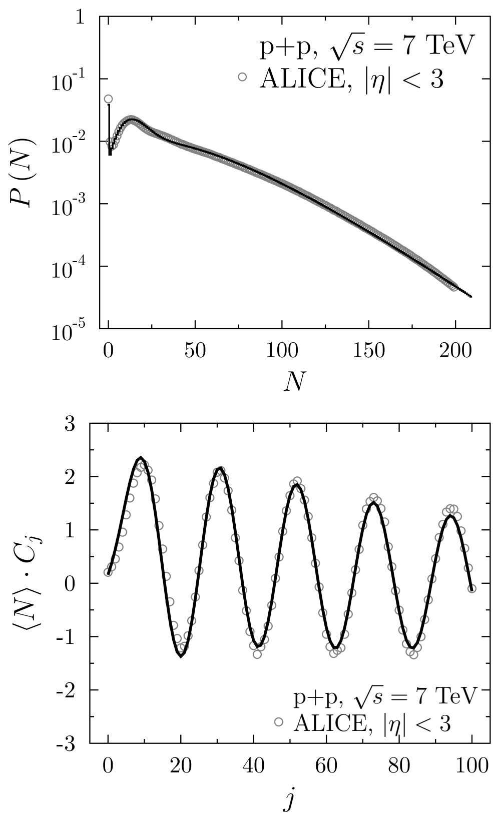

Fig. 3. Multiplicity distributions $P(N)$ measured in pp collisions by ALICE [25] (upper panel) and the corresponding modified combinants C_j (lower panel). Data are fitted using a two compound distribution (BD+NBD) given by Eqs. (25) and (24) with the parameters: $K_1 = K_2 = 3$, $p_1 = 0.9$, $p_2 = 0.645$, $k_1 = 2.8$, $k_2 = 1.34$, $m_1 = 5.75$, $m_2 = 23.5$, $w_1 = 0.24$ and $w_2 = 0.76$

BD with a Poisson distribution, one gains control over the period of oscillations (now equal to 2λ) and their amplitude. However, it turns out that such a combination does not allow us to fit data.

4. Multicomponent

The situation improves substantially, when one uses a multi-CBD based on Eq. (22). But the agreement is not yet satisfactory. It turns out that the situation improves dramatically, if one replaces the Poisson distribution by NBD and, additionally, uses a two-component version of such CBD with

$$P(N) = \sum_{i=1,2} w_i h\left(N; p_i, K_i, k_i, m_i\right) \tag{24}$$

with the generating function of each component equal to

$$H(z) = \left[p\left(\frac{1-p'}{1-p'z}\right)^k + 1 - p \right]^K. \tag{25}$$

In such a case, as can be seen in Fig. 3, one gains a satisfactory control over the periods of oscillations, their amplitudes, and their behavior as a function of the rank j. Moreover, one can nicely fit $P(N)$ and C_j. Of special importance is the fact that the enhancement $P(0) > P(1)$ is also reproduced in this approach.

The above result also explains the apparent success in fitting the experimentally observed oscillations of C_j by using a weighted sum of the three NBD used in [26]. Such a distribution uses freely selected weights and parameters (p, k) of NBDs and, therefore, resembles the compound distribution of BD with NBD. However, we note that the sum of M variables (with $M = 0,\ 1,\ 2, ...$), each from NBD characterized by parameters (p, k), is described by NBD characterized by (p, Mk). Therefore, as discussed before, it cannot reproduce the void probability $P(0)$. This can be reproduced only in the case where $M = 0,\ 1, ..., K$ is distributed according to BD, and we have a K-component NBD (where the consecutive NBDs have precisely defined parameters k),

$$P(N) = \sum_{M=0}^{K} P_{\mathrm{BD}}(M) P_{\mathrm{NBD}}(N; p, Mk). \tag{26}$$

In this case, one also has the $M = 0$ component, which is lacking in the previous multi-NBD case used in [26]. This is the reason for that, whereas the compound (BD&NBD) distribution reproduces the void probability, $P(0)$, the single NBD (or any combination of NBDs) do not. This means that the observation of the peculiar behavior of the void probability discussed above signals the necessity of using some compound distribution based onBD to fit data for $P(N)$ (and the C_j obtained from it).

5. Summary and Conclusions

Since the time of Ref. [8], one encounters essentially no detailed experimental studies of the combinants and only rather sporadic attempts at their phenomenological use to describe the multiparticle production processes. We demonstrate that the modified combinants C_j are a valuable tool for the investigations of multiplicity distributions, and C_j deduced from the measured multiplicity distributions, P(N), could provide additional information on the dynamics of the particle production. This, in turn, could allow us to reduce the number of possible interpretations presented so far and, perhaps, answer some of the many still open fundamental questions (that this is possible, despite experimental errors, has been shown in [7, 26]). Finally, let us note that a large number of papers suggest some kind of universality in the mechanisms of hadron production in e^+e^- anihilations and in pp and $p\bar{p}$ collisions. This arises from observations of the average multiplicities and relative dispersions in both types of processes (cf., e.g., [27, 28]). However, as we have shown here, the modified combinant analysis reveals differences between these processes. Namely, while, in e^+e^- annihilations, we observe oscillations of C_j with period 2, the period of oscillations in pp collisions is ~ 10 times longer, and the amplitude of oscillations in both types of processes differs dramatically. At the moment, this problem remains open and awaits a further investigation.

This research was supported in part by the Polish Ministry of Science and Higher Education (Contract No. DIR/WK/2016/2010/17-1), by the National Science Centre (NCN) (Contract No. DEC-2016/22/M/ST/00176) (G.W.), and by the NCN grant 2016/23/B/ST2/00692 (M.R.). We would like to thank Dr. Nicholas Keeley for reading the manuscript.

1. W. Kittel, E.A. De Wolf. *Soft Multihadron Dynamics* (World Scientific, 2005).
2. Ding-wei Huang. Multiplicity distribution with enhanced void probability. *J. Phys. G* **23**, 895 (1997).
3. S. Dutta, A.H. Chan, C.H. Oh. Mod. Void probability enhanced multiplicity distribution of produced hadrons in p–p collision at lhc energies. *Phys. Lett. A* **27**, 1250145 (2012).
4. G. Wilk, Z. Włodarczyk. How to retrieve additional information from the multiplicity distributions. *J. Phys. G* **44**, 015002 (2017).
5. G. Wilk, Z. Włodarczyk. Some intriguing aspects of multiparticle production processes. *Int. J. Mod. Phys. A* **33**, 1830008 (2018).
6. M. Rybczyński, G. Wilk, Z. Włodarczyk. Intriguing feature of multiplicity distributions. *Eur. Phys. J. Web Conf.* **206**, 03002 (2019).
7. M. Rybczyński, G. Wilk, Z. Włodarczyk. Intriguing properties of multiplicity distributions. *Phys. Rev. D* **99**, 094045 (2019).
8. S.K. Kauffmann, M. Gyulassy. Multiplicity distribution. *J. Phys. A* **11**, 1715 (1978).
9. J. Bartke. On the description of multiplicity distributions in multiple production processes in terms of combinants. *Phys. Scripta* **27**, 226 (1983).
10. A.B. Balantekin, J.E. Seger. Description of pion multiplicities using combinants. *Phys. Lett. B* **266**, 231 (1991).
11. Bao-An Li. Pion multiplicity distributions and combinants in relativistic heavy ion collisions. *Phys. Lett. B* **300**, 14 (1993).
12. S. Hegyi. Correlation studies in quark jets using combinants. *Phys. Lett. B* **463**, 126 (1999).
13. A.B. Balantekin. Combinant analysis of multiplicity distributions. *AIP Conf. Proc.* **276**, 346 (1993).
14. A.Z. Mekjian, T. Csörgö, S. Hegyi. A Bose–Einstein model of particle multiplicity distributions. *Nucl. Phys. A* **784**, 515 (2007).
15. J.F. Fiete Grosse-Oetringhaus, K. Reygers. Charged-particle multiplicity in proton–proton collisions. *J. Phys. G* **37**, 083001 (2010).
16. P. Ghosh. Negative binomial multiplicity distribution in proton-proton collisions in limited pseudorapidity intervals at LHC up to $\sqrt{s} = 7$ TeV and the clan model. *Phys. Rev. D* **85**, 0541017 (2012).
17. A. Giovannini, R. Ugoccioni. Signals of new physics in global event properties in pp collisions in the TeV energy domain. *Phys. Rev. D* **68**, 034009 (2003).
18. I.J. Zborovsky. A three-component description of multiplicity distributions in pp collisions at the LHC. *J. Phys. G* **40**, 055005 (2013).
19. I.M. Dremin, V.A. Nechitailo. Independent pair parton interactions model of hadron interactions. *Phys. Rev. D* **70**, 034005 (2004).
20. S.V. Chekanov, V.I. Kuvshinow. Multifractal multiplicity distribution in bunching parameter analysis. *J. Phys. G* **22**, 601 (1996).
21. B.E.A.Saleh, M.K. Teich. Multiplied-Poisson noise in pulse, particle, and photon detection. *Proc. IEEE* **70**, 229 (1982).
22. R. Botet, M. Płoszajczak. *Universal Fluctuations. The Phenomenology of Hadronic Matter*, (World Scientific, 2002).
23. D. Buskulic *et al.* (ALEPH Collaboration). Measurements of the charged particle multiplicity distribution in restricted rapidity intervals. *Z. Phys. C* **69**, 15 (1995).
24. H.W. Ang, A.H. Chan, M. Ghaffar, Q. Leong, M. Rybczyński, G. Wilk, Z. Włodarczyk. Modified combinant analysis of the e^+e^- multiplicity distributions. *Modern Phys. Lett. A* **34**, 1950324 (2019).

25. J. Adam *et al.* (ALICE Collaboration). Measurement of D-meson production versus multiplicity in p-Pb collisions at $\sqrt{s_{NN}} = 5.02$ TeV. *J. High Energy Phys.* **78**, 1608 (2016).
26. I. Zborovsky. Three-component multiplicity distribution, oscillation of combinants and properties of clans in pp collisions at the LHC. *Eur. Phys. J. C* **78**, 816 (2018).
27. A. Biswas. Charged multiplicity distributions in e^+e^- annihilation and pp collision. *J. Phys. G* **12**, 1 (1986).
28. J.F. Grosse-Oetringhaus, K. Reygers. Charged-particle multiplicity in proton–proton collisions. *J. Phys. G* **37** 083001 (2010).

Received 08.07.19

М. Рибчинськi, Г. Вiлк, З. Влодарчик

ПОГЛЯД НА МНОЖИННІ РОЗПОДІЛИ
ЧЕРЕЗ МОДИФІКОВАНІ КОМБІНАНТИ

Р е з ю м е

Експериментально вимiрянi розподiли по множинностi пiсля їх ретельного аналiзу демонструють незвично пiдвищену ймовiрнiсть порожнечi i осциляторну поведiнку модифiкованих комбiнантiв. Ми показуємо, що обидвi цi риси можна використати як додатковi джерела iнформацiї, ще не використанi в повнiй мiрi в механiзмах багаточастинкового народження. Ми надаємо їх теоретичну iнтерпретацiю в термiнах компаундних розподiлiв.

https://doi.org/10.15407/ujpe64.8.745

L.M. SATAROV,[1,2] I.N. MISHUSTIN,[1,2] A. MOTORNENKO,[1,3] V. VOVCHENKO,[1,3] M.I. GORENSTEIN,[1,4] H. STOECKER [1,3,5]

[1] Frankfurt Institute for Advanced Studies
(1, Ruth-Moufang-Str., D-60438 Frankfurt am Main, Germany; e-mail: satarov@fias.uni-frankfurt.de)
[2] National Research Center "Kurchatov Institute"
(1, Kurchatov Sq., 123182 Moscow, Russia)
[3] Institut für Theoretische Physik, Goethe Universität Frankfurt
(1, Max-von-Laue-Str., D-60438 Frankfurt am Main, Germany)
[4] Bogolyubov Institute for Theoretical Physics, Nat. Acad. of Sci. of Ukraine
(14b, Metrologichna Str., 03143 Kyiv, Ukraine)
[5] GSI Helmholtzzentrum für Schwerionenforschung GmbH
(1, Planck-Str., D-64291 Darmstadt, Germany)

PHASE TRANSITIONS AND BOSE–EINSTEIN CONDENSATION IN ALPHA-NUCLEON MATTER

The equation of state and the phase diagram of an isospin-symmetric chemically equilibrated mixture of α particles and nucleons (N) are studied in the mean-field approximation. We use a Skyrme-like parametrization of mean-field potentials as functions of the partial densities of particles. The parameters of these potentials are chosen by fitting the known properties of pure N- and pure α-matters at zero temperature. The sensitivity of results to the choice of the αN attraction strength is investigated. The phase diagram of the $\alpha - N$ mixture is studied with a special attention paid to the liquid-gas phase transitions and the Bose–Einstein condensation of α particles. We have found two first-order phase transitions, stable and metastable, which differ significantly by the fractions of α's. It is shown that the states with α condensate are metastable.

K e y w o r d s: phase transitions, mean-field model, Bose–Einstein condensation, chemical equilibrium.

1. Introduction

At subsaturation densities and low temperatures, the nuclear matter has a tendency to the clusterization, when small and big nucleon clusters are formed under the conditions of thermal and chemical equilibrium. This state of excited nuclear matter is realized in nuclear reactions at intermediate energies known as the multifragmentation of nuclei [1, 2]. It is believed that the clusterized nuclear matter is also formed in outer regions of neutron-stars and in supernova explosions [3].

In our recent paper [4], we studied the equation of state (EoS) of an idealized system composed entirely of α-particles. Their interaction was described by a Skyrme-like mean-field potential. We have found that such a system exhibits two interesting phenomena, namely, the Bose–Einstein condensation (BEC) and the liquid-gas phase transition (LGPT). Earlier, the cold alpha matter was considered microscopically, by using phenomenological $\alpha\alpha$ potentials in Ref. [5].

However, by introducing such one-component system, one disregards a possible dissociation of alphas into lighter clusters and nucleons. The binary $\alpha - N$ matter in chemical equilibrium with respect to the reactions $\alpha \leftrightarrow 4N$ was considered in [6], by using the virial approach. Due to the neglect of quantum statistics and three-body forces, such approach may be justified only at small baryon densities.

In this paper, we briefly discuss the results of our recent article [7], where we studied the isospin-symmetric $\alpha - N$ matter under the conditions of chemical equilibrium. The EoS of such matter was calculated in the mean-field approach, by using Skyrme-like mean-field potentials. In our study, we simultaneously take into account the LGPT and BEC effects.

2. Mean-Field Model for Interacting $\alpha - N$ Matter

Let us consider the iso-symmetric system (with equal numbers of protons and neutrons) composed of nucleons (N) and alpha-particles (α). A small difference between the proton and neutron masses and the Coulomb interaction effects will be neglected. Our consideration will be restricted to small temperatures $T \lesssim 30$ MeV. In this case, the production of pions and other mesons, as well as the excitation of baryonic resonances, become negligible. In addition, the masses $m_N \simeq 938.9$ MeV and $m_\alpha \simeq 3727.3$ MeV are much larger than the system temperature. Thus, a non-relativistic approximation can be used in the lowest order in T/m_N.

In the grand canonical ensemble, the pressure $p\,(T,\mu)$ is a function of the temperature T and baryon chemical potential μ. The latter is responsible for the conservation of the baryon charge. The chemical potentials of N and α satisfy the relations

$$\mu_N = \mu, \quad \mu_\alpha = 4\mu, \tag{1}$$

which correspond to the condition of chemical equilibrium in the $N-\alpha$ mixture due to the reactions $\alpha \leftrightarrow 4N$.

Let us denote, by n_N and n_α, the partial number densities of N and α, respectively. The baryonic density $n_B\,(T,\mu) = n_N + 4n_\alpha$, entropy density s, and energy density ε can be calculated from $p\,(T,\mu)$, by using the equations

$$n_B = \left(\frac{\partial p}{\partial \mu}\right)_T, \quad s = \left(\frac{\partial p}{\partial T}\right)_\mu, \quad \varepsilon = Ts + \mu n_B - p. \tag{2}$$

To characterize the relative abundances of α's, we introduce their mass concentration $\chi = 4n_\alpha/n_B$.

In our mean-field model, we consider multiparticle interactions in the $\alpha - N$ matter, by introducing a temperature-independent "excess part" of the pressure Δp

$$p = p_N^{\rm id}(T, n_N) + p_\alpha^{\rm id}(T, n_\alpha) + \Delta p\,(n_N, n_\alpha), \tag{3}$$

where the first and second terms on the right-hand side (RHS) are, respectively, the pressure of the ideal gas of nucleons and α's. At known Δp, one can calculate the chemical potentials of N and α as functions of T, n_N, n_α. Solving further Eqs. (1), we get all thermodynamic quantities at given T,μ.

Earlier, we suggested a similar scheme to describe the particle interactions in one-component α [4] and nucleon [8] matters. This corresponds, respectively, to the limiting cases $n_N \to 0$ and $n_\alpha \to 0$. In the case of binary $\alpha-N$ mixture, we use a generalized Skyrme-like parametrization [7] for the excess pressure

$$\Delta p\,(n_N, n_\alpha) = -(a_N n_N^2 + 2a_{N\alpha} n_N n_\alpha + a_\alpha n_\alpha^2) + \\ + b_N\,(n_N + \xi\, n_\alpha)^{\gamma+2}. \tag{4}$$

Using Eqs. (3) and (4) and applying the thermodynamic relations, we get the expressions

$$\mu_N = \widetilde{\mu}_N(T, n_N) - 2\,(a_N n_N + a_{N\alpha} n_\alpha) + \\ + \frac{\gamma+2}{\gamma+1}\, b_N (n_N + \xi\, n_\alpha)^{\gamma+1}, \tag{5}$$

$$\mu_\alpha = \widetilde{\mu}_\alpha(T, n_\alpha) - 2\,(a_{N\alpha} n_N + a_\alpha n_\alpha) + \\ + \frac{\gamma+2}{\gamma+1}\, b_N\, \xi\,(n_N + \xi\, n_\alpha)^{\gamma+1}. \tag{6}$$

Here, $\widetilde{\mu}_i(T, n_i)$ is the chemical potential of the ideal gas of ith particles with the density n_i ($i = N, \alpha$). The second and third terms on RHS correspond to the attractive and repulsive parts of mean-field potentials for N ans α. Note that, in the region of BEC, $\widetilde{\mu}_\alpha$ reaches its maximum possible value $\widetilde{\mu}_\alpha = m_\alpha$, and n_α contains the contribution of Bose-condensed α's. In our calculations, we separate the states which are (meta)stable with respect to fluctuations of particle densities [1].

To choose the model parameters a_N, b_N, γ, we fit the ground-state (GS) properties of the cold ($T = 0$) iso-symmetric nuclear matter. This is the state with zero pressure and minimal energy per baryon. We assume the GS-values $\mu_N = 923$ MeV, $n_N = 0.15$ fm^{-3} [8] and choose $\gamma = 1/6$ [2]. The parameters a_α, ξ are estimated, by using the properties of a cold α matter. We fit the values of density ($n_\alpha = 0.036$ fm^{-3}) and binding energy per baryon ($E/B = -12$ MeV) obtained in Ref. [5] for the GS of this matter.

The cross-term coefficient $a_{N\alpha}$ determines the attractive part of the $N\alpha$ mean-field potential. It is

[1] For such states, the matrix $||\partial\mu_i/\partial n_j||$ is positive definite.

[2] As shown in Refs. [7, 8], such γ gives reasonable values of nuclear compressibility.

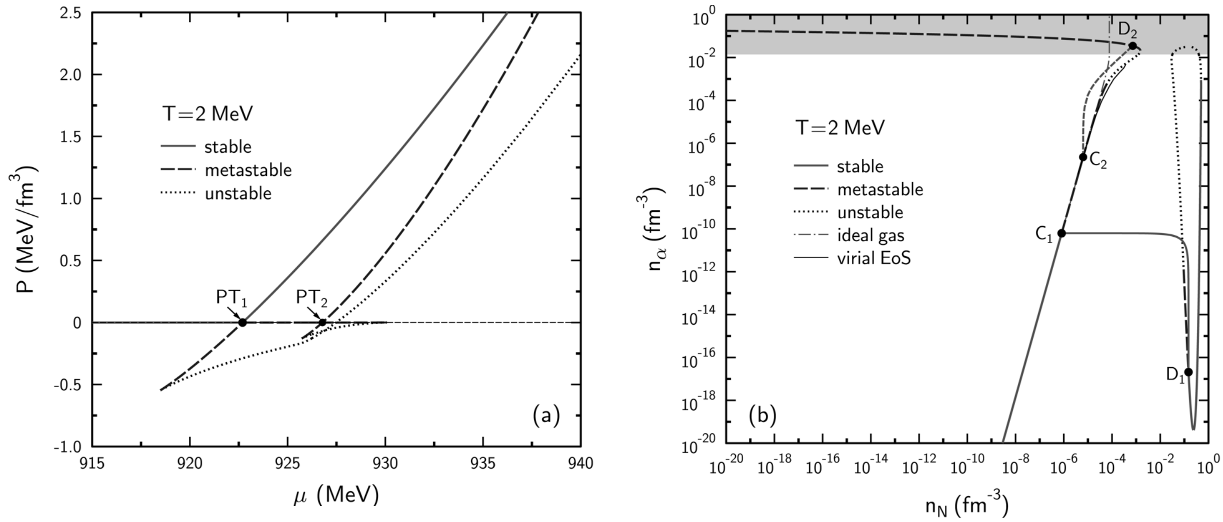

Fig. 1. Isotherm $T = 2$ MeV of $\alpha - N$ matter on the (μ, p) (a) and (n_N, n_α) (b) planes. The stable, metastable, and unstable parts of the isotherm are shown, respectively, by the solid, dashed, and dotted lines. The dots PT_1 and PT_2 in (a) show the positions of stable and metastable LGPT, respectively. The dash-dotted line in (b) is calculated for the ideal $\alpha - N$ gas. Lines C_1D_1 and C_2D_2 correspond to the mixed–phase states of PT_1 and PT_2, respectively. The thin solid line represents the isotherm $T = 2$ MeV from Ref. [6]

the only model parameter which is not fixed in our approach. To constrain this coefficient, we consider contours of the energy per baryon for the cold $\alpha - N$ matter on the (n_B, χ) plane. Our calculations show [7] that the properties of GS of such matter change drastically at some critical value $a_{N\alpha} = a_* \simeq 2.1$ GeVfm^3. In the overcritical region $a_{N\alpha} > a_*$, the model predicts nonzero fractions of α in the GS of the $\alpha - N$ matter. In this case, the GS is stronger bound as compared to the pure nucleon matter. Apparently, this is in contradiction with phenomenological properties of the nuclear matter. Therefore, we consider only subcritical values of $a_{N\alpha}$. To probe the sensitivity to this coefficient, we made calculations for $a_{N\alpha} = 1$ and 1.9 GeVfm^3. From the comparison with results of Ref. [6], we found that the latter value is more reasonable. Our "preferred" values of model parameters are given in Table 1.

3. Phase Diagram of $\alpha - N$ Matter

By substituting (5) and (6) into (1) and solving the resulting equations, we get the isotherms of the $\alpha - N$ matter for different μ. At low enough temperatures, one obtains, in general, several solutions for the pressure at given T, μ. Solutions with the largest (smallest) pressure correspond to stable (unstable) states. This is a typical situation for LGPT.

Figure 1, a represents the isotherm $T = 2$ MeV on the (μ, p) plane. According to the Gibbs rule, the intersection points of (meta)stable branches of the pressure as functions of μ correspond to phase transitions (PTs). As one can see from Fig. 1, a, there are two PTs at $T = 2$ MeV. The first transition, PT_1, occurs at a smaller baryon chemical potential than for PT_2. The states on the dashed lines have smaller pressure as compared to states with the same μ on the solid lines. Therefore, the second transition PT_2 is metastable.

Figure 1, b shows the same isotherm $T = 2$ MeV, but on the (n_N, n_α) plane. The shading represents the region of BEC. The states between C_1 and D_1 (C_2 and D_2) are mixed-phase states for the stable (metastable) PT. As compared to PT_1, the concentrations of α are much larger for the mixed-phase states of PT_2. A strong suppression of α is predicted at large nucleon densities. According to our calculation, BEC states are metastable (see the dashed line in the shaded domain).

Table 1. **Model parameters**

γ	a_N, GeV fm^3	b_N, GeV fm$^{3.5}$	a_α, GeV fm^3	ξ	$a_{N\alpha}$, GeV fm^3
1/6	1.17	1.48	3.83	2.006	1.9

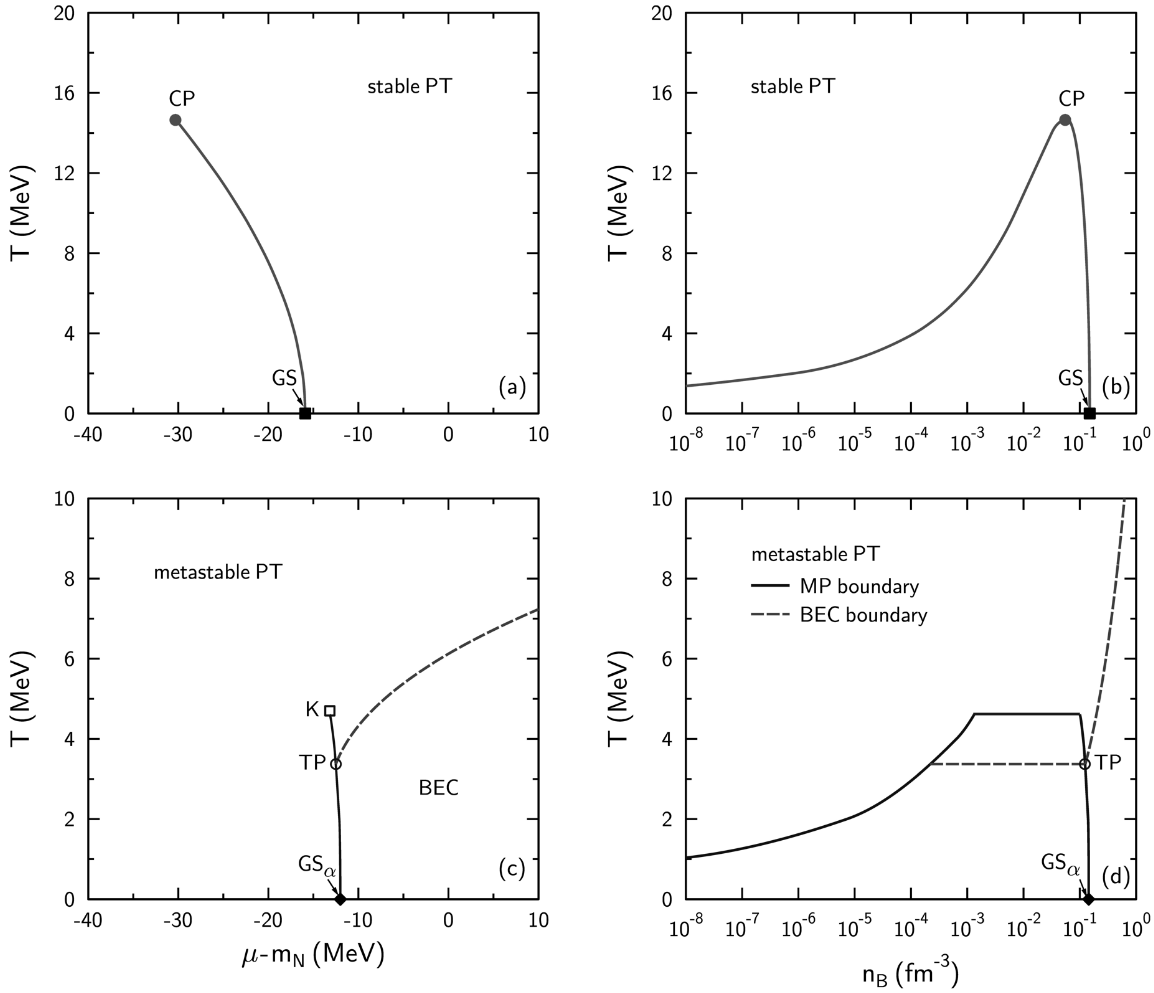

Fig. 2. Left panels: critical lines of stable (a) and metastable (c) PT of the $\alpha - N$ matter on the (μ, T) plane. Right panels: boundaries of the mixed phase for stable (b) and metastable (d) PT of the $\alpha - N$ mixture on the (n_B, T) plane. Full circles in (a) and (b) show positions of the critical point. The dashed lines in (c) and (d) represent boundaries of the BEC region. The open square (circle) marks the end (triple) point of the metastable PT. The full squares and diamonds show, respectively, the GS positions for the pure nucleon and pure alpha matters, respectively

Table 2. **Characteristics of phase transitions in $\alpha - N$ matter**

Stable PT				Metastable PT			
$T_{\rm CP}$, MeV	$\mu_{\rm CP}$, MeV	$n_{B\rm CP}$, fm^{-3}	$\chi_{\rm CP}$	T_K, MeV	μ_K, MeV	χ_K	$T_{\rm TP}$, MeV
14.7	908.6	5.3×10^{-2}	6.9×10^{-2}	4.6	925.7	0.46–0.86	3.4

Analyzing the results at different T, we get the phase diagram of the $\alpha - N$ matter. The stable and metastable parts of this diagram are shown in the upper and low panels of Fig. 2. Characteristics of PT$_1$ and PT$_2$ are shown in Table 2. Note that the metastable PT disappears at the temperature $T_K \simeq$ $\simeq 5$ MeV which is much less than the critical temperature $T_{\rm CP} \simeq 15$ MeV of the stable PT.

4. Conclusions

Our model describes both the phase transitions and BEC of the $\alpha - N$ matter. The results of this paper may be used for studying the nuclear cluster production in heavy-ion reactions, as well as in astrophysics. We think that the present formalism can be also used for the binary mixtures of fermionic atoms and bosonic molecules, like $H + H_2$ or $D + D_2$.

1. J.P. Bondorf. Heavy ion reactions between 30 and a few hundred MeV/nucleon. *J. Phys. Colloq.* **37**, 5 (1976).
2. J.P. Bondorf, A.S. Botvina, A.S. Illjinov, I.N. Mishustin, K. Sneppen. Statistical multifragmentation of nuclei. *Phys. Rep.* **257**, 133 (1995).
3. J.M. Lattimer, F.D. Swesty. A generalized equation of state for hot, dense matter. *Nucl. Phys. A* **535**, 331 (1991).
4. L.M Satarov, M.I. Gorenstein, A. Motornenko, V. Vovchenko, I.N. Mishustin, H. Stoecker. Bose-Einstein condensation and liquid-gas phase transition in strongly-interacting matter composed of α particles. *J. Phys. G* **44**, 125102 (2017).
5. J.W. Clark, T.-P. Wang. Theory of α matter. *Ann. Phys.* **40**, 127 (1966).
6. C.J. Horowitz, A. Schwenk. Cluster formation and the virial equation of state of low-density nuclear matter. *Nucl. Phys. A* **776**, 55 (2006).
7. L.M. Satarov, I.N. Mishustin, A. Motornenko, V. Vovchenko, M.I. Gorenstein, H. Stoecker. Phase transitions and Bose–Einstein condensation in alpha-nucleon matter. *Phys. Rev. C* **99**, 024909 (2019).
8. L.M. Satarov, M.N. Dmitriev, I.N. Mishustin. Equation of state of hadron resonance gas and the phase diagram of strongly interacting matter. *Phys. At. Nucl.* **72**, 1390 (2009).

Received 08.07.19

Л.М. Сатаров, І.Н. Мішустін, А. Моторненко,
В. Вовченко, М.І. Горенштейн, Х. Штокер

ФАЗОВІ ПЕРЕТВОРЕННЯ
ТА КОНДЕНСАЦІЯ БОЗЕ–ЕЙНШТЕЙНА
В АЛЬФА-НУКЛОННІЙ МАТЕРІЇ

Р е з ю м е

Рівняння стану та фазова діаграма ізоспін-симетричної хімічно рівноважної суміші α частинок та нуклонів (N) вивчається в наближенні середнього поля. Ми застосовуємо параметризацію Скірма для потенціалів середнього поля як функцій парціальних густин частинок. Параметри цих потенціалів знайдені як результат підгонки відомих властивостей чистої N- та чистої α-матерії при нульовій температурі. Вивчена чутливість результатів до вибору величини αN притягання. Фазова діаграма $\alpha - N$ суміші вивчається з особливою увагою до процесів фазового перетворення рідина-газ та конденсації Бозе–Ейнштейна для α-частинок. Ми знаходимо два фазові перетворення, стабільний та метастабільний, які значно відрізняються концентраціями α-частинок. Показано, що стани з α-конденсатом є метастабільними.

https://doi.org/10.15407/ujpe64.8.750

W. SCHÄFER,[1] I. BABIARZ,[1] A. CISEK,[2] A. SZCZUREK[1]

[1] Institute of Nuclear Physics, Polish Academy of Sciences
(152, Ul. Radzikowskiego, PL-31-142 Kraków, Poland; e-mail: wolfgang.schafer@ifj.edu.pl)
[2] Faculty of Mathematics and Natural Sciences, University of Rzeszów,
(1, Ul. Pigonia, PL-35-310 Rzeszów, Poland)

RECENT RESULTS ON INCLUSIVE QUARKONIUM PAIR PRODUCTION IN PROTON-PROTON COLLISIONS

Recently, there has been much interest in the pair production of charmonia. One of the main motivations behind these studies is that the production of quarkonium pairs is expected to receive an important contribution from the double parton scattering (DPS) production mode. A large effective cross-section $\sigma_{\rm eff}$ is found from the empirical analysis of the J/ψ-pair production – about a factor 2.5 smaller than the usually accepted $\sigma_{\rm eff} = 15$ mb. Here, we present the recent results of our calculations of the χ_c pair production, mainly in the single parton scattering (SPS) mode. An important feature is that the single-gluon exchange mechanism can to some extent mimic the behavior of the DPS production.

Keywords: perturbative QCD, quarkonia, multiparton processes.

1. Introduction

The production of J/ψ-pairs has been suggested as a probe of the double-parton scattering (DPS) processes [1]. More generally, the DPS production mode is expected to be especially important in the charm sector [2]. Therefore, recently, there has been much interest in the quarkonium pair production in proton-proton collisions also from the experimental side. Among others, the cross-sections for the production of J/ψ-pairs were measured at the Tevatron [3] and the LHC [4–7].

A number of puzzles remain with these data, however. For example, the single parton scattering (SPS) leading order of $\mathcal{O}(\alpha_S^4)$ (see, e.g., [8, 9]) does not describe well all the kinematic distributions in the case of the ATLAS and CMS data. Especially, when the rapidity distance Δy between two J/ψ mesons is large, it falls short of experimental data. If one ascribes the whole discrepancy to DPS processes, the normalization of DPS comes out a factor ~ 2.5 larger than in other hard processes. It is still an open issue at the moment whether this points to a nonuniversality of DPS effects or whether there are additional single parton scattering mechanisms not taken into account up to now.

This problem motivated our recent studies of the χ_c-pair production in the k_T-factorization [10] and of the production of χ_c-pairs associated with a gluon (jet) in the collinear factorization [11]. We summarize these works in this contribution.

2. Production of χ_c-Pairs

In the standard hard scattering approach, the cross-section of the production of a pair of quarkonia a, b is calculated from a convolution of parton densities with a parton-level cross-section (see the left diagram in Fig. 1). However, at high energies, favored by a rise of the gluon distribution at small x, there is a sizable contribution from processes in which two or more hard processes proceed in the same proton-proton collision (see the right diagram in Fig. 1).

One commonly assumes the factorized ansatz for the production cross- section in the DPS mode:

$$\frac{d\sigma_{\rm DPS}(pp\to abX)}{dy_a dy_b d^2\mathbf{p}_{aT} d^2\mathbf{p}_{bT}} = \\ = \frac{1}{1+\delta_{ab}}\,\frac{1}{\sigma_{\rm eff}}\,\frac{d\sigma(pp\to aX)}{dy_a d^2\mathbf{p}_{aT}}\,\frac{d\sigma(pp\to bX)}{dy_b d^2\mathbf{p}_{bT}}. \quad (1)$$

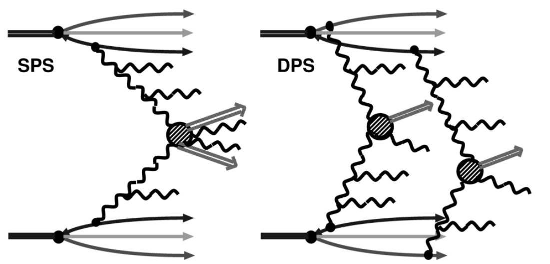

Fig. 1. Sketch of the single parton scattering (SPS) and double parton scattering (DPS) production modes

The DPS cross-section is written as a product of the inclusive single-particle spectra, and the cross-section is normalized by the "effective cross-section" $\sigma_{\rm eff}$. The latter is not the cross-section for a specific process – the real parameter is rather its inverse, which is related in the simplest model to the overlap of parton densities in the transverse plane, $t_N(\mathbf{b})$:

$$\frac{1}{\sigma_{\rm eff}} = \int d^2\mathbf{b}\, T^2_{NN}(\mathbf{b}),$$
$$T_{NN}(\mathbf{b}) = \int d^2\mathbf{s}\, t_N(\mathbf{s}) t_N(\mathbf{b}-\mathbf{s}). \tag{2}$$

The salient features of DPS are obvious from Eq. (1). Important for us is the observation that each of the single particle spectra is a fairly broad function of $y_{a,b}$. Thus, the DPS distribution in rapidity distance $\Delta y = y_b - y_a$ will be very broad as well. As far as the effective cross-section is concerned, it is usually taken in the ballpark of $\sigma_{\rm eff} = 15$ mb, which is within the line of a fair amount of hard processes, see, e.g., a table in [5].

In the case of J/ψ-pair production, the lowest-order "box-diagram" mechanism suggests a very clean separation of SPS versus DPS modes. Indeed, the explicit calculations performed in the k_T-factorization [9] show that the J/ψ-pair distribution is sharply peaked around $\Delta y = 0$.

A main point of this presentation is the fact that the situation looks completely different in the case of production of a pair of χ_c mesons. Indeed, the χ_{cJ} states, which come in three different spins $J = 0, 1, 2$ have positive C-parity and thus couple to two gluons in a color singlet state. Hence, the mechanism of Fig. 2 with the t-channel exchange of a single gluon is possible. It is well understood that it will lead to a $gg \to \chi\chi$ cross-section independent of the cm-energy in the high-energy limit. The matrix element for this

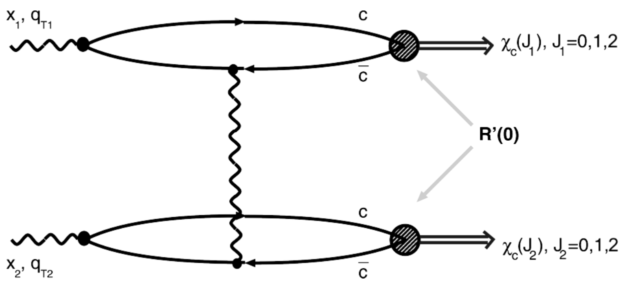

Fig. 2. Gluon t-channel exchange mechanism for the production of $\chi_c\chi_c$ pairs

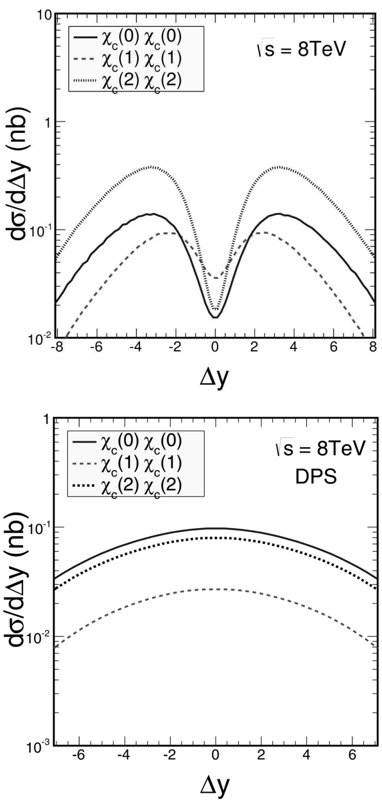

Fig. 3. Distribution of χ_c-pairs in the rapidity difference between mesons. Top panel: SPS mode, lower panel: DPS mode

process thus puts no penalty on a large rapidity distance Δy between the χ_c-mesons.

The relevant amplitudes can be obtained from effective $g^*g^* \to \chi_{cJ}$ vertices for the fusion of two spacelike off-shell gluons. These have been obtained in Ref. [10] for all possible spin-states of the χ_c family. We also performed calculations in the k_T-factorization including the transverse momenta of incoming gluons. In the upper panel of Fig. 3, we

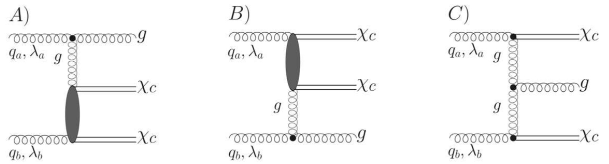

Fig. 4. Feynman diagrams for the production of a χ_c-pair associated with a gluon

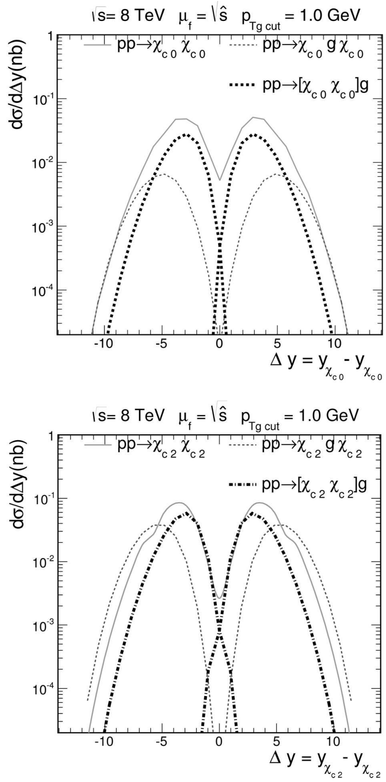

Fig. 5. Distribution in rapidity between χ_0 mesons (top panel) and χ_{c2} mesons for the following different processes: Born-level production of χ_c-pairs, production of χ_c pairs with a leading gluon, and production of χ_c-pairs with a central gluon

show the distribution in rapidity distance Δy between mesons. Note that we only show, as an example, the production of pairs of identical mesons, the full array of all possible combinations can be found in Ref. [10]. In the lower panel of Fig. 3, we show distributions in Δy for the DPS mode, by using $\sigma_{\rm eff} = 15$ mb. We see that these distributions are very broad and in the same ballpark as the SPS contribution. Of course, there is no minimum at $\Delta y = 0$ for the DPS distributions. Thus, we observe rather similar distributions in Δy for single and double parton scattering productions of different χ_c-quarkonia states. This shows that both contributions must be included in the analysis of future data on the $\chi_{cJ_i}\chi_{cJ_j}$ production. Now, one would observe that the large rapidity distance between mesons means a large phase space for the emission of additional gluons. To investigate this situation, we studied the associated production of χ_c pairs with a gluon in the standard collinear factorization in Ref. [11]. There are two main contributions shown in the diagrams of Fig. 4: first, the emission of a "leading gluon", where the gluon jet carries a large fraction of the momentum carried by one of the incoming gluons, and, second, the production of "central" gluons, which are emitted in the rapidity space between two mesons with a large difference in rapidity from either one. Some distributions, again in rapidity distance Δy between mesons, are shown in Fig. 5. The production of leading gluons adds to the Born-result to recover the k_T-factorization result, while the production of central gluons gives rise to an about 20% enhancement of the cross-section. Here, one may think of $\alpha_S\,\Delta y$ as a large parameter which could be resummed in the future using the BFKL formalism.

3. Conclusions

The pair production of quarkonia is a topic that still poses puzzles to theorists. The quantitative understanding of DPS contributions requires not only a reliable formalism for its calculation but also a good understanding of SPS processes that can show a similar behavior as DPS in many kinematic variables.

For the theoretically simplest case, the production of χ_c-pairs, we have shown that the cross-sections for different combinations of χ_c quarkonia, the SPS and DPS cross-sections, are of the similar size, and both involve very broad distributions in the rapidity distance Δy.

We have also shown that an enhancement of the pair production cross-section for χ_c-pairs can be expected from the higher-order corrections, due to the large phase space of the gluon emission.

However, it turns out that the feed-down from χ-pairs into the J/ψ-pair channel does not resolve the discrepancy between different determinations of $\sigma_{\rm eff}$.

It might be necessary to look deeper into the fundamentals of the DPS theory (see, e.g., [13]) to understand the peculiar behavior of the charmonium pair production.

The participation of W.S. in the conference New Trends in High Energy Physics 2019 has been partially supported by the Polish Academy of Sciences.

1. C. H. Kom, A. Kulesza, W. J. Stirling. Pair production of J/ψ as a probe of double parton scattering at LHCb. *Phys. Rev. Lett.* **107**, 082002 (2011).
2. M. Łuszczak, R. Maciuła, A. Szczurek. Production of two $c\bar{c}$ pairs in double-parton scattering. *Phys. Rev. D* **85**, 094034 (2012).
3. V.M. Abazov *et al.*, [D0 Collaboration]. Observation and studies of double J/ψ production at the Tevatron. *Phys. Rev. D* **90**, 111101 (2014).
4. V. Khachatryan *et al.*, [CMS Collaboration]. Measurement of prompt J/ψ pair production in pp collisions at $\sqrt{s} = 7$ Tev. *JHEP* **1409**, 094 (2014).
5. M. Aaboud *et al.*, [ATLAS Collaboration]. Measurement of the prompt J/ ψ pair production cross-section in pp collisions at $\sqrt{s} = 8$ TeV with the ATLAS detector. *Eur. Phys. J. C* **77**, 76 (2017).
6. R. Aaij *et al.*, [LHCb Collaboration]. Observation of J/ψ pair production in *pp* collisions at $\sqrt{s} = 7$ TeV. *Phys. Lett. B* **707**, 52 (2012).
7. R. Aaij *et al.*, [LHCb Collaboration]. Measurement of the J/ψ pair production cross-section in pp collisions at $\sqrt{s} = 13$ TeV. *JHEP* **1706**, 047 (2017); Erratum: *JHEP* **1710**, 068 (2017).
8. S.P. Baranov. Pair production of J/ψ mesons in the k_t-factorization approach. *Phys. Rev. D* **84**, 054012 (2011).
9. S.P. Baranov, A.M. Snigirev, N.P. Zotov, A. Szczurek, W. Schäfer. Interparticle correlations in the production of J/ψ pairs in proton-proton collisions. *Phys. Rev. D* **87**, 034035 (2013).
10. A. Cisek, W. Schäfer, A. Szczurek. Production of χ_c pairs with large rapidity separation in k_T factorization. *Phys. Rev. D* **97**, 114018 (2018).
11. I. Babiarz, W. Schäfer, A. Szczurek. Associated production of χ_c pairs with a gluon in the collinear-factorization approach. *Phys. Rev. D* **99**, 074014 (2019).
12. W. Schäfer. Production of quarkonium pairs in high-energy proton-proton collisions. *EPJ Web Conf.* **199**, 01021 (2019).
13. J. R. Gaunt, R. Maciuła, A. Szczurek. Conventional versus single-ladder-splitting contributions to double parton scattering production of two quarkonia, two Higgs bosons and $c\bar{c}c\bar{c}$. *Phys. Rev. D* **90**, 054017 (2014).

Received 26.01.18

В. Шефер, І. Бабяж, А. Чішек, А. Щурек

НОВІ РЕЗУЛЬТАТИ
ПРО ІНКЛЮЗИВНЕ НАРОДЖЕННЯ
ПАР КВАРКОНІУМУ
В ПРОТОН-ПРОТОННИХ ЗІТКНЕННЯХ

Р е з ю м е

Останнім часом спостерігається значний інтерес до процесів парного народження шармонія. Однією з причин інтересу є те, що продукування пар кварконіуму в значній мірі зумовлене подвійним розсіянням партонів (DPS). З емпіричного аналізу народження пар J/ψ знайдено велике значення ефективного перерізу $\sigma_{\rm eff} = 15$ мб. Ми представляємо нові результати наших розрахунків продукування пар χ_c в моді одинарного партонного розсіяння (SPS). Важливим моментом є те, що однопіонний обмін в деякій мірі може симулювати ефект подвійного партонного обміну (DPE).

https://doi.org/10.15407/ujpe64.8.754

V. SKALOZUB

Oles Honchar Dnipro National University

(72, Gagarin Ave., Dnipro 49010, Ukraine; e-mail: Skalozubv@daad-alumni.de)

INDUCED COLOR CHARGES, EFFECTIVE $\gamma\gamma G$ VERTEX IN QGP. APPLICATIONS TO HEAVY-ION COLLISIONS

We calculate the induced color charges $Q^3_{\rm ind}, Q^8_{\rm ind}$ and the effective vertex $\gamma - \gamma$-gluon generated in a quark-gluon plasma with the A_0 condensate because of the color C-parity violation at this background. To imitate the case of heavy-ion collisions, we consider the model of the plasma confined in the narrow infinite plate and derive the classical gluon potentials $\bar\phi^3$ and $\bar\phi^8$ produced by these charges. Two applications – the scattering of photons on a plasma and the conversion of gluon fields in two photons radiated from the plasma – are discussed.

K e y w o r d s: quark-gluon plasma, heavy-ion collision, Polyakov's loop, effective vertex.

1. Introduction

Investigations of the deconfinement phase transition (DPT) and the quark-gluon plasma (QGP) are in the center of modern high energy physics. These phenomena happen at high temperature due to the asymptotic freedom of strong interactions. The researches are carried out either in experiments on hadron collisions or in quantum field theory. The order parameter for DPT is Polyakov's loop (PL), which is zero at low temperatures and nonzero at high temperatures $T > T_d$, where $T_d \sim 160$–180 MeV [1] is the phase transition temperature. The standard information on DPT is adduced, in particular, in [2].

The PL is defined as [3]:

$$PL = \int\limits_C dx_4 \; A_0(x_4, \mathbf{x}). \tag{1}$$

Here, $A_0(x_4, \mathbf{x})$ is the zero component of the gauge field potential, the integration contour is going along the fourth direction and back to an initial point in the lattice Euclidean space-time. The PL was introduced in pure gluodynamics. It violates the center of the color group symmetry $Z(3)$ that results in the nonconservation of the color charges Q^3 and Q^8.

The QGP state consists of quarks and gluons liberated from hadrons. Polyakov's loop is not a solution to the local Yang–Mills equations. The local order parameter for DPT is the A_0 condensate, which is a constant at $T > T_d$. It can be calculated, in particular, from a two-loop effective potential. More details on different calculations carried out in analytic quantum field theory can be seen in [4]. Taking these results into consideration, we have to consider QGP as a state at the A_0 background, which breaks the color C-parity symmetry. So, new type phenomena may happen.

In the SU(2) gluodynamics, the gluon spectra at A_0 were calculated and investigated in Ref. [5, 6]. In particular, the induced color charge $Q^3_{\rm ind}$ was also computed. It was shown that the state with a condensate is free of infrared instabilities existing in a gluon plasma in the empty space. Thus, the ground state with A_0 is a good approximation to the plasma after DPT.

In Ref. [7], the induced charges $Q^3_{\rm ind}, Q^8_{\rm ind}$ generated by quark loops in QCD were calculated. In what follows, we consider the QCD case, but the precise values of the induced charges will not be specified.

The paper is organized as follows. In Sect. 2, the color induced charges $Q^3_{\rm ind}$ and $Q^8_{\rm ind}$ generated by tadpole quark loops with one gluon lines, which are nonzero due to Furry's theorem violation, are calculated. In Sect. 3, we consider a simple model of the plasma confined in a plate narrow in one dimension and infinite in two other dimensions with the A_0 condensate and induced charges. We compute the classical gluon potentials $\bar\phi^3$ and $\bar\phi^8$ generated by the induced charges $Q^3_{\rm ind}$ and $Q^8_{\rm ind}$. In Sect. 4, the effective $\gamma\gamma G$ vertex generated in the plasma is calculated in the high-temperature approximation. In Sect. 5, the processes of photon scattering on these potentials and the conversion of gluons in two photons are considered as the application. These new phenomena have to happen due to the three-linear effective vertices.

2. Induced Color Charges and Quark Propagator

In what follows, we consider the case of A_0^3 background field and present the color field potential in the form $Q_\mu^a \to A_0 \delta^{a3}\delta_{\mu 4} + Q_\mu^a$, where Q_μ^a is a quantum field. The calculation of $Q^8_{\rm ind}$ is similar (see [7]), and the final results will be adduced only.

The explicit expression is given by the form $Q_\mu^a Q^3_{\rm ind}\delta_{\mu 4}\delta_{a3} = Q_4^3 Q^3_{\rm ind}$, where

$$Q^3_{\rm ind} = \frac{g}{\beta}\sum_{p_4}\int \frac{d^3p}{(2\pi)^3}\,{\rm Tr}\left[\gamma^4 \frac{\lambda^3_{ij}}{2} G^{ij}(p_4, \mathbf{p}, A_0)\right]. \quad (2)$$

Here, λ^3 is the Gell-Mann matrix, and $\beta = 1/T$ is the inverse temperature. The expressions for the propagators are

$$G^{11} = \frac{\gamma^4(p_4 - A_0) + \mathbf{p}\,\boldsymbol{\gamma} + m}{(p_4 - A_0)^2 + \mathbf{p}^2 + m^2},$$
$$G^{22} = \frac{\gamma^4(p_4 + A_0) + \mathbf{p}\,\boldsymbol{\gamma} + m}{(p_4 + A_0)^2 + \mathbf{p}^2 + m^2}. \quad (3)$$

For brevity, we denoted $A_0 = gA_0/2$ entering the interaction Lagrangian. Accounting for the trace ${\rm Tr}[(\gamma^4)^2] = -4$, the diagonal values of λ^3, and ${\rm Tr}[\gamma^4\boldsymbol{\gamma}] = 0$, we get

$$Q^3_{\rm ind} = \frac{4g}{\beta}\sum_{p_4}\int \frac{d^3p}{(2\pi)^3}\frac{p_4 + A_0}{(p_4 + A_0)^2 + \mathbf{p}^2 + m^2}. \quad (4)$$

The sum over $p_4 = \frac{\pi(2n+1)}{2\beta}$ can be calculated, by using the formula

$$\frac{1}{\beta}\sum_{p_4} f(p_4) = -\frac{1}{4\pi i}\int\limits_C \tan\left[\frac{\beta\omega}{2}\right] f(\omega), \quad (5)$$

where the contour C encloses clockwise the real axis in the complex plane ω.

The calculations (after transformation to the spherical coordinates and angular integrations) give

$$Q^3_{\rm ind} = \frac{g\sin(A_0\beta)}{\pi^2}\int\limits_0^\infty p^2 dp \frac{1}{\cos(A_0\beta) + \cosh(\epsilon_p\beta)}, \quad (6)$$

where $\epsilon_p^2 = p^2 + m^2$.

Considering the high-temperature limit $\beta \to \infty$, we obtain

$$Q^3_{\rm ind} = gA_0\left[\frac{4}{3}\beta^{-2} - \frac{2m^2}{3\pi^2}\beta + O(\beta^3)\right]. \quad (7)$$

Hence, we see that the first term is independent of the mass and dominant at high temperatures.

Now, for completeness, we calculate the temperature sum in Eq. (4).

The integrand in Eq. (4) has the form

$$f(p_4) = \frac{p_4 + A_0}{(p_4 - p_4^{(1)})(p_4 - p_4^{(2)})}, \quad (8)$$

where $p_4^{(1)} = -A_0 + i\epsilon_p$, $p_4^{(2)} = -A_0 - i\epsilon_p$. The sum in Eq. (5) after computing the simple residues equals

$$S_1 = \frac{1}{\beta}\sum_{p_4} f(p_4) = -\frac{1}{2}\left[\frac{i\epsilon_p}{p_4^{(1)} - p_4^{(2)}}\tan\left(\frac{\beta}{2}p_4^{(1)}\right) + \right.$$
$$\left. + \frac{-i\epsilon_p}{p_4^{(2)} - p_4^{(1)}}\tan\left(\frac{\beta}{2}p_4^{(2)}\right)\right]. \quad (9)$$

Substituting the corresponding parameters and fulfilling elementary transformations, we find

$$S_1 = \frac{1}{2}\frac{\sin(A_0\beta)}{\cos(A_0\beta) + \cosh(\epsilon_p\beta)}. \quad (10)$$

By substituting S_1 in Eq. (4), we obtain Eq. (6).

Performing similar calculations for $Q^8_{\rm ind}$, we get [7]

$$Q^8_{\rm ind} = gA_0^8\left[\frac{16}{3\sqrt{3}}\beta^{-2} - \frac{8m^2}{3\sqrt{3}\pi^2}\beta + O(\beta^3)\right]. \quad (11)$$

Here, A_0^8 is the background field generated in the plasma. For our problem, it is a given number.

Now, we calculate the quark propagator accounting for the induced charge by means of Schwinger–Dyson's equation. In the Euclidean space-time, it reads

$$S^{-1}(p) = -\left(\gamma^4\left(p_4 - \frac{\lambda^3}{2}gA_0\right) + \boldsymbol{\gamma}\mathbf{p}\right) + m - \Sigma(p), \quad (12)$$

where $\Sigma(p)$ is a quark mass operator. In our problem, to consider the presence of the induced charge, we separate the part of radiation corrections $\Sigma^{(\rm tp.)}$ equaling to the sum of the tadpole diagrams with one gluon line G_4^3, which relates the quark bubble to a quark line. In Eq. (12), we also substitute the A_0 expression explicitly. In the rest frame of the plasma, where the actual calculations are carried out, the velocity vector is $u_\mu = (u_4 = 1,\ \mathbf{u} = 0)$.

Next, we have to consider the gluon field propagator $G^3_{44}(k)$. For that, we use the generalized Green's function of neutral gluons. It reads (in the Lorentz–Feynman gauge) [5, 6]

$$(G^3_{44})^{-1} = k^2 - \Pi_{44}(k_4, \mathbf{k}), \tag{13}$$

where $\Pi_{44}(k^2)$ is the $4-4$ component of a polarization tensor. For $k_4 = 0$, $\mathbf{k} \to 0$, it defines Debye's temperature mass having the order $m_D^2 \sim g^2T^2$. This mass is responsible for the screening of the Coulomb color fields.

The component of interest G^3_{44} taken at zero momenta reads [5, 6]

$$G^3_{44}(p = 0) = \frac{1}{m_D^2}. \tag{14}$$

Using the vertex of interactions in Eq. (12) and Eqs. (6), (14), we obtain

$$\Sigma^{(\mathrm{tp.})} = -\frac{\lambda^3}{2}\gamma^4 \frac{gQ^3_{\mathrm{ind}}}{m_D^2}. \tag{15}$$

Substituting this result in Eq. (12), we conclude that the resummation of tadpole insertions results in the replacement $gA_0 \to gA_0 + g\frac{Q^3_{\mathrm{ind}}}{m_D^2}$ in the initial propagator.

3. Potentials of Classical Color Fields

The presence of the induced color charges in the plasma leads to the generation of classical gluon potentials. To describe this phenomenon, we introduce a simple model motivated by heavy-ion collisions. In this case, the plasma is created for a short period of time in a finite space volume which has a much smaller size in the direction of collisions compared to the transversal ones.

We consider the QGP confined in the plate of the size L in the z-axis direction and infinite in the x-, y-directions. For this geometry, we calculate the classical potentials $\bar\phi^3 = G^3_4, \bar\phi^8 = G^8_4$ by solving the classical field equations for the gluon fields G^3_4, G^8_4 generated by the induced charges $Q^3_{\mathrm{ind}}, Q^8_{\mathrm{ind}}$. In doing so, we account for the results of Refs. [5, 6], where the gluon modes at the A_0 background were calculated. For our problem, we are interested in the longitudinal modes of the fields G^3_4, G^8_4 that have temperature masses $\sim g^2T^2$.

The classical potential $\bar\phi^3$ is calculated from the equation

$$\left[\frac{\partial^2}{\partial x_\mu^2} - m_D^2\right]\bar\phi^3 = -Q^3_{\mathrm{ind}}. \tag{16}$$

Making Fourier's transformation to the momentum k-space, we derive the spectrum of modes $-\ k_4^2 = k_x^2 + k_y^2 + k_z^2 + m_D^2$, where $k_z^2 = (\frac{2\pi}{L})^2 l^2$ and $l = 0, \pm 1, \pm 2, \dots$. The discreteness of k_z is due to the periodic boundary condition for the plane: $\bar\phi^3(z) = \bar\phi^3(z + L)$. The general solution to Eq. (16) is

$$\bar\phi^3(x_4, \mathbf{x}) = d + a\ e^{-i(k_4x_4 - \mathbf{k}\,\mathbf{x})} + b\ e^{i(k_4x_4 - \mathbf{k}\,\mathbf{x})}. \tag{17}$$

In the case of zero induced charge, $d = 0$, and we have two well-known plasmon modes. In the case of $Q^3_{\mathrm{ind}} \neq 0$, the values a, b, d calculated from the confinement boundary condition

$$\bar\phi^3\left(z = -\frac{L}{2}\right) = \bar\phi^3\left(z = \frac{L}{2}\right) = 0 \tag{18}$$

result in the expression

$$\bar\phi^3(z)\frac{Q^3_{\mathrm{ind}}}{m_D^2}\left[1 - \frac{\cos(k_z z)}{\cos(k_z L/2)}\right]. \tag{19}$$

The generated potential depends on the z-variable only. There are no dynamical plasmon states at all. The same result follows for the potential $\bar\phi^8(z)$. This is the main observation. In the presence of the induced charges, the static classical color potentials have to be realized in the plasma.

For applications, it is also necessary to get the Fourier transform $\bar\phi^3(k)$ of potential (19). Fulfilling that for the interval of $z[-\frac{L}{2}, \frac{L}{2}]$, we obtain

$$\bar\phi^3(k) = \frac{Q^3_{\mathrm{ind}}L}{m_D^2}\ \frac{\sin(kL/2)}{(kL/2)}\frac{k_z^2}{k_z^2 - k^2}, \tag{20}$$

where the values of k_z are given by Eq. (16).

The energy for a mode with momentum k_z is positive and equals

$$E_l = \frac{(Q^3_{\mathrm{ind}})^2}{m_D^4}\frac{k_z^2}{2}L = \frac{(Q^3_{\mathrm{ind}})^2}{m_D^4}\frac{2\pi^2}{L}l^2. \tag{21}$$

The total energy is given by the sum over l of energies (21). Similar results hold for the potential $\bar{\phi}^8$.

Thus, in the presence of the induced charges, the static gluon potentials with positive energy should be generated. This is a consequence of condition Eq. (18). Obviously, such a situation is independent of the specific form of the bag, where the plasma is confined. In general, we have to expect that the color static potentials $\bar{\phi}^3$, $\bar{\phi}^8$ should be present in the QGP that results in a new type of processes.

4. Effective $\gamma\gamma G$ vertices in QGP

Other interesting objects, which have to be generated in QGP with the A_0 condensate, are the effective three-line vertices $\gamma\gamma G^3, \gamma\gamma G^8$. They also should exist due to Furry's theorem violation and relate the colored and white states. These vertices, in particular, lead to observable processes such as the inelastic scattering of photons, splitting (or conversion) of gluon $\bar{\phi}^3$, $\bar{\phi}^8$ potentials in two photons.

In this and next sections, we calculate the vertex $\gamma\gamma G^3$ and investigate the mentioned processes.

Let us consider the vertex $\Gamma^{\nu}_{\mu\lambda}$ corresponding to the diagram depicted in the plot. The second diagram is obtained by changing the direction of the quark line. We set that all the momenta are ingoing, the first photon is $\gamma_1(k^1_\mu)$, the second photon is $\gamma_2(k^3_\lambda)$, a color $a = 3$ gluon – $Q^3(k^2_\nu)$, and $k^1 + k^2 + k^3 = 0$. $k^{1,2,3}$ are the momenta of external fields.

We consider the contributions coming from the traces of four γ-matrices, which are proportional to the quark mass and dominant for small photon momenta $k^1, k^3 \ll m$. The analytic expression (common factor is $e^2 gm$) is

$$\Gamma^{\nu}_{\mu\lambda}(k^1,k^3) = \Gamma^{\nu,(1)}_{\mu\lambda}(k^1,k^3) + \Gamma^{\nu,(2)}_{\mu\lambda}(k^1,k^3), \tag{22}$$

where

$$\Gamma^{\nu,(1)}_{\mu\lambda}(k^1,k^3) = \frac{1}{\beta}\sum_{p_4}\int \frac{d^3p}{(2\pi)^3}\frac{N_1}{D(\tilde{P})D(\tilde{P}-k^1)D(\tilde{P}+k^3)}. \tag{23}$$

Here, the summation is over $p_4 = \frac{2\pi}{\beta}(l+1/2), l = 0, \pm1, \pm2, ...$, the integration is over three-dimensional momentum space p, N_1 denotes the numerator coming from the first diagram, $\tilde{P} = (\tilde{P}_4 = p_4 - A_0, \mathbf{p})$, $D(\tilde{P}) = (p_4 - A_0)^2 + \mathbf{p}^2 + m^2 = \tilde{P}_4^2 + \epsilon_p^2$, and $\epsilon_p^2 =$

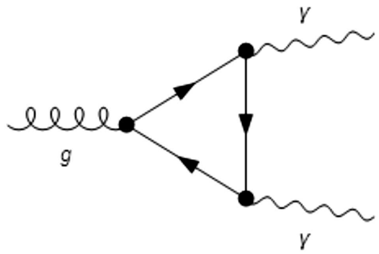

$= \mathbf{p}^2 + m^2$ is the squared energy of a free quark. The functions $D(\tilde{P}-k^1), D(\tilde{P}+k^3)$ assume a corresponding shift in the momentum. The numerator N_1 is

$$(N_1)_{\mu\nu\lambda} = \delta_{\mu\nu}(\tilde{P}-k^2)_\lambda + \delta_{\lambda\nu}(\tilde{P}-k^2)_\mu + \delta_{\mu\lambda}(\tilde{P}-q)_\nu, \tag{24}$$

where $q = k^3 - k^1$ is the photon momentum transferred.

The expression for the second term in (22) comes from the second diagram and can be obtained from (23), (24) by the substitutions $k^1 \to -k^1$, $k^2 \to -k^2$, $q \to -q$. We denote the second numerator by N_2. In what follows, we carry out actual calculations for the first term in (22) and adduce the results for the second one.

Now, we consider the fact that, in the high temperature limit, the large values of the integration momentum p give the leading contribution. Therefore, we can present the functions

$$D(\tilde{P}), \quad D(\tilde{P}-k^1), \quad D(\tilde{P}+k^3)$$

in the form:

$$\begin{aligned} D(\tilde{P}) &= \tilde{P}_4^2 + \epsilon_p^2 = \tilde{P}^2, \\ D(\tilde{P}-k^1) &= \tilde{P}^2\Big(1 - \frac{2\tilde{P}\,k^1 - k_1^2}{\tilde{P}^2}\Big), \\ D(\tilde{P}+k^3) &= \tilde{P}^2\Big(1 + \frac{2\tilde{P}\,k^3 + k_3^2}{\tilde{P}^2}\Big) \end{aligned} \tag{25}$$

with $k_1^2 = (k_4^1)^2 + \mathbf{k}_1^2, k_3^2 = (k_4^3)^2 + \mathbf{k}_3^2$. At high temperature and $\tilde{P}^2 \to \infty$, the k-dependent terms are small. So, we can expand in these parameters. Now, the integrand in Eq. (23) reads

$$\text{Intd.} = \frac{N_1}{(\tilde{P}^2)^3}\left[1 + \sum_{i=1}^{4} A_i\right], \tag{26}$$

where

$$A_1 = -2\frac{(\tilde{P}\,q)}{\tilde{P}^2}, \quad A_2 = -\frac{k_3^2 - k_1^2}{\tilde{P}^2},$$

$$A_3 = -4\frac{(\tilde{P}\,k^1)(\tilde{P}\,k^3)}{\tilde{P}^2}, \quad A_4 = 4\frac{(\tilde{P}\,k^1)^2 + (\tilde{P}\,k^3)^2}{\tilde{P}^2}, \tag{27}$$

and the vector $q_\mu = (q_4, \mathbf{q})$.

For the second diagram, we have to substitute $q \to \to -q$, other terms are even and do not change.

Further, we concentrate on the scattering of photons on the potential Q_4^3 in the medium rest frame and set the thermostat velocity $u_\nu = (1, \mathbf{0}), \nu = 4$. The corresponding terms in the numerators are

$$N_1 \to \delta_{\mu\lambda}(\tilde{P} + q)_4, \quad N_2 \to \delta_{\mu\lambda}(\tilde{P} - q)_4. \tag{28}$$

In this case, $\tilde{P}_4 = p_4 - A_0$ and $\tilde{P}^2 = (p_4 - A_0)^2 + \epsilon_p^2$.

We have to calculate, in general, the series of two types corresponding to these numerators:

$$S_1^{(n)} = \frac{1}{\beta}\sum_{p_4}\frac{p_4 - A_0}{(\tilde{P}^2)^n}, \quad S_2^{(n)} = \frac{1}{\beta}\sum_{p_4}\frac{q_4}{(\tilde{P}^2)^n}, \tag{29}$$

$n = 3, 4, 5$.

These functions can be calculated from the $S_1^{(1)}$ and $S_2^{(1)}$, by computing a number of derivatives with respect to ϵ_p^2. The latter series result in simple expressions. First is the one calculated already for the tadpole diagram Eq. (10). But now, we have to change the sign $A_0 \to -A_0$. The function $S_2^{(1)}$ is

$$S_2^{(1)} = \frac{1}{\beta}\sum_{p_4}\frac{q_4}{\tilde{P}^2} = -\frac{q_4}{2\epsilon_p}\frac{\sinh(\epsilon_p\beta)}{\cos(A_0\beta) + \cosh(\epsilon_p\beta)}. \tag{30}$$

Let us adduce the expressions for A_i obtained after some simplifying algebraic transformations:

$$A_1 = -2\frac{(p_4 - A_0)q_4}{\tilde{P}^2}, \tag{31}$$

$$A_3 = -\frac{4}{\tilde{P}^2}\left[\left(1 - \frac{\epsilon_p^2}{\tilde{P}^2}\right)k_4^1 k_4^3 + \frac{(\mathbf{p}\,\mathbf{k}_1)(\mathbf{p}\,\mathbf{k}_3)}{\tilde{P}^2}\right], \tag{32}$$

$$A_4 = \frac{4}{\tilde{P}^2}\left[\left(1 - \frac{\epsilon_p^2}{\tilde{P}^2}\right)((k_4^1)^2 + (k_4^3)^2) + + \frac{(\mathbf{p}\,\mathbf{k}_1)^2 + (\mathbf{p}\,\mathbf{k}_3)^2}{\tilde{P}^2}\right]. \tag{33}$$

Finally, the resulting amplitude consists of the terms

$$M_1 = 2\delta_{\mu\lambda}\frac{p_4 - A_0}{(\tilde{P}^2)^3}(1 + A_1 + A_3 + A_4) \tag{34}$$

and

$$M_2 = -4\delta_{\mu\lambda}\frac{(p_4 - A_0)q_4^2}{(\tilde{P}^2)^4}. \tag{35}$$

Thus, all the contributions of the $S_2^{(n)}$ series are cancelled in the total. Now, we turn to the d^3p integration.

We present calculation of high temperature asymptotic considering the first term in Eq. (34) which is calculated as the second derivative of $S_1^{(1)}$ over ϵ_p^2 and equals to

$$S_3 = -A_0\beta\,\frac{\mathrm{sech}(\beta\epsilon_p/2)^4}{64p^3}(-2\beta\epsilon_p + + \beta\epsilon_p\cosh(\beta\epsilon_p) + \sinh(\beta\epsilon_p)). \tag{36}$$

Performing integration in the spherical coordinates and taking the leading order approximation, $\epsilon_p\beta = = p\beta$, we get

$$I_3 = \int_{-\infty}^{\infty} d^3p\,S_3 = -A_0\pi\beta\ (0.3348). \tag{37}$$

In such a way all the other integrations in Eqs. (34), (35) can be carried out.

5. Scattering of Photons on the Potentials

Relations (19), (20) give the calculated expressions for the potential $\bar{Q}_4^3 = \bar{\phi}^3$ in the plasma plate. Here, we consider the scattering of photons on potential (20). Let us denote the momenta of ingoing and outgoing photons as k_μ^1 and k_λ^3, respectively. The matrix element of the process is

$$M = (2\pi)^4\delta(k^1 + k^2 - k^3)\ \frac{e_\mu^{\sigma_1}}{\sqrt{2\omega_1}}\ \bar{\phi}^3\ \Gamma_{\mu\lambda}^4\ \frac{e_\lambda^{\sigma_3}}{\sqrt{2\omega_3}}. \tag{38}$$

Here, $e^{\sigma_1}{}_\mu, e^{\sigma_2}{}_\lambda$ are polarization amplitudes of photons, and ω_1, ω_3 are the corresponding energies, $\Gamma_{\mu\lambda}^4(k^1, k^3)$ is the effective vertex calculated in the previous section.

We assume that the beams are not polarized, $\sum_{\sigma_3} e_\mu^{\sigma_1} e_{\mu'}^{\sigma_1} = = \delta_{\mu\mu'}$, $\sum_{\sigma_3} e_\lambda^{\sigma_3} e_{\lambda'}^{\sigma_3} = \delta_{\lambda\lambda'}$. Then the probability

$$P = MM^+ = (\bar{\phi}^3(k))^2\ \Gamma_{\mu\lambda}^4\Gamma_{\mu\lambda}^4\frac{C}{4\omega_1\omega_3}\ \delta(k^1 + k^2 - k^3), \tag{39}$$

where C is some nonrelevant number. In this expression (accounting for the momentum conservation),

$\omega_3 = [(\omega_x^1)^2 + (\omega_y^1)^2 + (\omega_z^1 + k_z^2)^2]^{1/2}$. The value of k_z^2 is a free parameter of the problem. It indicates the point, at which the actual scattering happens in the z-plane. Since this is not known, we have to sum up the probability over k_z^2, i.e., over l. In this expression, all the parameters and functions are known. So, the scattering on the induced color potentials can be calculated. Analogous process has to happen for the classical field $\bar{\phi}^8(k)$. This kind of scattering drastically differs from that for the plasma consisting of free chaotically moving particles.

Another related process is the conversion of classical gluon fields $\bar{\phi}^3(k), \bar{\phi}^8(k)$ in two photons coming out from the QGP due to the effective vertex $\Gamma^{\nu}_{\mu\lambda}(k^1, k^3)$. In the rest frame of the plasma, two photons moving in opposite directions and having specific energies, which correspond to the energy levels E_l Eq. (21), have to be observed. The amplitude is described by Eq. (38) with corresponding changes of momenta.

6. Conclusions

We have demonstrated that, in QGP with the A_0 condensates, the induced color charges $Q^3_{\rm ind}, Q^8_{\rm ind}$ and the static classical gluon fields $\bar{\phi}^3, \bar{\phi}^8$ have to be present. This results in specific new phenomena. In particular, the conversion of gluons in photons happened due to the effective $\Gamma^{\nu}_{\mu\lambda}$ vertex could influence the exit of direct photons from the plasma.

1. Y. Aoki, *et al.* The QCD transition temperature: results with physical masses in the continuum limit II. arxiV: 0903.4155 (2009).
2. H. Satz. Extreme states of matter in strong interaction physics: An introduction. *Lect. Notes Phys.* **841**, 237 (2012).
3. M. Srednicki, I. Susskin. Colored monopoles on the lattice. *Nucl. Phys. B* **179**, 239 (1981).
4. O.A. Borisenko, J. Bohacik, V.V. Skalozub. A_0 condensate in QCD. *Fortschr. Phys.* **43**, 301 (1995).
5. O.K. Kalashnikov. Infrared properties of the hot gauge theory after symmetry breaking. *Progr. Theor. Phys.* **92**, 1207 (1994).
6. O.K. Kalashnikov. Self-energy peculiarities of the hot gauge theory after symmetry breaking. *Mod. Phys. Lett. A* **11**, 1825 (1996).
7. I.A. Baranov, V.V. Skalozub. Induced charges and quark polarization operator at A0 background. *J. Phys. Electron.* **26 (1)**, 3 (2018).

Received 26.07.19

В. Скалозуб

ІНДУКОВАНІ КОЛЬОРОВІ ЗАРЯДИ,
ЕФЕКТИВНА $\gamma\gamma G$-ВЕРШИНА У КВАРК-ГЛЮОННІЙ
ПЛАЗМІ. ЗАСТОСУВАННЯ ДО ЗІТКНЕНЬ
ВАЖКИХ ІОНІВ

Р е з ю м е

Ми обчислюємо індуковані кольорові заряди $Q^3_{\rm ind}, Q^8_{\rm ind}$ та ефективну $\gamma - \gamma$-глюон вершину, які генеруються у кварк-глюонній плазмі в присутності A_0 конденсату внаслідок порушення кольорової C-парності в таких умовах. Для імітації зіткнення важких ядер ми розглядаємо модель плазми, що знаходиться всередені вузької пластини необмежених поперечних розмірів. Для таких умов ми отримуємо потенціали класичних глюонних полів $\bar{\phi}^3, \bar{\phi}^8$, що виникають у присутності індукованих зарядів. У якості застосування розглядаються два процеси – розсіювання фотонів на плазмі та конвертація класичних глюонів у два фотони, що випромінюються із плазми.

https://doi.org/10.15407/ujpe64.8.760

I. SZANYI,[1] V. SVINTOZELSKYI[2]

[1] Eötvös Loránd University
(1/A, Pázmány Péter Walkway, 1117 Budapest, Hungary; e-mail: istvan.szanyi@cern.ch)
[2] Taras Shevchenko National University of Kyiv
(64/13, Volodymyrska Str., Kyiv 01601, Ukraine; e-mail: 1vladimirsw@gmail.com)

POMERON-POMERON SCATTERING

The central exclusive diffractive (CED) production of meson resonances potentially is a factory producing new particles, in particular, a glueball. The produced resonances lie on trajectories with vacuum quantum numbers, essentially on the pomeron trajectory. A tower of resonance recurrences, the production cross-section, and the resonances widths are predicted. A new feature is the form of a non-linear pomeron trajectory, producing resonances (glueballs) with increasing widths. At LHC energies, in the nearly forward direction, the t-channel both in elastic, single, or double diffraction dissociations, as well as in CED, is dominated by the pomeron exchange (the role of secondary trajectories is negligible, however a small contribution from the odderon may be present).

Keywords: Regge trajectory, pomeron, glueball, CED, LHC.

1. Introduction

The central exclusive diffractive (CED) production continues attracting attention of both theorists and experimentalists (see, e.g., [1] and references therein). Interest in this subject is triggered by LHC's high energies, where even the subenergies at an equal partition is sufficient to neglect the contribution from secondary Regge trajectories. Consequently, CED can be considered as a gluon factory to produce exotic particles such as glueballs.

Below, we will study CED shown in Fig. 1 with topology 4. Its knowledge is essential in studies with diffractive excited protons, topologies 5 and 6.

In the single-diffraction dissociation or single dissociation (SD), one of the incoming protons dissociates (topology 2 in Fig. 1), in double-diffraction dissociation or double dissociation (DD), both protons dissociate (topology 3), and, in central dissociation (CD) or double-Pomeron exchange (DPE), none of the protons dissociates (topology 4). These processes are tabulated below as

SD $pp \to Xp$
or $pp \to pY$
DD $pp \to XY$
CD (DPE) $pp \to pXp$,

where X and Y represent diffractive dissociated protons.

2. Pomeron/Glueball Trajectory

Regge trajectories $\alpha(s)$ connect the scattering region, $s < 0$, with that of particle spectroscopy, $s > 0$. In this way, they realize the crossing symmetry and anticipate the duality, *i.e.*, the dynamics of two kinematically disconnected regions is intimately related: the trajectory at $s < 0$ should "know" its behavior in the cross channel and vice versa. Most of the familiar meson and baryon trajectories follow the above regularity: with their parameters fitted in the scattering region, they fit the masses and spins of relevant resonances, see, e.g., [2]. The behavior of trajectories both in the scattering and particle regions is close to linear, which is an approximation to reality. Resonances on real and linear trajectories imply unrealistic infinitely narrow resonances. Analyticity and unitarity also require that the trajectories be non-linear complex functions [3,4]. Constraints on the threshold and asymptotic behaviors of Regge trajectories were derived from dual amplitudes with Mandelstam analyticity [4]. Accordingly, near the threshold (see also [5–7])

$$\Im m\alpha(s)_{s\to s_0} \sim (s-s_0)^{\alpha(s_0)+1/2}, \qquad (1)$$

while the trajectories are constrained asymptotically by [4]

$$\left|\frac{\alpha(s)}{\sqrt{s}\ln s}\right|_{s\to\infty} \le \text{const.} \tag{2}$$

The above asymptotic constrain can be still lowered to a logarithm by imposing (see [8] and earlier references) the wide-angle power behavior for the amplitude.

The above constrains are restrictive, but still leave much room for the model building. In Refs. [9, 10], the imaginary part of the trajectories (resonances' widths) was recovered from the nearly linear real part of the trajectory by means of dispersion relations and fits to the data.

While the parameters of meson and baryon trajectories can be determined both from the scattering data and from the particle spectra, this is not true for the pomeron (and odderon) trajectory, known from fits to scattering data only (negative values of its argument). An obvious task is to extrapolate the pomeron trajectory from negative to positive values to predict glueball states at $J = 2, 4, ...$ was not solved. Given the nearly linear form of the pomeron trajectory, known from the fits to the (exponential) diffraction cone, little room is left for variations in the region of particles ($s > 0$.) The non-observability of any glueball state in the expected values of spins and masses may have two explanations: 1. glueballs appear as hybrid states mixed with quarks, which makes their identification difficult; 2. their production cross-section is low and their widths is large. To resolve these problems, one needs a reliable model to predict cross-sections and decay widths of the expected glueballs, in which the pomeron trajectory plays a crucial role.

Models for the pomeron/glueball trajectories were proposed and discussed in quite a number of papers [11–14]. They range from simple phenomenological (also linear) models to quite sophisticated ones, involving QCD, lattice calculations, extra dimensions, etc. The basic problem of the production cross-sections and the decay widths of produced glueballs in the cited papers remains open. Close to the spirit of the present approach are papers [12–14], where the pomeron/glueball trajectory, including the threshold singularities is manifestly non-linear, and the real part terminates.

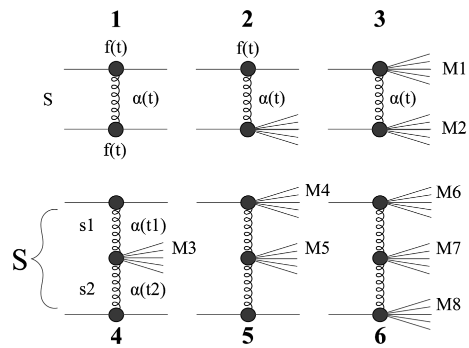

Fig. 1. Regge-pole factorization

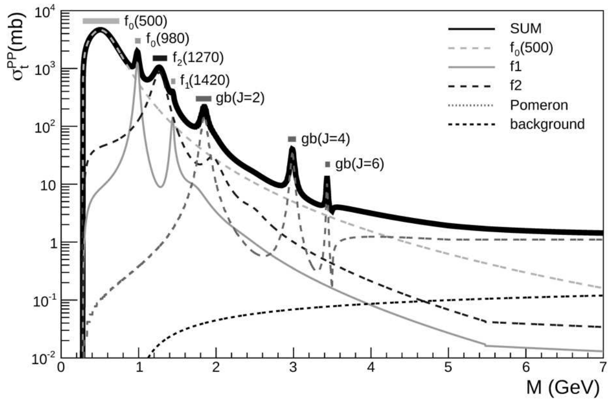

Fig. 2. Pomeron-pomeron total cross-section in CED calculated in Ref. [1]

We continue the lines of researches initiated in Refs. [1, 15] in which an analytic pomeron trajectory was used to calculate the pomeron-pomeron cross-section in the central exclusive production measurable in the proton-proton scattering, e.g., at the LHC. The basic idea in that approach is the use of a non-linear complex Regge trajectory for the pomeron satisfying the requirements of the analytic S-matrix theory and fitting the data. Fits imply high-energy elastic proton-proton scattering data. For the scattering amplitude, the simple and efficient Donnachie–Landshoff model [16] was used. The essential difference with respect to many similar studies lies in the non-linear behavior of the trajectories. They affect crucially the predicted properties of the resonances. Our previous papers [1, 15] contain more than that: the fitted trajectories are used to calculate pomeron-pomeron scattering cross-sections in the central exclusive diffraction at the LHC. Figure 2 shows the result of those calculations.

Papers [1, 15] contain detailed analyses and fits of both the pomeron and non-leading (also complex!) Regge trajectories, the emphases being on the pomeron/gluon one. In the present study, we revise the basic object, namely the model of a pomeron trajectory, postponing other details (secondary reggeons, CED, *etc.*) to a forthcoming study.

2.1. Scattering amplitude, cross-sections, resonances

In Ref. [1], the contribution of resonances to the pomeron-pomeron (PP) cross-section was calculated from the imaginary part of the amplitude with the use of the optical theorem:

$$\sigma_t^{PP}(M^2) = \Im m\, A(M^2, t=0) =$$

$$= a \sum_{i=f,P} \sum_J \frac{[f_i(0)]^{J+2}\, \Im m\, \alpha_i(M^2)}{(J - \Re e\, \alpha_i(M^2))^2 + (\Im m\, \alpha_i(M^2))^2}. \quad (3)$$

In this section, we concentrate on the pomeron. In this case, Eq. (3) reduces to

$$\sigma_t^{PP}(M^2) = a \sum_J \frac{k^{J+2}\, \Im m\, \alpha(M^2)}{(J - \Re e\, \alpha(M^2))^2 + (\Im m\, \alpha(M^2))^2}, \quad (4)$$

where $k = f_i(0)$, and, for simplicity, we set $k = 1$.

We start by comparing the resulting glueball spectra in two ways: first, we plot the real and imaginary parts of the trajectory (Chew–Frautchi plot) and calculate the resonances' widths by using the relation (see, e.g., Eq. (18) in [15])

$$\Gamma(s = M^2) = \frac{2\Im m\alpha(s)}{|\alpha'(s)|}, \quad (5)$$

where $\alpha'(s) = d\Re e\alpha(\sqrt{s})/d\sqrt{s}$.

2.2. Analytic Regge trajectories

In the previous studies [1, 15, 18], the following two types of trajectories were considered:

$$\alpha(s) = \alpha_0 + \alpha_1 s + \alpha_2(\sqrt{s_0 - s} - \sqrt{s_0}), \quad (6)$$

and

$$\alpha(s) = \alpha_0 + \alpha_2(\sqrt{s_0 - s} - \sqrt{s_0}) + \alpha_3(\sqrt{s_1 - s} - \sqrt{s_1}), \quad (7)$$

In trajectory Eq. (7), the second, heavy threshold was introduced to mimic the nearly linear rise of the trajectory for $s < s_1$, avoiding an indefinite rise as in Eq. (6), thus securing the asymptotic square-root upper bound (2). As realized in Refs. [1, 15], these trajectories result in "narrowing" the resonances (here, a glueball) whose widths decrease, as their masses increase. Below, we show that this deficiency is remedied in a trajectory that satisfies the constraint of the analytic S-matrix theory, namely, the threshold behavior and asymptotic boundedness, and produces fading resonances (glueballs), whose widths are rising with mass.

The trajectory is:

$$\alpha(s) = \frac{a + bs}{1 + c(\sqrt{s_0 - s} - \sqrt{s_0})}, \quad (8)$$

where $s_0 = 4m_\pi^2$, and a, b, c are adjustable parameters, to be fitted to scattering ($s < 0$) data with the obvious constraints: $\alpha(0) \approx 1.08$ and $\alpha'(0) \approx 0.3$. Trajectory Eq. (8) has square-root asymptotic behavior, in accord with the requirements of the analytic S-matrix theory.

With the parameters fitted in the scattering region, we continue trajectory Eq. (8) to positive values of s. When approaching the branch cut at $s = s_0$, one has to choose the right Riemann sheet, For the $s > s_0$ trajectory Eq. (8) may be rewritten as

$$\alpha(s) = \frac{a + bs}{1 - c(i\sqrt{s - s_0} + \sqrt{s_0})} \quad (9)$$

with the sign "minus" in front of c, according to the definition of the physical sheet.

For $s \gg s_0, |\alpha(s)| \to \frac{b}{c}\sqrt{|s|}$. For $s > s_0$ (on the upper edge of the cut), $\Im m\, \alpha > 0$.

The intercept is $\alpha(0) = a$, and the slope at $s = 0$ is

$$\alpha'(0) = b + \frac{ac}{2\sqrt{s_0}}. \quad (10)$$

To anticipate subsequent fits and discussions, we note that the presence of the light threshold $s_0 = 4m_\pi^2$ (required by unitarity and the observed "break" in the data) results in the increasing, compared with the "standard" value of ≈ 0.25 GeV^{-2}, intercept.

2.3. Simple Regge-pole fits to high-energy elastic scattering data

High-energy elastic proton-proton and proton-antiproton scatterings, including ISR and LHC energies, were successfully fitted with non-linear pomeron trajectories Eqs. (6) and (7) in a number of papers, see [17] and references therein. Here, we are interested in the parametrization of the pomeron (and odderon) trajectories, dominating the LHC energy region, and concentrate on the LHC data, where the secondary trajectories can be completely ignored in the near forward direction.

At lower energies (e.g., at the ISR), the diffraction cone shows the almost perfect exponential behavior corresponding to a linear pomeron trajectory in a wide span of $0 < -t < 1.3$ GeV^2, which is violated only by the "break" near $t \approx -0.1$ GeV^2. At the LCH, it is almost immediately followed by another structure, namely, by the dip at $t \approx -0.6$ GeV^2. The dynamics of the dip (diffraction minimum) has been treated fully and successfully [18]. However, those details are irrelevant to the behavior of the pomeron trajectory in the resonance (positive s) region and the expected glueballs there, that depend largely on the imaginary part of the trajectory and basically on the threshold singularity in Eq. (8).

In Fig. 3, we show a fit to the low-$|t|$ elastic proton-proton differential cross-section data [19] at 13 TeV with a simple model:

$$A_P(s,t) = a_P e^{b_P t} e^{-i\pi\alpha_P(t)/2}(s/s_{0P})^{\alpha_P(t)}, \tag{11}$$

where $\alpha_P(t)$ is given by Eq. (8) (changing the variable s to the variable t).

We used the norm

$$\frac{d\sigma}{dt} = \frac{\pi}{s^2}|A_P(s,t)|^2. \tag{12}$$

Figure 4 shows the normalized form of the differential cross-section (used by TOTEM [19]) illustrating the low-$|t|$ "break" phenomenon [17] related to the non-linear square-root term in the pomeron trajectory. However, it should be also noted that the "break" may be resulted from the two-pion threshold both in the trajectory and the non-exponential residue, as discussed in [17].

2.4. Extrapolating the pomeron trajectory to the resonance region, $s > 0$

Fitting to the measured pp scattering data, the values of the pomeron trajectory parameters became known. Changing back the variable t to the variable s (crossing symmetry), we can extrapolate now the

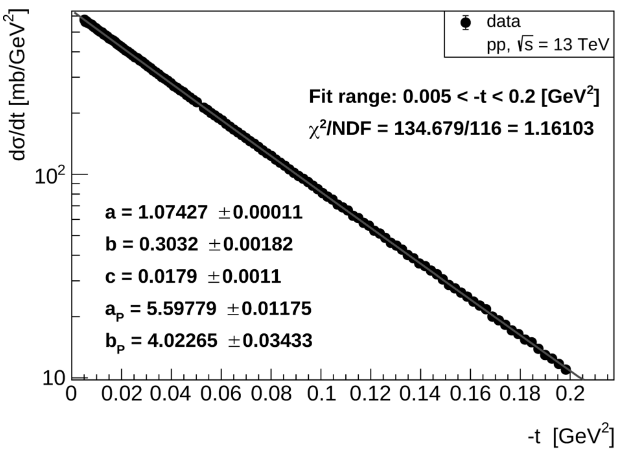

Fig. 3. Fitted pp differential cross-section at 13 TeV using amplitude Eq. (11) and trajectory Eq. (8)

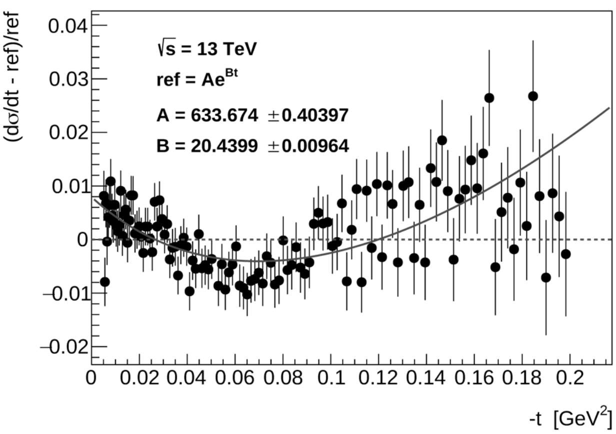

Fig. 4. Normalized form of the fitted pp differential cross-section at 13 TeV using amplitude Eq. (11) and trajectory Eq. (8)

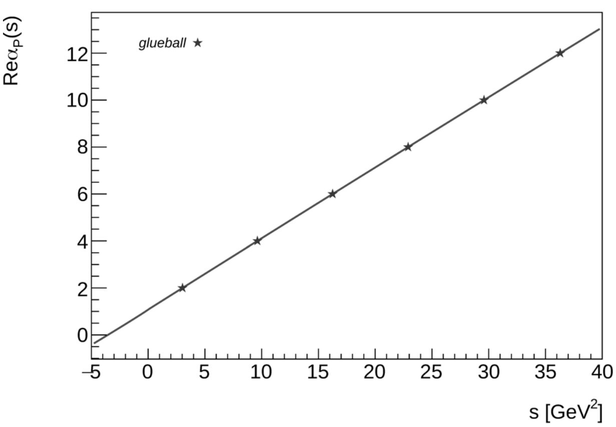

Fig. 5. Real part of the pomeron trajectory Eq. (8) as a function of s

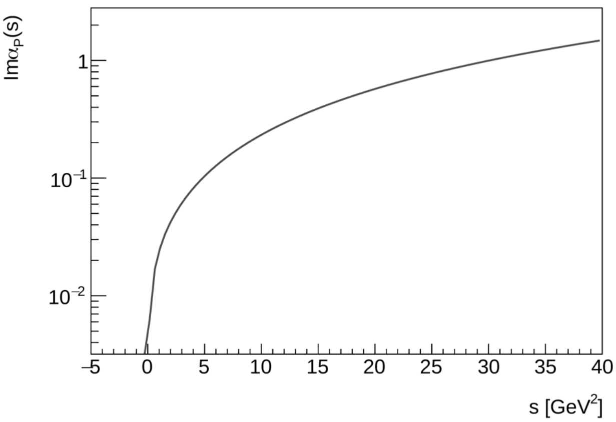

Fig. 6. Imaginary part of the pomeron trajectory Eq. (8) as a function of s

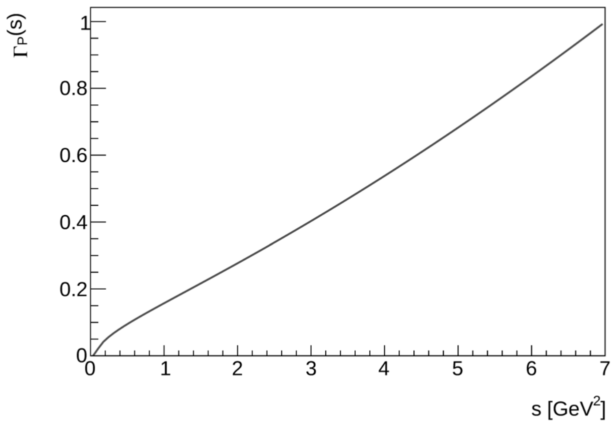

Fig. 7. Resonance width Eq. (5) calculated with trajectory Eq. (8)

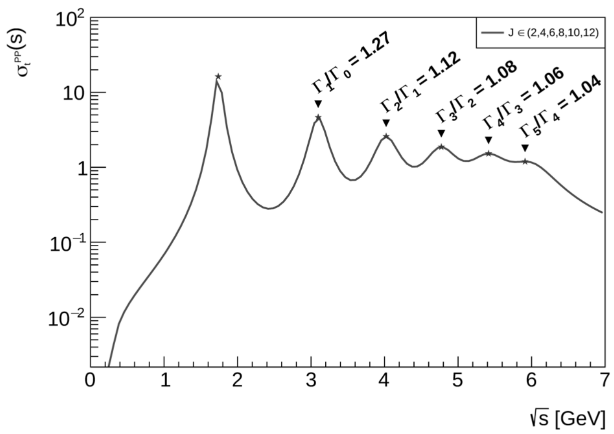

Fig. 8. Pomeron-pomeron total cross-section Eq. (4) (setting $a = 1$ and $J \in (2, 4, 6, 8, 10, 12)$) calculated with trajectory Eq. (8) showing also the ratios of neighboring resonances' widths

pomeron trajectory to the resonance region, $s > 0$. Figures 5 and 6 show, respectively, the real and imaginary parts of the trajectories (during the calculations, the trajectory parameter values are taken from the fit shown in Fig. 3). Figure 5 shows the glueball spectra lying on the pomeron trajectory. Such glueballs have even integer spins ($J \equiv \mathrm{Re}\,\alpha_P(s) = 2,\ 4,\ 6,\ ...$) and mass square $M^2 = s$.

In Figs. 8 and 7, we can see, respectively, the resonance width and the pomeron-pomeron total cross section.

3. Summary

Using a simple pomeron pole model fit to the 13-TeV pp low-$|t|$ differential cross-section data, we have extrapolated the pomeron trajectory from negative to positive values to predict glueball states at $J = 2$, 4, 6, 8, 10, and 12. We have predicted also the cross-sections and decay widths of the expected glueballs. Applying the pomeron trajectory Eq. (8), we have obtained such resonances (glueballs) whose widths increase with their masses.

We thank the organizers of the New Trends in High-Energy Physics 2019 for their support and the inspiring discussions provided by the Conference. We thank also László Jenkovszky for his guidance during the preparation of the manuscript. The work of I. Szanyi was supported by the "Márton Áron Szakkollégium" program.

1. R. Fiore, L. Jenkovszky, R. Schicker. Exclusive diffractive resonance production in proton-proton collisions at high energies. *Eur. Phys. J. C* **78**, 468 (2018).
2. P.D.B. Collins. *An Introduction to Regge Theory and High Energy Physics* (Cambridge Univ. Press, 1977).
3. A. Degasperis, E. Predazzi. Dynamical calculation of Regge trajectories. *Nuovo Cimento A* **65**, 764 (1970).
4. A.I. Bugrij, G. Cohen-Tannoudji, L.L. Jenkovszky, N.A. Kobylinsky. Dual amplitudes with Mandelstam analyticity. *Fortschritte der Physik* **21**, 427 (1973).
5. A.O. Barut, D.E. Zwanziger. Complex angular momentum in relativistic S-matrix theory. *Phys. Rev.* **127**, 974 (1962).
6. V.N. Gribov, Ya.I. Pomeranchuk. Properties of the elastic scattering amplitude at high energies. *Nucl. Phys.* **38**, 516 (1962).
7. R. Oehme. Complex angular momentum in elementary particle scattering, in *Proceedings of the Scottish Universities Summer School* Edinburgh 1963, edited by R. G. Moorhouse, p.129 (1964).

8. L.L. Jenkovszky. High-energy elastic hadron scattering. *La Rivista del Nuovo Cimento* **10**, 1 (1987).
9. R. Fiore, L.L. Jenkovszky, F. Paccanoni, A. Prokudin. Baryonic Regge trajectories with analyticity constraints. *Phys. Rev. D* **70**, 054003 (2004).
10. R. Fiore, L.L. Jenkovszky, V. Magas, F. Paccanoni, A. Papa. Analytic model of Regge trajectories. *Eur. Phys. J. A* **10**, 217 (2001).
11. M.N. Sergeenko. Gluonium states and the Pomeron trajectory. arXiv:0807.0911.
12. M.M. Brisudova, L. Burakovsky, T. Goldman, A. Szczepaniak. Nonlinear Regge trajectories and glueballs. arXiv:nucl-th/0303012.
13. T. Goldman, A. Szczepaniak. Nonlinear Regge trajectories and glueballs. arXiv:hep-ph/0009126.
14. M.M. Brisudova, L. Burakovsky, T. Goldman. Spectroscopy "windows" of quark-antiquark mesons and glueballs with effective Regge trajectories. arXiv:hep-ph/0008212.
15. R. Fiore, L. Jenkovszky, R. Schicker. Resonance production in Pomeron–Pomeron collisions at the LHC. *Eur. Phys. J. C* **76**, 38 (2016).
16. A. Donnachie, P.V. Landshoff. Hard diffraction: Production of high pT jets, W or Z, and Drell–Yan pairs. *Nucl. Phys. B* **303**, 634 (1988).
17. L. Jenkovszky, I. Szanyi, CI. Tan. Shape of proton and the pion cloud. *Eur. Phys. J. A* **54**, 116 (2018).
18. I. Szanyi, N. Bence, L. Jenkovszky. New physics from TOTEM's recent measurements of elastic and total cross-sections. *J. Phys. G: Nucl. Part. Phys.* **46**, 055002 (2019).
19. The TOTEM collaboration. First determination of the ρ parameter at $\sqrt{s} = 13$ TeV – probing the existence of a colourless three-gluon bound state. arXiv:1812.04732.

Received 08.07.19

І. Сані, В. Свінтозельський

ПОМЕРОН-ПОМЕРОННЕ РОЗСІЮВАННЯ

Р е з ю м е

Центральне ексклюзивне дифракційне (ЦЕД) народження мезонних резонансів потенційно може бути фабрикою нових частинок, зокрема глюболів. Отримані резонанси лягають на траєкторії з вакуумними квантовими числами, переважно на траєкторію померона. Отримано ширини резонансів та їхній поперечний переріз. Новою особливістю є використання нелінійної траєкторії для померона, що продукує резонанси (глюболи) зі зростаючою шириною. При енергіях ВАК, у майже прямому напрямку в t-каналі як при пружних – одинарної чи подвійної дифракційної дисоціації, так і в ЦЕД домінує обмін померонами (вплив вторинних траєкторій нехтовний, хоча можливе врахування невеликого внеску оддерона).

https://doi.org/10.15407/ujpe64.8.766

M. SZYMAŃSKI,[1] M. BLUHM,[1,2,3] K. REDLICH,[1,3] C. SASAKI[1]

[1] Institute of Theoretical Physics, University of Wrocław
(PL-50204 Wrocław, Poland; e-mail: michal.szymanski@ift.uni.wroc.pl)
[2] SUBATECH UMR 6457 (IMT Atlantique, Université de Nantes, IN2P3/CNRS)
(4 rue Alfred Kastler, 44307 Nantes, France)
[3] Extreme Matter Institute EMMI, GSI
(Planckstr. 1, D-64291 Darmstadt, Germany)

SEARCHING FOR THE QCD CRITICAL POINT WITH NET-PROTON NUMBER FLUCTUATIONS

Net-proton number fluctuations can be measured experimentally and, hence, provide a source of important information about the matter created during relativistic heavy ion collisions. Particularly, they may give us clues about the conjectured QCD critical point. In this work, the beam-energy dependence of ratios of the first four cumulants of the net-proton number is discussed. These quantities are calculated using a phenomenologically motivated model in which critical mode fluctuations couple to protons and antiprotons. Our model qualitatively captures both the monotonic behavior of the lowest-order ratio, as well as the non-monotonic behavior of higher-order ratios, as seen in the experimental data from the STAR Collaboration. We also discuss the dependence of our results on the coupling strength and the location of the critical point.

K e y w o r d s: net-proton number fluctuations, QCD critical point, heavy-ion collisions.

1. Introduction

The theoretical and experimental investigations of the phase diagram of strongly interacting matter are an important subject of modern high-energy physics. One of the unresolved questions concerns the existence and location of the QCD critical point (CP) in the T and μ planes. Strong fluctuations of the critical mode, σ, in the vicinity of CP, although not directly observable, are expected to couple to physically measurable quantities such as fluctuations of conserved charges [1, 2].

Fluctuations of the net-proton number serve as an experimental probe of baryon number fluctuations. Recent, but still preliminary results of the STAR Collaboration [3–5] show a non-monotonic beam energy dependence of the ratios of higher-order net-proton number cumulants. However, the interpretation of the data is still unclear [6–9]. Therefore, effective models are needed to improve our understanding of these quantities.

One of such models was developed in [10], where the impact of resonance decays on net-proton number cumulant ratios was studied. This model could qualitatively describe the non-monotonic behavior of the C_3/C_2 and C_4/C_2 ratios. However, it also showed a strong non-monotonic behavior of the C_2/C_1 ratio which is not observed experimentally. Recently, this model was re-examined [11] to account for the scaling properties of the baryon number and chiral susceptibilities obtained within effective models [12, 13]. This reduces the effect of critical fluctuations in the net-proton number variance and, thus, allows for a better description of the STAR data.

Here, we discuss the beam energy dependence of the ratios of net-proton number cumulants obtained using the refined model from Ref. [11] and study their dependence on the coupling strength between the critical mode and (anti)protons, as well as their dependence on the location of the critical point.

2. Model Setup

As a baseline model to calculate the net-proton number cumulants, we choose the hadron resonance gas (HRG) model in which the number density of each particle species is given by the ideal gas formula,

$$n_i(T,\mu_i) = d_i \int \frac{d^3k}{(2\pi)^3} f_i^0(T,\mu_i). \qquad (1)$$

Here, d_i is the degeneracy factor, and

$$f_i^0 = \frac{1}{(-1)^{B_i} + e^{(E_i - \mu_i)/T}} \tag{2}$$

is the equilibrium distribution function, where $E_i = \sqrt{\mathbf{p}^2 + m_i^2}$ is the dispersion relation, and $\mu_i = B_i\mu_B + S_i\mu_S + Q_i\mu_Q$ is the chemical potential of a particle with mass m_i, baryon number B_i, strangeness S_i, and electric charge Q_i; μ_B, μ_Q and μ_S denote the baryon, strangeness and charge chemical potentials.

Since the QCD pressure is approximated in the HRG model by a sum of partial ideal gas pressures corresponding to different particles, there are only thermal fluctuations in this approximation. To include critical fluctuations on the top of thermal ones, we follow the phenomenological approach employed in Ref. [10]. In this approach, the particle mass is assumed to be composed of critical and non-critical parts as suggested in linear sigma models,

$$m_i \sim m_0 + g_i\sigma, \tag{3}$$

where m_0 is a non-critical contribution, and g_i is the coupling strength between the critical mode and the particle of type i. Critical mode fluctuations modify the distribution function into $f_i = f_i^0 + \delta f_i$, where a change of the distribution function due to critical mode fluctuations reads

$$\delta f_i = \frac{\partial f_i}{\partial m_i}\delta m_i = -\frac{g_i}{T}\frac{v_i^2}{\gamma_i}\delta\sigma, \tag{4}$$

with $v_i^2 = f_i^0((-1)^{B_i} f_i^0 + 1)$ and $\gamma_i = E_i/m_i$.

Fluctuations of the particle number in the thermal medium can be quantified in terms of cumulants. The n-th order cumulant of the i-th particle species reads

$$C_n^i = VT^3 \frac{\partial^{n-1}(n_i/T^3)}{\partial(\mu_i/T)^{n-1}}\bigg|_T, \tag{5}$$

where the temperature T is kept constant. In this work, we consider the first four cumulants of the net-proton number, $N_{p-\bar{p}} = N_p - N_{\bar{p}}$, which are given by [10]

$$C_n = C_n^p + (-1)^n C_n^{\bar{p}} +$$

$$+ (-1)^n \langle (V\delta\sigma)^n \rangle_c (m_p)^n (J_p - J_{\bar{p}})^n, \tag{6}$$

where C_n^p and $C_n^{\bar{p}}$ are the n-th order proton and antiproton cumulants obtained within the baseline model, respectively, $\langle (V\delta\sigma)^n \rangle_c$ is the n-th critical mode cumulant, and

$$J_i = \frac{gd}{T}\int \frac{d^3k}{(2\pi)^3}\frac{1}{E} f_i^0(1 - f_i^0). \tag{7}$$

Moreover, the contributions of other particles and resonance decays are neglected.

In general, cumulants of the critical mode cannot be calculated analytically. Following the approach introduced in Ref. [10], we model them using the universality class arguments which state that different physical systems belonging to the same universality class exhibit the same critical behavior close to the critical point [14]. Under the assumption that QCD belongs to the same universality class, as the three-dimensional Ising model [16–18], we can identify the QCD order parameter, σ, with the magnetization, M_I, the order parameter of the spin model. Hence, the critical mode cumulants can be written as [10]

$$\langle (V\delta\sigma)^n \rangle_c = \left(\frac{T}{VH_0}\right)^{n-1} \frac{\partial^{n-1} M_I}{\partial h^{n-1}}\bigg|_r, \tag{8}$$

where $r = (T - T_c)/T_c$ is the reduced temperature, and $h = H/H_0$ is the reduced magnetic field. The critical point is located at $r = h = 0$.

In the net-proton number cumulants, the singular part of the second cumulant receives a contribution from the first derivative of the order parameter with respect to the reduced magnetic field,

$$C_2^{\text{sing.}} \propto \frac{\partial M_I}{\partial h}. \tag{9}$$

The right-hand side of this equation is the magnetic susceptibility of the Ising model which, due to universality, can be identified with the chiral susceptibility of QCD. However, C_2 is related to the baryon number susceptibility which is known to diverge weaker than the chiral one [12, 13, 19]. Therefore, the model introduced in Ref. [10] requires some modifications [11]. This can be done using the following relation obtained by calculations within the effective model on the mean field level [12, 13]:

$$\chi_{\mu\mu} \simeq \chi_{\mu\mu}^{\text{reg}} + \sigma^2\chi_{\text{chiral}}, \tag{10}$$

in which the singular contribution to the baryon number susceptibility is proportional to the chiral susceptibility times the squared order parameter, and $\chi_{\mu\mu}^{\text{reg}}$

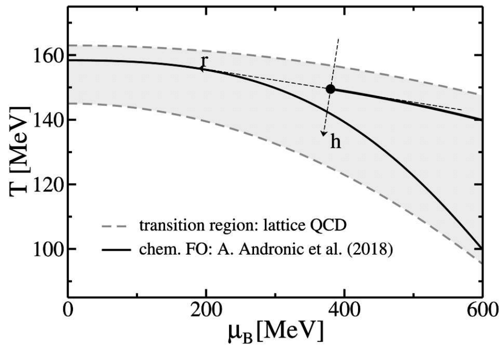

Fig. 1. The model setup used in this work. The filled band between two dashed curves shows the lattice QCD constraints for the chiral crossover transition. The green dot denotes the critical point with the spin model coordinate system attached to it and the first-order phase transition line for a larger baryon chemical potential. The solid blue line corresponds to the chemical freeze-out curve from [15]

is the regular part of the baryon number susceptibility. To obtain such a form of the second cumulant, the proton mass in Eq. (6) should be replaced by the order parameter, σ, such that the new C_2 reads

$$C_2 = C_2^p + C_2^{\bar{p}} + g^2\sigma^2\langle(V\delta\sigma)^n\rangle(J_p - J_{\bar{p}})^2. \tag{11}$$

The modified higher-order cumulants are

$$C_3 = C_3^p - C_3^{\bar{p}} - g^3\sigma^3\langle(V\delta\sigma)^n\rangle(J_p - J_{\bar{p}})^3 \tag{12}$$

and

$$C_4 = C_4^p + C_4^{\bar{p}} + g^4\sigma^4\langle(V\delta\sigma)^n\rangle(J_p - J_{\bar{p}})^4. \tag{13}$$

Since the cumulants are volume-dependent, it is convenient to consider their ratios in which this dependence cancels out,

$$\frac{C_2}{C_1} = \frac{\sigma^2}{M}, \quad \frac{C_3}{C_2} = S\sigma, \quad \frac{C_4}{C_2} = \kappa\sigma^2, \tag{14}$$

where $M = C_1$ is the mean, $\sigma^2 = C_2$ the variance, $\kappa = C_4/C_2^2$ the kurtosis, and $S = C_3/C_2^{3/2}$ the skewness.

To use the universality class arguments discussed above, a mapping between the QCD phase diagram and the reduced temperature and a magnetic field of the spin model is needed. Such a mapping is non-universal and has to be modeled for each system separately. In this work, we use a linear mapping [20, 21] in which the critical point is located at $r = h = 0$, the r axis is tangential to the QCD first-order phase transition line, and the positive direction of the h axis points toward the hadronic phase. Schematically, this is shown in Fig. 1, where the green line denotes the first-order phase transition, and the filled band shows lattice QCD constraints on the location of the chiral crossover region.

To calculate the order parameter and its cumulants, we use the parametric representation of the magnetic equation of state [22]. For a more detailed discussion of the mapping, lattice limits, and the magnetic equation of state, we refer the reader to the papers [10, 11].

Finally, assuming that the matter created during a heavy ion collision forms a thermal medium characterized by the temperature and chemical potentials, experimental data on event-by-event multiplicity fluctuations can be compared with model results. To this end, we calculate the net-proton number cumulants at the chemical freeze-out. The chemical freeze-out conditions used in this work were obtained by the analysis of hadron yields [23–28]. The blue line in Fig. 1 shows the recently obtained parametrization [15].

3. Numerical Results

In this section, we discuss numerical results on net-proton number cumulant ratios obtained within the current model. The set of model parameters includes the coupling strength g between (anti)protons and the critical mode, the parameters of the magnetic equation of state, as well as the size of a critical region in the (T, μ) plane. Their values and a detailed discussion can be found in Refs. [10, 11]. Moreover, the location of the QCD critical point is unknown. To study the effect of its position in the QCD phase diagram on the refined model results, we consider three different locations of the CP listed in Table and shown in Fig. 2, where the distance to the freeze-out curve is the farthest for CP_1 and closest for CP_3.

The first step of our discussion is the comparison between the C_2/C_1 ratio obtained using the model from Ref. [10], where the n-th net-proton number cumulant is given by Eq. (6), and the refined model [11] for the critical point location CP_1. This is shown in Fig. 3. Results obtained using the original model exhibit a clear non-monotonic behavior and deviate strongly from the non-critical baseline (the black-dotted line) even for the small coupling, $g = 3$, which becomes more pronounced for $g = 5$ (the red solid and dashed lines, respectively). Using the current approach, we find a substantial reduction of the criti-

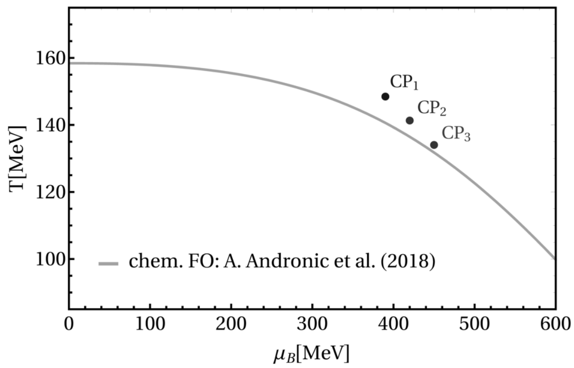

Fig. 2. QCD critical point locations from Table plotted with the chemical freeze-out curve [15] used in this work

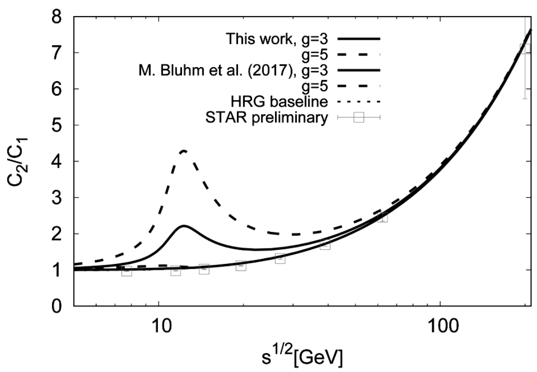

Fig. 3. Second to first net-proton number cumulant ratio for $g = 3$ and 5 calculated following Ref. [10] (red solid and dashed lines, respectively) compared to the refined model results [11] (blue solid and dashed lines, respectively). The preliminary STAR data on the net-proton number fluctuations [5] (squares with the error bars containing both statistical and systematic errors) and HRG baseline result (black dotted line) are also shown for comparison

Locations of the QCD critical point in the (μ_B, T)-plane considered in this work. These locations in the QCD phase diagram are shown in Fig. 2

CP_i	μ_{cp} [MeV]	T_{cp} [MeV]
1	390	149
2	420	141
3	450	134

cality in the C_2/C_1 ratio even for larger values of g (see the blue curves in Fig. 3). The refined model results for the C_2/C_1 ratio agree with the experimental data from the STAR Collaboration [5]. On the other hand, the original model would require an exceptionally small coupling strength in order to capture the experimentally observed behavior.

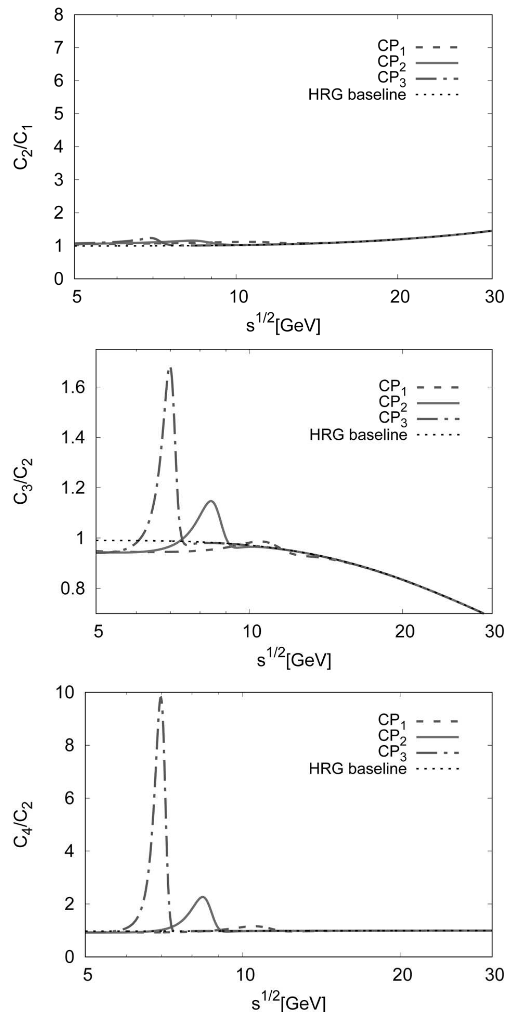

Fig. 4. Ratios of net-proton number cumulants calculated in the refined model [11] for the fixed coupling $g = 5$ and for different locations of the QCD critical point (listed in Table)

The net-proton cumulant ratios obtained in the refined model for different locations of the critical point (as listed in Table) and with a fixed value of the coupling, $g = 5$, are shown in Fig. 4. We find that a non-monotonic behavior of the cumulant ratios becomes more pronounced, when the critical point is closer to the freeze-out line. Moreover, the deviation from the non-critical HRG baseline becomes larger for higher-order cumulant ratios.

Finally, Fig. 5 shows the coupling strength dependence of the net-proton number cumulant ratios ob-

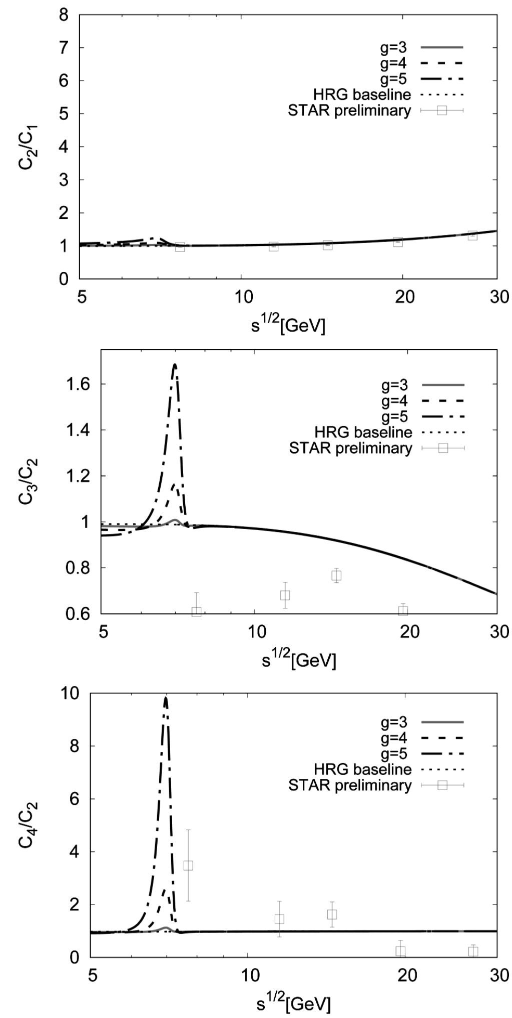

Fig. 5. Ratios of net-proton number cumulants calculated in the refined model [11] with CP_3 and for the coupling strengths, $g = 3$, 4 and 5 (orange solid, green long-dashed, and red dash-dotted lines, respectively). The preliminary STAR data on the net-proton number fluctuations [5] (squares with the error bars containing both statistical and systematic errors) and HRG baseline results (black dotted lines) are also shown for comparison

tained for CP_3. We find a strong g dependence of all ratios. This is expected, since, in our refined model, the n-th cumulant scales as g^{2n}, according to Eqs. (7) and (11)–(13). When our model results are compared to the STAR data [5], we find a qualitative agreement with the C_2/C_1 and C_4/C_2 ratios. On the other hand, the C_3/C_2 ratio does not follow the systematics seen in the data, i.e., our model results overshoot the HRG baseline, while the data stay below.

Our results suggest that the appropriate choice of model parameters, as well as the location of the QCD critical point, allows us to describe some of the experimentally observed cumulant ratios. Especially, the smooth dependence of C_2/C_1 and the strong increase of C_4/C_2 at low beam energies, $\sqrt{s} < 20$ GeV, seen by the STAR Collaboration, suggest that the QCD critical point may be located close to the freeze-out curve. However, in this case, the C_3/C_2 ratio should increase beyond the non-critical baseline, which is not seen in the experimental data. Therefore, it seems unlikely that the QCD critical point is close to the freeze-out curve. This conclusion requires, however, additional theoretical and experimental justifications due to uncertainties in the model parameters as well as in the experimental data.

4. Conclusions

We have presented the ratios of net-proton number cumulants obtained within an effective model in which the coupling between (anti)protons and critical mode fluctuations is introduced by connecting the particle masses to the order parameter. We have modified the existing approach [10] to account for the correct scaling properties of the baryon number susceptibility, as dictated by the universality hypothesis.

Model results were compared with the recent experimental data on net-proton number fluctuations from the STAR Collaboration. We find a substantial reduction of the signal coming from the presence of the QCD critical point in the C_2/C_1 ratio which stays in agreement with the experimental data. Moreover, we find that the model discussed in the present work allows us to describe some of the experimentally observed features in the net-proton number cumulant ratios. Particularly, the smooth dependence of C_2/C_1 and an increase in C_4/C_2 at lower beam energies ($\sqrt{s} < 20$ GeV) suggest that the critical point may be located close to the freeze-out curve. However, the experimentally observed C_3/C_2 ratio does not follow the behavior expected from such a scenario.

Therefore, it seems unlikely that the QCD critical point is located close to the phenomenological freeze-out curve. However, because of uncertainties on both theoretical and experimental sides, this statement requires a further investigation.

M.S. and M.B. acknowledge the support of the Polish National Science Center (NCN) under grant Po-

lonez UMO-2016/21/P/ST2/04035. M.B. was partly supported by the program "Etoiles montantes en Pays de la Loire 2017". This work is partly supported by the Polish National Science Center (NCN) under Maestro grant No. DEC-2013/10/A/ST2/00106 and Opus grant No. 2018/31/B/ST2/01663. K.R. also acknowledges the partial support of the Polish Ministry of Science and Higher Education. We thank F. Geurts and J. Thäder for providing the preliminary STAR data [5] shown in Figs. 3 and 5.

1. M.A. Stephanov, K. Rajagopal, E.V. Shuryak. Signatures of the tricritical point in QCD. *Phys. Rev. Lett.* **81**, 4816 (1998).
2. M.A. Stephanov, K. Rajagopal, E.V. Shuryak. Event-by-event fluctuations in heavy ion collisions and the QCD critical point. *Phys. Rev. D* **60**, 114028 (1999).
3. X. Luo, [STAR Collaboration]. Energy dependence of moments of net-proton and net-charge multiplicity distributions at STAR. *PoS CPOD* **2014**, 019 (2015).
4. X. Luo. Exploring the QCD phase structure with beam energy scan in heavy-ion collisions. *Nucl. Phys. A* **956**, 75 (2016).
5. J. Thäder [STAR Collaboration]. Higher moments of net-particle multiplicity distributions. *Nucl. Phys. A* **956**, 320 (2016).
6. G.A. Almasi, B. Friman, K. Redlich. Baryon number fluctuations in chiral effective models and their phenomenological implications. *Phys. Rev. D* **96**, 014027 (2017).
7. F. Karsch. Lattice QCD results on cumulant ratios at freeze-out. *J. Phys. Conf. Ser.* **779**, 012015 (2017).
8. A. Bzdak, V. Koch. Net-baryon multiplicity distribution consistent with lattice QCD. *Phys. Rev. C* **99**, 024913 (2019).
9. V. Koch, A. Bzdak. Fluctuations and the QCD phase diagram. *Acta Phys. Polon. B* **47**, 1867 (2016).
10. M. Bluhm, M. Nahrgang, S.A. Bass, T. Schäfer. Impact of resonance decays on critical point signals in net-proton fluctuations. *Eur. Phys. J. C* **77**, 210 (2017).
11. M. Szymański, M. Bluhm, K. Redlich, C. Sasaki. Net-proton number fluctuations in the presence of the QCD critical point. *arXiv*:1905.00667 [nucl-th].
12. C. Sasaki, B. Friman, K. Redlich. Quark number fluctuations in a chiral model at finite baryon chemical potential. *Phys. Rev. D* **75**, 054026 (2007).
13. C. Sasaki, B. Friman, K. Redlich. Chiral phase transition in the presence of spinodal decomposition. *Phys. Rev. D* **77**, 034024 (2008).
14. J. Zinn-Justin. *Quantum Field Theory and Critical Phenomena* (Clarendon Press, 2002).
15. A. Andronic, P. Braun-Munzinger, K. Redlich, J. Stachel. Decoding the phase structure of QCD via particle production at high energy. *Nature* **561**, 321 (2018).
16. F. Wilczek. Application of the renormalization group to a second-order QCD phase transition. *Int. J. Mod. Phys. A* **07**, 3911 (1992).
17. A.M. Halasz, A.D. Jackson, R.E. Shrock, M.A. Stephanov, J.J.M. Verbaarschot. Phase diagram of QCD. *Phys. Rev. D* **58**, 096007 (1998).
18. H.-T. Ding, F. Karsch, S. Mukherjee. Thermodynamics of strong-interaction matter from Lattice QCD. *Int. J. Mod. Phys. E* **24**, 1530007 (2015).
19. Y. Hatta, T. Ikeda. Universality, the QCD critical/tricritical point and the quark number susceptibility. *Phys. Rev. D* **67**, 014028 (2003).
20. S. Mukherjee, R. Venugopalan, Y. Yin. Real time evolution of non-Gaussian cumulants in the QCD critical regime. *Phys. Rev. C* **92**, 034912 (2015).
21. C. Nonaka, M. Asakawa. Hydrodynamical evolution near the QCD critical end point. *Phys. Rev. C* **71**, 044904 (2005).
22. R. Guida, J. Zinn-Justin. 3-D Ising model: The scaling equation of state. *Nucl. Phys. B* **489**, 626 (1997).
23. B. Abelev *et al.*, [ALICE Collaboration]. Centrality dependence of π, K, p production in Pb–Pb collisions at $\sqrt{s_{NN}} = 2.76$ TeV. *Phys. Rev. C* **88**, 044910 (2013).
24. B.B. Abelev *et al.*, [ALICE Collaboration]. K^0_S and Λ production in Pb–Pb collisions at $\sqrt{s_{NN}} = 2.76$ TeV. *Phys. Rev. Lett.* **111**, 222301 (2013).
25. B.B. Abelev *et al.*, [ALICE Collaboration]. Multi-strange baryon production at mid-rapidity in Pb–Pb collisions at $\sqrt{s_{NN}} = 2.76$ TeV. *Phys. Lett. B* **728**, 216 (2014), Erratum: [*Phys. Lett. B* **734**, 409 (2014)].
26. B.B. Abelev *et al.*, [ALICE Collaboration]. $K^*(892)^0$ and ffl(1020) production in Pb–Pb collisions at $\sqrt{sNN} =$ $= 2.76$ TeV. *Phys. Rev. C* **91**, 024609 (2015).
27. J. Adam *et al.*, [ALICE Collaboration]. ${}^3_\Lambda\mathrm{H}$ and ${}^3_{\overline{\Lambda}}\overline{\mathrm{H}}$ production in Pb–Pb collisions at $\sqrt{s_{\mathrm{NN}}} = 2.76$ TeV. *Phys. Lett. B* **754**, 360 (2016).
28. J. Adam *et al.*, [ALICE Collaboration]. Production of light nuclei and anti-nuclei in pp and Pb–Pb collisions at energies available at the CERN large hadron collider. *Phys. Rev. C* **93**, 024917 (2016).

Received 18.07.19

М. Шиманскі, М. Блум, К. Редліх, К. Сасакі

ПОШУКИ КРИТИЧНОЇ ТОЧКИ
КХД З ФЛУКТУАЦІЄЮ ЧИСЛА ПРОТОНІВ

Р е з ю м е

Флуктуації повного числа протонів можна вимірювати експериментально, отримуючи таким чином важливу інформацію про речовину, що народжується під час зіткнень релятивістських іонів. Зокрема вона може містити інформацію про критичну точку КХД. В даній роботі ми обговорюємо залежність відношень перших чотирьох кумулянтів числа протонів від енергії струменя частинок. Ці величини розраховані за допомогою феноменологічної моделі, в якій флуктуації з критичною модою пов'язані з протонами та антипротонами. Наша модель якісно відтворює як монотонну поведінку відношення найнижчих порядків, так і немонотонну поведінку відношень високих порядків, як це спостерігається в результатах колаборації STAR. Ми обговорюємо також залежність наших результатів від сили зв'язку і місцезнаходження критичної точки.

https://doi.org/10.15407/ujpe64.8.772

M. TRZEBIŃSKI

Institute of Nuclear Physics Polish Academy of Sciences
(152, Radzikowskiego Str., 31-342 Cracow, Poland; e-mail: maciej.trzebinski@ifj.edu.pl)

DIFFRACTIVE PHYSICS AT THE LHC

Diffractive processes possible to be measured at the LHC are listed and briefly discussed. This includes soft (elastic scattering, exclusive meson pair production, diffractive bremsstrahlung) and hard (single and double Pomeron exchange jets, γ +jet, W/Z, jet-gap-jet, exclusive jets) processes as well as Beyond Standard Model phenomena (anomalous gauge couplings, magnetic monopoles).

K e y w o r d s: LHC, AFP, ALFA, TOTEM, pomeron, diffraction, exclusive processes, beyond standard model.

1. Introduction

About a half of collisions at the LHC are of diffractive nature. In such events, a rapidity gap [1] between the centrally produced system and scattered protons is present. Due to the exchange of a colorless object – photon (electromagnetic) or Pomeron (strong interaction) – one or both outgoing protons may stay intact.

Studies of diffractive events are an important part of the physics program of the LHC experiments. The diffractive production could be recognized by the search for a rapidity gap in the forward direction or by the measurement of scattered protons. The first method is historically a standard one for the diffractive pattern recognition. It uses the usual detector infrastructure: *i.e.* tracker and forward calorimeters. Unfortunately, the rapidity gap may be destroyed by *e.g.* particles coming from the pile-up – parallel, independent collisions happening in the same bunch crossing. In addition, the gap may be outside the acceptance of a detector. In the second method, protons are directly measured. This solves the problems of gap recognition in the very forward region and a presence of a pile-up. However, since protons are scattered at small angles (few hundreds microradians), additional devices called “forward detectors” are needed to be installed.

At the LHC, the so-called Roman pot technology is used. In ATLAS [1], two systems of such detectors were installed: ALFA [2, 3] and AFP [4]. At the LHC interaction point 5, Roman pots are used by CMS [5] and TOTEM [6,7] groups. Since protons are scattered at small angles, there are several LHC elements (*i.e.*, magnets and collimators) between them and the IP which influence their trajectory. The settings of these elements, commonly called machine optics, determine the acceptance of forward detectors. The detailed description of the properties of optics sets used at the LHC can be found in [8].

In both experiments, a large community works on both phenomenological and experimental aspects of diffraction. In this paper, the diffractive processes possible to be measured will be briefly described.

2. Soft Diffraction

Collisions at hadron accelerators are dominated by soft processes. The absence of a hard scale in these events prevents one from using perturbation theory. Instead, in order to calculate the properties of the produced particles such as the energy or angular distributions, one has to use approximative methods.

The elastic scattering process has the simplest signature that can be imagined: two protons exchange their momentum and are scattered at small angles. At the LHC, the measurement of protons scattered elastically requires a special settings commonly named the high-β^* optics. Properties of the elastic scattering were measured by both ATLAS and TOTEM Collaborations for center-of-mass energies of 7 [9, 10], 8 [11, 12], and 13 TeV [13].

Another soft process is a diffractive bremsstrahlung. It is typically of electromagnetic nature. However, high-energy photons can be radiated in the elastic

[1] A space in the rapidity devoid of particles.

proton-proton scattering as postulated in [14]. This idea was further extended in [15] by introducing the proton form-factor into the calculations and by considering other mechanisms such as a virtual photon re-scattering. The feasibility studies presented in [16] suggest that such measurement should be possible at the LHC. The requirements are high-β^* optics, proton measurement in ALFA/TOTEM and photon measurement in Zero Degree Calorimeter.

Last of the processes described in this section is the exclusive meson pair production, a $2 \to 4$ process in which two colliding protons result in two charged mesons and two scattered protons present in the final state. In the non-resonant pion pair production (also called continuum), a Pomeron is "emitted" from each proton resulting in four particles present in the final state: scattered protons and (central) pions [17]. The object exchanged in the t-channel is an off-shell pion. Exclusive pions can also be produced via resonances, *e.g.*, f_0 [18]. Although the dominant diagram of the exclusive pion pair continuum production is a Pomeron-induced one, the production of a photon-induced continuum is also possible. On the top of that, a resonant ρ^0 photo-production process may occur [19].

Recently, the models of elastic scattering, exclusive meson production, and diffractive bremsstrahlung were added to the GenEx Monte-Carlo generator [20–22].

3. Hard Diffraction

Hard diffractive events can be divided into the single diffractive and double Pomeron exchange classes. In the first case, one proton stays intact, whereas the other one dissociates. In the second case, both interacting protons "survive". In addition, the sub-case of the exclusive production can be considered – a processes in which all final-state particles can be measured by ATLAS and CMS/TOTEM detectors.

Depending on the momentum lost during the interaction, the emitting proton may remain intact and be detected by a forward proton detector. However, it may happen that the soft interactions between the protons or the proton and the final-state particles can destroy the diffractive signature. Such effect is called the gap survival probability. For the LHC energies, the gap survival is estimated to be of about 0.03–0.1 depending on the process [23].

From all hard events, the diffractive jets have the highest cross-section [2]. By studying the single diffractive and double Pomeron exchange jet productions, a Pomeron universality between *ep* and *pp* colliders can be probed. As was discussed in [24], the tagging of diffractive protons will allow the QCD evolution of gluon and quark densities in the Pomeron to be tested and compared to the ones extracted from the HERA measurements. Another interesting measurement is the estimation of the gap survival probability. A good experimental precision will allow for comparison to theoretical predictions and differential measurements of the dependence of the survival factor on, *e.g.*, the mass of the central system.

An interesting class of jet events is one with a rapidity gap is present between jets – the so-called jet-gap-jet production. In such events, an object exchanged in the t-channel is a color singlet and carries a large momentum transfer. When the gap size is sufficiently large, the perturbative QCD description of jet-gap-jet events is usually performed in terms of the Balitsky–Fadin–Kuraev–Lipatov (BFKL) model [27–29]. The jet-gap-jet topology can be produced also in the single diffractive and double Pomeron exchange processes. Properties of such events were never measured – the determination of the cross-section should enable the tests of the BFKL model [30].

Jets produced in the processes described above are typically of gluonic nature. In order to study the quark composition of a Pomeron, diffractive photon + + jet productions should be considered. In such cases, one Pomeron emits a gluon, whereas the other one delivers a quark. A measurement of the photon + jet production in the DPE mode can be used to test the Pomeron universality between HERA and LHC. Moreover, HERA was not sensitive to the difference between the quark components in a Pomeron. This means that the fits assumed the equal amounts of light quarks, $u = d = s = \bar{u} = \bar{d} = \bar{s}$. The LHC data should allow more precise measurements [25].

Another interesting process is the diffractive production of W and Z bosons. Similarly to γ + jet, it is sensitive to the quark component, since many of the observed production modes can originate from a quark fusion. As was discussed in [26], by measuring the ratio of the W production cross-section to the Z one, the d/u and s/u quark density values in the

[2] Depends on the jet transverse momentum.

Pomeron can be estimated. In addition, a study of the DPE W asymmetry can be performed [26]. Such measurement can be used to validate theoretical models.

The feasibility studies of all measurements described above in this section are described in Ref. [31].

Diffractive jets can be produced in the exclusive mode. Usually, it is assumed that one gluon is hard, whereas the other one is soft [32, 33]. The role of the soft gluon is to provide the color screening in order to keep the net color exchange between protons equal to zero. The exclusivity of the event is assured via the Sudakov form factor [34], which prohibits an additional radiation of gluons in higher orders of perturbative QCD. In [35], a discussion about the feasibility of such measurement in the case of the ATLAS detector and both tagged protons is held. A semiexclusive measurement, when one of the protons is tagged, is discussed in [36, 37].

4. Anomalous Couplings and Beyond Standard Model Physics

The presence of an intact proton can be used to search for a new phenomena. The Beyond Standard Model (BSM) processes are usually expected to be on a high mass, which makes them visible in forward detectors.

One example of the BSM physics is anomalous couplings: $\gamma\gamma WW$, $\gamma\gamma ZZ$, $\gamma\gamma\gamma\gamma$ or $WW\gamma$. As was shown in [38, 39], the possibility of the forward proton tagging provides a much cleaner experimental environment which improves the discovery potential. Authors expect that, with 30–300 fb^{-1}, the data collected with the ATLAS detector with information about scattered protons tagged in AFP should result in a gain in the sensitivity of about two orders of magnitude over a standard ATLAS analysis.

Finally, the presence of protons with a high energy loss and a lack of energy registered in the central detector might be a sign of a new physics, for example, magnetic monopoles [31].

5. Conclusions

The Large Hadron Collider gives possibility to study the properties of diffractive physics in a new kinematic domain. Diffractive events can be identified in all major LHC experiments using the rapidity gap recognition method. In addition, as ATLAS and CMS/TOTEM are equipped with the set of forward detectors, it is possible to use the proton tagging technique.

In this paper, a brief summary of the diffractive processes measurable at the LHC was done. Using special settings of the LHC – high-β^* optics – the processes of elastic scattering, exclusive meson pair production, and diffractive bremsstrahlung can be studied. Hard diffractive events, due to smaller cross-sections, should be measured with the standard LHC optics. The studies of properties of the diffractive di-jet, photon+jets, and the W/Z boson production processes should lead *i.a.* to the determination of a gap survival probability and a Pomeron structure. Studies of diffractive jet-gap-jet events should bring more insight into the description of the Pomeron, *i.a.* to verify predictions of the BFKL model. On the top of that, the measurement of the jet production in the exclusive (double proton tag) and semiexclusive (single tag) modes can be performed. Finally, the additional information about a scattered proton may improve the searches for a New Physics including such phenomena as anomalous gauge couplings or magnetic monopoles.

Development of the GenEx Monte Carlo generator was partially supported by the Polish National Science Center grant: UMO-2015/17/D/ST2/03530.

1. ATLAS Collaboration. The ATLAS experiment at the CERN Large Hadron Collider. *JINST* **3**, S08003 (2008).
2. ATLAS Luminosity and Forward Physics Community. *Technical Design Report*, CERN-LHCC-2008-004.
3. S. Abdel Khalek *et al.* The ALFA Roman Pot Detectors of ATLAS. *JINST* **11**, P11013 (2016).
4. ATLAS Collaboration. *Technical Design Report for the ATLAS Forward Proton Detector*, CERN-LHCC-2015-009, ATLAS-TDR-024.
5. CMS Collaboration. The CMS experiment at the CERN large hadron collider. *JINST* **3**, S08004 (2008).
6. TOTEM Collaboration. *Technical Design Report* CERN-LHCC-2004-002.
7. TOTEM Collaboration. *TOTEM Upgrade Proposal* CERN-LHCC-2013-009.
8. M. Trzebinski. Machine optics studies for the LHC measurements. In *Proceedings of XXXIV-th IEEE-SPIE Joint Symposium*, SPIE 0277-786X, vol. 9290, (2014), p. 26.
9. ATLAS Collaboration. Measurement of the total cross section from elastic scattering in pp collisions at $\sqrt{s} = 7$ TeV with the ATLAS detector. *Nucl. Phys. B* **889**, 486 (2014).
10. TOTEM Collaboration. Proton-proton elastic scattering at the LHC energy of $\sqrt{s} = 7$ TeV. *EPL* **95**, (2011).
11. ATLAS Collaboration. Measurement of the total cross section from elastic scattering in pp collisions at $\sqrt{s} = 8$ TeV with the ATLAS detector. *Phys. Lett. B* **761**, 158 (2016).

12. TOTEM Collaboration. Measurement of elastic pp scattering at $\sqrt{s} = 8$ TeV in the coulomb-nuclear interference region – determination of the ρ parameter and the total cross-section. *Eur. Phys. J. C* **76**, 661 (2016).
13. TOTEM Collaboration. First measurement of elastic, inelastic and total cross-section at $\sqrt{s} = 13$ TeV by TOTEM and overview of cross-section data at LHC energies. *Eur. Phys. J. C* **79**, 103 (2019).
14. V.A. Khoze, J.W. Lamsa, R. Orava, M.G. Ryskin. Forward physics at the LHC: Detecting elastic *pp* scattering by radiative photons. *JINST* **6**, P01005 (2011).
15. P. Lebiedowicz, A. Szczurek. Exclusive diffractive photon bremsstrahlung at the LHC. *Phys. Rev. D* **87**, 114013 (2013).
16. J.J. Chwastowski, S. Czekierda, R. Staszewski, M. Trzebinski. Diffractive bremsstrahlung at high-β^* LHC case study. *Eur. Phys. J. C* **77**, 216 (2017).
17. P. Lebiedowicz, O. Nachtmann, A. Szczurek. Central exclusive diffractive production of $\pi^+\pi^-$ continuum, scalar and tensor resonances in *pp* and *pp* scattering within tensor pomeron approach. *Phys. Rev. D* **93**, 054015 (2016).
18. P. Lebiedowicz, O. Nachtmann, A. Szczurek. Exclusive central diffractive production of scalar and pseudoscalar mesons tensorial vs. vectorial pomeron. *Annals Phys.* **344**, 301 (2014).
19. P. Lebiedowicz, O. Nachtmann, A. Szczurek. The ρ^0 and Drell–Soding contributions to central exclusive production of $\pi^+\pi^-$ pairs in proton-proton collisions at high energies. *Phys. Rev. D* **91**, 074023 (2015).
20. R.A. Kycia, J. Chwastowski, R. Staszewski, J. Turnau. GenEx: A simple generator structure for exclusive processes in high energy collisions. *Commun. Comput. Phys.* **24**, 860 (2018).
21. P. Erland, R. Staszewski, M. Trzebinski, R. Kycia. Elastic hadron scattering in various Pomeron models. *Acta Phys. Pol. B* **48**, 981 (2017).
22. R.A. Kycia, J. Turnau, J.J. Chwastowski, R. Staszewski, M. Trzebinski. The adaptive Monte Carlo toolbox for phase space integration and generation. *Commun. Comput. Phys.* **25**, 1547 (2019).
23. A.B. Kaidalov, V.A. Khoze, A.D. Martin, M.G. Ryskin. Probabilities of rapidity gaps in high energy interactions. *Eur. Phys. J. C* **21**, 521 (2001).
24. C. Royon. Forward physics with tagged protons at the LHC: QCD and anomalous couplings. In *Proceedings of the Low x 2013 workshop* (Weizmann Institute of Sci., 2013).
25. C. Marquet, C. Royon, M. Saimpert, D. Werder. Probing the Pomeron structure using dijets and γ+jet events at the LHC. *Phys.Rev. D* **88**, 074029 (2013).
26. K. Golec-Biernat, C. Royon, L. Schoeffel, R. Staszewski. Electroweak vector boson production at the LHC as a probe of mechanisms of diffraction. *Phys. Rev. D* **84**, 114006 (2011).
27. L.N. Lipatov. Reggeization of the vector meson and the vacuum singularity in non-Abelian Gauge theories. *Sov. J. Nucl. Phys.* **23**, 338 (1976).
28. E.A Kuraev, L.N. Lipatov, V.S. Fadin. The pomeranchuk singularity in non-Abelian Gauge theories. *Sov. Phys. JETP* **45**, 199 (1977).
29. I.I. Balitsky, L.N. Lipatov. The Pomeranchuk singularity in quantum chromodynamics. *Sov. J. Nucl. Phys.* **28**, 822 (1978).
30. C. Marquet, C. Royon, M. Trzebinski, R. Zlebcik. Gaps between jets in double-Pomeron-exchange processes at the LHC. *Phys. Rev. D* **87**, 034010 (2013).
31. K. Akiba *et al. LHC Forward Physics*, SLAC-PUB-16364, DESY 15-167.
32. V.A. Khoze, A.D. Martin, M.G. Ryskin. Central jet production as a probe of the perturbative formalism for exclusive diffraction. *Eur. Phys. J. C* **48**, 467 (2006).
33. M.G. Albrow, T.D. Coughlin, J.R. Forshaw. Central exclusive particle production at high energy hadron colliders. *Prog. Part. Nucl. Phys.* **65**, 149 (2010).
34. V.V. Sudakov. Vertex parts at very high energies in quantum electrodynamics. *Sov. Phys. J. E. T. P.* **30**, 65 (1956).
35. ATLAS Collaboration. *Exclusive jet production with forward proton tagging feasibility studies for the AFP project*, ATL-PHYS-PUB-2015-003.
36. M. Trzebinski, R. Staszewski, J. Chwastowski. On the possibility of measuring the single-tagged exclusive jets at the LHC. *Eur. Phys. J. C* **75**, 320 (2015).
37. M. Trzebinski. Exclusive jet measurement in special LHC runs – feasibility studies. *Acta Phys. Pol. B* **47**, 1745 (2016).
38. E. Chapon *et al.* Anomalous quartic $\gamma\gamma WW$, $\gamma\gamma ZZ$, and trilinear $WW\gamma$ couplings in two-photon processes at high luminosity at the LHC. *Phys. Rev. D* **81**, 074003 (2010).
39. S. Fichet *et al.* Probing new physics in diphoton production with proton tagging at the Large Hadron Collider. *Phys. Rev. D* **89**, 114004 (2014).

Received 08.07.19

М. Тшебіньскі

ДИФРАКЦІЯ НА LHC

Р е з ю м е

Перераховано і коротко обговорено дифракційні процеси, які можна вимірювати на LHC. Список включає м'які (пружне розсіяння, ексклюзивне продукування мезонних пар, дифракційне гальмівне випромінювання) та жорсткі (струмені з обміном одного або двох померонів, фотон + струмінь, W/Z, струмінь-розрив-струмінь, ексклюзивні струмені) процеси, а також явища поза рамок Стандартної Моделі (аномальні калібрувальні зв'язки, магнітні монополі).

https://doi.org/10.15407/ujpe64.8.776

TO THE 110th ANNIVERSARY OF ACADEMICIAN M.M. BOGOLYUBOV BIRTHDAY

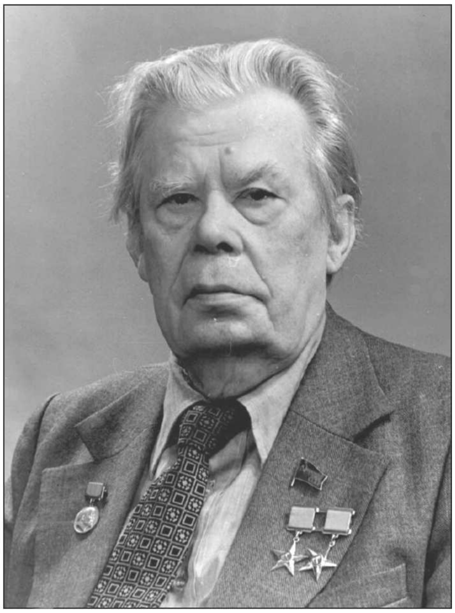

The 110th anniversary of Mykola Bogolyubov provides a good opportunity to recollect the scientific achievements of this brilliant scientist and to discuss once again his invaluable contribution to the development of various fields of theoretical and mathematical physics – nonlinear mechanics, nuclear physics, quantum field theory, high-energy physics, condensed matter physics, etc. The departments, research groups, and even whole institutes founded by him continue to work nowadays. The Bogolyubov scientific school, which has grown on his ideas, is successfully developing already in its fourth generation.

Mykola Bogolyubov was born on August 21, 1909 in Nizhny Novgorod. That very year the Bogolyubov family moved from Nizhny Novgorod to Nizhyn, Chernihiv province, where Mykola's father – by that time already known theologist Mykola Mykhailovych Bogolyubov – got the position of Professor of scripture at the Prince Bezborodko Historical and Philological Institute. It should be noted that this institute had a long educational traditions and a high reputation. Mykola Hohol, Yevhen Hrebinka, Leonid Hlibov, and many other outstanding figures had been its students. Four years later, Mykola Mykhailovych became a professor of theology at St. Vladimir' University and the family moved to Kyiv.

In 1917, when Bogolyubov was eight, he entered the preparatory class of the First Alexander Classic Kyiv Gymnasium, but he studied there for less than two years. In 1920, Soviet power was finally established in Kyiv, the Department of Theology was closed, and Mykola's father was forced to take a parish in the village of Velyka Krucha, Poltava province. Mykola began to attend the Velykokruchans'ka seven-year school and graduated in 1922. When recollecting this school, Bogolyubov said that it's pedagogical team would be honor to the best schools of the capital. By the way, the certificate on the graduation of the seven-year school was the only document on education that Bogolyubov received in his life, and the words about his officially received education are "I became a scientist in Velika Krycha". Due to school and home education, at the age of 13 Mykola Bogolyubov had knowledge at the graduate level of the faculty of physics and mathematics of the university.

In 1922, the Bogolyubov family returned to Kyiv. Bogolyubov's father asked the famous mathematician Academician Dmytro Grave for advise concerning the further education of his elder son. Professor Grave, after acquaintance with young Bogolyubov, told his father that attending lectures at any university would make no sense for the young man, but advised to continue education individually. Since then Bogolyubov began to participate in the seminars of

Academician Grave. In the spring of 1923 young Bogolyubov met his teacher, mentor, and future colleague Academician Mykola Krylov, who began to give special classes in mathematics and mechanics for Bogolyubov. When Mykola Bogolyubov was 15 years old, he published his first scientific paper, and on June 1, 1925, a special decree was adopted by the Ukrhlavnauka, which stated: "In view of phenomenal gift for mathematics, to consider M. Bogolyubov as a postgraduate student of the Department of Mathematics since July 18, 1925. Add him to the payroll list".

In 1930, Bogolyubov received his first recognition – he got the Award of the Academy of Sciences of Bologna (Italy). The same year, namely, on April 6, 1930, at the General Meeting of the Department of Physics and Mathematics of the All-Ukrainian Academy of Sciences (VUAN), on the recommendation of D. Grave and M. Krylov, the degree of Doctor of Sciences was awarded to Bogolyubov without thesis. Academic title of Professor on the Department of Theory of Functions was conferred on Bogolyubov in 1936 after he had began teaching at Kyiv University. Later, in 1939, M. Bogolyubov was elected a corresponding member, in 1948 – Academician of the Academy of Sciences of the Ukrainian SSR. In 1947, he became a Corresponding Member of the Academy of Sciences of the USSR, and in 1953 he became its full member.

The topmost results of Bogolyubov in 1932–37 include the foundation, together with his teacher, of a new section of mathematical physics – the theory of nonlinear oscillations, that later would be called nonlinear mechanics. In particular, they have developed new methods for integrating nonlinear differential equations describing vibration processes. These results have been summarized in many joint monographs by Bogolyubov and Krylov of this period. Among them are "On Some Formal Decompositions at Nonlinear Mechanics", "New Methods of Nonlinear Mechanics", "Application of Methods of Nonlinear Mechanics to the Theory of Stationary Oscillations", "Introduction to Nonlinear Mechanics". In 1955, a fundamental monograph by Bogolyubov and Mitropolsky "Asymptotic Methods in the Theory of Nonlinear Oscillations" was published.

In 1935–1936, Bogolyubov represents the Department of Mathematical Physics of VUAN abroad. He gives lectures on the theory of nonlinear oscillations at Henri Poincaré Institute in France, Belgian Mathematical Society, and Belgian Research Institute. In 1940, after the unification of the Northern Bukovyna with Ukraine Bogolyubov participated in the formation of the mathematical department at the Physics and Mathematics Faculty of Chernivtsi University.

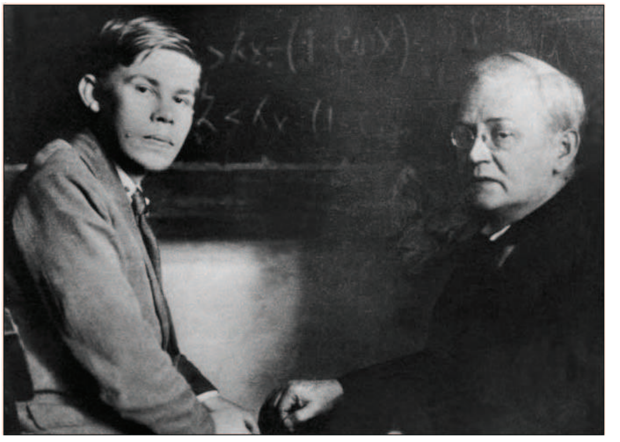

Fig. 1. M.M. Bogolyubov and Academician M.M. Krylov

Fig. 2. Opening of a new building of the Institute for Theoretical Physics

In summer of 1941, M. Bogolyubov was evacuated to Ufa and then sent to Moscow. At this time, as Mykola Mykolayovych writes in his autobiography, he, while continuing theoretical studies in nonlinear mechanics, was mainly concerned with defense topics. Bogolyubov returned to Kyiv in early 1944.

One of the most fruitful periods of creativity of Bogolyubov is associated with Kyiv. Just here

Fig. 3. Academicians O.S. Davydov, O.G. Sitenko, and M.M. Bogolyubov after the opening of a new building of the Institute (1970)

Fig. 4. M.M. Bogolyubov and his disciples, Academicians O.S. Parasyuk (left) and Yu.O. Mytropol's'kyi (right)

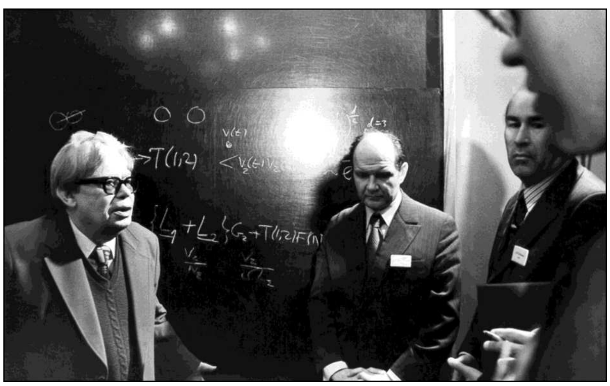

Fig. 5. M.M. Bogolyubov with Academicians I.R. Yukhnovskyi and D.Ya. Petryna

M. Bogolyubov initiated new fields of theoretical and mathematical physics, in particular, wrote his classical works on modern statistical theory. Particularly, in 1946, M. Bogolyubov published the world-famous book "Problems of the Dynamic Theory in Statistical Physics". The results given in this work have initiated a new stage in the progress of statistical mechanics after the achievements related to Maxwell, Boltzmann, Gibbs. Bogolyubov proposed a dynamic approach to the formulation of the kinetic theory based on the chain of equations for equilibrium and nonequilibrium many-particle distribution functions – the chain of Bogolyubov–Borne–Green–Kirkwood–Yvon equations (it should be noted that Bogolyubov gave the most general and mathematically rigorous chain derivation). Using a small-scale expansion of this chain and applying the assumption of the existence of a hierarchy of time scales (known in the world literature as the hierarchy of Bogolyubov's characteristic times), Bogolyubov obtained closed kinetic equations for one-particle distribution functions not only for neutral gas but also for plasma. The latter equation today is called the Bogolyubov–Balescu–Lennard kinetic equation. Instead of Boltzmann's hypothesis of molecular chaos, he proposed the principle of complete weakening of initial correlations (Bogolyubov's principle), which made it possible to calculate collision integrals on the basis of a reduced chain of equations for distribution functions. To describe the next stage in the evolution of the system, Bogolyubov obtained the equations of hydrodynamics.

1947 – another brilliant result: the microscopic theory of superfluidity. The article in which this theory was formulated has remained, for many years, one of the most cited works of our time. In this work, Bogolyubov for the first time applied a new mathematical technique known today as Bogolyubov's canonical transformation. On the example of a weakly idealized Bose gas, Bogolyubov explained from the first principles the formation of the excitation spectrum of a superfluid helium and thus the nature of this macroscopic quantum phenomenon. He later summarized his mathematical formalism for the foundation of a microscopic theory of superconductivity. Bogolyubov perfectly studied the methods of secondary quantization for quantum statistical systems. His "Lectures on Quantum Statistics", published in 1949, could be a good illustration of effective application of this method to quantum statistics. This contributed to his interest in the problems of quantum field theory, where he also managed to obtain a number of outstanding results. A brilliant example is the development of a method for eliminating divergences in the quantum field theory based on the use of the subtraction procedure, and proving one of the central theorems of the renormalization theory, known as the Bogolyubov–Parasyuk theorem. The discovery of the general form of the subtraction procedure and its justification were of great importance for the further development of high-energy physics. It made it possible, in particular, to prove the renormality of a unified theory of electroweak interactions, as well as of supersymmetric theories, to obtain operator expansions at short distances, to study phase transitions, and so on.

In 1951–1953, Mykola Bogolyubov worked at the top-secret object of the Soviet Union – "Arzamas-16" (Sarov), as well as at the Institute of Atomic Energy (now "Kurchatov Institute" in Moscow), where, in parallel with the mathematical studies of the problems related to the creation of hydrogen weapons, he worked on the problems concerning the magnetic fusion reactor. It should be noted that the results obtained then by Bogolyubov in the field of nuclear fusion have not been published, since they were a part of secret reports. Only after removing the mark of secrecy from these results it turned out to be that a considerable part of the results on the kinetic plasma theory had been obtained by Bogolyubov before they were obtained and published independently by other authors in open literature.

From 1948, M. Bogolyubov along with his work in Kyiv began to head the Department of Mathematical Physics at the Institute of Chemical Physics in Moscow, and from 1949 – also the Department of Theoretical Physics of the Steklov Mathematical Institute of the Academy of Sciences of the USSR. In 1956, Mykola Bogolyubov became the Director of the Laboratory of Theoretical Physics of the Joint Institute for Nuclear Research (JINR) in Dubna. In January 1965, at the session of the plenipotentiaries of the governments of the member states of the Institute, Mykola Bogolyubov was elected the Director of JINR, which he has headed for over 20 years. Since 1957, Mykola Bogolyubov also headed the Laboratory of the Theory of Atomic Nuclei and Elementary Particles at the Institute of Physics of the Academy of Sciences of the Ukrainian SSR.

Among other results by Bogolyubov concerning the perturbation methods in the quantum field theory, one should also mention the method of renormalization group – the new general approach in theoretical physics, which has found application in various fields.

Mykola Bogolyubov is a founder of a new field of research in the quantum theory that was later called the axiomatic field theory. In particular, the proposed derivation of the dispersion relations has led to the development of a new mathematical approach to the analytic continuation of the generalized functions of many variables. For these studies in 1966, Mykola Bogolyubov was awarded the Danny Heinemann Award. In his welcome address, Professor R. Jost said: "You made an unforgettable impression on me. Most theorists at the time were disrespectful of mathematics, and logical deduction was "trampled". Only the romantic influence of genius could have value. And then you appeared, a person who knows both mathematics and physics and who is ready to solve complex problems that require their logical combination. It seems to me that this is a reflection of the national character of your great people".

In 1961, M. Bogolyubov introduced the fundamental concept of quasiaverages and thus, in fact, a new theory of phase transformations was created. The spread of these ideas to the physics of elementary particles was called spontaneous symmetry breaking – another fundamental result of Mykola Bogolyubov, which is important for quantum physics.

During the period of 1964–1966, Bogolyubov published important papers on the symmetry theory and quark models of elementary particles. One of the important results in this field is the introduction of the new quantum number for quarks, now known as color, proposed by him and his disciples A.N. Tavkhelidze and B.V. Struminskii for quarks. Now this parameter is known as color.

Bogolyubov's scientific activity revealed the unity of the mathematical structure of theories for different branches of physics. The follower of Bogolyubov Academician V. Vladimirov noted: "Combination of mathematics and physics in the works of M.M. Bogolyubov made it possible for him to contribute considerably to the development of theoretical physics and in fact to create the foundations of modern mathematical physics, which continues the traditions of Hilbert, Poincare, Einstein, Dirac".

Fig. 6. E.C.G. Sudarshan (USA), R.E. Marshak (USA), M.M. Bogolyubov, and V.P. Shelest at the Institute for Theoretical Physics during the XV International Conference on High Energy Physics (Kyiv, 1970)

Fig. 7. First International Conference on Plasma Theory (Kyiv, Institute for Theoretical Physics of the Academy of Sciences of the UkrSSR, 1971)

Mykola Bogolyubov had the talent of a great researcher and outstanding organizer of science. An example confirming his organizational skills is the foundation in 1966 of the Institute for Theoretical Physics that since 1993 is called by his name. It should be noted that the creation of an elite physical institute in Kyiv was an extremely difficult task. There were several reasons. These include the existence in the USSR of the Institute for Theoretical Physics of the USSR Academy of Sciences in Chornogolovka (now the Landau Institite for Theoretical Physics of RAS), and the inconsistency to the "general line", according to which the priority in the development of fundamental research belonged obviously not to Ukraine, and problems with the formation of highly skilled staff capable to perform competitive research. It was necessary to have the influence and weight of Mykola Bogolyubov to succeed. It was also important that the First Secretary of the Communist Party of Ukraine Petro Shelest and President of the Academy of Sciences of Ukrainian SSR Borys Paton gave him great help and assistance in this matter. As a result of their joint efforts, on January 5, 1966, the Council of Ministers of the Ukrainian SSR adopted a decree "On the Establishment of the Institute for Theoretical Physics of the Academy of Sciences of the Ukrainian SSR", and in 1970, during the Rochester Conference, a new building of the Institute was opened on the site chosen by Bogolyubov.

Everything related to the foundation of the Institute has been done with the direct participation of Bogolyubov – from the choice of the site for the institute building to staff appointments. He formulated the main fields of scientific activity of the Institute, namely: elementary particle theory, theory of nuclei and nuclear reactions, and statistical physics. Mykola Bogolyubov invited outstanding scientists to the Institute, including his talented students. Among the scientists with world names whom he invited were Academicians O. Davydov, A. Petrov, O. Sitenko, I. Yukhnovsky; students of Bogolyubov: A. Tavhelidze (later Academician of the Russian Academy of Sciences), Academicians of the NAS of Ukraine O. Parasyuk, D. Petryna, Corresponding Member of the Academy of Sciences of Ukraine V. Shelest and others. As a result, for the first seven years of the directorship of Mykola Bogolyubov, the Institute has become a powerful center of theoretical physics, well-known not only in Ukraine, but also far beyond its borders.

Bogolyubov paied much attention to the development of international cooperation, in particular the organization of international conferences such as Rochester Conference on high-energy physics and international conferences on plasma theory initiated by him together with O. Sitenko. These conferences proved to be so successful that they were called the "Kyiv Conferences on Plasma Theory" and were held under this name in many countries around the world, periodically returning to Kyiv in 1976, 1987, and 2006.

As already mentioned, the scientific fields formulated by Mykola Bogolyubov have determined the activities of the Institute for many years. Today its main activities are related to high-energy physics and astrophysics, nucleus theory, quantum field theory, symmetry theory, the theory of nonlinear phenomena in condensed matter and plasmas, as well as the kinetic theory of highly nonequilibrium processes. In fact, this corresponds to somewhat extended trends formulated by Bogolyubov. We can say that much of the research activities of the Institute are related to the application and development of the ideas of Mykola Bogolyubov. In particular, in the field of theoretical high-energy physics, this concerns the dynamic generation of masses, spontaneous symmetry breaking, quantum chromodynamics, and the application of symmetry theory in quantum field theory. The same concerns Bogolyubov's ideas in the kinetic theory. As noted above, Mykola Bogolyubov is one of the founders of the theory of many-particle systems. Previously, such theory was used to describe gases and plasma.

But Bogolyubov's methods have also proved to be efficient for describing much more complex systems, in particular for the study of dusty plasmas, i.e., a mixture of plasmas and solid particles. Creative inheritance of Bogolyubov is also used today to solve the problems of condensed matter physics. These include the description of high-temperature superconductivity, the phenomenon of Bose condensation in various systems, nonlinear phenomena in solids and liquids, transport processes in molecular systems, and the kinetics of electron transport in nanoobjects. Methods of quantum field theory are, in turn, widely used in the study of low-dimensional and so-called Dirac structures, as well as new materials.

Along with scientific research and organizational activities, Bogolyubov carried out impressive pedagogical work. In 1936–1941 and 1944–1949, he taught at Kyiv State University, in 1945–1948 he was Dean of the Faculty of Mechanics and Mathematics, where he founded and headed the Department of Mathematical Physics. From November 1943, he was Professor at the Lomonosov Moscow University. In January 1953, Bogolyubov was elected the Head of the Department of Theoretical Physics of the University, where, in 1966, he also founded the well-known Bogolyubov Department of Quantum Statistics and Field Theory.

It is important to note that Mykola Bogolyubov's life and work from the first years till the last days were closely connected with Ukraine. Being ethnic Russian by origin, he was brought up in the atmosphere of deep love to Ukraine, he felt great respect for the land where his childhood and adolescence passed, where he made his first steps in science and gained worldwide name. Desiring to share the fate of the Ukrainian people in everything, he considered himself Ukrainian, as he wrote about himself in all questionnaires and personal papers. The same entry was in his Soviet passport. Mykola Mykolayovych's attitude to Ukraine is comprehensively characterized by Alexey Bogolyubov's words about his elder brother: "Mykola Mykolayovych had two homelands – Russia and Ukraine and two native languages – Russian and Ukrainian. Beginning from the Velyka Crucha years, he became associated with Ukraine, and Shevchenko's poetry was, in fact, the first poetry he became interested in. The young graduate student of the Department of Mathematical Physics wrote the minutes of the seminars of the department in Ukrainian, and his first works were also written in Ukrainian." Further: "Mykola Mykolayovych, in the difficult times for Ukraine, when the Ukrainian intelligentsia started to be destroyed, when the shameful process of the Ukrainian Liberation Union took place in Kharkiv and Ukrainian books burned, he admitted himself to be a Ukrainian and so considered himself for his whole life. It is an indisputable fact that all the development of his personality and the acquisition of features of scientific creativity took place in Ukraine, and were also closely associated with Ukraine. He used to call Kyiv his favorite city, equating to him only Paris". Although these words are well known and have been cited for many times in articles about the Ukrainian period of Bogolyubov and memories of him, we have to mention them here, because they reveal the origins of Bogolyubov's love for Ukraine. Mykola Mykolayovych's attitude to his native Ukrainian land, to the Ukrainian language, should be a good example for many of our compatriots.

Mykola Bogolyubov passed away on February 13, 1992. He has left invaluable scientific heritage, numerous scientific schools, a large cohort of students and followers, with whom he always shared scientific ideas and interesting research.

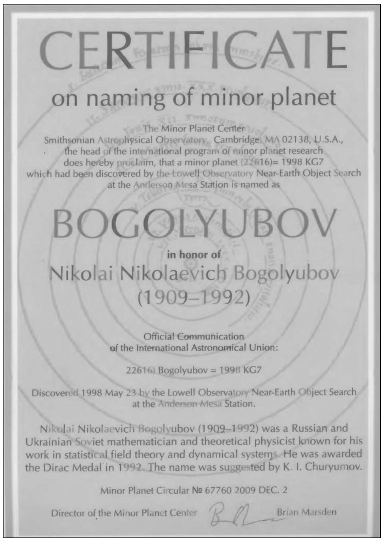

CERTIFICATE

on naming of minor planet

The Minor Planet Center
Smithsonian Astrophysical Observatory, Cambridge, MA 02138, U.S.A.,
the head of the international program of minor planet research
does hereby proclaim, that a minor planet (22616)= 1998 KG7
which had been discovered by the Lowell Observatory Near-Earth Object Search
at the Anderson Mesa Station is named as

BOGOLYUBOV

in honor of

Nikolai Nikolaevich Bogolyubov
(1909–1992)

Official Communication
of the International Astronomical Union:

22616) Bogolyubov = 1998 KG7

Discovered 1998 May 23 by the Lowell Observatory Near-Earth Object Search
at the Anderson Mesa Station.

Nikolai Nikolaevich Bogolyubov (1909–1992) was a Russian and Ukrainian Soviet mathematician and theoretical physicist known for his work in statistical field theory and dynamical systems. He was awarded the Dirac Medal in 1992. The name was suggested by K. I. Churyumov.

Minor Planet Circular № 67760 2009 DEC. 2

Director of the Minor Planet Center Brian Marsden

Fig. 8. Certificate on naming of a minor planet in the solar system as Bogolyubov

M.M. Bogolyubov was a scholar of wide international recognition. He was elected a member of 10 foreign academies of sciences and was awarded the honorary doctorate of 10 foreign universities. Foreign state and scientific awards also testify to the recognition of Bogolyubov's contribution to the world science. In particular, he is a winner of the Prize of the Academy of Sciences of Bologna (1930, Italy), Heinemann Prize of the American Physical Society (1966), Helmholtz Gold Metal (1969), Max Planck Prize of the Physical Society of Germany (1978), Franklin Prize (1974, USA), Prize of the Slovak Academy of Sciences (1975), Paul Dirac Prize (1992), and others.

In 1987, the International Center for Theoretical Physics in Trieste founded the Bogolyubov Prize for outstanding achievements in mathematics and solid state physics for scientists from developing countries. The National Academy of Sciences of Ukraine has also established the Bogolyubov Prize for the research in mathematics and physics. The Russian Academy of Sciences founded in 1999 the Bogolyubov Gold Medal, for researches in the fields of mathematical physics and mathematics. The Bogolyubov Gold Medal was also founded in JINR. In 2018, the Bogolyubov Institute for Theoretical Physics started awarding Bogolyubov Prizes for the best works in theoretical and mathematical physics.

The monuments of Academician Bogolyubov were erected in Nizhny Novgorod and Dubna, and his busts were located in Kyiv at the Bogolyubov Institute for Theoretical Physics and at the JINR Laboratory of Theoretical Physics. A memorial plaque honoring Mykola Bogolyubov decorates the Red Building of Taras Shevchenko National University of Kyiv. A memorial sign in honor of Mykola Mykolayovych was erected in the village of Velyka Krucha.

The 100th anniversary of Bogolyubov birth is widely celebrated in Ukraine. The International Bogolyubov Conference "Modern Problems of Theoretical and Mathematical Physics" and the II Ukrainian Mathematical Congress were held in Kyiv, and the anniversary Bogolyubov Conference was also held in Lviv; books and articles about the life and work of the great scientist were published. The anniversary coin and the Bogolyubov Medal of the Ukrainian Mathematical Congress were minted.

On December 3, 2009, at the application of the famous Ukrainian astronomer K.I. Churyumov initiated by the Bogolyubov Institute for Theoretical Physics, the International Astronomical Union adopted the decision to give the minor planet of the Solar System (22616) = 1998 KG7 the name Bogolyubov.

A brilliant scientist continues his life in the works of his students and numerous followers, including those who work at the Bogolyubov Institute for Theoretical Physics, and we are sure that the ideas of Mykola Bogolyubov will inspire many theorists for many years.

V.G. BAR'YAKHTAR, A.G. ZAGORODNY,
V.M. LOKTEV, I.M. MRYGLOD,
M.F. SHUL'GA, I.R. YUKHNOVS'KYI

AUTHOR'S INDEX